

**AMYOTROPHIC LATERAL SCLEROSIS  
MOLECULAR MECHANISMS TO DIAGNOSTICS**

By

Srikanth Ranganathan

M.Sc. Zoology, “Jnanabharathi”, Bangalore University, 1990

M.S. Biology, Georgia Institute of Technology, 1994

Submitted to the Graduate Faculty of the School of Medicine,

Department of Cellular and Molecular Pathology

in partial fulfillment of the requirements for the degree of

Doctor of Philosophy

University of Pittsburgh

2004

University of Pittsburgh

School of Medicine

This dissertation was presented

by

Srikanth Ranganathan

It was defended on

November 15<sup>th</sup> 2004

and approved by

Cristian Achim, M.D., Ph.D., Chairman  
Associate Professor, Department of Pathology

Charleen Chu, M.D., Ph.D.  
Assistant Professor, Department of Pathology

Ian Reynolds, Ph.D.  
Professor, Department of Pharmacology

Reza Zarnegar, Ph.D.  
Professor, Department of Pathology

Robert Bowser, Ph.D.  
Dissertation Director  
Associate Professor, Department of Pathology

## COPYRIGHT

This document is copyright free for educational and scientific development.

Permission was granted to the use of parts from:

1. **Ranganathan, S.,** and Bowser, R. (2003) Alterations in G1 to S phase cell cycle regulators during amyotrophic lateral sclerosis. *Am. J. Pathol* 162(3): 823-835
2. Functional Neuroanatomy: An Interactive Text and Manual, Jeffrey T. Joseph and David L. Cardozo, Copyright © (2004, John Wiley and Sons, Inc.).

Documentation of permission letters is on file with Srikanth Ranganathan

# **AMYOTROPHIC LATERAL SCLEROSIS**

## **MOLECULAR MECHANISMS TO DIAGNOSTICS**

**Srikanth Ranganathan**

**University of Pittsburgh, 2004**

### **ABSTRACT**

Amyotrophic lateral sclerosis (ALS) is a relentlessly progressive and fatal motor neuron disease, characterized by loss of motor neurons in the cortex, brainstem and spinal cord. Clinical management is plagued by a lack of biomarkers and effective treatment. In spite of numerous scientific advancements, molecular mechanisms involved in its initiation and progression remain an enigma. At the mechanistic level, ALS is considered multifactorial. Extracellular signals may modulate nuclear events with a possible consequence being the reactivation of cell cycle-related genes and protein alterations in the terminally differentiated motor neurons.

In the first specific aim, we hypothesized that re-entry of post-mitotic motor neurons into the cell cycle, concurrent with altered activity or distribution of transcription factors will result in apoptosis of motor neurons during ALS. To address this hypothesis, we utilized archived human autopsy material from the cortical and spinal cord regions of ALS and age-matched control cases. We conclude that surviving ALS motor neurons in these regions exhibited increased levels of G1 to S phase regulators (Cyclin D1, CDK4, hyperphosphorylated -pRb and E2F-1). It also revealed two intriguing results: (i) E2F-1, a transcription factor, was cytoplasmic and (ii) increased nuclear p53 was noted in spinal motor neurons but absent in neurons of the motor

cortex. In addition there was increased protein levels of apoptotic death markers (BAX, FAS, Caspases) and DNA fragmentation. Therefore we have identified a potential role for cell cycle proteins in an apoptotic mode of motor neuron death in ALS.

In the second specific aim we hypothesized that a mass spectrometry-based proteomics approach will identify diagnostic biomarkers and molecular targets for drug discoveries. We used cerebrospinal fluid (CSF) from ALS and control subjects to identify and validate a biomarker panel specific to ALS. Furthermore, utilizing peptide map fingerprinting and tandem mass-spectrometry, we have identified three of the protein peaks to be a carboxyl-terminal fragment of neurosecretory chaperone protein 7B2 (3.44kDa), Cystatin C (13.3kDa) and monomer of transthyretin (13.78kDa).

Taken together, this body of work furthers the understanding of both the mechanisms leading to selective motor neuron loss in ALS and paves the way for diagnostics and therapeutics.

## TABLE OF CONTENTS

AMYOTROPHIC LATERAL SCLEROSIS .....	i
COPYRIGHT .....	iii
ABSTRACT .....	iv
LIST OF TABLES.....	xi
LIST OF FIGURES .....	xii
ABBREVIATIONS .....	xv
ACKNOWLEDGEMENTS .....	xix
1. INTRODUCTION .....	1
1.1. Neurons, Glia and Synapse.....	1
1.2. The Central Nervous System.....	4
1.2.1. Brain and Brainstem .....	4
1.2.2. Spinal cord .....	7
1.3. The Motor System.....	7
1.4. The Tracts .....	9
1.5. Motor Neuron Diseases.....	10
1.6. Amyotrophic Lateral Sclerosis (ALS) .....	13
1.6.1. Epidemiology .....	13
1.6.2. Clinical Features.....	15
1.6.3. Diagnosis.....	16
1.6.4. Neuropathology .....	18
1.6.5. “ALS –Plus”: A Multisystem Disorder?.....	20
1.6.6. Genetics of ALS .....	22
1.6.7. Pathogenic Mechanisms of SALS .....	26
1.6.7.1. Oxidative Stress and SOD1-mediated toxicity.....	29
1.6.7.2. Excitotoxicity .....	34
1.6.7.3. Mitochondrial dysfunction .....	36
1.6.7.4. Cytoskeletal Abnormalities .....	36

1.6.7.5.	Astrogliosis.....	38
1.6.7.6.	Autoimmunity.....	39
1.6.7.7.	Other mechanisms (DNA Damage, Growth Factors, Viruses).....	40
1.7.	Cell Cycle and Cell death.....	41
1.7.1.	Cell cycle Regulators and Neurological disorders.....	44
1.8.	Types of Cell Death during Neurodegeneration.....	44
1.8.1.	Apoptosis during Neurodegeneration.....	46
1.8.2.	Apoptotic Pathways in ALS.....	48
1.9.	Current Therapeutics and Clinical Trials.....	48
1.10.	Drug design and therapy – The “Omics” approach.....	50
1.10.1.	Clinical Proteomics.....	51
1.10.2.	Two Dimensional Gel Electrophoresis (2D-GE).....	52
1.10.3.	Mass Spectrometry.....	53
1.10.4.	MS-Based Proteomics.....	54
1.11.	Statement of Problem.....	56
2.	Abortive Re-entry of Motor Neurons into Cell Cycle.....	57
2.1.	Abstract.....	57
2.2.	Introduction.....	58
2.3.	Materials and Methods.....	60
2.3.1.	Source of Tissue Samples.....	60
2.3.2.	Antibodies.....	60
2.3.3.	Immunohistochemistry – Light and Confocal Microscopy.....	63
2.3.4.	Protein Extraction.....	64
2.3.5.	Immunoblotting.....	65
2.3.6.	Electrophoretic Mobility Shift Assay (EMSA).....	66
2.3.7.	Statistical Analysis.....	66
2.4.	Results.....	67
2.4.1.	Increased immunoreactivity of G1 to S phase cell cycle proteins in ALS spinal cord motor neurons.....	67
2.4.2.	Cellular distribution of cell cycle proteins in motor cortex.....	70
2.4.3.	Cell cycle proteins in white matter of ALS spinal cord and motor cortex.....	72

2.4.4.	Co-localization of ppRb, E2F-1 and p53 in ALS motor neurons using laser scanning confocal microscopy .....	74
2.4.5.	Co-localization of ppRb, E2F-1 and p53 in the white matter of ALS spinal cord and motor cortex using laser scanning confocal microscopy.....	80
2.4.6.	Analysis of protein levels by Western immunoblotting .....	80
2.4.7.	DNA-binding activity of E2F-1 .....	83
2.5.	Discussion.....	85
3.	Neuronal Cell death in ALS: Role of p53 mediated apoptosis .....	91
3.1.	Abstract .....	91
3.2.	Introduction .....	92
3.3.	Materials and Methods.....	95
3.3.1.	Antibodies .....	96
3.3.2.	Electrophoretic Mobility Shift Assay (EMSA).....	96
3.3.3.	Terminal deoxynucleotidyl transferase-mediated biotinylated UTP nick end labeling staining (TUNEL) .....	96
3.4.	Results.....	97
3.4.1.	Analysis of death marker protein levels by Western immunoblotting .....	97
3.4.2.	Increased immunoreactivity of p53 in ALS spinal cord but not motor cortex ...	102
3.4.3.	Subcellular distribution of apoptotic death markers in spinal cord and motor cortex .....	105
3.4.4.	Co-localization of cell cycle proteins and apoptotic death markers in ALS spinal cord and motor cortex.....	106
3.4.5.	DNA fragmentation as a marker for apoptosis .....	110
3.4.6.	DNA-binding activity of p53 .....	115
3.5.	Discussion.....	116
4.	Assessment of human CSF Proteome stability by SELDI-TOF-MS.....	123
4.1.	Abstract .....	123
4.2.	Introduction .....	124
4.3.	Materials and Methods.....	125
4.3.1.	Study Population and Sample Preparation.....	125
4.3.2.	Chip Preparation.....	126

4.3.3.	SELDI-TOF-MS.....	126
4.3.4.	Data Analysis .....	127
4.4.	Results and Discussion.....	128
5.	Post-mortem CSF is not an ideal candidate for biomarker discovery .....	135
5.1.	Abstract .....	135
5.2.	Introduction .....	136
5.3.	Materials and Methods.....	137
5.3.1.	Study Population .....	137
5.3.2.	Sample and Chip Preparation.....	138
5.3.3.	SELDI-TOF-MS.....	138
5.3.4.	Data Analysis .....	139
5.4.	Results and Discussion.....	140
6.	Discovery and identification of ALS-specific biomarkers by mass spectrometry- based proteomics .....	152
6.1.	Abstract .....	152
6.2.	Introduction .....	154
6.3.	Materials and Methods.....	157
6.3.1.	Study Population and CSF .....	157
6.3.2.	SELDI-TOF-MS.....	157
6.3.3.	Data Analysis .....	159
6.3.4.	Biomarker Identification by Mass Spectrometric Analysis.....	161
6.3.5.	Biomarker Validation .....	162
6.3.5.1.	Immuno-SELDI-TOF-MS.....	162
6.3.5.2.	Immunoblotting .....	163
6.3.5.3.	Immunohistochemistry.....	163
6.4.	Results.....	164
6.4.1.	Identification of differentially expressed protein peaks in ALS by univariate analysis .....	164
6.4.2.	CSF Biomarker panels.....	167
6.4.2.1.	BPS Analysis.....	167
6.4.2.2.	RL Analysis.....	169

6.4.2.3.	Site of Disease Onset .....	173
6.4.3.	Protein Identification .....	174
6.4.4.	Protein Validation.....	179
6.4.5.	Western Immunoblotting for Cystatin C and Transthyretin .....	181
6.4.6.	Immunohistochemistry for Transthyretin .....	183
6.5.	Discussion.....	183
7.	Future Directions .....	195
7.1.	<i>In vitro</i> motor neuron cultures to dissect the functional role for cell cycle proteins, p53 and pro-death molecules during ALS .....	195
7.2.	Dissect the role for re-activation of cell cycle and p53-mediated motor neuron death in animal models of ALS ( <i>in vivo</i> ) .....	199
7.3.	Determine the Functional Role for Cytoplasmic E2F-1.....	202
7.4.	MS-based proteomics approach to study protein alterations during ALS in an animal model using plasma and spinal cord tissue samples.....	204
7.5.	A longitudinal biomarker study in ALS patients .....	207
7.6.	Proteomics for ALS: The future .....	208
8.	Concluding Remarks.....	210
	BIBLIOGRAPHY .....	213

## LIST OF TABLES

Table 1	Spectrum of Motor Neuron Diseases .....	12
Table 2	List of the cases utilized in this study.....	61
Table 3	List of Antibodies.....	62
Table 4	Features utilized by BPS for classification and prediction.....	149
Table 5	List of cases in the training set.....	158
Table 6	List of cases in the blinded test set.....	159
Table 7	Multivariate analysis of blinded dataset using RL.....	170
Table 8	RL analysis of validation and blinded sample sets .....	171
Table 9	RL analysis of all subjects .....	173
Table 10	RL analysis of site of disease onset in ALS subjects .....	174

## LIST OF FIGURES

Figure 1	Schematic Representation of a Motor Neuron.....	2
Figure 2	Neuronal Synapse.....	3
Figure 3	Central Nervous System (CNS).....	4
Figure 4	Regions of the Brain and Brainstem.....	5
Figure 5	Spinal Cord – Gross anatomy and histology .....	6
Figure 6	Homunculus and the tracts.....	8
Figure 7	Spinal Degeneration in ALS .....	18
Figure 8	Ubiquitin Positive Inclusion Bodies in Lower Motor Neurons .....	19
Figure 9	Normal Function for Cu/Zn cytoplasmic SOD – A schema.....	23
Figure 10	ALS Pathogenesis: Do all roads lead to motor neuron death ?.....	27
Figure 11	Hypothesized Mechanisms for the “Gain of Toxic Function” in Mt SOD1.....	31
Figure 12	Hypothesis: Aberrant re-activation of G1 to S phase Regulators .....	42
Figure 13	Immunohistochemical analysis of G1 to S phase regulators in human spinal cord tissues.....	70
Figure 14	Immunohistochemical analysis of G1 to S phase regulators in human motor cortex .....	71
Figure 15	Immunohistochemical analysis of ppRb and E2F-1 in glia in the white matter of ALS spinal cord and motor cortex .....	73
Figure 16	Immunohistochemical co-localization analysis of ppRb, E2F-1 and p53 in motor neurons of ALS spinal cord and motor cortex.....	76
Figure 17	Immunohistochemical co-localization analysis of ppRb, E2F-1 and p53 in activated astrocytes of ALS spinal cord and motor cortex .....	78
Figure 18	Immunohistochemical co-localization analysis of ppRb, E2F-1 and p53 in activated microglia of ALS spinal cord.....	80
Figure 19	Protein levels in total cell extracts from human spinal cord and motor cortex .....	82

Figure 20	E2F-1 DNA binding activity is unaltered in ALS.....	84
Figure 21	Model of motor neuron cell death induced by activation of cell cycle proteins.....	89
Figure 22	Increased p53 and death markers in ALS spinal cord tissue lysates.....	99
Figure 23	Decreased p53, p73 and no change in death markers in ALS motor cortex tissue lysates.....	101
Figure 24	Increased immunoreactivity of p53 in spinal cord motor neurons but not in the motor cortex .....	103
Figure 25	Increased immunoreactivity of death markers in spinal cord motor neurons.....	104
Figure 26	No change in immunoreactivity of death markers in cortical motor neurons .....	106
Figure 27	Cell cycle transcription factors co-localize with death markers in spinal motor neurons .....	107
Figure 28	Cell cycle transcription factors co-localize with death markers in cortical motor neurons .....	109
Figure 29	Fas and Caspase-8 co-localize in spinal motor neurons.....	110
Figure 30	Increased DNA fragmentation in spinal but not cortical motor neurons.....	112
Figure 31	No change in p53 DNA binding activity in ALS motor neurons.....	114
Figure 32	CSF spectra representing m/z region of 11 to 15kDa depicting temperature dependent changes in proteome stability .....	129
Figure 33	Percent variance and coefficient of variance as measures of CSF proteome stability .....	131
Figure 34	GMSD as a statistical measure of variance in the CSF proteome.....	132
Figure 35	Representative spectrogram illustrating differences in CSF proteome profile of post-mortem and recently diagnosed ALS patients in the mass range of 2 - 20kDa and 4 -8kDa .....	141
Figure 36	Differences in spectral patterns when CSF from living ALS patients (190, 390 or 1400 days from time of symptom onset) are compared to post-mortem (PM) CSF sample .....	143
Figure 37	Clustering of spectra using BPS.....	144
Figure 38	Univariate analysis of CSF from living patients and post-mortem cases.....	146
Figure 39	BPS classification analyzing post-mortem ALS and age-matched post-mortem non-neurological and neurological controls .....	148

Figure 40	Comparison of mass spectra between ALS and Controls using SAX2 chip .....	165
Figure 41	Univariate analysis of analytes from SAX2 and Zn-IMAC30.....	166
Figure 42	Multivariate analysis of SAX2 (A) and Zinc-IMAC30 (B) datasets using BPS ...	168
Figure 43	Enrichment of biomarkers by fractionation.....	175
Figure 44	1D SDS-PAGE, in-gel tryptic digests of the 13.38kDa and 13.78kDa peaks .....	176
Figure 45	Peptide mass fingerprinting of the 13.38 and 13.78kDa digests.....	178
Figure 46	Validation of transthyretin (monomer) by Immuno-SELDI-TOF-MS .....	179
Figure 47	Validation of the 13.78 and 13.38kDa protein peaks by Western blotting .....	180
Figure 48	Decreased immunoreactivity of transthyretin in ALS spinal motor neurons .....	182
Figure 49	Schematic representation for murine spinal motor neuron cultures.....	196
Figure 50	Immunofluorescent staining for $\alpha$ -tubulin, MAP2, p75 .....	197
Figure 51	Motor neuron culture protocol to test aberrant cell cycle hypothesis .....	198
Figure 52	Spinal cord sections from G93A SOD1 transgenics and non-transgenic littermates immunostained for ppRb, E2F-1 and p53 .....	200
Figure 53	Western immunoblot for ppRb and E2F-1 in G93A spinal cord.....	201
Figure 54	Human lumbar sections from control and ALS cases were double-labeled for E2F-1 and TRAF2 .....	203
Figure 55	Identification and validation of glial fibrillary acidic protein (GFAP) in ALS spinal cord lysates .....	206
Figure 56	Motor neuron death in ALS .....	211

## ABBREVIATIONS

ACN	Acetonitrile
ACST	Anterior corticospinal tract
AD	Alzheimer's disease
AEC	3-amino-9 ethylcarbazole
ALS	Amyotrophic lateral sclerosis
ALS2	ALSIN
ALS-PDC	Amyotrophic lateral sclerosis – Parkinsonism dementia complex
BPS	Biomarker pattern software
CBT	Corticobulbar tract
CC	Cystatin C
CCS	Copper chaperone for SOD1
CDK	Cyclin dependent kinases
CNS	Central nervous system
COV	Coefficient of variance
CSF	Cerebrospinal fluid
CT-7B2	Carboxy terminal fragment of 7B2 protein
Ctl	Control
CV	Coefficient of variation
E13	Embryonic day 13
EAM	Energy absorbing molecule
EMSA	Electrophoretic mobility shift assay

FALS	Familial amyotrophic lateral sclerosis
FTD	Frontal temporal dementia
GFAP	Glial fibrillary acidic protein
GMSD	Grand sum mean deviation
HD	Huntington's disease
IHC	Immunohistochemistry
kDa	Kilodaltons
LCST	Lateral corticospinal tract
LMN	Lower motor neurons
LSC	Lumbar spinal cord
m/z	mass / charge
mAb	Monoclonal antibodies
MALDI-TOF	Matrix assisted laser desorption / ionization – Time of flight
MND	Motor neuron disease
MS	Mass spectrometry
NF-H, -L, -M	Neurofilament-Heavy chain, -light chain and medium chain
pAb	Polyclonal antibodies
PBP	Progressive bulbar palsy
PC2	Prohormone convertases 2
PD	Parkinson's disease
PLS	Primary lateral sclerosis
PM	Post-mortem
PMA	Progressive muscular atrophy

pRb	Hypophosphorylated retinoblastoma protein
ppRb	Hyperphosphorylated retinoblastoma protein
RCC1	Regulator of chromatin condensation 1
RL	Rule Learner
RT	Room temperature
SALS	Sporadic amyotrophic lateral sclerosis
SAX2	Strong anionic exchange chip array
SBMA	Spino-bulbar muscular atrophy
SD	Standard deviation
SDS-PAGE	Sodium dodecyl sulfate – Polyacrylamide gel electrophoresis
SELDI-TOF-MS	Surface enhanced laser desorption / ionization – Time of flight – Mass spectrometry
SEM	Standard error of mean
SMA	Spinal muscular atrophy
SOD1	Superoxide dismutase 1 (Cu <sup>++</sup> /Zn <sup>++</sup> –SOD1)
SOP	Standard operating protocols
SPA	Sinapinic Acid
2D-GE	Two-dimensional gel electrophoresis
TdT	Terminal deoxynucleotidyl transferase
TFA	Trifluoroacetic acid
TNF- $\alpha$	Tumor necrosis factor -alpha
TRAF	TNF- $\alpha$ receptor associated factors
TSA	Tyramide signal amplification

TTR	Transthyretin
TUNEL	Terminal deoxynucleotidyl transferase-mediated biotinylated UTP nick end labeling
UMN	Upper motor neurons
VAR	Variance
Zn-IMAC30	Zinc ion – treated immobilized metal affinity capture chip array

## ACKNOWLEDGEMENTS

*Om Namō Guruvayurappa Rakshamaum*

*“Mathru Devo bhava*

*Pithru Devo bhava*

*Aacharya Devo bhava*

*Athithi Devo bhava” – The Vedas*

*Regard your mother (“Mathru”), father (“Pithru”), preceptor (“Aacharya”),  
and guest (“Athithi”) as god (“Devo”).*

This study was made possible by the combined efforts of many individuals who made my graduate career a truly rewarding experience.

I would like to express my deepest gratitude to my advisor, Dr. Robert Bowser (Bob) for his untiring efforts in guiding me through all stages of this investigation and in the completion of this thesis. The consistent encouragement, the interest, the thoughtful kindness, supervision and advice proffered by Bob will be forever remembered. It was a pleasure to work in close association with Bob because of his scientific motivation, cutting-edge ideas, enthusiasm and sincerity towards the scientific development of graduate students.

Sincere appreciation is expressed to my committee members – Drs. Cris Achim, Charleen Chu, Ian Reynolds and Reza Zarnegar for their valuable advice and constructive criticism towards the development of the contents of this thesis, as also to Drs. Clayton Wiley, Ron Hamilton, Billy Day, and Marielena McGuire. Grateful acknowledgements are extended to Drs. Robert Brown Jr., and Merit Cudkowicz at the Massachusetts General Hospital (MGH), who

generously provided the valuable clinical samples. Without their courtesy and collaboration the opportunity for this research may not have been possible.

Special thanks to Aaron, Peter, Rama, Nandini, Sriram, Madhuri, Malini and Mihaela for their helpful suggestions and technical discussions encountered in the study.

I cannot express thanks to a number of people, who have made significant contributions to the preparation of this body of work in many ways. Among them, recognition must be given to Drs. Vanathi Gopalakrishnan and James Lyons-Weiler for their careful guidance in the field of bioinformatics. My heartfelt thanks to Dr. Stephen Phillips for his forthright willingness to always have his doors open for every graduate student in need like me and to have his sincere interest during my pre-doctoral training. Special thanks to him and the BGSA for having provided me the opportunity to actively serve on the admissions committee, which truly is an experience I will cherish. This section will be incomplete without my acknowledging Cindy, Sandi, Jen and Carol in the graduate student administration as also LaTonya, Sara, Ada, Karen and Nicole amongst others in the Department of Pathology all of whom had ample patience in making this experience smooth and fun.

Thanks also to the numerous patients and their family for having contributed not only to the University of Pittsburgh ALS tissue bank and MGH but also to the scientific community as a whole. Without their involvement this work would be non-existent. I would like to acknowledge NINDS for generously providing the pre-doctoral training support.

Special thanks to all my colleagues in the lab, present and past (Jamie, John, , Georgie, Fran, Dave, Courtney, Jing, Kelly, Sarah, Rama, Kate, Heather, Jason and Jiyan) for their support and scientific discussions. Gratitude extended also to the numerous graduate and undergraduate students who helped me at various stages throughout my project.

My journey to my pre-doctoral training was as important as my journey during the past 5 years here at the University of Pittsburgh. In this regard, I would like to acknowledge Drs. Parthasarathy, Gururaj and Akhila Javed, all my teachers in school especially my school principal, Smt. Kamalam Sethuraman, Ms. Leela, Sarada and my biology teacher in high school, my friends from KVM and KVH, wonderful lecturers and friends in college during my bachelors (Badhri), dear friends of mine (Ravi, Vittal, Bhags, Sunita, Swapna, Priya and others) who made my life at “Jnanabharathi” truly memorable, all my friends at Georgia Tech (Srini, Sujatha, Ramesh, Sam, Shanthi-Narayanan, Padma-Sudarshanan, Annajee, Babu) who helped me make Atlanta my second home and last but not the least the excellent group of friends (KK, Vegitha, Subbi, Venkat, RV, Shyam, Sonali, Aditi, Vidya and others) in College Park, MD for providing me the chance to enjoy life thoroughly. Thank you also to all my friends (Nandini, Anand, Asli, Casey, Vivek, Prajakta, Kavitha and others) who made my life in Pittsburgh enjoyable.

At the scientific level, I would like to acknowledge my Masters advisor, Dr. Dwight Hall for giving me my first shot at graduate school in this country and Dr. Judith Whittum-Hudson for believing in me during my first real job. Finally Dr. John Laterra, I can't thank enough for moulding me towards my second essay of graduate school. Thanks are also due to members of the Drs. Laterra and Bressler lab: Drs. Roger Abounader for his everlasting patience and parting of his knowledge, Bachchu, Carey, Adam, Luisia, Kyung, Ahamed Hossain amongst others.

I would like to thank my family (my lovely niece and nephews, siblings – Akka, Ganesh and Kannan; Rama, Yogi, Madhuri, Malini and my in-laws) who have always stood by me providing their endearing love, who patiently listened and helped me to put things into perspective during this endeavor, egging me to never give up.

I would also like to convey my respectful gratitude to my late uncle, Sri. Natarajan and my grandparents who helped me during trying times.

To my wife, Rama, for her utmost patience and having put my interests before her own – Sincere gratitude.

Finally, but foremost, **“to those from whom I took the most, more than I can ever give back – to my parents”**, who taught me the value of education, for their constant love, thoughtfulness, understanding and continued support in every way, which sustained me throughout my education.

**To my dear parents - I dedicate this doctoral degree  
and all my achievements, past and future**

# 1. INTRODUCTION

## 1.1. Neurons, Glia and Synapse

The nervous system is one of the most complex and intriguing circuitry that controls and integrates all body activities. It is primarily organized into the central (brain and spinal cord) and the peripheral (connecting the central nervous system (CNS) to rest of the body) nervous systems. Principally the nervous system comprises of two types of cells: Nerve cells or Neurons and Neuroglial cells or Glia. Dr. Cajal suggested neurons to be the structural and functional units of the nervous system in the “Neuron Doctrine” [1-3]. Neurons can be classified based on their functions (motor, sensory), shape (pyramidal, stellate), size (small sized granule cells or large motor neurons) number of processes found on the cell body (uni-, bi-, or multipolar), or named after scientists (Purkinje, Betz) (Fig 1).

Neuroglial cells, which literally mean “Nerve Glue”, function as ancillary cells in the nervous tissue. There are four types of neuroglial cells in the CNS: Astrocytes, Microglia, Oligodendrocytes, and Ependymocytes. In addition to providing structural support, astrocytes possess glutamate transporters that aid in uptake of the excitatory neurotransmitter glutamic acid. Astrocytes and microglial cells have the ability to undergo rapid mitosis leading to tumor formation, inflammation in response to injury or neurodegenerative diseases [4-7]. “Reactive astrocytes” stain positive for glial acidic fibrillary protein (GFAP), a cytoskeletal intermediate filament protein universally considered as a marker of activated astrocytes and phenotypically appears with a number of processes. Microglia act as delegates of the immune system in the

brain and are considered macrophages of the nervous system. Upon injury, microglia dramatically increase in number due to additional infiltration of blood monocytes via blood vessels, which in turn mature into macrophages. Oligodendrocytes (ODC) form myelin sheath around axons of CNS neurons analogous to Schwann cells in the peripheral nervous system (PNS). The ependymal cells form the lining of cerebral cavities or brain ventricles and the central canal of the spinal cord. Their ciliated form aids in the flow of the cerebrospinal fluid (CSF) that fills these spaces.

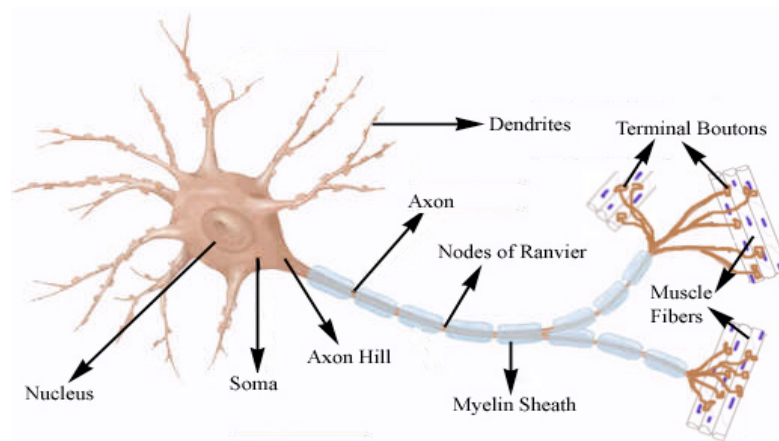


**Figure 1 Schematic Representation of a Motor Neuron**

*Motor neurons are characterized by a large cell body (Soma) with a distinct nucleus and a long myelinated axon. Dendritic arborization, which receive impulses and spines are evident. The axon innervates the muscle fibers forming the motor end plate. Modified from [www.macalester.edu/~psych/whathap/UBNRP/dreaming/images/neuron.jpg](http://www.macalester.edu/~psych/whathap/UBNRP/dreaming/images/neuron.jpg)*

Communications between neurons occur through the synapse of one neuron (pre-synaptic) to another (post-synaptic) with a resultant extracellular space in between the two cells termed the synaptic cleft. The release of neurotransmitters from the pre-synaptic membrane depolarizes the post-synaptic membrane (for instance, motor neurons) and results in an influx of  $\text{Ca}^{2+}$  into the post-synaptic neuron [2, 8]. Ongoing research in this area also focuses on the

involvement of these proteins during synaptic loss during neurodegenerative diseases such as Alzheimer's disease [9-11]. In order for optimal neurotransmission without excessive neurotransmitters present in the synaptic milieu, proper functioning of the support cells or neuroglia is critical (Fig 2).

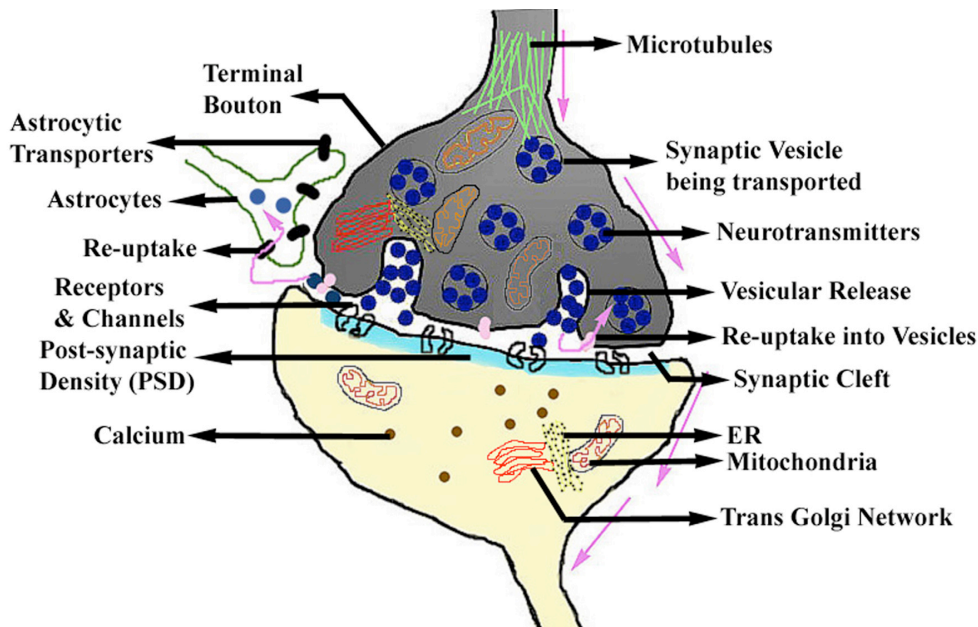


**Figure 2      Neuronal Synapse**

*The dendritic spines of the pre-synaptic neuron communicate with the post-synaptic neuron and transduce nerve impulses (direction of the pink arrow) thus de-polarizing the post-synaptic membrane. Vesicles containing glutamate (blue circles) are transported with the help of cytoskeletal proteins such as microtubules and released into the synaptic cleft. This initiates a signaling cascade with an influx of calcium (brown circles) into the post-synaptic neuron and a concentration of proteins at the post-synaptic membrane termed the post-synaptic density (PSD). Glutamate is efficiently recycled via astrocytic and neuronal transporters. Excess glutamate or inefficient removal of glutamate has been implicated in neurodegenerative diseases such as ALS.*

## 1.2. The Central Nervous System

The CNS comprised of the cortex, brainstem and spinal cord is a functionally well-organized conglomeration of cells that continually receives / transmits and perceives information along the neuronal highway (Fig 3). The motor neurons in the CNS are affected during amyotrophic lateral sclerosis (ALS).

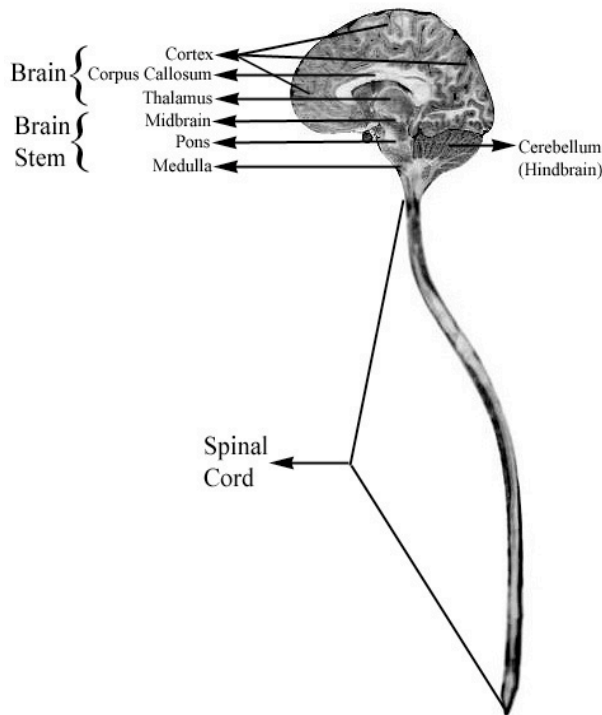


**Figure 3 Central Nervous System (CNS)**

*The brain, brainstem and the spinal cord form the CNS. The brain is comprised amongst other regions the cerebral cortex, thalamus, and the cerebellum. The brainstem consists of the midbrain, pons and the medulla, which continues into the spinal cord.*

*Modified from Functional Neuroanatomy: An Interactive Text and Manual, Jeffrey T. Joseph and David L. Cardozo, Copyright © (2004, John*

*Wiley and Sons, Inc.). Reprinted with permission of John Wiley & Sons, Inc.*

### 1.2.1. Brain and Brainstem

The average normal male and female brain weighs approximately 1350g and 1250g, respectively. In old age and during neurodegenerative diseases such as in Alzheimer's disease, there is reduction in brain weight due to atrophy [12]. The brain analyzes sensory input and then appropriate motor signals are transmitted back to the target muscles via the spinal cord. Three

layers of connective tissue, termed the dura mater, arachnoid and pia mater cover the brain and the spinal cord. Cerebrospinal fluid (CSF) secreted by the choroid plexus into the brain ventricles and the central canal of the spinal cord fills the subarachnoid space in the cranium.

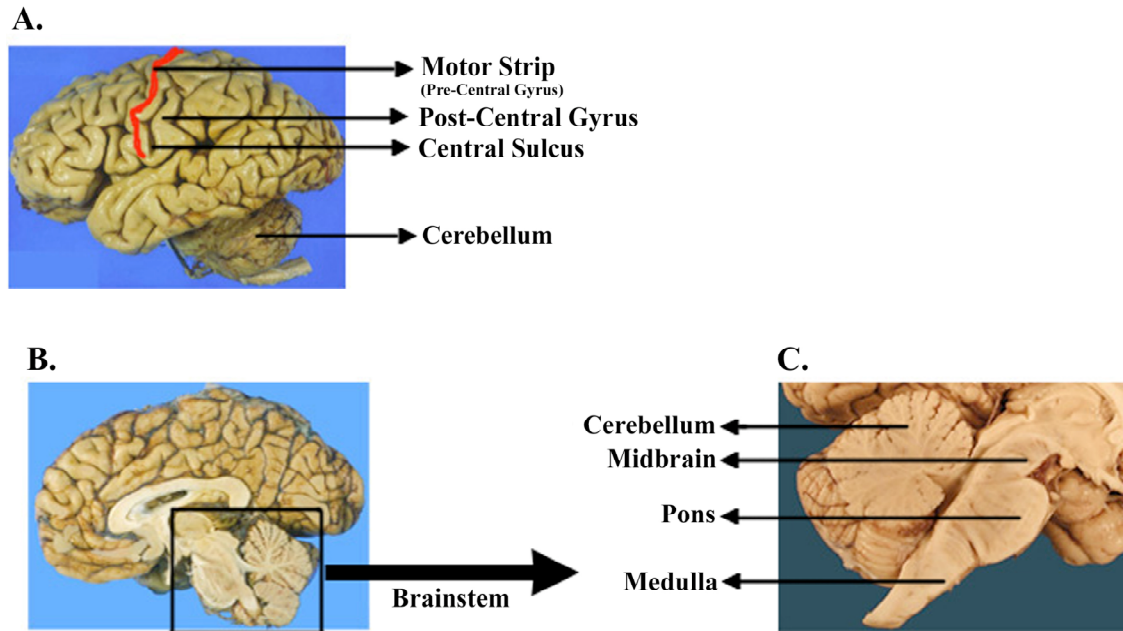


**Figure 4**      **Regions of the Brain and Brainstem**

*In panel A, the gross anatomy of the cortical region is shown. The central sulcus demarcates the pre-central gyrus (motor cortex / highlighted strip) and the post-central gyrus (sensory cortex). Panel B is a sagittal section through the cortex with the boxed region (brainstem) magnified in C. The rightmost panel depicts the different regions that constitute the brainstem. Modified from *Functional Neuroanatomy: An Interactive Text and Manual*, Jeffrey T. Joseph and David L. Cardozo, Copyright © (2004, John Wiley and Sons, Inc.). Reprinted with permission of John Wiley & Sons, Inc.*

The medulla, pons and midbrain together comprise the brain stem of the CNS and are present deep within the brain continuous with the spinal cord containing motor and sensory nuclei (group of nerve cell bodies). Some of the functions the brainstem controls include

breathing, swallowing, heart rate, ability to sleep and probably laughing. Nerve fibers in the brain stem typically do not regenerate and hence injury may result in permanent loss of function (Fig 4).

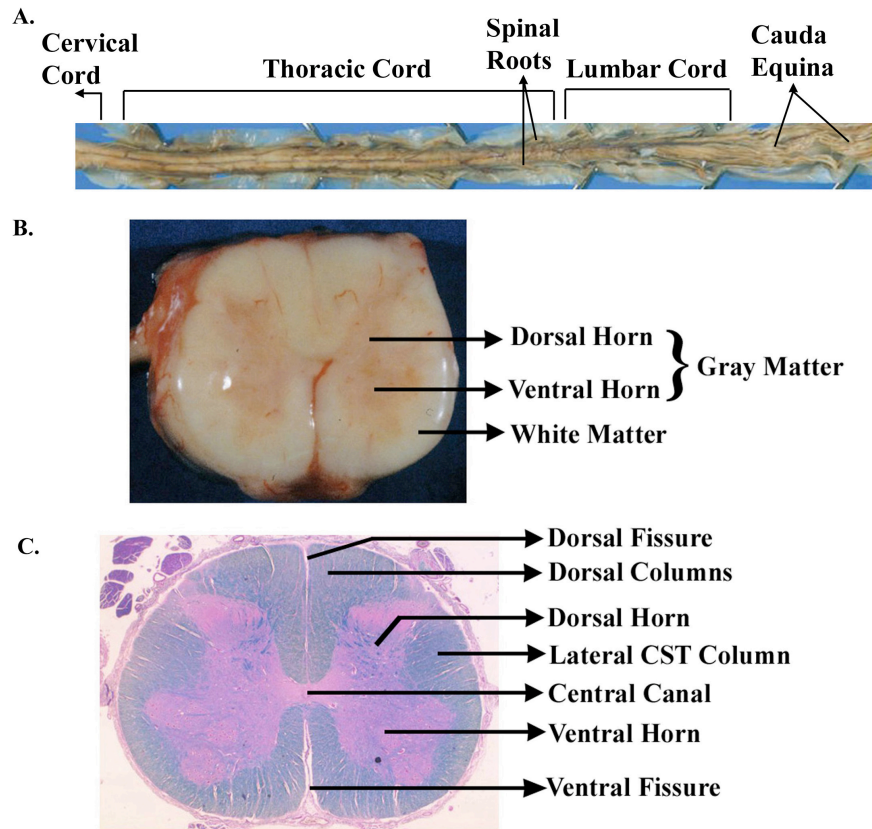


**Figure 5 Spinal Cord – Gross anatomy and histology**

(A) Gross anatomical representation of spinal cord. The spinal roots and cauda equina (the collection of the nerve fibers) are evident. (B) Fresh cord at the level of the lumbar region. The distinct “butterfly” shaped gray matter is seen with an enlarged ventral horn that houses the motor neurons. (C) Transverse section through a cord stained with luxol fast blue and haematoxylin / eosin. Modified from *Functional Neuroanatomy: An Interactive Text and Manual*, Jeffrey T. Joseph and David L. Cardozo, Copyright © (2004, John Wiley and Sons, Inc.). Reprinted with permission of John Wiley & Sons, Inc.

### **1.2.2. Spinal cord**

The spinal cord is covered by the bony vertebral column and is a cylindrical structure slightly flattened dorsoventrally (Fig 5A, B). The cord is divided into five different levels [cervical (8 pairs of nerves), thoracic (12 pairs), lumbar (5 pairs), sacral (5 pairs), coccygeal (1 pair)] depending on the regions of the human body that the spinal “mixed” nerves innervate. These are "mixed" nerves because each contains both sensory and motor axons. In a transverse section of the spinal cord, the gray matter is butterfly shaped in the form of the letter “H” with the white matter at the surface (Fig 5C). The dorsal / posterior horn comprises of the sensory neuronal cell bodies while the ventral / anterior horn possesses the large cell bodies of the motor neurons.

### **1.3. The Motor System**

The muscle fibers and the motor neurons that innervate them, together, are termed the “motor unit”. The size of these motor units vary depending on the range of functions that a particular muscle mass performs. Usually the motor neurons are influenced by dorsal root afferents for spinal reflexes with the intervention of interneurons and by several descending tracts for the control of motor activity by the brain. The more complex forms of motor movements are governed in part by the lower motor neurons (LMN) in the spinal cord, and the upper motor neurons (UMN), which include all the nuclei in the brain stem and motor cortex. Much of the motor system is organized in a hierarchical fashion with successive levels for motor control. In the 19<sup>th</sup> century, it was discovered that the most excitable area for generating movements is a cortical area anterior to the central gyrus, designated also as the motor cortex or the precentral gyrus or the gyrus of Rolandi [2, 13]. The motor innervation of the entire human

body is shown as a distorted human figure frequently referred to as the “Homunculus” with an orderly progression of focal areas (Fig 6A). The motor cortical regions that have been utilized in this study (chapters 2 and 3) include the mid- (regions #2 - #5 in Fig 6B) and the superior-motor cortical regions (regions 6 and 7 in Fig 6B).

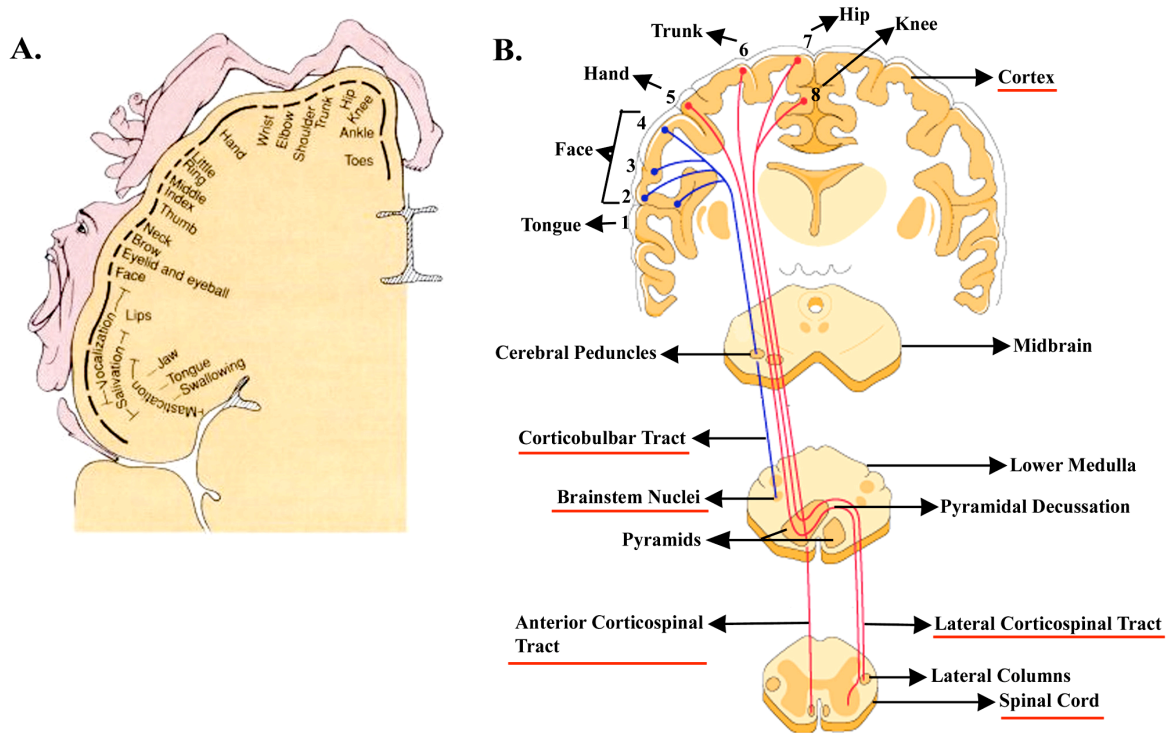


**Figure 6 Homunculus and the tracts**

(A) The upper motor neurons residing in the pre-central gyrus are arranged in a stereotypical fashion, which is graphically represented in the form of a distorted human figure called the “Homunculus”. The size of the face and mouth as well as the limbs is depicted large because many motor nerve fibers innervate these parts of human body.

(B) The axons originating from the motor cortex form a bundle of fibers and traverse through the cerebral peduncle in the midbrain. The axons that innervate the face are present medially in the lower medulla and form the corticobulbar tract (CBT) terminating in the brainstem / cranial

*motor nuclei. The axons innervating the lower limbs are laterally present in the peduncles and form the lateral corticospinal tracts (LCST) aggregating to form the pyramids in the lower medulla. About 80-90% of these tracts then crossover to the other side of the lower medulla (pyramidal decussation). The anterior CST does not decussate and continues in an ipsilateral manner. These axons then synapse on the lower motor neurons situated in the ventral horn of the spinal cord. During ALS, the CBT and the CST degenerate resulting in loss of connectivity between the upper motor centers and the brainstem nuclei or the spinal cord (red underlines).*

*Modified from (A) <http://faculty.etsu.edu/currie/images/homunculus1.JPG>*

*and (B) [http://diagnosis.hallym.ac.kr/multimedia/img/sin\\_563p.gif](http://diagnosis.hallym.ac.kr/multimedia/img/sin_563p.gif)*

#### **1.4. The Tracts**

The  $\alpha$ - and  $\gamma$ -motor neurons in the spinal cord are controlled by the axons originating in the precentral gyrus, thus forming the corticospinal tract, also known as the pyramidal tract. At the level of the medulla, 85% of the fibers cross over to the opposite side (pyramidal decussation) and form the lateral corticospinal tract (LCST) (Fig 6B). The LCST fibers synapse on the lateral motor nuclei of the ventral horn. Axons, which do not cross (15%) continue as the anterior or ventral corticospinal tract (A/VCST) and preferentially innervate the axial / trunk muscle groups. The ACST axons synapse on the medial motor nuclei of the ventral horn. Some of the pyramidal tract fibers can terminate in the bulbar (medulla) cranial motor nuclei forming the corticobulbar tract (CBT), which controls facial muscles (Fig 6B). Giant neurons called Betz cells in cortical layer V give rise to about 3% of the corticospinal tract fibers [13]. The corticospinal and corticobulbar fibers regarded, as the pathways of voluntary movements are both affected in some motor neuron diseases such as ALS.

## **1.5. Motor Neuron Diseases**

The term “motor neuron diseases (MND)” is used in plural to designate the entire spectrum of diseases of the anterior horn cells and the motor system. However, the term MND is used in the United Kingdom synonymously to ALS, with the latter being preferred by the United States. Clinico-pathologically, the spectrum of MND presents with loss of upper and/or lower motor neurons (UMN/LMN) resulting in muscle wasting or atrophy (Table 1). Parkinson’s disease (PD) and Huntington’s disease (HD) fall into the class of neuromuscular diseases and are not conventionally classified as MND with their involvement of the extra-pyramidal motor system. In some disorders (such as ALS), the axons from the motor cortex to the brain stem (corticobulbar tracts) or spinal cord (corticospinal tracts) are involved; in others (such as bulbar palsies), motor nuclei in the brain stem (bulbar nuclei) are selectively affected [14-16].

Injuries to the UMN in the cortex or their axons before they enter the pyramidal decussation result in contralateral spastic paralysis. Injuries to the pyramidal tract below the decussation or to the LMN cause ipsilateral paralysis. The neuromuscular junction or the muscle fibers can also be affected as in myasthenia gravis, or myopathies [14, 17]. However, it is intriguing to note that in some MND such as ALS there is selective sparing of motor neuronal populations. While the somatic motor neurons that control eye movements (extraocular muscles) remain unaffected, those that control bladder/bowel function (Onufrowitz’s nucleus) show inclusions but they are affected to lesser degree than other motor neurons during ALS [18-20].

Historically, it was Aran in 1850 who introduced the term progressive muscular atrophy (PMA) to a muscle disorder that was first described by Duchenne in 1849. The term glosso-labio-laryngeal paralysis was described by Duchenne in 1858 but was later changed to

progressive bulbar palsy (PBP) by Wachsmuth in 1859. Charcot (1874) who studied the pathological features observed earlier by Luys and Clarke (1860), and noted the involvement of the corticospinal tracts, suggested the term ALS. It was Déjerine a French neurologist in 1882 who established the relationship of PBP to ALS [14, 21-23].

In a much more rare form, Betz cells in the motor cortex and corticospinal tracts are principally affected with rare involvement of the lower motor neurons. Spiller (1904) defined the lack of muscular atrophy with myelopathic weakness and the spinobulbar spasticity associated with this disease to be primary lateral sclerosis (PLS). In PLS, there is rarely evidence of the degeneration of spinal motor neurons or muscle wasting (amyotrophy) that occurs in ALS, which it resembles. However, PLS is considered to present with predominantly, but not exclusive motor neuron involvement. The disease, which scientists believe is not hereditary, progresses gradually over a number of years, or even decades [23-26]. Onset of PLS usually occurs after the age of 50. Symptoms include spasticity with slight weakness in the lower limbs and eventually speech with emotional problems. Sometimes PLS can be misdiagnosed to be ALS but if there is a continued lack of LMN involvement, then ALS is ruled out [23-26].

About a century after Charcot proposed the term ALS, Brain (1962) introduced the term motor neuron disease (MND) in recognition of the relationship between ALS, PBP and PMA, depending on the topography of motor neuron cell loss. PMA involves only LMNs, progressive bulbar palsy involves LMNs of the face and throat muscles and Pseudobulbar Palsy affects the UMNs of the face and throat muscles [16, 27]. The spectrum of motor neuron diseases includes the inherited spinal muscular atrophies (SMA) that affect infants and adults. These disorders affect only LMNs and are slowly progressive in adults. Kennedy's Disease or X-linked

Spinobulbar Muscular Atrophy (SBMA) that affects only males (expanded polyglutamine repeats in the gene for androgen receptor) is marked by proximal weakness in the limbs, facial muscles, decreased fertility, and enlarged breasts [28-30]. This disease does not shorten life expectancy but may result in mild to moderate disability and may mimic ALS [28].

Motor Neuron Diseases	Affected CNS Regions	Associated Cause
Spinobulbar Muscular Atrophy (SBMA)	BS and SC (adult onset)	CAG repeats in Androgen Receptor gene
Spinal Muscular Atrophy (SMA)	SC (No UMN) (Infant/Juvenile)	Survivor of motor neuron (SMN) gene
Primary Lateral Sclerosis (PLS)	UMN and CST (no LMN)	Idiopathic (Slow progression)
Progressive Bulbar Palsy (PBP)	Mainly BS	Idiopathic
Progressive Muscular Atrophy (PMA)	LMN (no UMN)	Idiopathic
Sporadic Amyotrophic Lateral Sclerosis (SALS)	MC, BS, SC	Idiopathic / Multifactorial
Familial Amyotrophic Lateral Sclerosis (FALS)	MC, BS, SC	SOD1 (21q22.1), ALS2 (2q33), NF-H
ALS of Guam	MC, BS, SC, Extrapyramidal system	Aluminum, Cycad Nuts
ALS with Parkinsonism	MC, BS, SC, Extrapyramidal system	Tau (17q21)
ALS with Frontotemporal Dementia (FTD)	MC, BS, SC, Extrapyramidal system	9q21-22
Lathyrism	UMN	BOAA, Dietary cyanide (India)
Konzo	UMN	BOAA, Dietary cyanide (Central Africa)

**Table 1 Spectrum of Motor Neuron Diseases**

*The wide gamut of MND can vary in the CNS regions affected. The causative agents for some sporadic MND (ALS of Guam) or familial MND (SMA, SBMA) are known but most others remain idiopathic. CAG – codon for the amino acid, glutamine; BS – brainstem; SC – spinal cord; UMN - upper motor neurons; CST - corticospinal tract; LMN - lower motor neurons; MC - motor cortex; BOAA - [β-N-oxalylamino-L-alanine.*

## **1.6. Amyotrophic Lateral Sclerosis (ALS)**

Amyotrophic Lateral Sclerosis (ALS) is also known as *Maladie de Charcot* or Lou Gehrig's disease. Jean-Martin Charcot was the French neurologist who first coined the term in circa. 1874. He studied a case of muscle wasting ("amyotrophy") caused by the hardening of the lateral columns of the spinal cord due to gliosis of the corticospinal tracts ("lateral sclerosis"). The disease spread to the bulbar and spinal cord motor neurons [22, 23]. Thus the clinical aspects of both the gray matter and white matter were defined. Lou Gehrig was the famous New York Yankee baseball player who had earned the name "iron horse" (for his 2130 consecutive games) before succumbing to this rapidly progressive motor neuron disease. This latter reason is why the name Lou Gehrig's disease is more common to the general population in the United States.

ALS affects the corticomotoneuronal system, selectively the large pyramidal Betz cells in the motor cortex and motor neurons in brain stem and spinal cord. When voluntary muscles fail to receive impulses from the motor neurons, they weaken and waste away (atrophy) leading to spasticity [14, 31, 32]. The process of neuronal loss can induce proximal and distal axonopathy in related nerve fiber projections leading to a "dying back" degeneration [14, 33]. There are multiple forms of ALS, which will be discussed later, but the predominant form is sporadic (SALS). As discussed later, the lack of biomarkers and multifactorial nature of the disease have deterred early diagnosis and impeded discovery of effective treatments. Patients who suffer from this debilitating disease rely mainly on palliative care and sound clinical care management.

### **1.6.1. Epidemiology**

ALS affects persons regardless of race, creed or the socioeconomic stature. Geographically, there is no preference in the disease prevalence with a few regional exceptions. There is a high

prevalence of ALS and its variants (see section 1.3.5) in certain populations of the western Pacific islands (Guam and Rota), two areas of the Japanese Kii peninsula, off the western coast of Indonesia (Irian Jaya), and an isolated tribe in the gulf of Carpentaria (Northern Australia) [34, 35]. According the National Institute of Health, about 5000 new cases are diagnosed every year with a prevalence of approximately 1 in 13,600 individuals in the United States. Globally there is an incidence of 4-6 cases in every 100,000 people [32, 34, 36]. Statistically, the incidence rate might increase with improved understanding of disease mechanisms and better diagnostics but the prevalence should decrease which is the target for efficient health care specialists. Indeed studies have documented an increase in mortality rates, which could be due to an artifact of increased diagnosis of the disease [32, 36].

Although this disease can inflict anyone at anytime, typical disease onset ranges from 40 to 70 years with an average age of 55 years [31, 37]. With age the prevalence of ALS increases by an order of magnitude [38]. Also, depending on the age and site of onset, the rate of disease progression from diagnosis is rapid, ranging from 1-5 years with a median survival of about 3 years [32, 37]. Usually subjects with initial bulbar dysfunction will tend to have a more rapid disease progression and shorter survival than cases with limb onset. In familial cases, the average age at disease onset is about 45 years, about 10 years earlier than in sporadic cases and can sometimes have longer disease duration [39]. It is interesting to note that men are more likely to be affected by the MND than women (1.5 to 2:1) [31, 34]. However, this imbalance evens out with increasing age and post-menopause, suggesting the possible role of estrogens in disease initiation / progression [38, 40]. Indeed *in vitro* studies using rat spinal motor neurons have attributed a neuroprotective for estrogens from excitotoxic insults [41]. These population

parameters are important from the perspective of designing clinical trials and an unbiased interpretation of primary trial outcomes.

An interesting epidemiological study revealed the prevalence of ALS in young (aged 20-40 yrs) gulf war veterans [42-44]. The relatively young age for SALS with the patients having no familial history suggest that environmental exposures as a result of war could have triggered the disease pathogenesis in the genetically susceptible veterans. Warfare could induce undue increases in levels of chemical nerve agents (G-type compounds such as sarin) or heavy metals (such as Aluminum, depleted uranium, mercury) [42]. Such studies directly stress the importance of epidemiology and underscore the strong effects that the environment can have on the disease progression.

### **1.6.2. Clinical Features**

Due to the heterogeneity of the disease with respect to the site of onset (motor cortex / bulbar / spinal cord), direct and indirect symptoms for ALS can vary from one individual to another. Typically, one would experience asymmetric weakness of hands often manifesting itself by unusual and repeated dropping of objects, abnormal fatigue in the arms and difficulty performing motor tasks [31, 32]. The disease usually initiates unilaterally and then proceeds to become bilateral, making it difficult to perform simple tasks. If the disease affects the musculature of the lower limbs (25%) for instance, a simple task like walking will become difficult with a tendency to trip frequently. Bulbar (brainstem) involvement (25%) is characterized by difficulty in chewing, swallowing (dysphagia), coughing and speech (dysarthria). A clinical examination would reveal other symptoms such as drooping of the palate, a depressed gag reflex, pooling of saliva, tongue atrophy and muscle twitches. The patient is

commonly paralyzed in a few years from diagnosis. Eventually the diaphragm and respiratory muscles are afflicted which leads to death from an inability to breathe (dysapnea). Most often, patients in their end-stage have to be on an artificial respirator.

It is however very interesting to note that patients do not lose their ability to sense things. In addition, the patient's ocular muscles, bladder function and erectile function remain unaffected. Unlike in AD, cognition is typically unaffected. About 50% of the patients present with pseudobulbar characteristics such as pathological laughing or crying.

### **1.6.3. Diagnosis**

The World Federation of Neurology has established widely accepted criteria for the diagnosis of ALS [45, 46]. The El Escorial criteria depend on the level of certainty of the diagnosis that can vary from definite ALS to suspected ALS. There is no simple and rapid diagnostic test available for ALS. Routine clinical laboratory tests are obtained to exclude diseases that can mimic ALS. Such tests include a complete blood count and chemical analysis, thyroid function tests, serum protein electrophoresis, creatine kinase levels, erythrocyte sedimentation rate, antinuclear antibody, rheumatoid factor and when clinically indicated, hexosaminidase A and paraneoplastic antibodies [47-49]. Some of these tests however are performed to eliminate other disorders such as thyroid-related rather than to diagnose ALS. Anti-GM1 ganglioside antibody testing was considered a possible diagnostic tool, but it was soon found to yield false positives. Low titers of serum anti-GM1 antibodies are often found in the normal population and too rarely in significantly elevated amounts in ALS patients, making it impractical to use it for diagnostics [47, 50-52].

Electrophysiological tests are also conducted with repetitive stimulation and electromyography (EMG) to confirm LMN disorders and exclude disorders of the neuromuscular junction and peripheral nerves [53-56]. Findings of EMG indicative of denervation include fibrillations, positive sharp waves and complex repetitive discharge. Simultaneously reduced numbers and increased amplitude of motor unit potentials indicate reinnervations [53]. Neurologists also use muscle biopsies and neuroimaging techniques such as magnetic resonance imaging (MRI) and computed tomography (CT) scans to establish a profile when diagnosing ALS [32, 33, 57, 58]. Frequently, MRI scans of the brain or spine help to rule out tumors or degenerative spine disease [33, 59]. Muscle biopsies, though usually not required, typically show grouped atrophy consisting of shrunken and angulated muscle fibers amidst groups of uniform fiber types [60, 61]. Such detailed clinical analyses help in eliminating the possibilities of other neurological disorders.

There is a chance for misdiagnosis in about 15% of cases and post-mortem neuropathologic examination can confirm the clinical diagnosis of ALS [62-64]. Misdiagnosis include a wide array of diagnoses such as cervical spondylosis, monomelic amyotrophy of upper extremities, inflammatory neuropathy, myopathy, multiple sclerosis, parkinsonism, arsenical myopathy and lumbar spinal stenosis [47, 63, 65]. Other MND including Kennedy's disease or SBMA, PLS, PMA, PBP and multifocal motor neuropathy with conduction block (an autoimmune disorder that is responsive to immunosuppressive therapy) can be misdiagnosed as ALS. ALS diagnosis requires the presence of UMN degeneration by clinical examination, LMN degeneration by clinical, electrophysiological and neuropathological examinations and progressive spread of symptoms along with the absence of electrophysiological and neuroimaging evidence of other diseases or syndromes [31, 46].

#### 1.6.4. Neuropathology

At the gross level, unlike an AD brain, which atrophies, the brain in an ALS patient typically appears normal in spite of some amount of atrophy in the pre-central gyrus as evident in post-mortem analysis. There is however no apparent reduction in size and weight. However, it is common to observe marked atrophy all along the spinal cord and in the anterior roots (Fig 7A). There is also corticospinal tract pallor in myelin stains indicative of axonal loss [32, 66-68] (Fig 7B). Microscopically, ALS manifests itself by a reduction in the number and size of the upper and lower motor neurons including the motor nuclei in the brain stem. The disease is classically associated with astrogliosis and microgliosis (increased proliferation and activation of astrocytes and microglia, respectively) [69-71].

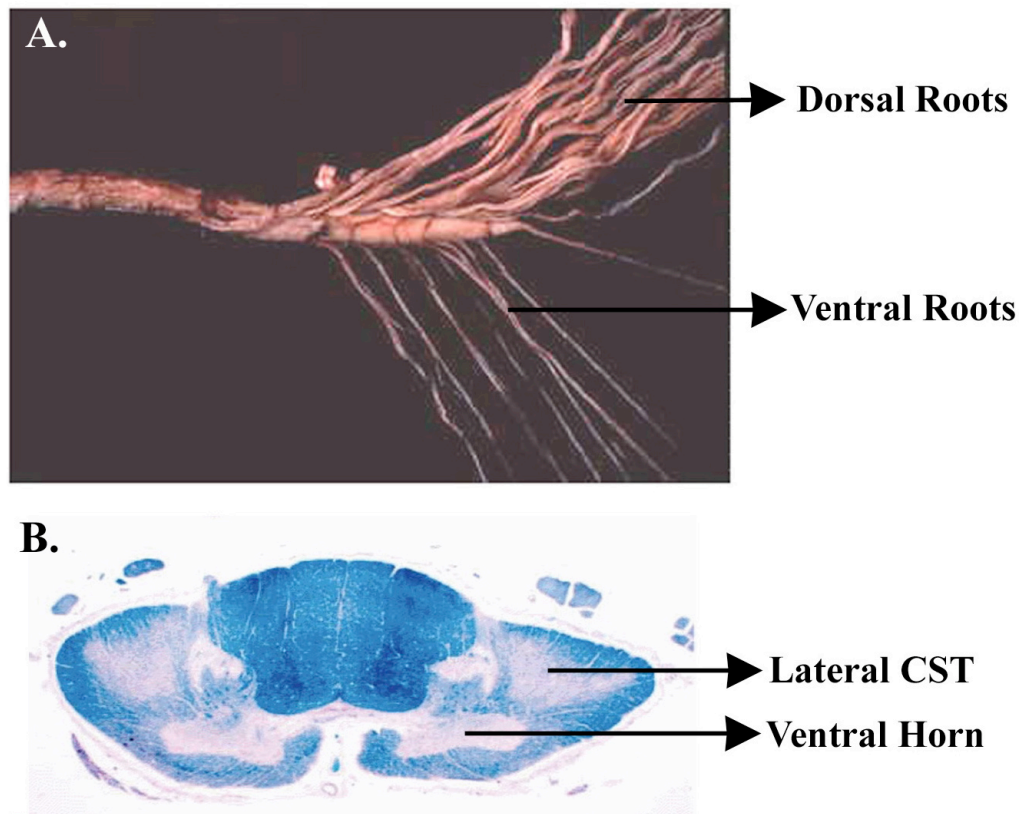


**Figure 7 Spinal Degeneration in ALS**

The pathological hallmark of an individual with ALS is atrophy along the spinal cord the axons due to loss of the LMN. Panel A shows distinct atrophy of the ventral roots that traverse from the LMN. Compare it to the healthy looking dorsal roots that arise from the sensory neurons, which remain unaffected during the disease process. Panel B is transverse section stained with Kluver-Berarra stain clearly indicating the pallor in the lateral corticospinal tract and the ventral horn again due to the selective degeneration of the motor neurons and the fibers that lead into and out of them.

(B) Modified from *Brain Pathol.* 13(1):10

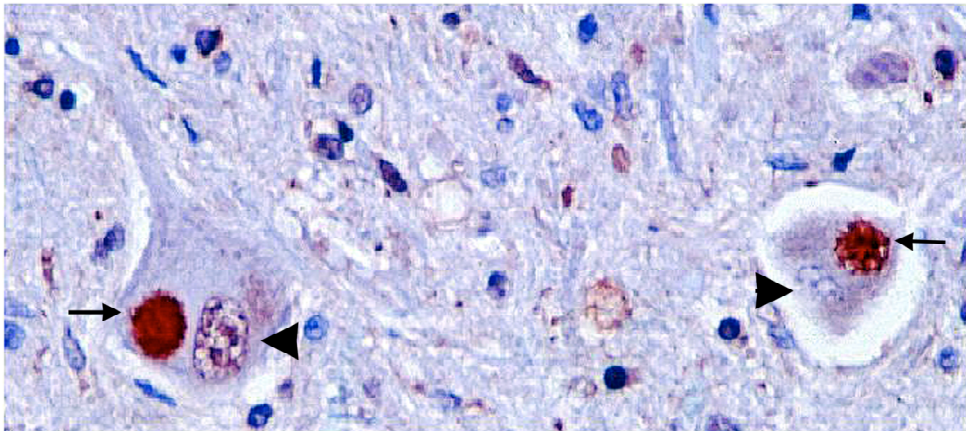


**Figure 8 Ubiquitin Positive Inclusion Bodies in Lower Motor Neurons**

Paraffin embedded section from human ALS spinal cord was immunostained for ubiquitin by 3-amino-9-ethylcarbazole (AEC) followed by counterstaining with hematoxylin. The motor neuron on the left with a process and another with somatodendritic attrition (on the right) reveal dark brown ubiquitin positive intranuclear aggregates (arrows). The arrowheads indicate the nuclei.

A number of cytoplasmic inclusions or protein aggregates are often found in affected neurons during ALS. Bunina bodies are small, round eosinophilic neuronal cytoplasmic inclusions and hyaline inclusions have been described in both upper and lower motor neurons.

These inclusions sometimes stain positive for ubiquitin and/or cystatin C, a small cysteine proteinase inhibitor [67, 68, 72-74] (Fig 8).

In addition, neurofilamentous swellings (spheroids) have been identified in ALS motor neuron bodies and proximal axons [75, 76]. This suggests an involvement of neurofilament, an intermediate cytoskeletal protein, in ALS pathogenesis. Lewy bodies are eosinophilic and found in the cytoplasm of cortical and brain stem neurons in Parkinson's disease (PD), some forms of dementia and occasionally ALS [77-79]. In PD, they are abundantly immunoreactive to 3 proteins:  $\alpha$ -synuclein, neurofilament and ubiquitin. However, the MND inclusions in ALS associated with parkinsonism are negative for  $\alpha$ -synuclein and tau [80-82]. Ubiquitin positive intraneuronal MND inclusions are observed in both the cytoplasm and nucleus of affected neurons and may be correlated to cognitive abnormalities in ALS patients referred to as ALS-Dementia or ALS-D [80, 82]. The neuronal Lewy body-like hyaline inclusion (LBHI) is a characteristic neuropathological marker of mutant SOD1-linked FALS with posterior column involvement (FALS-PCI) [83]. These SOD1 positive inclusions similar to the neuronal LBHIs have been discovered in astrocytes in certain patients with FALS exhibiting SOD1 gene mutations [83]. Thus the presence of protein aggregates during ALS in regions not pertaining to the motor system suggests variants of the disease to be more widespread and may be defined as being a multi-system disease.

#### **1.6.5. “ALS –Plus”: A Multisystem Disorder?**

According to El Escorial criteria, any rare combination of ALS with extra-motor neurological disorders such as dementia or “parkinsonism” is termed as “ALS-plus” [84]. Parkinsonism is a term used to describe symptoms as seen in PD, such as rigidity, loss of

balance, certain tremors or bent postures. In general ALS affects the populous independent of race or geographical location barring one exception. It occurs with higher than expected frequency among the indigenous population (Chamorros) on the Marianas Islands of Guam, where this disorder is very commonly associated with parkinsonism and dementia [35, 82, 85, 86]. This discovery led to the coining of the ALS variant ALS-Parkinsonism Dementia Complex (ALS-PDC). The incidence and prevalence of the Guam ALS-PDC has been estimated to be an order of magnitude higher than the worldwide average for ALS. It was recognized subsequently in two villages in the Kii Peninsula of Japan and among the Auyu and Jakai people of Irian Jaya (Western New Guinea), resulting in a total of three Western Pacific variants of ALS [35, 87].

Neuropathological analysis of ALS-PDC revealed fronto-temporal atrophy of the cortex associated with neuronal loss. Hyperphosphorylated tau protein, a microtubule-associated cytoskeletal protein, forms neurofibrillary tangles (NFTs). These are aberrations commonly associated with AD. However, these are also observed in ALS-PDC of both Guam and Kii peninsula [87, 88]. The phosphorylated epitopes are identical to those evident in AD [87]. However this variant of ALS differs from AD in that it lacks senile plaques, the NFTs are present in layers II and III as opposed to V and VI in AD, and these cytoskeletal abnormalities are observed in basal ganglia and brain stem in addition to neocortex and hippocampus [87]. These studies indeed suggest that the neurodegenerative process in ALS may provide us with more variants involving extra-motor neuronal system or the extra-pyramidal system, including the fronto-temporal region of the cortex, basal ganglia and the limbic system. The FTD-ALS patients whose behavioral deficits (similar to AD or Pick's disease) precede the MND symptoms exhibit behavioral and cognitive deficits such as emotional disinhibition, impairment of cognition and judgement, memory loss, reduced capacity for social conduct and behavior, personality change

amongst others [89]. Microscopically, ALS-FTD is defined by the presence of intraneuronal ubiquitin positive inclusion bodies in the fronto-temporal lobes. Thus ALS is growing from one that was restricted to the motor nuclei to a spectrum of ALS with variants that involve extra-motor systems.

#### **1.6.6. Genetics of ALS**

The etiology of about 5-10% of the ALS patients is considered to be genetic and these comprise both recessive and dominant inheritance patterns. Mutations in genes encoding for cytoplasmic Cu/Zn superoxide dismutase (SOD1), Alsin (ALS2), the 150kD subunit of dynactin (DCTN1) and Senataxin gene (ALS4) have been identified and have a direct effect on motor neuron degeneration [90-95].

Genetic studies in families with ALS revealed autosomal dominant mutations in the gene encoding SOD1 located on chromosome 21q22.1 [90]. Approximately 20% of familial disease (FALS) has been linked to 113 (100 substitutions, 4 deletions, 3 insertions, 5 polymorphisms and 1 compound) different mutations in the gene encoding SOD1. This major breakthrough in 1993 has enabled researchers to develop in vitro and transgenic experimental models to further dissect the molecular pathogenesis of ALS. This ubiquitously expressed 153-amino acid protein acts as a homodimer in scavenging and converting superoxide radicals into hydrogen peroxide, which is then converted to water by the action of catalase or glutathione peroxidase (Fig 9 A & B).

It remains unclear as to how and why this mutant protein causes selective motor neuron degeneration in spite of its ubiquitous expression. A number of these mutations result in loss of the dismutase activity to a variable degree [96-99]. Some mutations such as the G93A and D90A

result in ALS without any or negligible loss in enzymatic activity [97, 100, 101]. Furthermore, it was demonstrated that SOD1<sup>-/-</sup> mice were normal with no motor deficits and mice over-expressing mutant SOD1 protein developed MND with overt ALS-like symptoms, despite normal or elevated levels of the dismutase activity [102, 103]. These findings reveal that the SOD1 mutations do not result in a loss of function or enzymatic activity but due to “gain of a novel toxic function”. Studies with these mice have greatly helped in making inroads into the understanding of disease mechanisms and development of therapeutic strategies.

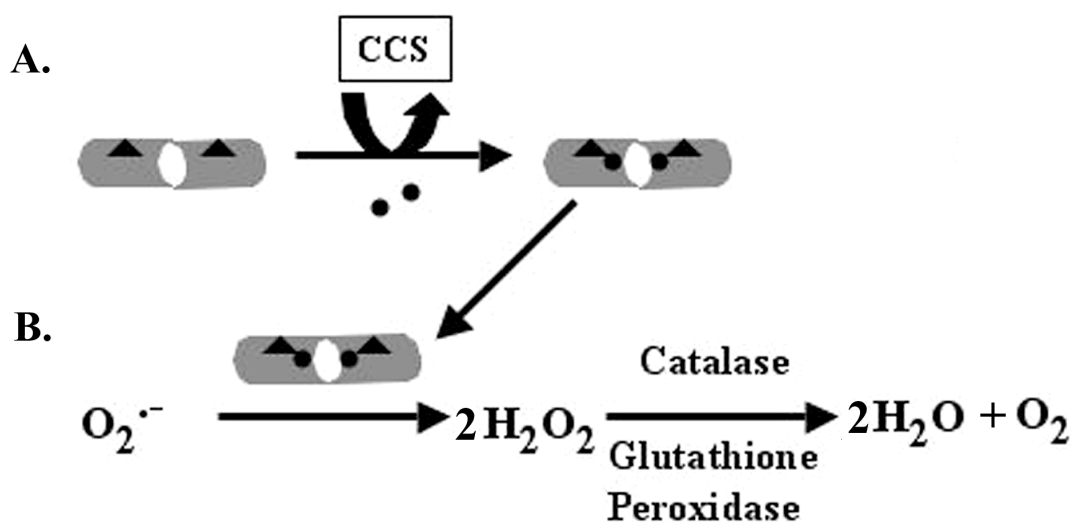


**Figure 9** Normal Function for Cu/Zn cytoplasmic SOD – A schema

*The copper chaperone for SOD1 (CCS) is a protein necessary to load copper ions (A; black circles) into the catalytic site for normal dismutase function of SOD1 (B). Zinc ions are represented by black triangles.*

Genetic studies have revealed a variation in disease progression, dependent on the mutation causing the disease. Patients with the most common form of the mutation, A4V have rapid progression with reduced survival (1.5 years) [104]. There are other mutations (E21G, G37R, H46R, D90A, G93C, I104F, I151T) that are slower in their progression with patients

exhibiting longer survival times (10 years or longer). The G37R and L38V mutations predicted an earlier age at onset. Such variations in part might be due to differential effects of these mutations on the newly acquired cytotoxic function of SOD1.

In addition to SOD1, other genes have been implicated in adult and juvenile FALS variants. Even though the majority of the inheritance is autosomal dominant, recessive and X-linked variants have been reported [32]. Two loci for a juvenile form of autosomal recessive cases (Juvenile onset AR-FALS) have been identified, on chromosome 2q33-q35 and on chromosome 15q15-21 [105, 106]. The disease-causing gene on chromosome 2q33-q35 has been identified to be ALSIN / ALS2 [91, 107]. These FALS cases have been predominantly reported in populations of North Africa and the Middle East. Disease onset in these cases is prior to 25 years of age and they also have a slower disease progression. ALSIN has a full-length 184 kD protein comprising 1657 amino acids as well as a smaller alternatively spliced variant with 396 amino acids (44 kD). Tunisian families with a severe disease phenotype have exhibited single-base pair (bp) deletions in exon 3 and patients with a milder form of ALS have deletions in exons 5 and 9. ALSIN contains multiple motifs with homology in the N-terminus to the regulator of chromosome condensation (RCC1), guanine exchange factor (GEF) domains (activating GTPases), pleckstrin domain (potential membrane attachment), two membrane occupation and recognition motifs (MORN). RCC1 acts on RAN, a protein involved in nuclear export and import. The C-terminus of ALSIN includes a vacuolar protein sorting-9 (VSP9) domain. Thus ALSIN might have a role in a variety of critical cellular functions such as signaling, membrane transport, modulating cytoskeletal assembly, and nuclear transport [91, 107, 108]. All of these important cellular functions are dysregulated during ALS. However, recent experiments with ALSIN transgenics have failed to mimic ALS. In spite of this being a setback, it probably points

to other modifying factors that might act in concert with ALSIN in causing the juvenile form of AR-FALS. Another gene associated with a rare form of juvenile-onset form of ALS has recently been identified to be senataxin [94, 109, 110]. Mutations in this gene lead to slower progression and longer life span than normal ALS. This study involved four unrelated families with members affected with the slowly progressing MND with minimal or no sensory nerve damage. Abnormalities in this protein are hypothesized to cause RNA processing defects, a defect that causes other MND such as SMA.

Other genetic alterations have been identified in FALS cases. Although a dominant form of ALS has been linked to chromosome Xp11-q12, the disease-causing gene is yet to be reported. Amyotrophy has been observed in cases with autosomal dominant mutations in the tau gene on chromosome 17q21-22 that are associated with frontotemporal dementia (FTD) and parkinsonism. These reports have been supported by the identification of ALS cases with involvement of the extra-pyramidal pathway and also by the observations that transgenics with mutated tau gene develop motor axonopathy and amyotrophy [111]. Additionally, a novel locus for autosomal dominant ALS has been identified at 18q21 [112].

In addition to these rare forms of FALS, a genetic basis for the occurrence of SALS has been implicated. In 5 unrelated SALS patients, rare heterozygous mutations (1%) in the heavy subunit of neurofilaments (NF-H) have been identified [113, 114]. The KSP repeat domains in the C-terminal region of the protein, where these mutations are localized, are important for NF assembly, crosslinking and phosphorylation. Recently other genes have been identified as modifiers such as the one encoding vascular endothelial growth factor (VEGF) implicating it as a risk factor for the disease. Animal studies involving G93A SOD1 transgenics have indicated levels of VEGF to directly correlate to the disease state [115]. In recent studies involving the

delivery of VEGF using a lentiviral system, disease onset was delayed with increased survival [116, 117]. There are other genes considered to be risk factors for SALS including those encoding apolipoprotein allele  $\epsilon 4$  (apo $\epsilon 4$ ), survivor of motor neuron (SMN), neuronal apoptosis inhibitory protein (NAIP) and leukocyte inhibitory factor (LIF) [34]. However, given the genetic heterogeneity of ALS, it is important to identify other candidate / modifier genes that might act with the environment or lifestyle of individuals.

Mechanistically, it remains unknown as to if motor neurons are affected by all these mutations through a common trigger. It is possible that protein aggregation (impairing protein or organelle transport), mitochondrial dysfunction (altering cellular energetics) and alteration at the nucleus may act as common trigger points for selective motor neuron death during ALS.

#### **1.6.7. Pathogenic Mechanisms of SALS**

ALS is a progressive neurodegenerative disorder involving both the UMN and LMN. Since 90-95% of ALS cases are sporadic, it is essential to understand factors implicated in its pathogenesis. Potential molecular mechanisms include oxidative stress, excitotoxicity, mitochondrial dysfunction, abnormalities in the cytoskeleton and proteasomal machinery, autoimmunity, and DNA damage [118] (Fig 10). One common mechanism leading to neuronal death in ALS is through apoptosis mediated by altered gene expression of both pro- / anti-apoptotic genes and cell cycle genes [119-122].

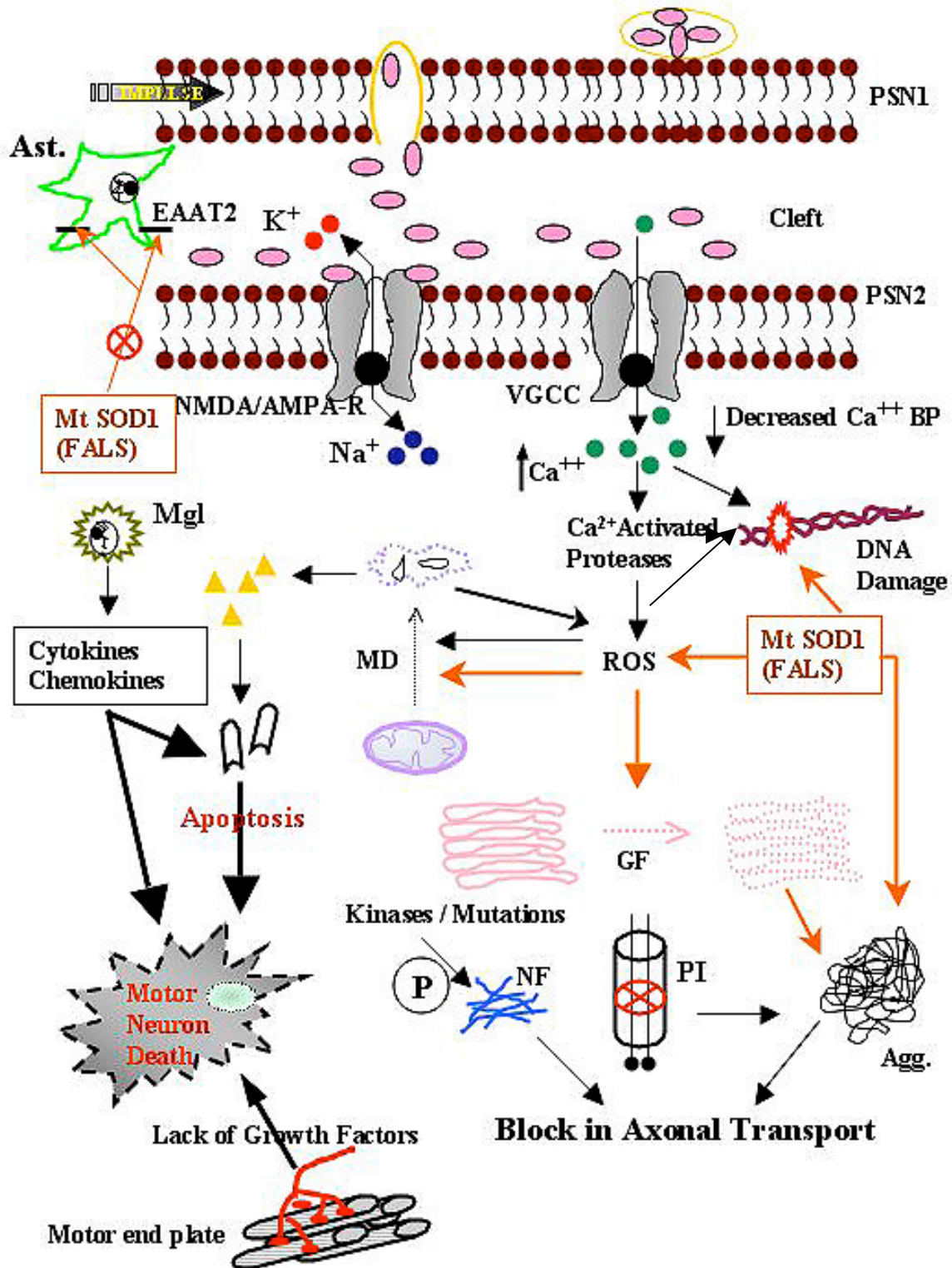


Figure 10 ALS Pathogenesis: Do all roads lead to motor neuron death ?

The pre-synaptic neuron membrane (PSN1) that transmits an impulse and the de-polarized post-synaptic membrane (PSN2) are schematically represented by the lipid bilayer (brown circles with hydrophobic tails). The membrane potential of the PSN2 is maintained by  $K^+$  (red circles) and  $Na^+$  (blue circles) channels. Glutamate (pink ovals) is released from the PSN1 vesicles serve as ligands for the NMDA/AMPA glutamate receptors. In ALS, mutations in SOD1 or other sporadic agents can cause alterations in the astrocytic (Ast.) glutamate transporters (EAAT2) resulting in inefficient re-uptake of glutamate. The excess glutamate in the cleft (excitotoxicity) due to decreased re-uptake and decreased amounts of  $Ca^{2+}$  binding proteins in the MN results in an increased influx of  $Ca^{2+}$  (green circles) through the voltage-gated  $Ca^{2+}$  channels (VGCC). This increase in intracellular  $Ca^{2+}$  can activate proteases with a concomitant generation of reactive oxygen species (ROS). Mutant SOD1 (mtSOD1) can also result in ROS and oxidative stress. Both excitotoxicity induced oxidative injury and direct oxidative stress can result in DNA damage. ROS via mtSOD1 causes mitochondrial vacuolation and dysfunction (MD), which in turn can account for increased ROS. MD results in cytochrome c release (orange triangles) and a caspase-dependent apoptosis of MN. In addition to mitochondrial vacuolation, mtSOD1 also results in the fragmentation of the golgi cisternae (pink stacks / GF). GF, endoplasmic reticular stress / reduced chaperone proteins (not shown), inhibition of the proteosomal machinery (cylinder / PI) and mutations / hyperphosphorylation of neurofilaments can all lead to improper protein folding and aggregate formation (Agg.). protein aggregates can block axonal transport with consequent damaging effects on the MN. MN can also be affected by decreased trophic factor support from the target muscle fibers. In addition, bystander effects via the release of cytokines and chemokines by activated microglia (Mgl.) can directly or indirectly through death receptor-mediated death cascades effect MND.

### 1.6.7.1. Oxidative Stress and SOD1-mediated toxicity

Several findings point to oxidative stress as one mediator of motor neuron injury. Due to a motor neuron's high-energy demands, these large cells with long axonal processes may be subjected to a higher degree of metabolic stress.  $\text{Cu}^{++}/\text{Zn}^{++}$  superoxide dismutase 1 is an abundant and ubiquitously expressed protein that normally scavenges free radicals thus reducing oxidative damage. As discussed above, mutations in SOD1 induce an adverse gain of cytotoxic function by the mutant protein. Over-expression (up to 6-fold) of wild type human SOD1 in G85R mice failed to affect disease onset, progression or pathology [123]. This and other studies (enumerated in section 1.3.6) led to the "gain of toxic function" hypothesis that these dominant mutations confer wherein disease is caused due to one or more aberrant properties of the mutant subunits[124]. The hypothesized mechanisms for SOD1-mediated toxicity include: i) conformational changes and zinc-deficient SOD1 that could enable peroxide or peroxynitrite to act as aberrant substrates resulting in increased free radicals, ii) Ineffective buffering of  $\text{Cu}^{++}$  resulting in increased copper-mediated toxicity, iii) aberrant SOD1 protein aggregation [37, 125]. Common to all SOD1 transgenic models of ALS, the downstream effects include the execution of caspase-mediated apoptotic cell death [125-128].

Mutant SOD1 accumulate in conditions of low  $\text{Zn}^{++}$  levels and have a lower affinity for  $\text{Zn}^{++}$  mainly due to the weakening of the backbone of SOD1 resulting in increased levels of superoxide [129, 130](Fig 11A). There are mutations such as L67R found in the Zn-binding loop of SOD1 [131]. Such substitutions of large amino acid with a positively charged amino acid can alter the conformation of the protein and open it for aberrant reactions with toxic substrates. Another line of investigation has pertained to metallothioneins (MT), the expression of which is elevated in the spinal cord of ALS patients and transgenic mice [132, 133]. While the expression

patterns of two of the isoforms (MT-I and MT-II) are glial, MT-III is expressed neuronally. The SOD1 G93A mice that are deficient in all three isoforms develop disease consistent with zinc depletion as a factor in SOD1-mediated toxicity [133, 134]. Production of superoxide that can react quickly with nitric oxide (NO) can result in peroxynitrite (ONOO<sup>-</sup>), which can then impair tyrosine receptors of growth factors by nitrosylating them or inhibit parts of the mitochondrial transport chain (Fig 11B). It has been reported that peroxynitrite treatment of astrocytes caused changes to their phenotype and activated them analogous to astrogliosis that is prevalent in ALS patients [135, 136]. When embryonic motor neurons were grown on top of these activated astrocytes, it resulted in apoptosis of the neurons, which was subsequently blocked by using inhibitors to inducible form of nitric oxide synthase (iNOS) or by using peroxynitrite scavengers [136]. In addition, in transgenics and human ALS spinal cord, there is an increase in free nitrotyrosine but no increase in protein-bound nitrotyrosine [137, 138]. However, there are conflicting reports to question the credence of a central role for peroxynitrite-mediated SOD1 toxicity. Levels of free nitro-tyrosine have not been found in ALS patients and in another study when wild type human SOD1 was over-expressed in G85R mice, it did not alleviate toxicity but actually exacerbated the disease state. Another aberrant substrate used by superoxides is hydrogen peroxide resulting in a very toxic hydroxyl radical (Fig 11C). Protein carbonyl formation and lipid peroxidation are significantly increased in the spinal cord in patients with SALS and SOD1 transgenics, respectively [139]. In addition oxidative damage to DNA have been demonstrated by immunocytochemical and biochemical assays [140]. These results strongly suggest that SOD1-mediated toxicity does not strongly depend on superoxides reacting with substrates such as peroxynitrite or hydrogen peroxide.

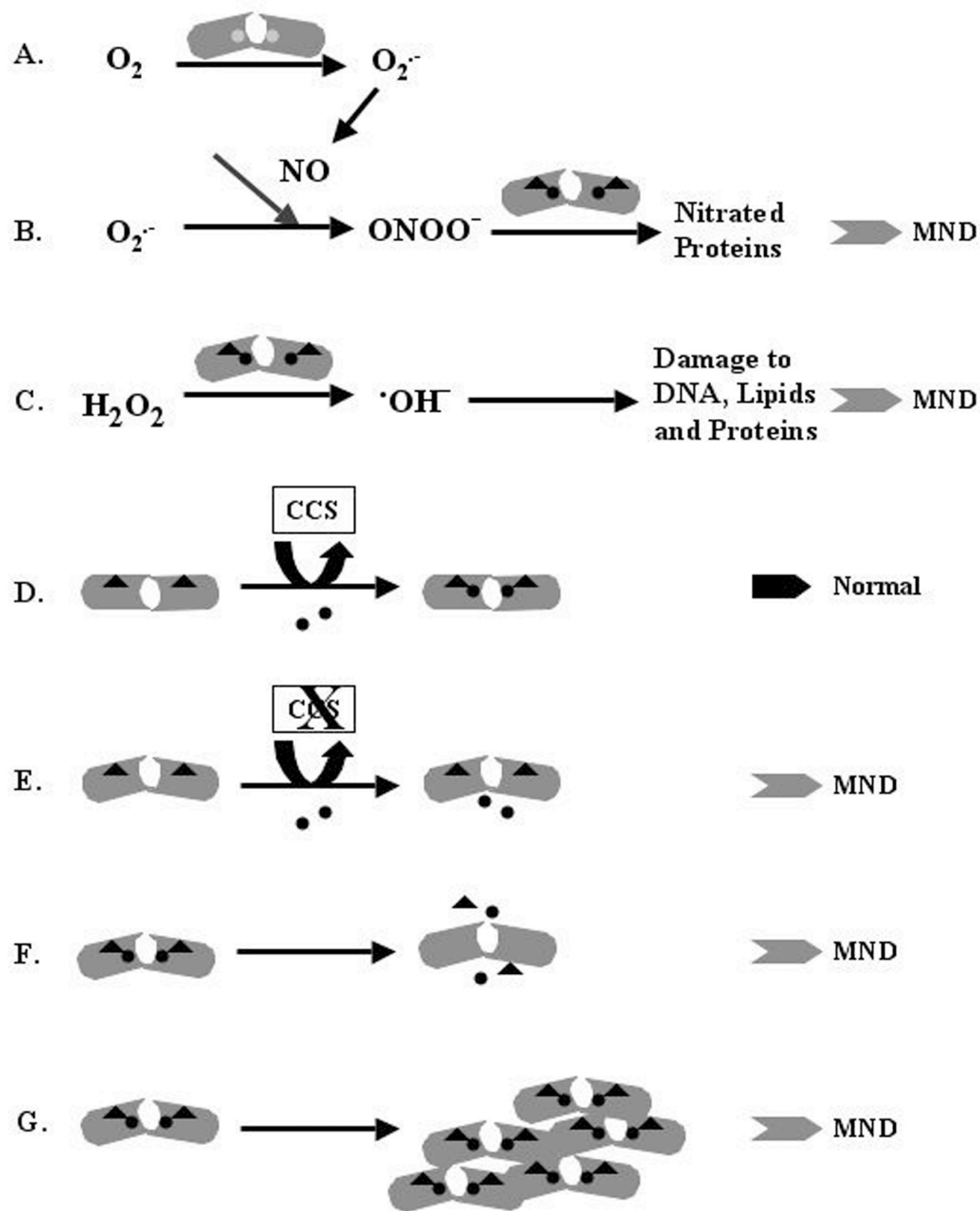


**Figure 11 Hypothesized Mechanisms for the “Gain of Toxic Function” in Mt SOD1**

(A) Zn-deficient (lack of black triangles) SOD1 rapidly results in reduced form of the protein that can subsequently react with oxygen to increase levels of superoxide. Also, NF can act as sink for binding Zn leading to increased Zn-deficient SOD1.

(B) *“Peroxynitrite hypothesis” relates to the generation of peroxynitrite (ONOO<sup>-</sup>), a highly reactive free radical formed through the reaction of superoxide with the highly diffusible small molecule, NO. ONOO<sup>-</sup> can then act as an aberrant substrate for mtSOD1 resulting in nitration of proteins such as tyrosine receptors.*

(C) *“Peroxidase hypothesis” suggests that hydrogen peroxide could act as an aberrant substrate for the mutant form of the protein generating very toxic and highly reactive hydroxyl radicals. These free radicals can cause oxidative damage to DNA, lipids and proteins.*

(D) *Copper chaperone for SOD1 is required for proper loading of copper onto the catalytic site of the protein.*

(E) *Crossbreeding studies using CCS knock-out (inefficient copper loading) and 3 mutant SOD1 transgenics failed to alleviate the motor neuron pathology.*

(F) *Mutant SOD1 might not bind copper and zinc tightly thus leading to free metal toxicity. Free copper might catalyze harmful reactions resulting in cellular damage.*

(G) *Mutant SOD1 may elevate the propensity to protein misfolding and hence aggregate formation. Aggregates could either play a role in enhancing the disease pathology or alternatively be protective.*

Copper chaperone for SOD1 (CCS) is a carrier protein that aids in incorporating copper into the catalytic site of SOD1 (Fig 11D). The copper ion but not zinc is important for the electron transfers that direct SOD1-mediated oxidative reactions. The production of both the toxic hydroxyl free radical and peroxynitrite depends on the proper binding of copper to SOD1. Amongst the four histidine residues involved in Cu-binding, two of them are mutated in ALS (H46R, H48R/H48Q). The levels of copper incorporation and SOD1 activity in CCS<sup>-/-</sup> mice are greatly reduced but the mice are viable [141] (Fig 11E). The CCS<sup>-/-</sup> / SOD1 mutant mice (G93A,

G37R and G85R) did not exhibit any change in protein levels of SOD1 and motor neurons were affected much like in SOD1 mutant mice [141]. Strikingly, the CCS<sup>-/-</sup> / SOD1 mutant mice exhibited no change in disease onset and progression. They also exhibited neuropathology similar to those observed in the SOD1 mutant mice. Thus this study negates a role for copper in SOD1-mediated toxicity.

However, the research group did not consider key issues. Low levels of free residual copper or its incomplete incorporation into SOD1 may not be sufficient for its complete enzymatic activity but may be enough to cause pathogenic oxidative mechanisms resulting in free copper mediated-toxicity (Fig 11F). This might explain the lack of amelioration of the disease phenotype in their study. In fact copper chelators that bind free copper alleviates the disease process in *in vitro* studies increasing motor neuron survival and enhancing neurite outgrowth [142]. In conclusion, although there is evidence against copper mediated toxicity, it cannot be excluded.

Furthermore, structural changes in SOD1 due to mutations can result in aberrant aggregates (Fig 11G). Aggregation is common to neurodegenerative diseases such as AD, PD, and a spectrum of polyglutamine diseases [143, 144]. In fact, SOD1 transgenics do exhibit aggregates that stain positive for SOD1, ubiquitin and neurofilaments. However, the mechanism by which aggregation can damage motor neurons is unknown. The recruitment of other proteins by the aggregates could lead to a loss of function such as those of transcription factors and chaperone proteins. It is documented that the proteasomal machinery and axonal transport systems are dysfunctional during ALS and this might also be the case in the SOD1 transgenics leading to aggregation [145, 146].

### 1.6.7.2. Excitotoxicity

Glutamate-mediated excitotoxicity represents another potential mechanism of neurodegeneration in ALS. Glutamate is derived from the reductive deamination of  $\alpha$ -ketoglutarate by glutamate dehydrogenase (GDH) or through the action of aminotransferases on amino acids [147]. In a normal state, glutamate is released from the pre-synaptic terminals upon depolarization, crosses the cleft and activates the post-synaptic neuron via the glutamate receptors. These receptors can either be ionotropic (N-methyl-D-aspartate (NMDA),  $\alpha$ -amino-3-hydroxy-5-methyl-4-isoxazole propionic acid (AMPA) and Kainate) or metabotropic (mGluR1-8). Amongst the major glutamatergic pathways are the corticobulbar and corticospinal tracts innervating the motor neurons. The primary mechanism for the inactivation of glutamate is simply its removal from extracellular space via a  $\text{Na}^+ / \text{K}^+$ -dependent transport system in astrocytes (EAAT1/GLAST and EAAT2/GLT-1) and neurons (EAAT3/EAAC1, EAAT4 and EAAT5).

Over-activation of synaptic glutamate receptors can lead to increased intracellular calcium ( $\text{Ca}^{++}$ ) resulting in oxidative stress-mediated synapse degeneration and cell death [148]. In addition to primary excitotoxicity such as in acute neurodegenerative diseases, secondary forms of glutamate toxicity can result in chronic forms of neuronal death. This occurs for instance through a drop in the energy levels of neurons resulting in a loss of membrane potential and activation of NMDA receptors.

Several lines of data support the excitotoxicity hypothesis in ALS. There is an increased concentration of glutamate and aspartate in CSF of ALS patients [149]. In organotypic spinal slices, neuronal toxicity by chronic levels of glutamate was selectively prevented by non-NMDA glutamate receptor antagonists and glutamate synthesis or release inhibitors, but not by NMDA

receptor antagonists [150]. The GluR2 subunits of pentameric AMPA receptors are normally calcium impermeable. In ALS motor neurons, the mRNA and protein levels of these subunits have been shown to be reduced resulting in increased calcium permeability [151, 152]. Increased levels of intracellular calcium are exacerbated by the relative lack of calcium buffering proteins such as calbindin, calretinin and parvalbumin leading to elevated levels of intracellular calcium [153, 154]. Additionally, RT-PCR studies of the disease-specific tissues, revealed two aberrant mRNA species of EAAT2, one that retains the 7th intron resulting in a truncated protein and another with exon-9 skipping [155]. This led to the speculation that aberrant mRNAs were the cause of the earlier reports of decreased expression of EAAT2 in ALS [156, 157]. Furthermore, EAAT2 knockout and knockdown mice have motor neuron degeneration. EAAT2 expression is also decreased in SOD-1 mice suggesting a link between oxidative damage to EAAT-2 and subsequent glutamate accumulation thus increasing susceptibility to excitotoxicity. The idea of aberrant splicing mechanisms of EAAT2 however has since been challenged because it has not been reproduced efficiently and also found to be a mechanism not exclusive to ALS [158-160].

In addition to these, environmental toxins such as b-N-oxalyl-amino-L-alanine (BOAA) (in chickling peas) and b-N-methylamino-L-alanine (BMAA) (in the seed of false sago palm) can cause only motor or sensorimotor pathology such as lathyrism and ALS-PDC (see section 1.3.5). Further the finding that Riluzole, a FDA approved drug that is the only current therapy diminishes pre-synaptic glutamate release provides added support to this theory. There seems to be a strong interplay between excitotoxicity, oxidative stress mechanisms and lack of mitochondrial efficacy all of which can result in increased levels of intracellular calcium. This is not only seen in ALS but also in many other neurodegenerative diseases.

### **1.6.7.3. Mitochondrial dysfunction**

In an elegant study using low copy G93A mutant mice, behavioral and muscle strength assays delineated four stages during disease progression – pre-muscle weakness (PMW), rapid decline of muscle strength (RD), slow decline (SD) and paralysis (Para) or end-stage [161]. The rapid decline stage was considered as the time of disease onset, which correlated to pathological changes without any death of motor neurons. The chief pathological change at the RD stage was mitochondrial vacuolation with a concomitant loss in muscle strength [161]. Another study also reported mitochondria to form vacuoles in a transgenic mouse model [162]. Electron microscopic studies have further demonstrated a process of inter-membrane space expansion (MWISE) resulting in these vacuoles and that these vacuoles contain peroxisomes in addition to SOD1 aggregates but not lysosomal proteins discounting a mechanism of autophagy [163].

Another group has recently corroborated prior ideas that mutant SOD1 is recruited specifically to the spinal cord mitochondria through the action of spinal cord specific factors [164]. Dysfunctional mitochondria can lead to improper release of pro-death molecules causing apoptotic death. It is interesting to note that mutations in the mitochondrial isoform of SOD (Mn<sup>++</sup> SOD or SOD2) do not have any effect on motor neurons but the overexpression of SOD2 in the transgenic line over-expressing G37R mutant SOD1 blocks motor neuron death [165]. These studies place mitochondria, which is present in close proximity to another calcium store (endoplasmic reticulum) in a central position to ALS pathogenesis.

### **1.6.7.4. Cytoskeletal Abnormalities**

Proper retention of neuronal energy status (mitochondria) and morphology along with the function of protein transport (cytoskeletal proteins) seem to be important in many

neurodegenerative diseases such as AD, PD, ALS and HD [166, 167]. Given that the axons of motor neurons extend a long distance, it is imperative for the structural integrity of the neuron and axon to be retained for efficient protein transport. Cellular protein and organelle trafficking depends on the integrity of endoplasmic reticulum (ER) and the golgi complex. Immunocytochemical evidence from human autopsy studies and ALS transgenics point towards an increase in fragmentation of golgi apparatus much like seen during the depolymerization of microtubules [168-171]. In the transgenic mouse model, golgi fragmentation was identified two months before onset of paralysis placing the event as an early mediator of ALS [172].

Another cytoskeletal protein abnormality that has led to many transgenic studies is the intermediate heteropolymers that are specific to neurons localized in axons and plays an important role in axonal transport. Neurofilaments (NF) are comprised of the light (NF-L), medium (NF-M) and high (NF-H) molecular weight subunits. The frequent neurofilamentous aggregates that co-localize with nitrotyrosine and SOD1 in different models of the disease have implicated these major intermediate filaments in ALS pathogenesis [118, 173, 174]. These could either be a result of the pathogenic process or the cause of ALS. Evidence discounting aggregate formation as the primary or only cause for the disease phenotype is from a study utilizing the G85R mutants. In these mutants, other defects such as slowing of axonal transport mostly due to defects in neurofilaments arose several months prior to aggregate formations [175]. The light chain of neurofilaments (NF-L) is required for cytoskeletal assembly and its deletion in the G85R mice delayed disease onset and resulted in fewer aggregates [175]. These results suggest that mitigating SOD1 aggregates is insufficient at disease amelioration.

Mice over-expressing mouse NF-L, human NF-H or mouse peripherin develop symptoms akin to ALS patients or the SOD1 transgenics [176, 177]. Also, transgenic mice with a point

mutation in NF-L subunit developed neurofilamentous aggregates in cell bodies and proximal axons causing selective degeneration of motor neurons [178]. Reduced slow axonal transport as seen in over-expressors of NF-H can result in aberrant accumulation of proteins. If NF-L is also over-expressed in these motor neurons, the transport defect and pathology can be reversed [179]. It has also been shown that NF transport in 3 different lines of mutant SOD1 mice is defective.

Genetic studies in families of ALS patients have revealed polymorphisms in the KSP repeats of NF-H and a recent study indicated mutations in genes encoding the dynein / dynactin protein complex [92, 93, 114]. The dynactin complex is important for transporting NF bidirectionally. The KSP repeats of NF-H and NF-M has been hypothesized to be phosphorylated by activated kinases such as the members of the mitogen activated protein kinase (MAPK) family and cyclin dependent kinase5 (CDK5), resulting in accumulation of NF in the SOD1 transgenics [180, 181]. Post-translational modifications can modulate axonal growth and transport of NF. Thus from all these studies, it is evident that cytoskeletal integrity is important for protein, organelle transport and normal functioning of the motor neurons.

#### **1.6.7.5. Astrogliosis**

Excessive proliferation and hypertrophy of the glial component is a neuropathological hallmark of the disease [182]. This event is termed astrogliosis wherein the astrocytes and microglial cells get activated, which may result in inflammatory cytokine / chemokine – mediated responses. These may then have a bystander effect on the adjacent motor neurons thus signaling the importance of the astroglial component of the CNS. A recent study in the transgenics has demonstrated that overexpression of mutant (G37R) human SOD1 driven by neuron-specific promoter did not result in motor neuron deficit, suggesting the importance of

glial interactions [183]. In another interesting study utilizing chimeric mice, it was demonstrated that the presence of SOD1 mutations in motor neurons is solely not sufficient in the disease pathogenesis [184]. Non-neuronal cells are also required to express the mutant SOD1 protein. Strikingly, they report that astroglial cells expressing wild-type SOD1 can delay motor neuron death and also extend survival of the affected motor neurons. Albeit this study used state of the art transgenic technology, the results did not shed any new light on ALS pathogenesis. It was convincingly demonstrated that the state of the glial cells (i.e., local environment) plays an equally important role in ALS. These studies provide important insight and guidance for any cell-based therapeutic approaches for ALS.

#### **1.6.7.6. Autoimmunity**

Autoimmunity has been hypothesized as a mechanism for SALS. Sera from SALS patients have exhibited levels of antibodies against voltage-gated calcium channels (VGCC), which could alter calcium channel function [185, 186]. Support for this hypothesis also stems from various studies that describe increase in microglial activation and inflammatory cytokines accompanying cell death in AD, PD and ALS. Activated microglia can act as antigen presenting cells (APC) and mount an autoimmune response as noticed in cases of multiple sclerosis and demyelinating inflammatory neuropathies. In fact a recent publication has documented increased expression of mature dendritic cell markers, microglia and chemokines in ALS spinal cord and CSF [187]. Microglial activation is an early response in ALS and it increases over time in transgenic mice models. Support for the role of immune response in ALS also comes from the fact that a cyclo-oxygenase 2 (COX2) inhibitor, minocycline has been demonstrated to extend lifespan of transgenic mice [188, 189].

#### **1.6.7.7. Other mechanisms (DNA Damage, Growth Factors, Viruses)**

Lipid peroxidation of proteins or other markers of oxidative damage are well documented for not only ALS but also for other neurodegenerative diseases [190-194]. Thus oxidative damage to proteins and DNA can be a common pathogenic mechanism for neurodegeneration. DNA damage can occur in glial or neuronal cells. Damage to mitochondrial DNA, activation of p53 and PARP have been reported in spinal motor neurons of both transgenic mice and post-mortem ALS tissues [195-200]. Antioxidant and DNA repair enzymes can counteract harmful effects of oxidative injury. Base excision repair (BER), which corrects the loss of single bases (AP sites) via the action of the apurinic / apyrimidinic endonuclease (APE) is one of the repair pathways. One group identified APE mutations in 8 of the 11 SALS and FALS patients [201]. While two groups reported reduced DNA repair activity in ALS patients, one other study did not show evidence for reduced enzymatic activity [202, 203]. Although inconclusive, these results suggest that DNA repair activity is compromised in disease states thus making cells susceptible to death via DNA damage. Another study suggested increased APE-1 activity in the surviving upper motor neurons and the astrocytes in the spinal cord of ALS patients [203]. Although this study does not directly corroborate the previous reports, it does support the DNA damage theory by suggesting that DNA repair activity is increased in an effort to compensate for the damage.

Other factors that may be involved in disease pathogenesis include target-derived trophic factor deprivation. Trophic factors or growth factors is a more viable hypothesis simply because their signaling is important for the survival of neurons and glia. It is likely that if there is a target-derived deprivation of these growth factors to the neurons, the death might be one of retrograde also termed the “dying back” phenomenon. This indeed is true in some ALS cases [14, 33]. Also, there have been a number of clinical trials involving the genetic manipulations of various growth

factors such as brain derived growth factor (BDNF), glial derived growth factor (GDNF), ciliary neurotrophic factor (CNTF), insulin-like growth factor-1 (IGF-1) and hepatocyte growth factor (HGF) amongst others [204-209]. Although most have proved unsuccessful in human trials, it nevertheless remains as a viable option to be explored in combinatorial therapeutic approach.

Although the viral hypothesis initially gained strength it has been mostly discounted. There have been contradictory reports suggesting the presence of enteroviruses [210-212]. A recent study has negated an earlier study by reporting the absence of echoviral RNA [213, 214]. Given the viral pathogenesis of poliomyelitis and the closeness in clinical symptoms between polio victims and ALS patients, cannot be entirely excluded without further investigations.

## **1.7. Cell Cycle and Cell death**

The cell cycle plays a pivotal role in determining the decision to proliferate or to withdraw from the cycle and enter a quiescent state. Thus, there is a distinct possibility that the molecular mechanisms that control cell division and cell death are interrelated. During cell division, there are transient and reversible changes that occur involving chromatin condensation, cell rounding and cytoskeletal rearrangements. However, in cell death these changes occur irreversibly and with destructive consequences [215-217].

Progression of the cell cycle through the four phases (G1, S, G2 and M) in eukaryotic cells is associated with the phase-specific expression of defined sets of genes and their regulation by transcriptional repressors and/or activators. Additionally, there are elaborate feedback mechanisms called checkpoints that regulate the transition of a cell through the cell cycle [218]. If irreparable damages to DNA or the mitotic apparatus itself are detected, cell death ensues. The p53 protein is an example of such an S-phase checkpoint controller that links cell cycle and cell

death mechanisms. Early G1 events are dependent on the binding of extracellular mitogens to cell surface receptors. There is a point in this phase termed the “restriction point” when cell cycle progression becomes independent of growth factors [217]. This point is characterized by the activation of the G1 cyclin dependent kinases (CDK), which are a family of cytosolic serine / threonine protein kinases and the subsequent inactivation of the tumor suppressor retinoblastoma protein (pRb), followed by increased DNA synthesis through transcriptional activation of S phase genes [219]. These kinases are tightly controlled by their regulatory subunits, the cyclins.

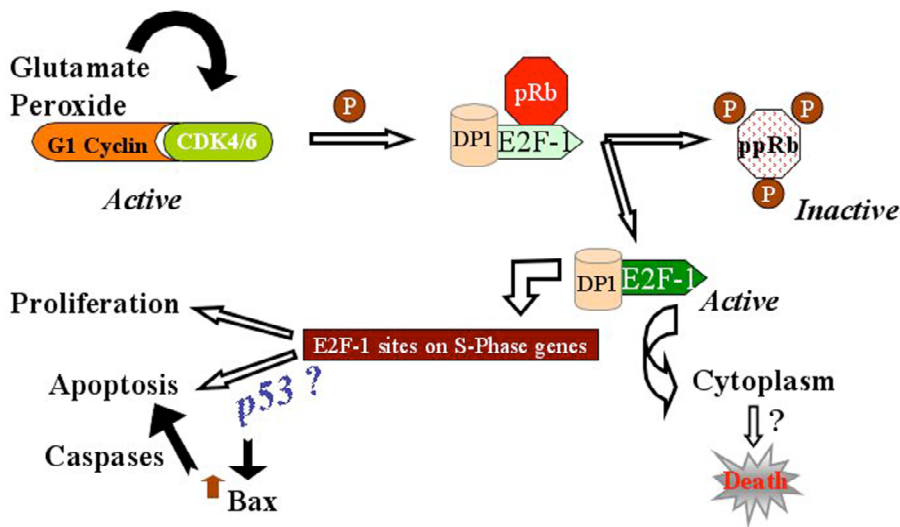


**Figure 12 Hypothesis: Aberrant re-activation of G1 to S phase Regulators**

*Phosphorylation of pRb by G1 cyclin (D1) - cyclin-dependent kinase 4/6 inhibits the ability of pRb to bind the E2F family of transcription factors. When released from inactive, hyperphosphorylated pRb, free and active E2F-1 in a dimeric complex with DPI protein enhances DNA binding activity, which activates transcription of S phase genes to induce proliferation or apoptosis. Proliferation is not likely to occur in post-mitotic neurons. Apoptosis could be dependent or independent of p53. Alternatively, E2F-1 in cytoplasm could initiate other death cascades.*

One of the substrates for Cyclin D1 / CDK4 (G1 phase) is pRb (p105) that normally exists in a hypophosphorylated form [220, 221]. It represses E2F/DP, a family of heterodimeric transcription factors important for regulating cell cycle genes [222-225]. pRb binds to the transactivating domain of E2F-1 acting as a transcriptional repressor. The overlying hypothesis for aberrant re-entry of post-mitotic motor neurons into cell cycle is depicted in Figure 12. Certain cellular signals such as glutamate and hydrogen peroxide can induce the kinase activity of CDK4 or CDK6 resulting in hyper-phosphorylating pRb (ppRb), which results in the release and de-repression of E2F-1 [220, 221]. Once E2F-1 is de-repressed, a number of genes related to cell cycle progression such as the p53 family of tumor suppressor genes, and genes encoding CDK inhibitors are transactivated.

The tumor suppressor protein, p53 is a sequence-specific DNA-binding protein that can regulate transcription. When wild-type p53 is over-expressed, it can suppress cell growth [226, 227] and promote cell death by apoptosis [228, 229]. It inhibits cell cycle progression through the activation of CDK inhibitors (CDKi) that blocks the activity of CDK/cyclin complexes. The existence of p53 knockout mouse indicates that functional p53 is not required during early development [230]. Co-expression of the wild-type p53 protein and E2F-1 in mouse embryo fibroblasts resulted in a rapid loss of cell viability through a process of apoptosis triggered by conflicting signals (growth arrest vs S phase entry). This E2F-1 mediated apoptosis may be dependent or independent of p53 [231-233]. These studies thus link the G1 to S phase regulators to p53 and apoptosis. In addition to the well-studied areas of development and cancer biology, the role for cell cycle during neurodegeneration and brain injury is emerging.

### **1.7.1. Cell cycle Regulators and Neurological disorders**

Although neuronal apoptosis is an important component of brain development, a growing body of evidence suggests that it also participates in the progression of neuropathological conditions such as stroke and neurodegenerative diseases [234-237]. Animal studies using sympathetic and cortical neuron cultures implicate cell cycle elements such as CDK4/6, pRb/p107, E2F-DP1 complex, and p53 in neuronal death evoked by DNA damage and  $\beta$ -amyloid [238-243]. In a study using a ALS mouse model expressing mutant human G37R SOD1, activity and levels of the G1 to S phase regulators such as CDK4, cyclin D1 and hyperphosphorylated Rb were elevated. However there was no change in the levels of CDK2 or CDK6 [244]. Thus, emergence from a post-mitotic state of selectively vulnerable populations of neurons and their subsequent “re-entry” into cell cycle such as in AD, PD, ALS and SIVE have been well documented [121, 242, 245-250]. There has been one report using fluorescent in-situ hybridization (FISH) suggesting ploidy in these post-mitotic neurons of AD brains [251]. However, these results have not been successfully reproduced. Thus the overlying hypothesis for the role of cell cycle proteins in post-mitotic adult neurons during neurodegeneration is one of “abortive re-entry leading to neuronal death via multiple pathways”.

### **1.8. Types of Cell Death during Neurodegeneration**

Depending on the kind of insult and the toxicity levels, different pathways can lead to neuronal cell death. In spite of the fact that most kinds of cell death is programmed, there are variations in the involvement of subcellular organelles and mechanisms. Neurons can degenerate via different types of death processes including apoptosis, necrosis, paraptosis and/or autophagy. In spite of a number of reports implicating caspases and classical apoptosis in acute and chronic

neurodegeneration, the lack of morphologically convincing apoptotic neurons has blunted a clear understanding of the relationship between neurodegenerative processes and apoptosis. In addition, in some studies the use of caspase inhibitors has either not had a significant effect on delaying onset or increasing survival while in others, it has been effective [252, 253]. This conundrum is probably due to the fact that it is very likely that many interrelated or independent pathways may regulate cell death. In fact, in several models of neuronal cell death such as after stroke or ischemia, the explosive necrotic death and the energy driven apoptotic type of death are considered to represent a continuum [254].

A variation of apoptosis termed “Paraptosis” has been defined and is hypothesized as an alternative form of neuronal cell death studies [255]. This form of death is characterized by the formation of empty spaces called vacuoles in the cell cytoplasm derived predominantly from the endoplasmic reticulum and later from the mitochondria. The process reveals mitochondrial swelling and a general lack of caspases except caspase-9.

An emerging concept in neurodegeneration is the role for autophagy, a catabolic process wherein the cytoplasm and other cellular organelles are phagocytosed by vacuoles and degraded in the lysosomes [256]. In a lurcher mouse model for ataxia, glutamate receptor-induced autophagy was evident in the Purkinje neurons [257]. In a PD model of methamphetamine-induced dopaminergic loss and in lewy bodies of post-mortem PD cases, autophagy has been documented [258, 259]. Furthermore trophic factor deprivation of *in vitro* cerebellar Purkinje neurons resulted in increased autophagosomes in a p75 low affinity NGF receptor dependent manner [260]. Thus it is fair to note that neuronal cell death can occur through more than one kind of mechanism.

### **1.8.1. Apoptosis during Neurodegeneration**

While multiple modes of cell death may contribute to ALS, apoptosis is the commonly proposed mechanism. Apoptosis (etymologically from Greek apo- from, detached, separate and ptosis- falling) is believed to function in molding the nervous system's cellular structure and function during brain development. Apoptotic events include DNA fragmentation, chromatin condensation, membrane blebbing, and cell shrinkage [261]. While it is favorable to have apoptosis to maintain cell number during neurodevelopment, if a cell sustains irreparable internal damage and initiates a death cascade when it should not, it becomes detrimental to the nervous system leading to, for instance, neuronal loss in ALS. Adult neurons aberrantly re-capture the ability to exhibit apoptosis during the process of aging, ischemia or stroke and neurodegeneration such as in ALS, AD, PD, and HD [119, 126, 262-272]. In a cortical injury model, it has been demonstrated that neuronal apoptosis in the thalamus is dependent on p53 and its downstream pro-apoptotic target, Bax [273, 274].

Cell disassembly is caused by the action of initiator proteases and effector proteases [275]. Proteases involved in programmed cell death have been termed "caspases". These are synthesized as cytoplasmic, inactive pro-caspases that are activated during apoptosis by the initiation of a cascade of proteolytic cleavage. Activation of an initiator caspase, in turn, activates effector caspases, resulting in cellular attrition. Different initiator caspases mediate distinct sets of signals. For instance, while caspase-8 is associated with apoptosis involving death receptors [276], caspase-9 is involved in death induced by cytotoxic agents [277]. Proapoptotic signals can cause mitochondrial membrane changes that induce the release of mitochondrial cytochrome c oxidase. This enzyme acts as a cofactor on the inactive Apaf-1 (Apoptosis promoting associated factor)/pro-caspase-9 complex and results in the formation of cytoplasmic

active caspase-9 [278]. This active caspase-9 through other intermediate proteases activates effector caspases such as caspase-3 and -7. A proteolytic cascade thus activated acts on various cellular substrates. A factor, DFF-45, is an inhibitor of the nuclease (CAD, caspase-activated deoxyribonuclease) responsible for DNA fragmentation, a hallmark of apoptosis [279, 280]. During apoptosis, caspase-3 cleaves DFF-45, thus de-suppressing CAD and results in DNA fragmentation [281]. Given the complexity of the system, it is conceivable that there could be redundancy in the activity of these different caspases in mediating death response through multiple signaling pathways.

Involvement of tumor necrosis factor (TNF- $\alpha$ ) receptors and FAS in conjunction with adaptor proteins containing death domains in apoptosis has also been extensively reported in various systems. Fas receptor and its downstream apoptotic signaling via caspases-8 and -3 have been implicated during neurogenesis and also in a model of transient spinal cord ischemia [282, 283]. TNF- $\alpha$  and FAS-ligand (FAS-L) can be released in response to inflammatory reactions by glial cells or by developing neurons, which would then activate caspases leading to neuronal death. In fact, the involvement of the Fas and its ligand (FasL) in p53-mediated neuronal apoptosis has been documented [284].

There are also reports of caspase-independent death mechanisms of such as in PD and stroke wherein DNA damage or oxidative stress can lead to the activation of poly (ADP-ribose) polymerase (PARP). PARP in turn leads to altered nuclear localization of apoptosis inducing factor (AIF) that can then trigger DNA fragmentation [285]. In fact evidence for AIF's in neuronal cell death also come from the "harlequin" mouse model, which has a mutation in the AIF gene [286, 287]. The cerebellar and retinal neurons in these mice are susceptible to oxidative stress, which then causes them to duplicate their DNA as they "re-enter the cell cycle".

Neuronal death via apoptosis in these mice in spite of reduced expression of AIF is suggestive of an antioxidant function of AIF. Thus in addition to causing apoptosis by nuclear translocation from the mitochondria, it is likely to scavenge free radicals that may arise through oxidative stress. This is a finding that directly connects oxidative stress to abortive re-entry into cell cycle.

### **1.8.2. Apoptotic Pathways in ALS**

Morphological and biochemical apoptotic characteristics have been observed in lower and upper motor neurons in ALS. It has been reported that there is enhanced chromatolysis, somatodendritic attrition, increased levels of DFF-45 and internucleosomal cleavage in spinal cord and motor cortex of ALS cases [288]. Also there is an increased level of cytosolic anti-apoptotic proteins (Bcl-2) in ALS cases, which reduces the chances of blocking cell death. Recent evidences from transgenic mice have establishes that mutant SOD1 selectively induce apoptosis in motor neurons [126, 289-291]. Many studies using caspase inhibitors or ablation of genes encoding caspases have not yielded expected results such as delay in disease onset and progression. It could be due to the fact that neuronal apoptosis is just one pathway of cell death and there would be the prevalence of caspase-independent pathways. To this effect there are reports in ALS transgenic mice of cell death mechanisms that are morphologically similar to paraptosis [103, 292].

### **1.9. Current Therapeutics and Clinical Trials**

Identifying therapeutic targets and developing an approach to stem the relentless loss of motor neurons is essential from a clinical perspective. The disease lacks diagnostic biomarkers and any long-term drug interventions [293]. Currently there is only one FDA approved drug,

riluzole/rilutek that increases lifespan by 2-3 months. Although the exact mechanism of its action is unknown, riluzole is thought to act through partially being an antagonist for glutamate release [294]. With ALS being heterogeneous simultaneous targeting of several pathways will probably be the most effective way to impede disease progression.

Antioxidant (Vitamin E and N-acetylcysteine), energy supplements (Creatine) and intrathecal / subcutaneous injections of neurotrophic factor (BDNF, CNTF and GDNF) were ineffective in drug trials [295]. Specifically, a double blind, placebo controlled human BDNF study failed to improve survival and was aborted. Although, some of these were very effective in animal studies, human trials failed. Another ongoing clinical trial uses minocycline (tetracycline-derivative with anti-inflammatory properties). It crosses the blood-brain barrier and has been effective in many paradigms such as PD, NMDA-mediated toxicity, and cerebral ischemia [296-299]. Its effects are possibly through inhibiting caspase activation / cytochrome c release, microglial activation and iNOS activity [298-301]

In recent animal studies (G93A mutant SOD1) a combination of creatine (supplement that improves mitochondrial function) and minocycline delayed disease onset and increased survival by 25% [302]. Another group used a cocktail of minocycline, riluzole and nimodipine (VGCC blocker) demonstrating delay in onset, slowed the loss of muscle strength and increase survival by about 6 weeks [303]. A recent gene therapy approach in SOD1 transgenics using IGF1 (myotrophin) delayed disease onset by 31 days and increased survival by 37 days when administered pre-symptomatically [206]. These mice also exhibited reduced pathology. IGF1 by far seems to be the most ideal candidate amongst growth factors. Caspase inhibitors (caspase-1 and -3) and over-expression of anti-apoptotic proteins (Bcl-2) in mutant SOD1 mice prolong their lifespan by upto 15% [290, 304, 305]. Furthermore, ongoing in vitro and animal studies

modulating the proteasome (ritonavir) increase survival and a molecule (Ceftriaxone) that increases glutamate transporter expression slows disease progression. Preliminary drug screening of G1 to S phase inhibitors (Eflornithine and Olumucine) that confer neuroprotection provides credence for cell cycle in ALS.

Numerous studies that are conducted in a laboratory fail to succeed in clinical trials due to a variety of reasons. Positive results from animal studies might be difficult to replicate in human studies because the time of disease course at which drugs are administered, mode of delivery, differences in drug metabolism and the fact that the transgenic animal models represents a very small fraction of ALS population. However, efficient early diagnosis, multi-system approach to disease marker discovery and drug intervention involving pharmacological, genetic and cell-based methodologies may be an efficient way to battle ALS.

#### **1.10. Drug design and therapy – The “Omics” approach**

Drug discovery and therapeutics relies on understanding molecular mechanisms, identification of drug targets and efficient utilization of novel approaches. Combinatorial approaches include high-throughput screening assays, genomics, proteomics and metabolomics. Over the past decade genomics has been used extensively to study the expression patterns of various genes. However mRNA does not directly correlate to levels of its product / protein mainly due to the prevalence of various post-transcriptional modifications and is a limitation to genomic studies. Thus the study of the entire set of proteins (“Proteome”) expressed by a genome, defined as “Proteomics” or the study of all the metabolites in a cell, also known as “Metabolomics” could result in successful drug discovery, design and better clinical management [306].

### **1.10.1. Clinical Proteomics**

The dynamic nature of the proteome of a cell or tissue is a strong reason to study disease at the proteomic level. Proteomics using complex systems such as cells, tissues, or body fluids (serum, plasma or CSF) provides the tool for identifying clinical biomarkers that extends the understanding of molecular mechanisms to drug discovery [307-310]. Biomarkers can be defined as any molecule that can be specifically associated with a biological process. Clinically a diagnostic biomarker can be utilized to correctly distinguish between a patient and a normal individual. Ideally one would like a validated diagnostic marker to predict at an early stage of the disease. It is thus important to understand the biology of the disease and stratify patients based on age, clinical symptoms, and drug regimen. Proteomics however has its disadvantages in that it has to deal with complex mixtures arising from alternative splicing and post-translational modifications. In addition, proteins found in low abundance cannot be amplified unlike low abundant DNA or RNA. Sometimes, high abundance proteins such as albumin present in elevated levels in serum and other body fluids may mask other proteins. These aspects necessitate the use of albumin depleting protocols, enrichment and fractionation methods coupled to sensitive techniques such as mass spectrometry (MS). Proteomic profiling can be performed either using a 2D-GE coupled to MS for protein identification or using protein chip-based tandem MS such as matrix-assisted laser desorption / ionization time of flight (MALDI-TOF), surface-enhanced laser desorption / ionization-TOF (SELDI) and electrospray ionization (ESI) [311]. While both 2D-GE and MS approaches have their advantages and disadvantages, in this study we have chosen the latter approach because of the following reasons: (i) MS-based proteomics is more rapid and sensitive; (ii) Protein chips require smaller amounts of sample; (iii) Proteins less than 10kDa can be better identified by MS but not 2D-GE; (iv) It is possible to

perform direct amino acid sequencing from the protein chips; (v) MS-based approach is better suited to identify post-translational modifications than 2D-GE.

### **1.10.2. Two Dimensional Gel Electrophoresis (2D-GE)**

2D-GE has been extensively used for proteomics but it presents certain caveats such as limited automation, difficulty in reproducing results and quantification. The latter two aspects were however solved by the fluorescence difference GE (DIGE) reducing the number of gels and increasing the efficacy of spot picking. This approach uses mass and charge-matched spectrally resolvable fluorescent dyes (Cy3 and Cy5) to label different protein samples *in vitro* before subjecting them to 2D electrophoresis [312]. In addition to providing a means to quantify protein differences, the DIGE technology can also identify any post-translational modifications. However the caveat to this technology is that the labeling step has to be optimized stoichiometrically. Once differentially expressed spots are picked from the 2D-GE they can be sequenced and validated by molecular techniques.

A combination of 2D-GE, Western immunoblotting and MS has been utilized in studying the proteomic patterns in the CSF and brain tissues of neurodegenerative and neuropsychiatric patients [313-318]. Studies have indicated oxidative damage to proteins involved in the neuronal proteasome machinery (ubiquitin carboxy-terminal hydrolase-L1, UHC-L1), oxidatively modified or nitrated protein differences in AD and PD brain samples [316, 317, 319-322]. In fact a recent study was published using a mouse model of HD and post-mortem samples from HD patients, wherein differences in serine protease inhibitors and chaperone proteins were reported [323, 324]. Other studies have involved Down's syndrome and Schizophrenic patients [318, 325,

326]. 2D-GE has thus yielded insights to disease-specific differences in the “neurome” (nervous system-specific proteome) and it can be handily coupled to the sensitivity of MS.

### **1.10.3. Mass Spectrometry**

The use of MS in biomedical sciences is a highly sensitive and analytical tool that bridges basic and clinical science. MS-based proteomics can detect signals with low amounts of clinical samples and aid in defining disease-specific “biosignatures”. All MS contain three parts: ionizer, analyzer, and detector. These instruments are based on the principle of desorbing and ionizing protein samples for analysis followed by their detection based on mass to charge ( $m/z$ ) ratios. The detector provides a pattern of spectral peaks, which discriminates disease from normal condition.

In the late 1980s, two new protein ionization techniques led to the discovery of matrix-assisted laser desorption / ionization (MALDI) and electrospray ionization (ESI) mass spectrometric instruments [327-329]. In MALDI, the sample of interest when mixed with an energy-absorbing matrix (EAM) forms a crystal and this is applied on a reusable metal plate with spots available for a number of different samples. When the samples are pulsed with laser, they are ionized accepting protons from the EAM and are desorbed from the plate in the gas phase being ejected into the mass analyzer. The mass analyzer helps in the separation of ions according to their  $m/z$  ratios prior to their detection. The mass analyzers can be of different kinds such as time-of-flight (TOF), quadrupole (Q), ion trap or a combination of these such as (TOF-TOF, Q-TOF). In a TOF analyzer, the mass is directly proportional to the speed at which the ions travel. The beam is focused by a reflector and directed towards a detector. Ions with a lower  $m/z$  ratio travel faster and are therefore quicker to be detected. In quadrupole analyzers, ions pass through

two pairs of oppositely charged parallel metal rods and are filtered based on the applied voltage prior to detection. Hybrids of these mass analyzers (TOF-TOF or Q-TOF) make for higher sensitivity to low abundance ions and also coupling the discovery phase of MS-based proteomics to the identification phase. MS however cannot be used for quantitative purposes much like 2D-GE. Nevertheless, similar to the DIGE system, a modification of MS termed isotope coded affinity tags (ICAT) has made it a quantifiable technique. In this approach, the samples are linked to isotopes and thus differences in the peak sizes isotope-labeled proteins / ions (heavy vs light) determine relative quantities.

Currently, a modified version of MALDI-TOF is used, termed surface-enhanced laser desorption / ionization-time of flight (SELDI-TOF) [330]. In SELDI, the samples are applied to spots on protein chip arrays that are biochemically modified with an active surface chemistry such as cation / anion exchange properties, hydrophobicity or metal affinity. All these approaches are closely associated with the use of bioinformatics, which provide the algorithmic tool for efficient data mining and interpretation [331]. They aid in determining discriminatory patterns of  $m/z$  values. Machine learning and classification tree based algorithms are used to discern differences [332-334]. Potential predictors of the disease can then be enriched and sequenced through MALDI based tandem MS/MS. The availability of such databases and the use of statistical methods emphasize the important role played by bioinformatics in proteomics.

#### **1.10.4. MS-Based Proteomics**

In a landmark “proof-of-principle study in 2002, this approach was published by a group from the National Cancer Institute using a training set of 100 serum samples from normal and ovarian cancer patients [335]. The model was then tested on a sample set of 116 of which 50

were diagnosed with cancer. They reported very high predictive value (95% specificity and 100% sensitivity) and biomarkers were utilized to develop commercial diagnostic tests. Re-analysis of this data by other groups revealed experimental artifacts generated by the limitations imposed by the Ciphergen-based SELDI-TOF machine and experimental protocol utilized to process the samples that questioned the credibility of the ovarian cancer study [336]. The SELDI-TOF does not provide high-resolution spectral data for proteins with high molecular weight (> 50 kDa). Usually researchers do not analyze m/z values less than 2kDa as they might present the matrix-related peaks and other experimental artifacts. Mass inaccuracy and spectral patterns that differ from machine to machine may also pose problems for interpretation. In spite of its limitations, MALDI / SELDI-TOF has been increasingly used in clinical research studies for identification of diagnostic biomarkers for diseases such as glioblastomas, breast, prostate, non-small cell lung carcinomas, renal cell carcinoma, cardiovascular diseases, allergies and neurological disorders such as AD, HIV-1 associated dementia [308, 316, 320, 337-345]. In an elegant study, clinical samples from HIV-1 infected individuals were analyzed for the identity of the soluble factor from CD8+ T lymphocytes that has been reported to inhibit HIV-1 replication. Using an immuno-SELDI-TOF-MS approach, this factor was identified to be  $\alpha$ -defensin 1, 2, and 3 [346]. This is further validation for the use of MS-based proteomics on clinical samples and identification of putative disease markers. Hence, although MS-based proteomics is in its infancy, it nevertheless provides an exciting prospect at identifying disease specific diagnostic markers and extending therapeutics even for such heterogeneous and fatal neurodegenerative diseases as ALS.

### 1.11. Statement of Problem

It is evident that the molecular mechanisms in chronic and fatal degeneration of motor neurons during ALS are far from being delineated. This relentless disease is devoid of early diagnostic biomarkers and therapeutic targets / drugs for long-term intervention. This study was undertaken so as to bridge two aspects that are lacking in the world of ALS. The role for cell cycle proteins and apoptosis has been reported in other neurodegenerative diseases but not ALS. *We hypothesized that aberrant re-activation of cell cycle proteins could lead to an apoptotic mode of motor neuron death furthering the understanding of disease mechanisms. In addition we hypothesized that a sensitive mass-spectrometry-based proteomic approach would not only yield ALS specific disease markers but also provide additional targets for drug design.*

## **2. Abortive Re-entry of Motor Neurons into Cell Cycle**

### **2.1. Abstract**

The mechanisms that regulate the initiation and/or progression of selective motor neuron loss during amyotrophic lateral sclerosis (ALS) remain enigmatic. Cell cycle events that occur during development and studied extensively during pathological states of tumorigenesis can be aberrantly recapitulated during neurodegeneration. Indeed recent data has implicated increased expression and activation of various cell cycle proteins in neuronal cell death. We have examined the expression and subcellular distribution of G1 to S phase cell cycle regulators in the spinal cord, motor cortex, and sensory cortex from clinically and neuropathologically diagnosed sporadic ALS cases and age-matched controls. Our results indicate hyperphosphorylation of the retinoblastoma protein in motor neurons during ALS, concurrent with increased levels of cyclin D, cyclin dependent kinase 4 (CDK4) and re-distribution of E2F-1 into the cytoplasm of motor neurons and glia. Furthermore, the cell cycle checkpoint, p53 co-localizes with hyperphosphorylated retinoblastoma and E2F-1 in spinal motor neurons. These results suggest that re-sensitization of cells to G1 to S phase activation occurs during ALS and may participate in molecular mechanisms regulating motor neuron death.

## 2.2. Introduction

The etiology of ALS is thought to be multifactorial with a number of different hypothesized factors as enumerated in chapter 1 (Fig 10). Signaling from the cell surface to the nucleus modulates chromatin structure and the activity of transcription factors, resulting in altered gene expression. In fact it is known that alteration in levels of pro- and anti-apoptotic genes can tilt the balance towards motor neuronal death [119]. Another potential cell death mechanism is the inappropriate expression or activation of cell cycle proteins [234]. Cell cycle is associated with the phase-specific expression or modification of defined sets of cell cycle genes that regulate cellular proliferation, differentiation or entry into a quiescent state [347]. However re-entry of quiescent, terminally differentiated neurons, into the cell cycle may result in a “mitotic catastrophe” and cell death [234, 235, 348]. For entry into the cell cycle, quiescent neurons of the adult brain must first exit G0 and enter the G1 phase of the cell cycle. Multiple cell cycle proteins regulate progression through G1, the most important being the products of retinoblastoma (pRb) tumor suppressor and E2F gene families [220]. In quiescent cells, the retinoblastoma protein (pRb) remains in a hypophosphorylated state and sequesters members of the E2F gene family of transcription factors, which suppresses cell cycle progression. The hyperphosphorylation of pRb (ppRb) releases and de-represses E2F-1 [219, 349].

Numerous lines of investigation have implicated pRb and E2F-1 in neuronal cell death [215, 239-242, 245-247, 350-352]. Studies using transgenic mouse models revealed that neuronal death in pRb knockouts was rescued by concurrent mutations in E2F-1, suggesting a role for E2F-1 in neuronal death [353, 354]. *In vitro* studies in PC12 cells or primary neuronal cultures suggest a role for pRb and E2F-1 in response to insults such as  $\beta$ -amyloid toxicity, over-expression of  $\beta$ -synuclein, UV irradiation, DNA damaging agents, trophic factor withdrawal,

and depolarizing conditions [242, 352, 355-358]. The functional role for these proteins has been established in mouse and rat cortical cultures using pharmacological inhibitors of CDK, dominant-negative and antisense constructs of CDK and/or E2F-1/DP-1 [240, 352, 359-361]. Human and animal post-mortem studies in AD, PD and SIV-E also suggest a plausible role for these regulators in selective neuronal death [121, 245, 248, 355, 358, 362]. There is one report in ALS wherein the G37R mutant SOD1 mouse model demonstrates increased levels of CDK4/cyclin D1 and ppRb [244]. This model does not reveal any changes in levels of CDK2 or CDK6 and the authors have not reported protein alterations downstream of ppRb.

Evidence from studies on non-neuronal cells suggests that E2F-1 induces cell death via apoptosis and can be either p53-dependent or independent [231, 232]. The role for p53 and E2F-1 in cortical neuronal cell death and DNA damage paradigms are well established [234, 363]. However, a role for these other cell cycle proteins in neurodegeneration during ALS is unknown. *We hypothesize that activation of G1 to S phase cell cycle transcriptional regulators in motor neurons during ALS leads to altered gene expression and regulates cell death.*

In this study, we report enhanced nuclear accumulation of hyperphosphorylated pRb (ppRb) and altered localization of E2F-1 in both lower and upper motor neurons in ALS patients. In addition, we show the co-localization of p53 with ppRb and E2F-1 in spinal cord motor neurons. These results suggest that, similar to *in vitro* models of neuronal cell death, motor neurons are induced to enter the G1 phase of the cell cycle, suggesting that hyperphosphorylation of pRb (ppRb) and altered localization of E2F-1 participates in motor neuron cell death during ALS.

## **2.3. Materials and Methods**

### **2.3.1. Source of Tissue Samples**

The lumbar spinal cord (see Fig 5A) and pre/post-central gyrus (motor/sensory cortex, see Fig 4A) region from eighteen cases of clinically diagnosed SALS, and nine non-ALS age-matched controls, were utilized to examine protein expression and distribution. All tissues were obtained from the University of Pittsburgh ALS tissue bank and approved for use by the University of Pittsburgh Institutional Review Board. The average age at death was  $60.05 \pm 12.22$  yrs for ALS cases (40-76 yrs) and was not significantly different from control cases ( $65.33 \pm 15.37$  yrs; 51-95 yrs;  $p = 0.34$ ). The average post-mortem interval times for ALS and control cases were  $6.02 \pm 3.35$  (2.5-14 hrs) and  $9.88 \pm 5.68$  hrs (5-20 hrs), respectively. The difference in the post-mortem interval time was statistically significant ( $p = 0.039$ ). Some of the controls and ALS cases (indicated with an asterisk in Table 1) were neuropathologically diagnosed as cases with possible AD (Braak II or III / VI). For immunohistochemistry, all tissues were fixed in 10% buffered formalin for 1 week and 8- $\mu$ m paraffin-embedded sections were examined.

### **2.3.2. Antibodies**

A list of antibodies and their dilutions used for experiments in Chapters 2 and 3 are shown in Table 3. Monoclonal antibodies were used to detect hypophosphorylated pRb (PharMingen, La Jolla, CA), E2F-1 (Santa Cruz Biotechnologies, Santa Cruz, CA), Cyclin D1 (Santa Cruz Biotechnologies, Santa Cruz, CA) and CD68 (DAKO, Carpinteria, CA). Polyclonal antibodies were utilized to detect hyperphosphorylated pRb (ser-795, NEN biolabs), active form of CDK4 (Santa Cruz Biotechnologies, Santa Cruz, CA), Actin (Chemicon, Temecula, CA) and GFAP (DAKO, Carpinteria, CA). Westerns were probed at dilutions of 1:750 (pRb, ppRb, E2F-

1), 1:200 (Cyclin D1, CDK4) or 1:10000 (Actin). For light microscopy, antibodies were utilized at dilutions of 1:150 (pRb, ppRb, E2F-1), 1:200 (CDK4, Cyclin D1) and for confocal laser scanning microscopy at 1:80 (ppRb, p53), 1:60 (E2F1), 1:100 (GFAP), and 1:30,000 (CD68).

Cases	Age / Sex	PMI (hrs)	Neuropathology Spinal Cord	Neuropathology Motor Cortex
Ctl 1	53 / F	7	No LMN loss or gliosis	No UMN loss or gliosis
Ctl 2	54 / M	6	No LMN loss or gliosis	No UMN loss or gliosis
Ctl 3	62 / M	5	No LMN loss or gliosis	No UMN loss or gliosis
Ctl 4	58 / F	5	No LMN loss or gliosis	No UMN loss or gliosis
Ctl 5*	82 / F	5	No LMN loss or gliosis	No UMN loss or gliosis
Ctl 6*	76 / M	13	No LMN loss or gliosis	No UMN loss or gliosis
Ctl 7	57 / F	11	No LMN loss or gliosis	No UMN loss or gliosis
Ctl 8	95 / M	20	No LMN loss or gliosis	No UMN loss or gliosis
Ctl 9	51 / F	17	No LMN loss or gliosis	No UMN loss or gliosis
ALS 1	71 / F	5	Severe LMN loss and gliosis	Moderate UMN loss and gliosis
ALS 2	71 / M	3	Severe LMN loss and gliosis	Moderate UMN and axonal loss
ALS 3	75 / M	2.5	Severe loss of LMN and gliosis	Moderate loss of UMN and gliosis
ALS 4	43 / M	4	Severe LMN loss, and gliosis	Severe UMN loss and gliosis
ALS 5	51 / F	5	Severe LMN loss, moderate gliosis	Severe UMN loss and gliosis
ALS 6	67 / M	4	Severe LMN loss and gliosis	Severe UMN loss and gliosis, Severe loss of axons
ALS 7	51 / M	5	Severe LMN loss, axonal loss, and Gliosis	Moderate UMN loss and mild gliosis, mild axonal loss
ALS 8	40 / M	6	Severe LMN and axonal loss, gliosis	Moderate UMN loss, mild gliosis
ALS 9	70 / F	3	Severe loss of LMN and gliosis	Moderate UMN loss and gliosis
ALS 10*	49 / M	14	Severe loss of LMN and gliosis	Moderate UMN loss and gliosis
ALS 11	44 / M	3	Severe loss of LMN, axonal loss and gliosis	Severe UMN loss, moderate gliosis, mild axonal loss
ALS 12	54 / F	6	Severe loss of LMN and gliosis	Moderate loss of UMN and gliosis
ALS 13	57 / M	3	Severe LMN loss, moderate gliosis	No loss of UMN and mild gliosis
ALS 14	73 / F	13	Moderate LMN loss and gliosis	No loss of UMN and mild gliosis
ALS 15	53 / M	10	Severe loss of LMN and gliosis	Moderate loss of UMN and gliosis
ALS 16	73 / F	11	Severe loss of LMN and gliosis	Mild loss of UMN and gliosis
ALS 17*	76 / F	6	Severe loss of LMN and moderate gliosis	Moderate loss of UMN and gliosis
ALS 18*	63 / F	5	Severe loss of LMN and gliosis	Moderate loss of UMN and gliosis

**Table 2** List of the cases utilized in this study

The post-mortem interval (PMI) and age in hours (average control, 9.88 hrs; ALS, 6.02 hrs) are indicated for the ALS (average age of 65.33 yrs) and age-matched controls (Cnts; 60.05 yrs), respectively. MN, motor neurons; UMN, Upper motor neurons; LMN, Lower motor neurons; asterisk next to cases indicates possible Alzheimer's disease. Reprinted from *Am J Pathol* 2003, 162:823-835 with permission from the American Society for Investigative Pathology.

Protein	Antibody	WB	L-IHC	C-IHC	Vendor
pRb	mAb	1:750	1:150	-----	Pharmlingen
ppRb	pAb	1:750	1:150	1:80	NEN Biolabs
E2F-1	mAb (KH95)	1:750	1:150	1:60	Santa Cruz
E2F-1	mAb (C-20)	-----	1:150	-----	Santa Cruz
Cyclin D1	pAb	1:200	1:200	-----	Santa Cruz
CDK4	pAb	1:200	1:100	-----	Santa Cruz
Actin	pAb	1:1500	-----	-----	Zymed
GFAP	pAb	-----	1:200	1:150	DAKO
CD68	mAb	-----	-----	1:30,000	DAKO
p53	mAb	1:750	1:150	1:80	Santa Cruz
p73	pAb	1:750	1:150	-----	Santa Cruz
BAX	pAb	1:1000	1:200	-----	Pharmlingen
Caspase-3	pAb	1:700	1:150	1:80	NEN Biolabs
Caspase-8	pAb	1:600	1:100	1:80	Stressgen

**Table 3 List of Antibodies**

The table illustrates all the antibodies with the respective dilutions they were used at for detection through Western immunoblotting (WB), immunohistochemistry at the light microscopic level (L-IHC) and laser scanning confocal microscopy (C-IHC). mAb and pAb indicate the type of antibody (monoclonal or polyclonal). Abbreviations of proteins are explained in the text. N/A

*represents either that the antibody was not used or that the detection of the protein by that particular technique was not performed. Also provided is the information regarding the vendor and the specific catalog number of the antibody utilized in these studies.*

*Reprinted from Am J Pathol 2003, 162:823-835 with permission from the American Society for Investigative Pathology.*

### **2.3.3. Immunohistochemistry – Light and Confocal Microscopy**

Paraffin-embedded tissue sections from lumbar or cervical spinal cord and mid-motor cortical regions (regions # 2 through #5 in Fig 6B) were microwave treated for 4 min at full power followed by 7 min at 40% power in 1X citra antigen retrieval (Biogenex, San Ramon, CA), cooled to room temperature for 90 min, and then incubated in 3% H<sub>2</sub>O<sub>2</sub> and 0.25% Triton X-100 in PBS (phosphate-buffered saline) for 30 min. The sections were then blocked in 5% milk/PBS for 1 hour. Primary antibodies at dilutions (see 2.3.2) were added in 1X PBS and incubated overnight at 4°C. After four 15-minute washes in PBS, sections were incubated in biotinylated goat anti-rabbit or anti-mouse IgG secondary antibody (1:1000; dilution Southern Biotechnology Labs, Birmingham, AL) for 1.5 hours. The signal was further amplified using biotinylated tyramide according to the manufacturer's protocol (TSA Biotin system, NEN Biolabs). On washing, the sections were incubated in streptavidin-Horseradish Peroxidase (HRP, 1:1000 dilution) for 1 hour and the reaction product visualized using 3-amino-9-ethylcarbazole (AEC for 3-5 mins) (Biogenex, San Ramon, CA). This reaction results in a red end product and all sections were then counterstained with hematoxylin. The study was conducted in a blinded fashion using 18 ALS and 10 age-matched control cases.

For laser scanning confocal microscopy, tissues were processed as for light microscopy with the following modifications. Primary antibodies were used at a higher concentration than

for light microscopy (Table 3) and the slides incubated overnight at 4°C. After incubations with biotinylated secondary antibodies, the signal was further amplified using the tyramide amplification kit as per manufacturer's protocol. The sections were finally incubated with a 1:500 dilution of streptavidin-Alexa Green (green) or streptavidin-Cy5 / Cy3 (red) at a dilution of 1:500. Co-localization was determined by the presence of yellow color (combination of green and red dyes). The sections were analyzed on a laser scanning confocal microscope (Zeiss). A total of 70-80 and 20-30 motor neurons in the spinal cord and cortex were counted, respectively at 400X magnification. The study was conducted in a blinded fashion using 11 ALS and 6 age-matched control cases. Post-mortem tissues are susceptible to auto-fluorescence through the presence of lipoproteinaceous deposits (lipofuscin). Single labeling and other control experiments were performed to determine optimal concentrations of primary and fluorescently labeled secondary antibodies. Omission of the primary antibody resulted in absence of fluorescent signal. Crossover control experiments were also performed to determine the specificity of the secondary antibody.

#### 2.3.4. **Protein Extraction**

Lumbar spinal cord and motor cortical (mid- and superior-motor cortical regions, #2 - #7 in Fig 6B) frozen tissue from controls and ALS cases (Table 2) were utilized for immunoblotting and DNA binding assays. For total cell lysates, tissue samples were homogenized using polytron homogenizer (PGC Scientific, Gaithersburg, MD) set at 15000 rpm for 45 seconds. It was carried out in lysis buffer containing 25mmol/L HEPES (pH 7.4), 50mmol/L NaCl, protease inhibitor cocktail II (SIGMA), and 1% triton-X 100. The homogenized product was spun at 14000 rpm in a cold microfuge and the supernatant saved as the total cell lysate. Nuclear and post-nuclear

extracts were extracted as described previously [121]. Briefly, protein extracts were prepared by detergent lysis on ice (0.1% Nonidet P-40, 10 mmol/L Tris (pH 8.0), 10 mmol/L MgCl<sub>2</sub>, 15 mmol/L NaCl, 0.5 mM phenylmethylsulfonyl fluoride, 2 µg/ml pepstatin A, and 1 µg/ml leupeptin). The nuclei were collected by low speed centrifugation at 800x g for 5 min. The supernatant was saved as the post-nuclear supernatant and the pellet containing the nuclei was further extracted with high salt buffer (0.42 mol/L NaCl, 20 mmol/L HEPES (pH 7.9), 20% glycerol, 0.5 mmol/L phenylmethylsulfonyl fluoride, 2 µg/ml pepstatin A, and 1 µg/ml leupeptin) on ice for 10 min. Residual insoluble material was removed by centrifugation at 14,000 x g for 5 min. The resulting supernatant fraction was collected and termed the "nuclear extract." Protein concentrations were determined by Bio-Rad assay (Bio-Rad, Richmond, CA).

### **2.3.5. Immunoblotting**

Total cell lysates, nuclear extracts and post-nuclear supernatants were fractionated by electrophoresis on an 8, 10 or 12% sodium dodecyl sulfate-polyacrylamide gels. The proteins were transferred to polyvinylidene difluoride nylon membranes (NEN Biolabs) and blocked in 5% nonfat milk / 1X PBS or 0.5% BSA / 0.15% glycine in 1X PBS overnight at 4°C. The blots were probed individually with the antibodies and concentrations overnight at 4°C in 0.5% milk/PBS (Table 3). The blots were washed three times in PBS / 0.1% Tween-20 for 15 min. Isotype-specific horseradish peroxidase-conjugated secondary antibodies (Chemicon) specific for each primary antibody were added for 2 hrs at room temperature. The secondary antibodies were washed extensively in PBS / 0.1% Tween-20 (three times for 20 min). The final reaction products were visualized using enhanced chemiluminescence (ECL; Pierce) and the band intensities were within the linear range of detection. Actin was used to normalize protein levels

within each sample. The density of bands was measured using the NIH Image software version 1.58 (National Institutes of Health, USA).

### **2.3.6. Electrophoretic Mobility Shift Assay (EMSA)**

Nuclear extracts (20-25 $\mu$ g) were preincubated with salmon sperm DNA (120ng) as a nonspecific competitor in 12-15 $\mu$ l EMSA buffer (20% glycerol, 150mmol/L KCl) prior to addition of  $^{32}$ P-labeled oligo to reduce nonspecific DNA-protein interactions. Wild type (WT E2F-1 5'-ATTTAAGTTTCGCGCCCTTTCTCAA-3') and mutant (MT E2F-1 5'-ATTTAAGTTTCGATCCCTTTCTCAA-3') oligonucleotides were synthesized and gel purified (Oligos ETC.). For competition reactions, unlabeled E2F-1 (3, 30, and 100ng) or unlabeled unrelated (5'-GATCATTCAGGTCATGACCTGA-3'; 100, and 300ng) competitor oligos were preincubated with the protein for 5 min on ice prior to addition of labeled probe. For positive controls of E2F1 DNA binding activity, nuclear extracts were prepared from NIH3T3 cells. The reaction mixture was loaded onto a 6% nondenaturing polyacrylamide gel and electrophoresed at 100 V in 1X Tris-borate-tetraethylenediaminetetraacetic acid. The gel was removed from the apparatus, dried, and exposed to autoradiography film. The density of the complexes was measured using the NIH Image software 1.58 (National Institutes of Health, USA).

### **2.3.7. Statistical Analysis**

Comparisons between any two groups of data were done using the single-factorial analysis of variance (ANOVA). A p-value of  $\leq 0.05$  was considered statistically significant. Numerical data were expressed as means  $\pm$  the standard deviation with "n" signifying the number of experiments or cases.

## **2.4. Results**

Based on the reported activation of cell cycle proteins in neurodegenerative diseases such as Alzheimer disease [121, 242, 246, 251], we investigated the expression and distribution of G1 to S phase cell cycle proteins in human post-mortem tissues from ALS and age-matched control cases. The G1 to S phase cell cycle transition is necessary for cell cycle progression and regulated by the activation of cyclin/cyclin-dependent kinases that hyperphosphorylate pRb, thus de-repressing the transactivational ability of E2F (Fig 12; [220, 223, 225, 347]). Therefore, the cell cycle proteins analyzed in this study include cyclin D1, CDK4, ppRb, and E2F-1. Co-localization studies involving these regulators and p53 were also performed. Since ALS affects the lower motor neurons in the spinal cord and upper motor neurons (Betz cells) in the cortex, we utilized tissue samples from both CNS regions to determine subcellular localization of cell cycle proteins by immunohistochemistry. Regions primarily unaffected during ALS, namely the dorsal horn of the cord (see Fig 5C) and the sensory cortex (see Fig 4A), were used as internal controls.

### **2.4.1. Increased immunoreactivity of G1 to S phase cell cycle proteins in ALS spinal cord motor neurons**

Sections of lumbar spinal cord and pre/post-central gyri were immunostained using commercially available antibodies (Table 3). For light microscopy, the antigen-antibody complex was visualized with 3-amino-9 ethylcarbazole (AEC) and counterstained with haematoxylin (see Materials and Methods). Cyclin D1, a D-type cyclin functional in the hyperphosphorylation of pRb and G1 to S phase transition of the cell cycle, exhibited increased cytoplasmic distribution in the spinal motor neurons of ALS patients (Fig 13, A and B). Sections were also stained for the active form of CDK4. Although active CDK4 immunoreactivity was primarily negligible in the

ventral horn of control cases (Fig 13D), increased and punctate CDK4 immunoreactivity was apparent in the cytoplasm and occasionally in the nucleus of ventral horn motor neurons of ALS patients (Fig 13E). CDK4 and cyclin D1 immunoreactivity were negligible in the dorsal horn sensory neurons and surrounding glia in the ALS patients (Fig13, C and F).

One downstream target of active cyclin D/CDK4 complex is the retinoblastoma protein (pRb), with cyclin D specific phosphorylation of serine at position 795. Therefore, we examined the phosphorylation state of pRb in ALS using a phospho-specific anti-pRb antibody to serine 795 that has been shown to detect increased pRb phosphorylation in AD [121, 242, 355]. We detected abundant nuclear and punctate cytoplasmic staining of Ser-795 phosphorylated pRb (ppRb) in the motor neurons of ALS spinal cord but not in the age-matched control tissues (Fig 13, G and H). When morphologically distinct motor neurons from multiple lumbar spinal cord sections of 18 ALS cases and 10 control cases were counted (total of 450 motor neurons / condition) the number of ppRb-positive lower motor neurons in ALS (85.5%) was significantly greater than controls (2.8%). The retinoblastoma protein regulates the transactivation ability of E2F family of transcription factors. We noted punctate E2F-1 immunoreactivity specific to the cytoplasm of ALS spinal motor neurons but not control motor neurons (Fig 13, J and K). The number of E2F-1 positive motor neurons in ALS cases was significantly greater (80.8%) than in control cases (4.5%). There were negligible levels of nuclear E2F-1 irrespective of the disease state. These results were reproduced using a second E2F-1 antibody that recognizes a distinct epitope not encompassing the pRb-binding domain (data not shown). In contrast to the motor neurons, the ALS sensory neurons were ppRb and E2F-1 negative (Fig 13, I and L).

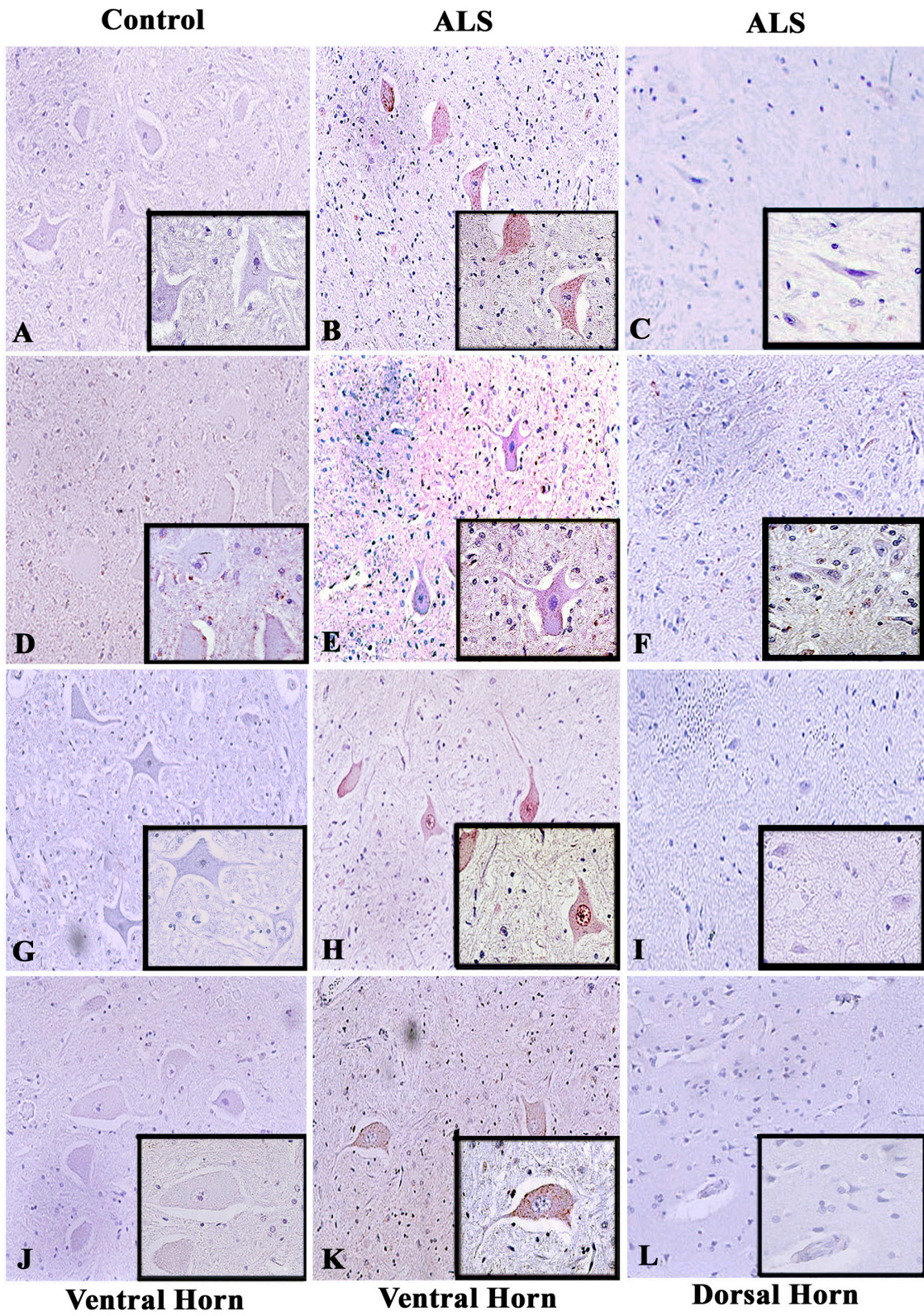


**Figure 13     Immunohistochemical analysis of G1 to S phase regulators in human spinal cord tissues**

*Lumbar spinal cord sections from 18 ALS and 9 non-neurological disease controls were immunostained for cyclin D1 (A-C), CDK4 (D-F), hyperphosphorylated Rb (ppRb, G-I), and E2F-1 (J-L). AEC was used to stain the antigens of interest (red) and each section was counterstained with hematoxylin. In relation to Table 2, panels represent cases C 2 (A, J), C 1 (D, G), ALS 4 (B, C), ALS 11 (E, F), ALS 5 (H, I) and ALS 8 (K, L). All insets are of the same cases as the lower magnification. Original magnifications: X200 (A to L); X400 (all insets). Reprinted from Am J Pathol 2003, 162:823-835 with permission from the American Society for Investigative Pathology.*

**2.4.2.            Cellular distribution of cell cycle proteins in motor cortex**

We next examined the expression patterns of cell cycle proteins in the motor and sensory cortex (pre- and post-central gyrus) of control and ALS patients. All ALS cases except one (ALS 10, Table 2) exhibited substantial loss of Betz cells and the presence of gliosis were used to identify the motor cortex when all Betz cells were absent. While cyclin D1 expression was largely cytoplasmic in any remaining large pyramidal neurons (Betz cells) of the motor cortex of ALS patients (Fig 14, A and B), CDK4 immunoreactivity was both nuclear and cytoplasmic in these neurons (Fig 14, D and E). There was variation in the level of CDK4 immunoreactivity within the motor cortex of ALS patients, though this did not correlate to any reported clinical information for the patients. The cortical neurons in the post-central gyrus of these patients exhibited little immunoreactivity for cyclin D1 or active CDK4 (Fig 14, C and F).

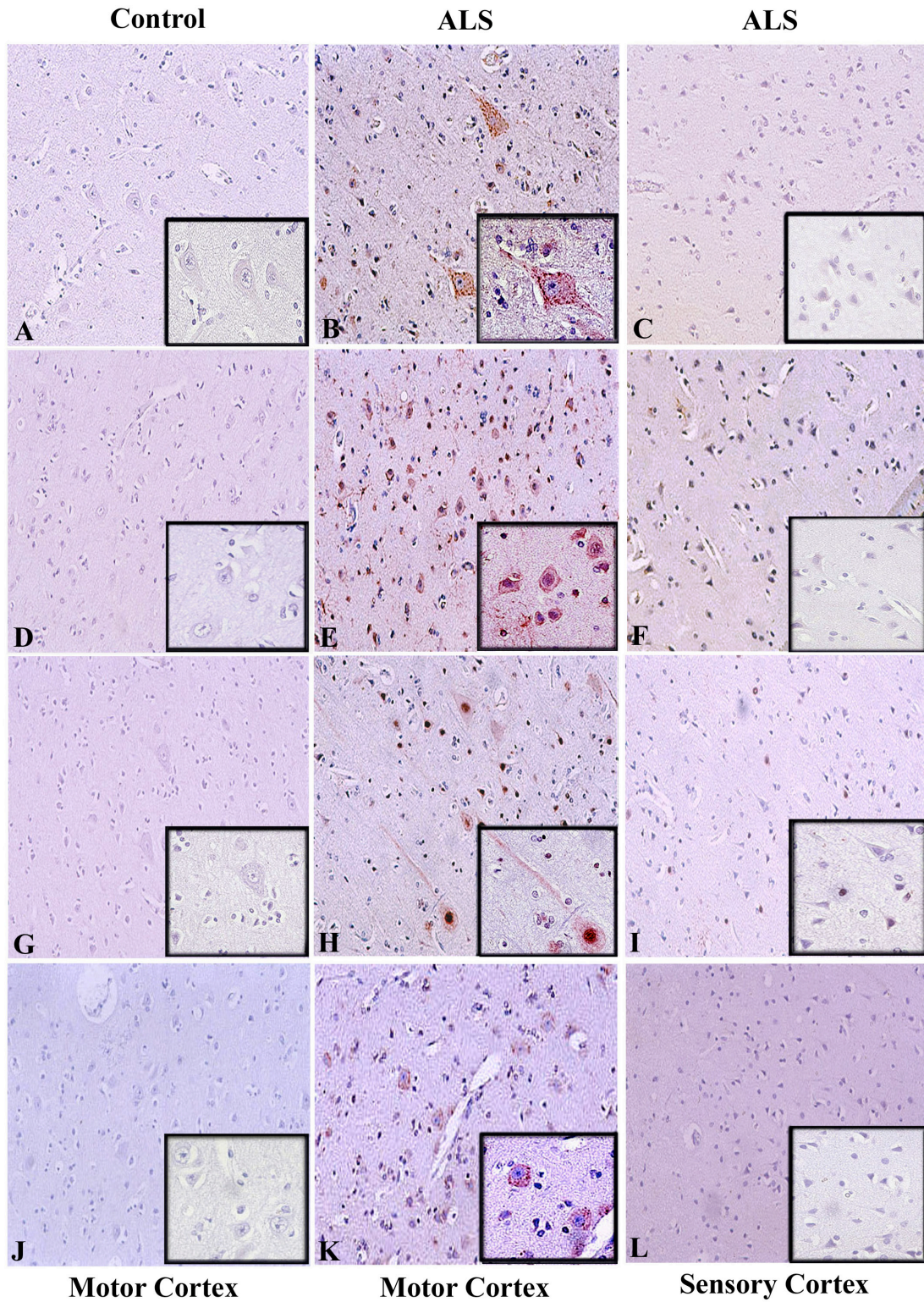


**Figure 14** Immunohistochemical analysis of G1 to S phase regulators in human motor cortex

*Precentral and post-central gyrus from 18 ALS and 9 non-neurological controls were immunostained for cyclin D1 (A-C), CDK4 (D-F), hyperphosphorylated Rb (ppRb, G-I), and E2F-1 (J-L). AEC was used to stain the antigens of interest (red) and sections were counterstained with hematoxylin. In relation to Table 2, panels represent cases C 1 (A, D, G, J), ALS 1 (B, C, H, I), ALS 4 (E, F, K, L). All insets are of the same cases as the lower magnification. Original magnifications: X200 (A to L); X400 (all insets). Reprinted from Am J Pathol 2003, 162:823-835 with permission from the American Society for Investigative Pathology.*

Hyperphosphorylated pRb (ppRb) was detected predominantly in the nucleus of many cortical neurons in the pre-central gyrus of ALS patients but not in control cases (Fig 14, G and H). The reactivity of ppRb in the cortical sensory neurons was low or negligible (Fig 14 I). E2F1 immunoreactivity was observed in the cytoplasm of neurons in the ALS motor cortex with no protein detected within control tissues (Fig 14, J and K). E2F-1 immunoreactivity was absent in the post-central gyrus (Fig 14 L). It is interesting to note that one ALS case lacking loss of upper motor neurons (ALS case #13, Table 2) exhibited little immunoreactivity for these G1 to S phase cell cycle regulators.

#### **2.4.3. Distribution of cell cycle proteins in white matter of ALS spinal cord and motor cortex**

Subsequently we investigated the presence of these proteins in cells with a glial morphology. We observed moderate immunoreactivity for cyclin D1 and CDK4 in cells with astrocytic morphology in the white matter of ALS lumbar spinal cord (data not shown). ppRb immunoreactivity appeared nuclear in the spinal cord white matter cells of ALS patients but not in control cases (Fig 15A). Furthermore, glial cells with morphology of activated astrocytes in the ALS lumbar spinal cord tissues were E2F-1 immunoreactive (Fig 15B). In the motor cortex,

ppRb was cytoplasmic in cells of the ALS white matter but not in control cases (Fig 15C). In consecutive sections, GFAP positive astrocytes were ppRB and E2F-1 positive (asterisk in Fig15, C-E). Some GFAP labeled astrocytes were E2F-1 positive but ppRb negative (arrowheads in Fig15, D-E).

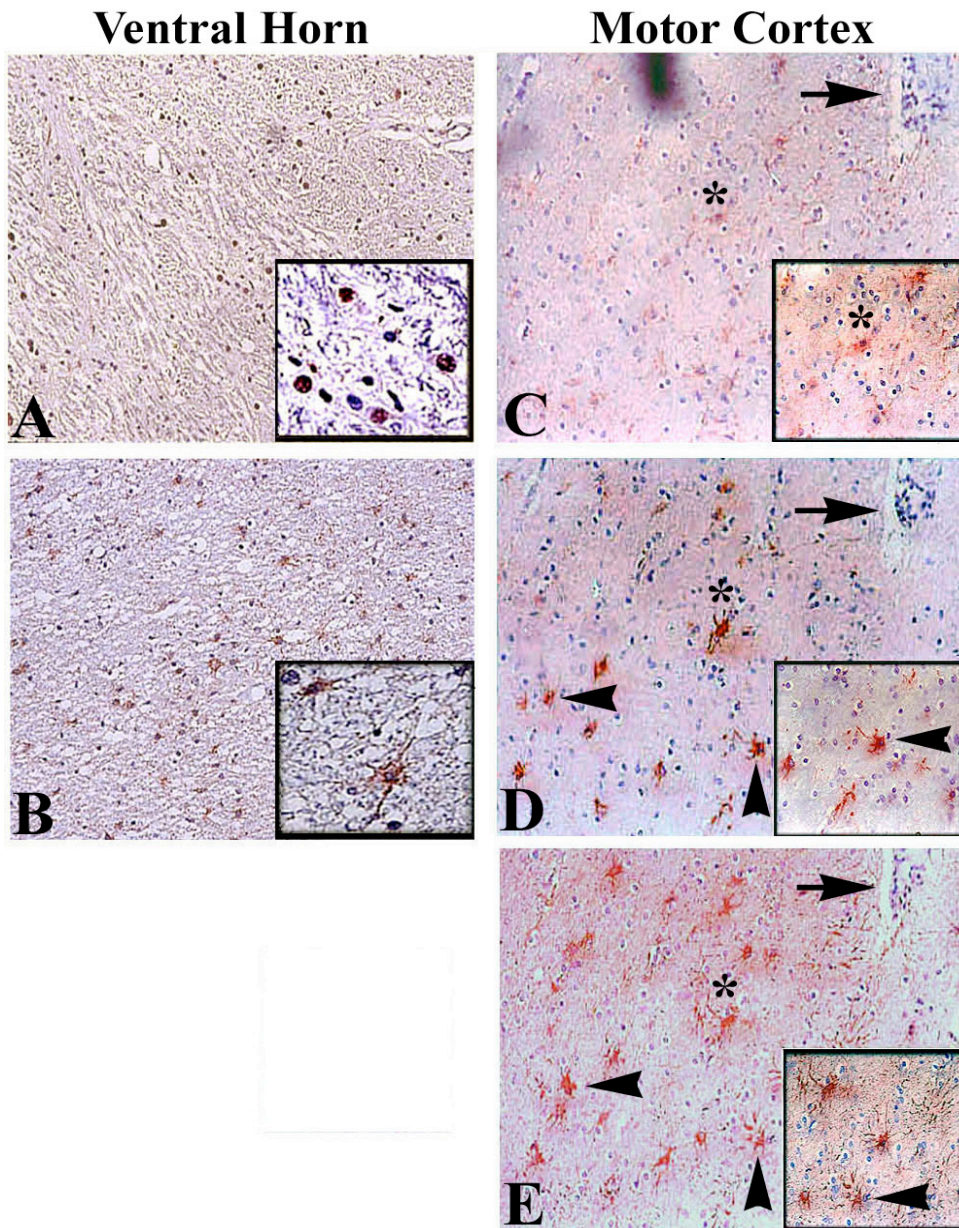


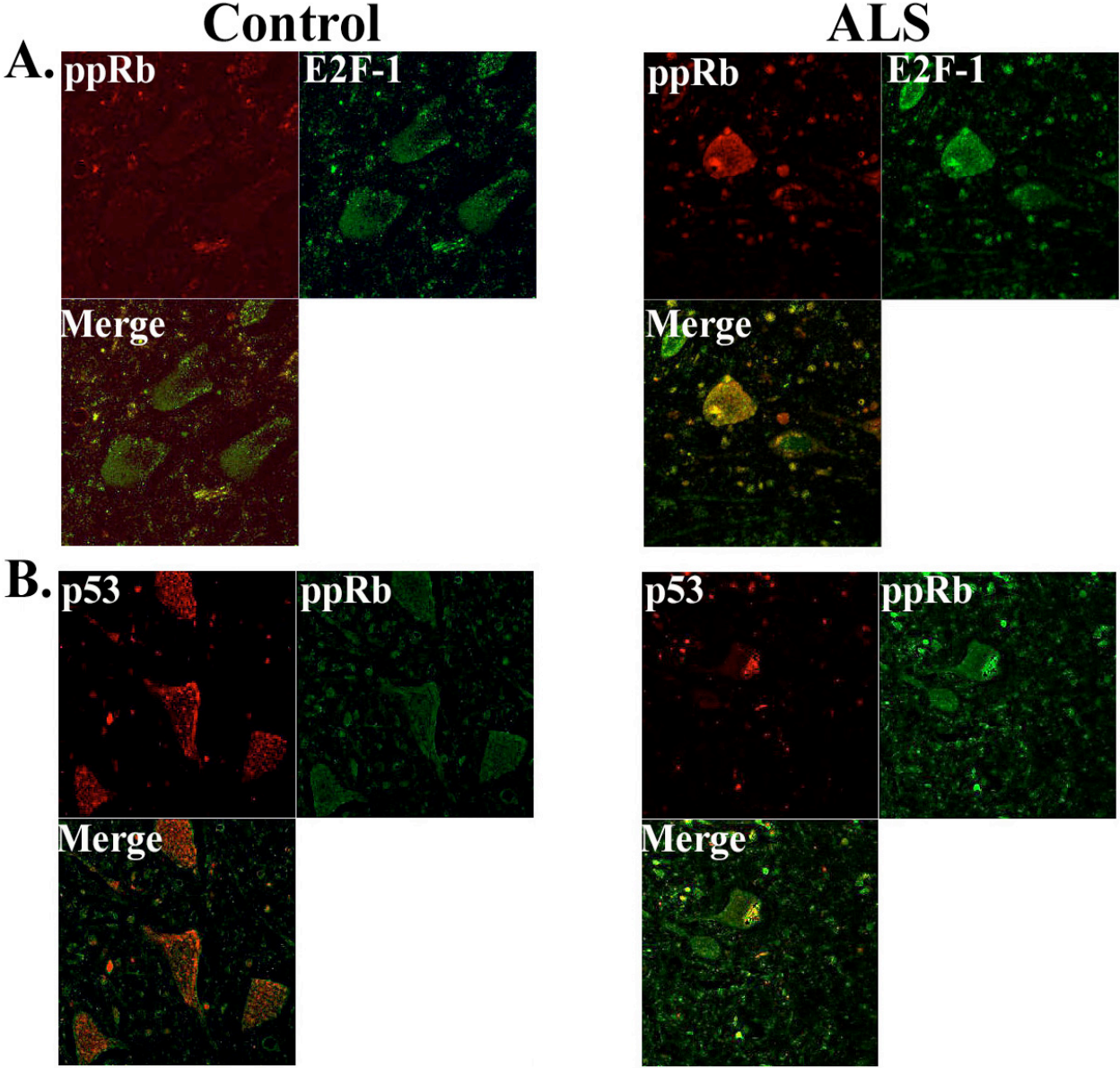
**Figure 15** Immunohistochemical analysis of ppRb and E2F-1 in glia in the white matter of ALS spinal cord and motor cortex

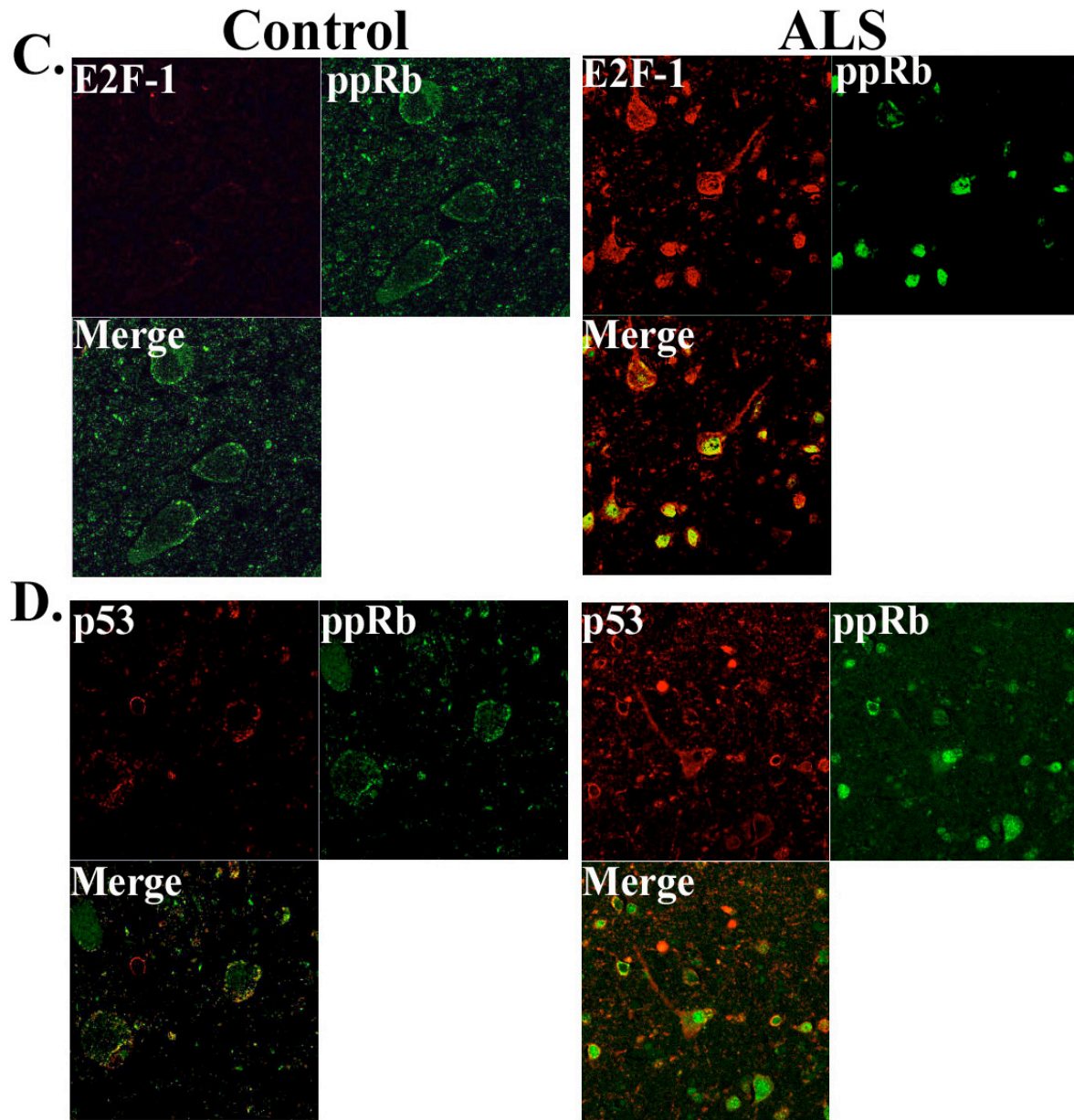
*Hyperphosphorylated Rb (ppRb) was in the nucleus of cells in the white matter of ventral horn of ALS spinal cord (A), while E2F-1 was cytoplasmic in cells that have an astrocytic morphology in ALS ventral horn white matter (B). However, both ppRb and E2F-1 appeared in the cytoplasm of cells in the motor cortex of ALS patients (C, D). Panels C, D and E represent ppRb, E2F-1 and glial fibrillary acidic protein (GFAP) staining in consecutive sections, with the arrow marking a blood vessel as landmark. The asterisk indicates a ppRb+GFAP+E2F-1+ cell, and arrowheads indicate E2F-1+GFAP+ cells. AEC was used to stain the antigens of interest (red) and each section counterstained with haematoxylin. Each panel is at a X200 magnification with the insets at X400. In relation to Table 2, panels represent cases ALS 8 (A), ALS 9 (B), ALS 4 (C, D, E). Reprinted from Am J Pathol 2003, 162:823-835 with permission from the American Society for Investigative Pathology.*

#### **2.4.4. Co-localization of ppRb, E2F-1 and p53 in ALS motor neurons using laser scanning confocal microscopy**

E2F-1 can transactivate tumor suppressor proteins such as p53 and p73, expressed in response to DNA damage. A more detailed analysis of p53 in human post-mortem ALS tissues will be presented in Chapter 3. To determine if ppRb, E2F-1 and p53 co-localize in the remaining motor neurons in the spinal cord and motor cortex, confocal microscopy was utilized. ALS spinal cord motor neurons that exhibited increased ppRb also demonstrated increased E2F-1 (68.5% of the motor neurons) and p53 (61%) (Fig 16, A and B). A total of 61 ALS motor neurons were counted. Abundant nuclear co-localization was specific in diseased lower motor neurons but not in control cases. In these studies, E2F-1 immunoreactivity was also present in the nucleus, contrasting the results from light microscopy or Western immunoblotting. While ppRb co-localized with E2F-1 in the remaining neurons (63.3% of 30 counted) in the ALS motor

cortex, there was no immunoreactivity of p53 detected in the motor neurons that expressed ppRb and E2F-1 (Fig 16, C and D).

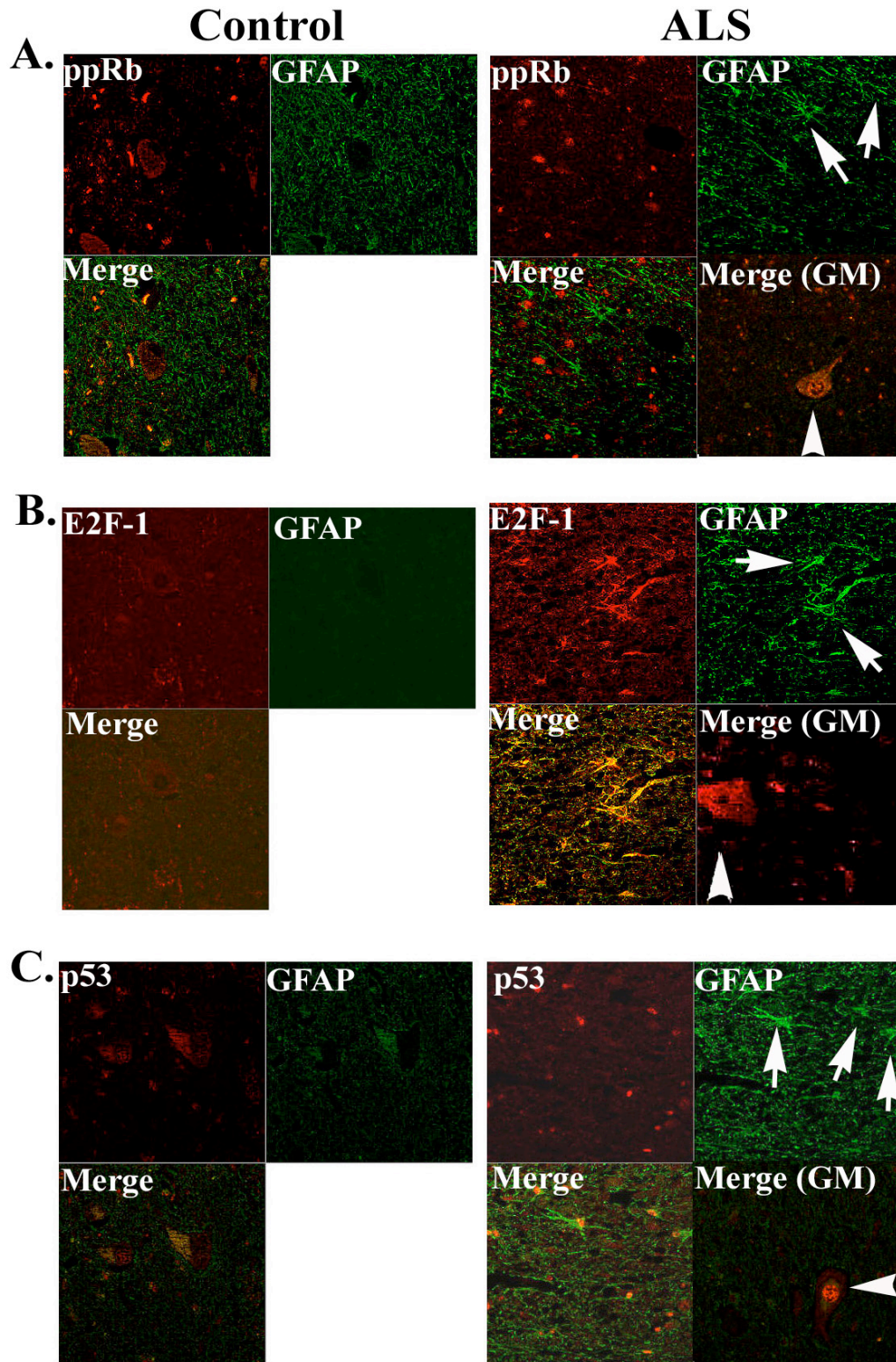




**Figure 16** Immunohistochemical co-localization analysis of ppRb, E2F-1 and p53 in motor neurons of ALS spinal cord (A, B) and motor cortex (C, D)

*Each of the panels are split into 4 quadrants with the top left representing antigen stained with a secondary antibody conjugated to a red dye (Cy5/Cy3) and the top right the antigen stained with a secondary antibody conjugated to a green dye (Alexa green), the bottom left represents the merged image with regions of protein co-localization appearing yellow and the bottom right*

remaining empty. The left and right sides represent control and ALS sections stained for the proteins pairs, respectively. All figures are at X400 magnification.



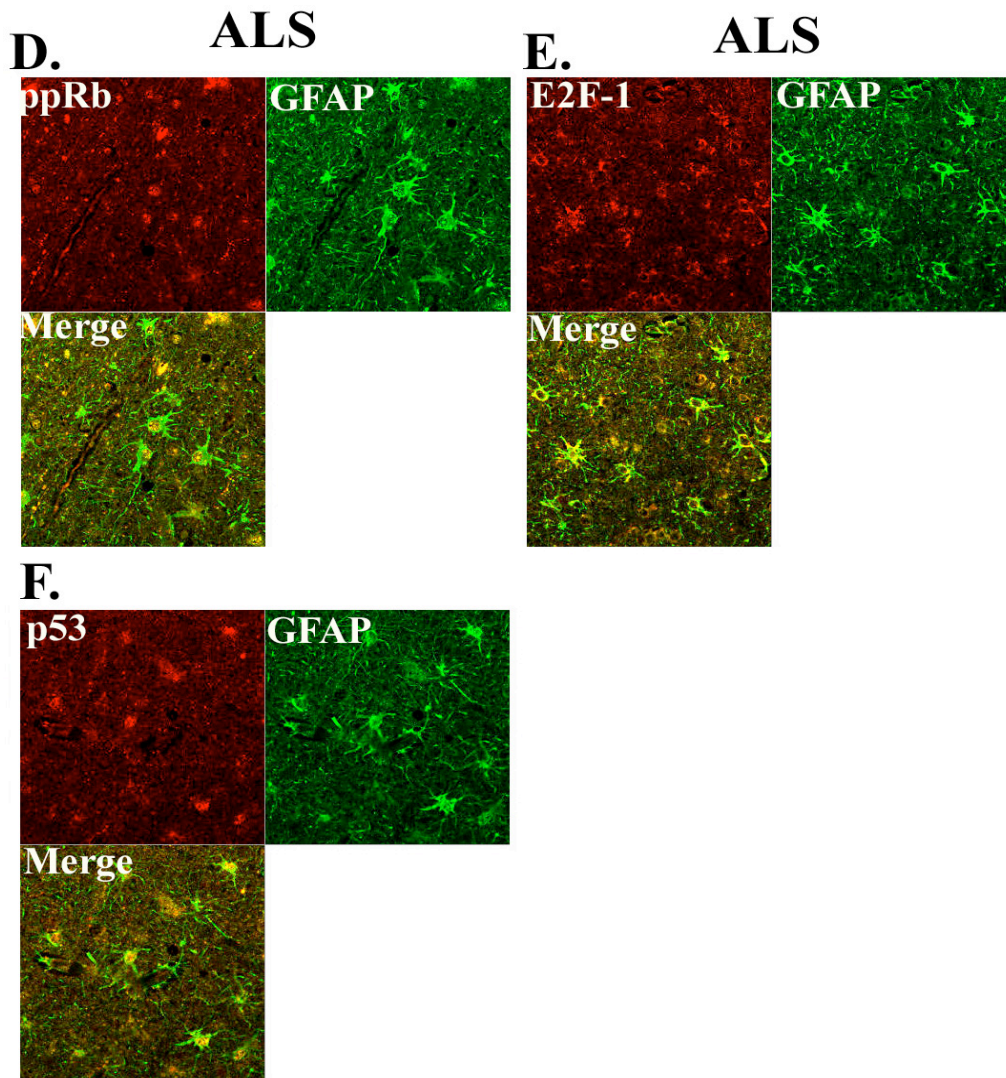


**Figure 17** Immunohistochemical co-localization analysis of ppRb, E2F-1 and p53 in activated astrocytes of ALS spinal cord (A-C) and motor cortex (D-F)

*GFAP is labeled with alexa green and the G1 to S phase regulators with Cy5 (red). (A-C) The merge panel shows GFAP(+) astrocytes that are ppRb+ (A), E2F-1+ (B), and p53+ (C). Arrows indicate astrocytes and arrowheads in merge panel (grey matter, GM) indicate motor neurons.*

*(D to F) GFAP(+) astrocytes in the motor cortex that are also positive for ppRb (nuclear, D), E2F-1 (cytoplasmic, E) and p53 (nuclear, F). All figures are at a magnification X400.*

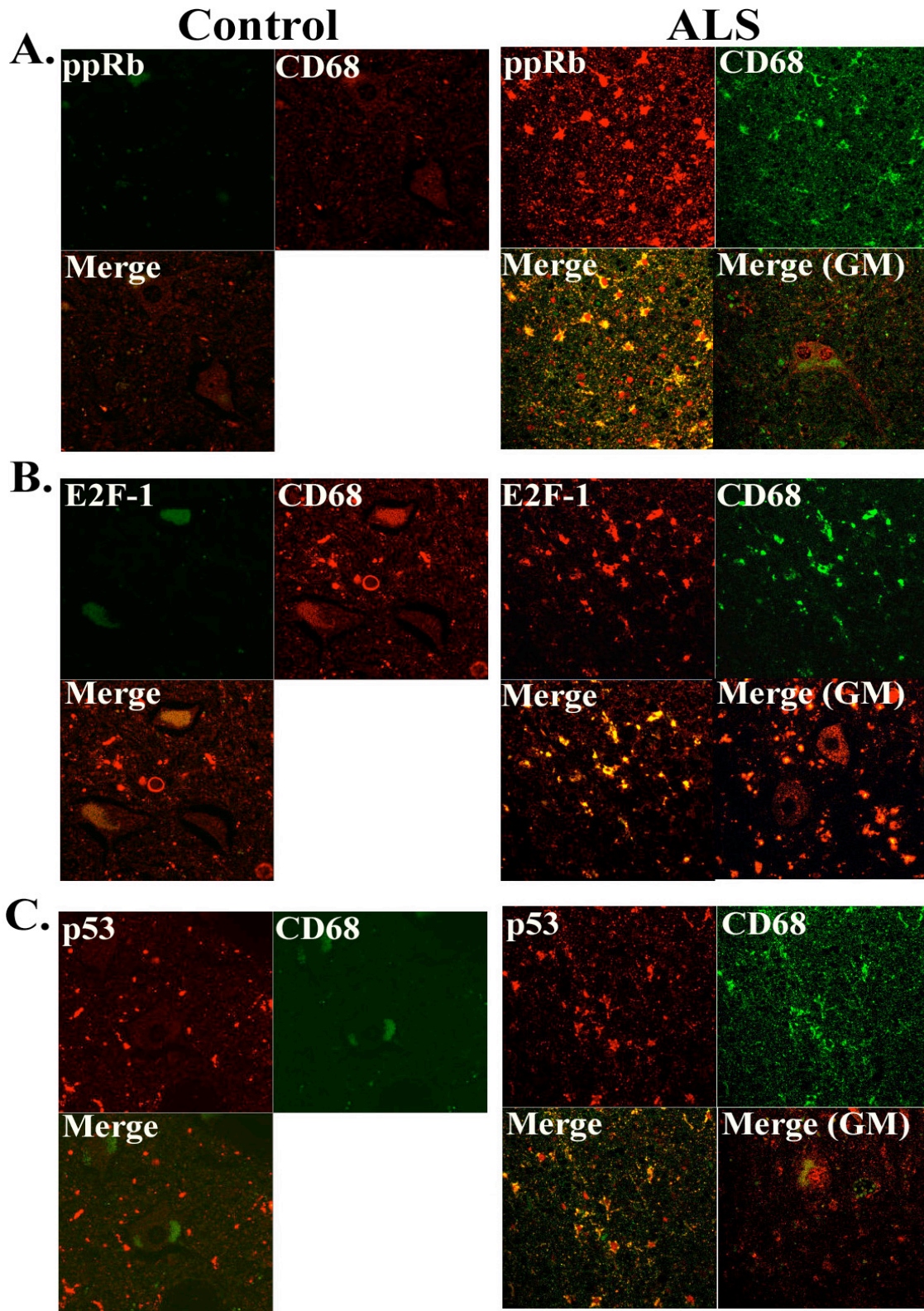


**Figure 18     Immunohistochemical co-localization analysis of ppRb, E2F-1 and p53 in activated microglia of ALS spinal cord (A-C)**

*Activated microglia have been labeled with alexa green with the G1 to S phase regulators labeled with Cy5 (red). Control panels are largely negative for all proteins. The merge panel shows CD68 (+) microglia that are ppRb+ (A), E2F-1+ (B), and p53+ (C). In the merge (grey matter, GM) panel, the ALS spinal cord motor neurons are CD68(-) but positive for ppRb (nuclear, A), E2F-1 (cytoplasmic, B), and p53 (nuclear, C).*

**2.4.5.            Co-localization of ppRb, E2F-1 and p53 in the white matter of ALS spinal cord and motor cortex using laser scanning confocal microscopy**

To corroborate the white matter staining at the level of light microscopy, the expression of these proteins in activated astrocytes and microglia of the spinal cord was analyzed using anti-GFAP and anti-CD68 antibodies, respectively. In the spinal cord, while ppRb and p53 appeared nuclear in GFAP positive activated astrocytes (Fig 17, A and C), E2F-1 localized in the cytoplasm and proteoplasmic processes of activated astrocytes (Fig 17B). In the motor cortex, ppRb and p53 were nuclear and E2F-1 was cytoplasmic in the activated astrocytes (Fig 17 D, F and E). Both ppRb and p53 appeared diffused in activated microglia (Fig 18, A and C). E2F-1 immunoreactivity in the cytoplasm and the processes of activated microglia (Fig 18B).

**2.4.6.            Analysis of protein levels by Western immunoblotting**

To determine if altered immunostaining correlates to increased protein levels in control and ALS spinal cords, we performed immunoblot analysis using total cell lysates from lumbar spinal cord tissues for 18 ALS and 9 control cases. We show representative data from ten ALS

and six control cases (Fig 19). The level of ppRb was significantly increased in the spinal cord of ALS patients, though the predominant pRb family member phosphorylated is p130 (Fig 19A & B). There was also an increase in phosphorylated Rb in nuclear extracts while it was undetected in post-nuclear supernatants (data not shown). We failed to detect altered levels of total pRb in nuclear extracts from control or ALS spinal cord, suggesting that phospho-pRb results from phosphorylation of pre-existing pRb (data not shown). Cyclin D1, CDK4 and E2F-1 expression exhibited increased levels in the total cell lysates (Fig 19A & B). Increased levels of Cyclin D1, ppRb and E2F-1 in ALS extracts were statistically significant ( $p \leq 0.05$ ). E2F-1 was increased specifically in soluble post-nuclear supernatants but undetectable in the nuclear fraction from spinal cord of ALS patients (data not shown). All protein levels were normalized to levels of actin and quantitated to demonstrate statistical significance of these findings (Fig 19).

We further examined protein expression in the motor cortex by immunoblot analysis. There was a decrease in levels of cyclin D1, CDK4, and E2F-1 in total cellular extracts (Fig 19C). This decrease was statistically significant for cyclin D1 ( $p \leq 0.05$ ). Hyperphosphorylated pRb (ppRb) was undetectable in the total cell extracts. However, we did notice a significant accumulation of ppRb in nuclear extracts of ALS patients but not in the post-nuclear supernatants (data not shown). Also, increased levels of cyclin D1 and E2F-1 were present in post-nuclear supernatants (data not shown). There was a significant 2-fold increase in the levels of active CDK4 in the nuclear fraction by immunoblot correlating with nuclear CDK4 immunoreactivity as noticed in many of the ALS cases (data not shown).

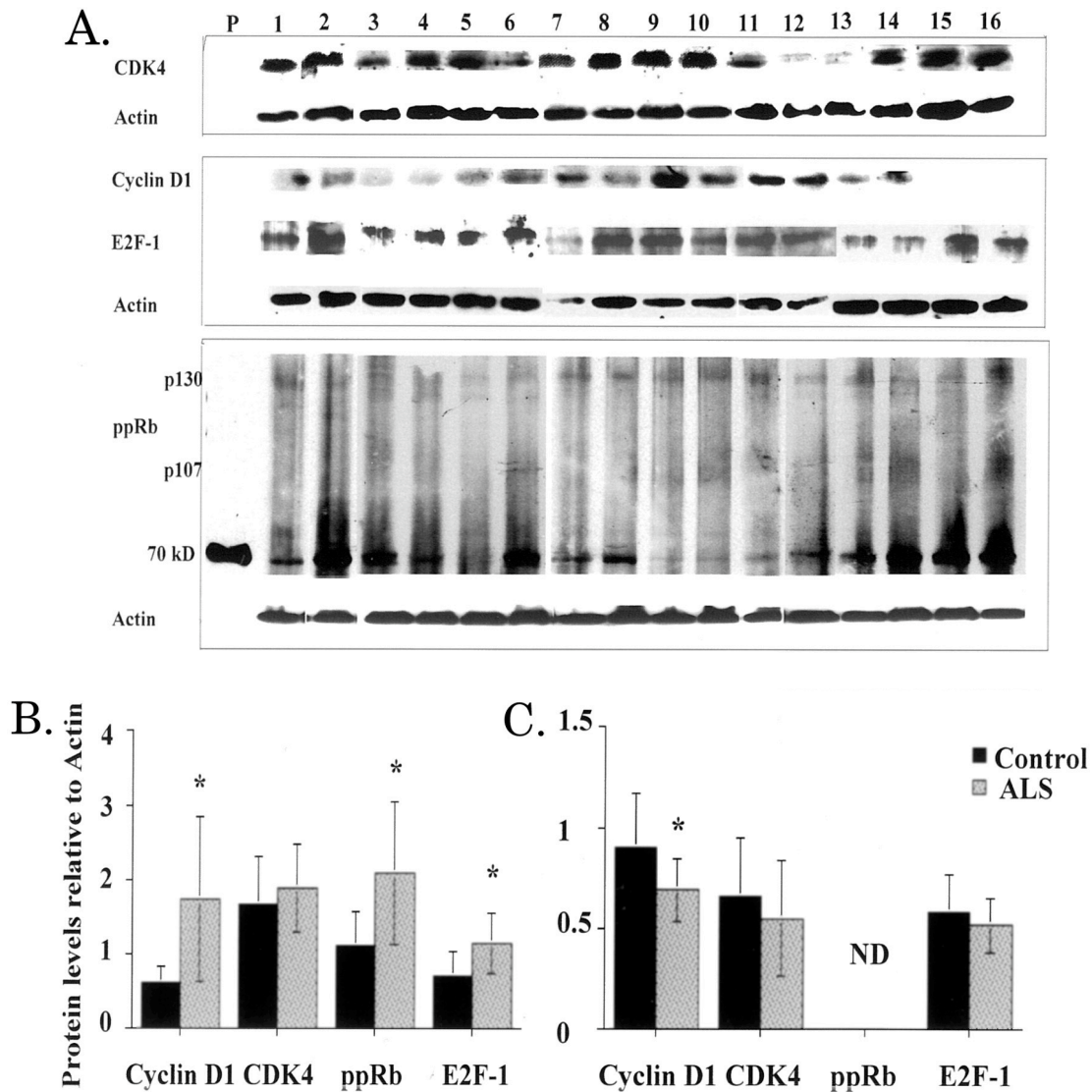


**Figure 19 Protein levels in total cell extracts from human spinal cord and motor cortex**

Protein extracts from lumbar spinal cord (A) and motor cortex (B) tissues of ten ALS (ALS 4 to 7, 13 to 18; Table 1) and six non-neurologic age-matched controls (C1, C4 to C7, C9; Table 1) were prepared as described in the Material and Methods. 150 µg of protein from each extract were loaded on SDS-PAGE and the resulting blots probed with antibodies specific to each protein. Immunoblots were repeated twice and all data quantified using NIH 1.58 software densitometry normalized to levels of actin in each sample. (A) Immunoblots of lumbar spinal

*cord total cellular extracts with the following lane assignments: P – Positive control (ppRb), Lanes 1-6 – Control cases, Lanes 7-16 – ALS cases; (B) and (C) are densitometric quantified representation of total cellular extracts from spinal cord and motor cortex, respectively with the bars denoting mean  $\pm$  standard deviation. Black bars are control cases (n = 6) and the gray bars are ALS cases (n = 10). ND indicates non-detectable levels. Statistical analysis was performed using single-factor ANOVA and asterisks indicate  $p \leq 0.05$ . In 19B, the p value for Cyclin D1, ppRb and E2F-1 was 0.046, 0.034 and 0.044, respectively. In 19C, the p value for Cyclin D1 was 0.04. Reprinted from Am J Pathol 2003, 162:823-835 with permission from the American Society for Investigative Pathology.*

#### **2.4.7. DNA-binding activity of E2F-1**

We next examined the DNA-binding activity of E2F-1 in control and ALS patients as a measure of E2F-1 functional activity. To evaluate DNA binding activity, gel mobility shift assays (EMSA) were performed using nuclear extracts from spinal cord and motor cortex, with extracts from proliferating NIH3T3 cells as positive control (see section 2.3.6). We first demonstrated that the very sensitive EMSA could detect nuclear E2F-1 that was below the limits of detection by immunoblot. The spinal and cortical nuclear extracts contained E2F-1 protein that bound the recognized E2F-1 binding element with specificity as demonstrated by competition with excess wild type cold oligos but not with excess mutant or unrelated oligos (Fig 20A). In Figure 20A, the slowest migrating complex is competed away by excess unlabelled oligos but not by mutant or unrelated and were interpreted to contain E2F-1. We next used nuclear extracts from proliferative 3T3 cell nuclear extracts as positive control (lane 2 in left panel of 20B) and competed the E2F-1 complex with increasing levels of excess cold oligo (Fig

20B, lanes 3 and 4). We next examined nuclear extracts of control and ALS spinal cord and motor cortex for E2F-1 DNA binding activity (Fig 20B). Densitometric measurement of the protein:DNA complex indicates no significant change in the intensity of DNA binding in spinal cord ( $p = 0.189$ ) or motor cortex ( $p = 0.724$ ) of ALS patients when compared to age-matched controls (Fig 20B&C).

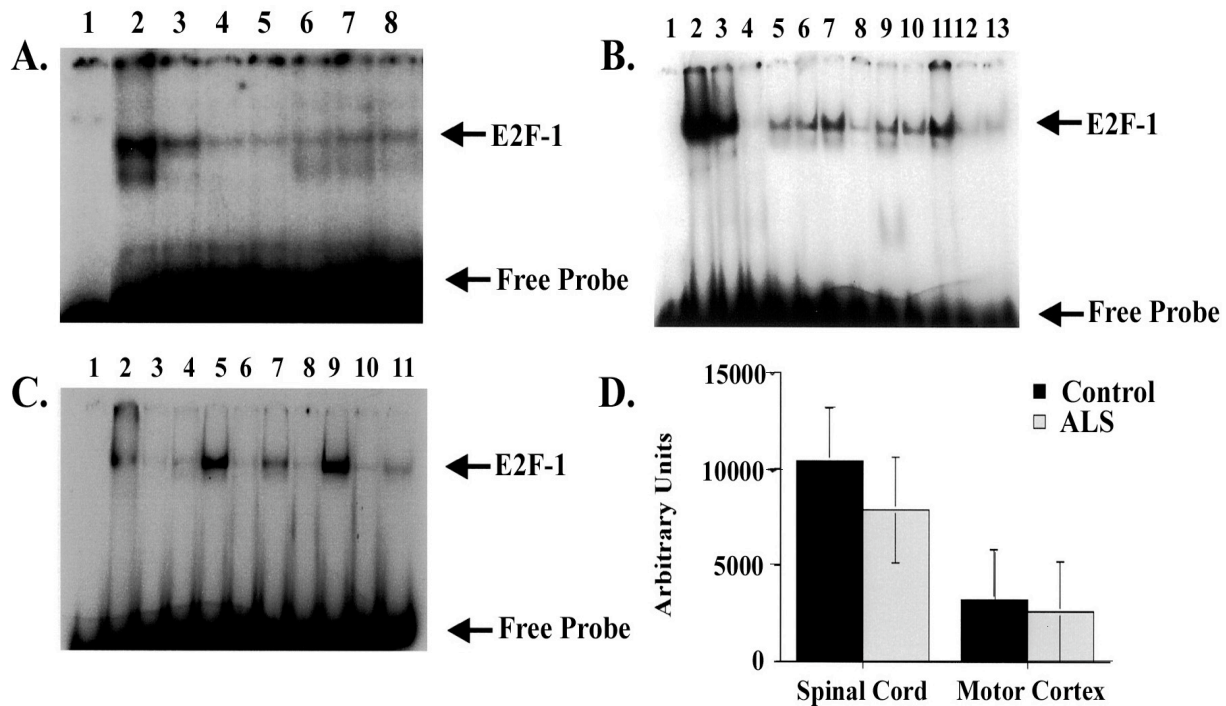


**Figure 20 E2F-1 DNA binding activity is unaltered in ALS**

*Nuclear extracts from spinal cord and motor cortex tissues of six ALS (case # 3-5, 9, 12 and 13, Table 2) and three non-neurologic age-matched controls (case # 1,2,3, Table 2) were used for electrophoretic gel mobility shift assay (EMSA). (A) is a competition EMSA using radiolabeled E2F-1 oligo and spinal cord nuclear extracts (25µg) indicating a concentration dependent competition (lanes 3 – 5) when excess cold oligos were used in the binding reaction. The complexes remain unaltered when excess mutant oligos (lanes 6 – 8) were utilized in the binding reactions. Lane assignments were as follows: Lane 1: Free probe, Lane 2: Hot probe, Lanes 3 –*

5: Excess cold oligos (3ng, 30ng, and 100ng, respectively), Lanes 6 – 8: Excess mutant oligos (30ng, 100ng, and 300ng, respectively). (B) is an EMSA using radiolabeled E2F-1 oligo and spinal cord nuclear extracts. Spinal cord gel lane assignments: 1: Free probe alone, 2: Positive control (3T3 cells), 3: Positive control with 3 ng cold oligo, 4: Positive control with 100 ng cold oligo, 5 – 7: Control cases (C1 – C3 from Table 1), 8 - 13: ALS cases (ALS 3-5, 9, 12, 13 from Table 1). (C) is an EMSA using radiolabeled E2F-1 oligo and motor cortex nuclear extracts. Motor cortex gel lane assignments: 1: Free probe alone, 2: Positive control (3T3 cells), 3 – 5: Control cases, 6 – 11: ALS cases (case # 3-5, 9, 12, 13 from Table 1). The E2F-1:DNA complex and free probes are indicated to the left of the figure. (D) depicts densitometric measurement of the E2F-1: DNA complex using NIH 1.58 software. Controls are denoted in black bars ( $n = 3$ ) and ALS cases in stippled bars ( $n = 6$ ). The  $p$ -values were 0.189 for spinal cord extracts and 0.724 for motor cortex using single-factor ANOVA with a 95% confidence interval. Reprinted from *Am J Pathol* 2003, 162:823-835 with permission from the American Society for Investigative Pathology.

## 2.5. Discussion

A delicate balance of signals regulates cellular homeostasis. Activation of cell cycle proteins via extracellular signals can be toxic to post-mitotic neurons in a number of model systems. We initiated this study to explore improper cell cycle activation and altered nuclear events as a possible mechanism in SALS. Aside from a previously published brief report and a study in a G37R mutant SOD1 transgenic mouse [121, 244], this is the first study examining a role for the G1 to S phase cell cycle proteins in pathogenesis of ALS [122]. We present evidence for nuclear accumulation of hyperphosphorylated pRb (ppRb) with concurrent increase in

cytoplasmic E2F-1 immunoreactivity suggesting a role for aberrant activation of G1 to S phase regulators.

Increased levels of cyclin D1 and its associated kinase, CDK4, in motor neurons of the affected region in ALS patients suggest aberrant re-activation of the cell cycle. The activation of G1 to S phase cyclins results in hyperphosphorylation and inactivation of the retinoblastoma proteins (ppRb). Post-mitotic motor neurons in ALS post-mortem tissues that exhibit altered levels of the regulators of the restriction point, namely ppRb and E2F-1, are considered to have “re-entered” the cell cycle. Sample-to-sample variation is likely due to the inherent cell type heterogeneity of the tissue sample extracts or due to protein degradation that may occur during the tissue extraction procedure.

During ALS, cellular insults to motor neurons can cause an aberrant activation of motor neurons and other cells into the G1 phase of the cell cycle. While conditions may not permit DNA replication and completion of the cell cycle, cell cycle proteins may increase the vulnerability of motor neurons to further toxic damage and cause apoptosis by reducing the threshold for cell death. The tumor suppressor, p53, is an important protein in making a cell’s decision to either arrest cell cycle or direct it towards apoptosis. The finding that G1 to S phase regulators (ppRb and E2F-1) are present in the same motor neurons that show aberrant levels of p53 in the lower motor neurons suggests that transactivation of genes downstream of E2F-1 (such as p53) can direct a cell to apoptose. It is intriguing that the remaining Betz cells in the cortical region of ALS subjects showed no immunoreactivity to p53. A more detailed analysis of p53 and discussion related to the dichotomous pattern of p53 immunoreactivity will follow in Chapter 3.

Improper activation of the cell cycle in motor neurons will alter the function of DNA binding proteins that can affect overall chromatin structure, thus permitting additional DNA damage via oxidative injury. Modifications to histones or E2F-1 itself can greatly affect the association of pRb/E2F-1 and transcriptional activity of E2F-1 or apoptosis [364]. ALSIN, a putative guanine exchange factor that has sequence homology to RCC1 (regulator of chromatin condensation) has been implicated in familial ALS (FALS) [91, 107]. RCC1 acts on RAN, a protein involved in nuclear import and export. Mutation in a protein that is homologous to a regulator of chromatin structure may make the cell more susceptible to DNA damage. DNA damage can be exacerbated by various endonucleases that signal various cell death pathways.

One of the intriguing results of our study was immunohistochemical data that indicates an altered localization of the E2F-1 transcription factor. Such alterations have been observed in studies using AD and SIV-E tissues [121, 245, 355, 362]. The E2F gene family comprises six members sharing homology in the Rb-binding domains [223, 225, 347]. These isoforms complex with the Rb family of proteins at different and defined periods of the cell cycle controlling gene expression within the G1 phase. The different binding states can translate to differences in subcellular localization of these proteins [365]. The re-distribution of E2F-1 during ALS may result from the formation of alternative protein:protein complexes containing E2F-1 or the retention of newly synthesized E2F-1 in the cytoplasm. Alternatively E2F-1 protein contained in the nucleus may not be recognized by the monoclonal antibody raised against the Rb-binding epitope and used throughout this study. To discern this, a second anti-E2F-1 antibody was utilized whose antigenic determinant site does not encompass the Rb-binding domain. Identical results were obtained with this antibody. Confocal microscopic results however indicate some E2F-1 immunoreactivity in the nucleus. This might be due to the higher sensitivity of the laser

scanning confocal microscope to identify low amounts of nuclear E2F-1. Nevertheless, the role of cytoplasmic E2F-1 in motor neuron cell death warrants further investigations within well defined in vitro model systems.

To examine the functional role of E2F-1 in the nucleus, gel shift assays were performed to determine DNA binding activity of E2F-1. The DNA binding activity of E2F-1 in the spinal cord and motor cortex did not show a significant difference between controls and ALS cases. This suggests that any changes in E2F-1 transactivational activity may be transient with a greater tendency for re-distribution into the cytoplasm. An alternate explanation to the cytosolic accumulation may be alterations in protein turnover. Reduced protein degradation through proteasomal inhibition may result in increased cytosolic E2F-1. In fact, ubiquitin positive protein aggregates are neuropathological hallmarks of ALS [67, 68, 73, 74]. Increased E2F-1 and p53 immunoreactivity was also found in the white matter of ALS spinal cord suggesting that cell cycle proteins in microglia and astrocytes may play a role in ALS. Activated glia can secrete neurotoxic substances such as cytokines and chemokines, which affect the neuronal milieu and result in neuronal death.

E2F-1 de-repression by pRb hyperphosphorylation leads to increased expression of downstream targets such as p53, p73, p14<sup>ARF</sup>, Apaf-1 and cytochrome c, which are involved in cell death pathways [366-370]. Although there are reports indicating an increased expression of p53 in both spinal cord and motor cortex further studies are required to examine the levels of other proteins regulated by E2F-1 [197]. p53 may directly activate pro-apoptotic genes [371]. Synergism between loss of pRb and activation of E2F-1 has been shown to contribute to p53-induced apoptosis [366, 372]. In addition, accumulated DNA damage through chromatin remodeling and de-repression of E2F-1 may contribute to p53-mediated apoptosis.

The data presented supports a model in which motor neurons are stimulated to enter the G1 phase of the cell cycle during ALS and activate cell cycle regulating proteins such as pRb and E2F-1, which assist in regulating motor neuron cell death (Fig 21). We have found increased levels of cyclin D1 and active CDK4 in the ventral spinal cord and motor cortex of ALS patients, concurrent with increased phosphorylation of pRb at a site (ser795). In addition, we have identified increased levels of E2F-1 protein in the cytoplasm of ALS motor neurons. These cell cycle-related changes may not be the cause for motor neuron death but would most likely reflect an event as a consequence of neuronal injury. This aspect however cannot be directly inferred from our study as it pertains to tissues from end-stage of disease. Further functional studies using in vitro cultures as enumerated in Chapter 7 can be performed to validate our current study.

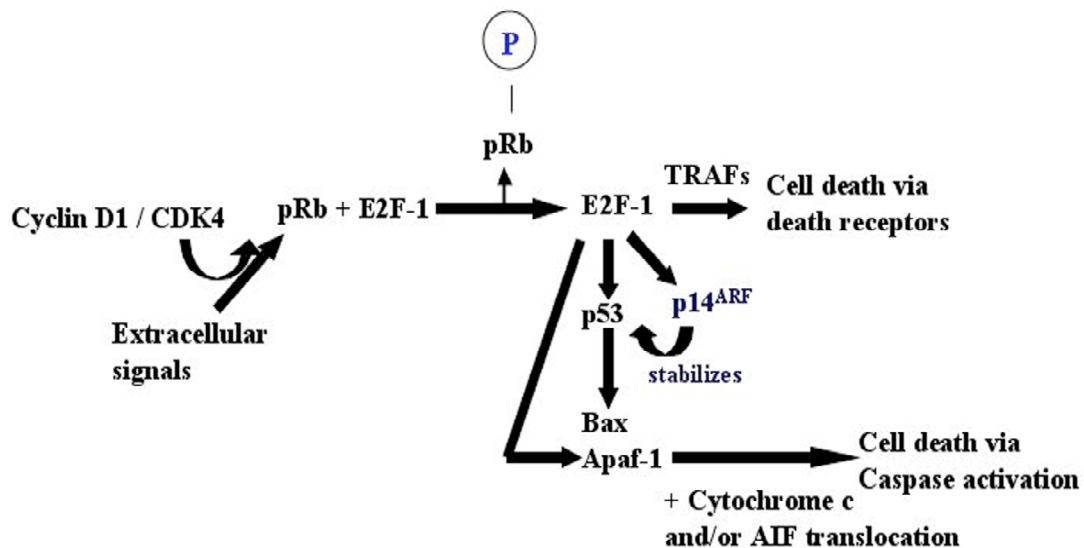


**Figure 21 Model of motor neuron cell death induced by activation of cell cycle proteins**

*In an adult post-mitotic neuron reduced levels of cyclin D-CDK4 results in repression of gene expression by the interaction of pRb with E2F-1. Also, TRAF proteins complexes with death receptors (DR) such as p75<sup>NTR</sup> blocking cell death. However, upon extracellular signals, increased levels of cyclin D-CDK4 result in hyperphosphorylation of pRb (ppRb) with release of*

*E2F-1. Transcriptional activity of E2F-1 results in initiating death signals via induction of p14<sup>ARF</sup>, p53, Bax, Apaf-1, and cytochrome C (Cyt C), apoptotic regulators that would in turn activate pro-apoptotic proteins such as caspase-9 and caspase-3. Alternatively, E2F-1 in the cytoplasm may interact with TNF receptor associated factors (TRAF) and permit DR mediated cell death. Activation of these pathways may sensitize the neuron to further toxic insults that pushes the susceptible neuron towards death. Reprinted from Am J Pathol 2003, 162:823-835 with permission from the American Society for Investigative Pathology.*

The results from this body of work are corroborated by a murine study, which demonstrates increased expression of CDK4/cyclin D1 and hyperphosphorylation of pRb [244]. This G37R SOD1 mouse model of ALS does not reveal any changes in levels of CDK2 or CDK6 and the authors have not reported anything related to proteins downstream of ppRb [244]. Whether other mouse models will reveal similar changes as from our human post-mortem study is speculative. However our study of a role for G1 to S phase regulators in ALS coupled with studies in other neurodegenerative diseases have led to a hypothesized link between oxidative damage and abortive cell cycling in post-mitotic neurons [373, 374]. Unless more studies indicate the existence of ploidy supporting the one study performed in AD, and the presence of G2 to M phase markers *in vitro*, the theory of an “abortive cell cycling without S phase progression” in neuronal death will predominate. Future studies will further define the intracellular signaling pathways involved in cell cycle activation and explore the functional role of p53 in motor neuron cell death. These studies may reveal that an abortive cell cycling event in susceptible populations of neurons can lead to a caspase-dependent or caspase-independent (AIF-mediated) neuronal death.

### 3. Neuronal Cell death in ALS: Role of p53 mediated apoptosis

#### 3.1. Abstract

Apoptosis is a mechanism of cell death reported to occur in many neurodegenerative diseases, including ALS. Furthermore, the demonstration that caspase inhibitors delay disease onset and prolong survival in animal models of ALS directly link this energy-dependent mode of cell death to motor neuron death during ALS (see Chapter 1). We have demonstrated a role for G1 to S phase regulators in ALS with alteration in the levels of ppRb, E2F-1 and p53 (Chapter 2). *We further hypothesize that altered levels of p53 will have a role in motor neuron death during ALS with concurrent changes in the levels of apoptotic death markers.* For this study we utilized archived human post-mortem motor cortex and spinal cord tissues of ALS and age-matched non-neurological controls. Through the use of western immunoblotting, light microscopy as well as laser scanning confocal microscopy, we report elevated levels of nuclear p53 in remaining ALS spinal cord motor neurons but not the surviving neurons in the motor cortex. In addition, we demonstrate increased protein levels of Bax, Fas, caspases-8 and -3 in ALS spinal motor neurons. While caspase-3 and TUNEL stained neurons were also positive for ppRb, E2F-1 and p53 in spinal motor neurons, we failed to observe this trend in Betz cells in the motor cortex of ALS subjects. In conclusion we have linked the aberrant re-activation of G1 to S phase cell cycle regulators to an apoptotic mode of cell death in a p53-dependent manner in ALS spinal cord motor neurons.

### **3.2. Introduction**

The control of cell proliferation or growth arrest is intimately linked to the control of programmed cell death or apoptosis. Cell cycle components such as pRb, E2F and p53 function in both cell cycle progression and apoptosis. In fact the promoters of p53, p73, human cytochrome c1 and apoptotic protease activating factor 1 (APAF1) contain E2F-1 binding sites suggesting a direct E2F-1-mediated transcriptional regulation [369, 370, 375, 376].  $\beta$ -amyloid-mediated toxicity in PC12 cells was found to be mediated by the E2F-1 – p53 – Bax pathway and the over-expression of E2F-1 in these cells led to the induction of p53 (by E2F-1) and Bax (by p53) proteins, as well as nuclear fragmentation [377]. These studies directly link E2F-1 to p53 and apoptosis. As the “guardian of the genome”, p53 regulates the cell cycle by triggering growth arrest or apoptosis due to the presence of errors in DNA acquired during replication or inability to properly repair DNA damage. Depending on the cell type, over-expression of p53 can result in either cell growth arrest or apoptosis [226-229]. Conversely, a knockout of p53 produces resistance to apoptosis with the mice typically dying from T-cell lymphomas [230, 378]. Thymocytes from these mice are resistant to DNA damaging agents such as ionizing radiation and topoisomerase II inhibitors (etoposide) but not to cell death induced by glucocorticoids or phorbol ester [379]. Thus both p53-dependent and independent cell death pathways exist. Furthermore, efficient p53-dependent apoptosis is through DNA strand breaks.

Upon completion of synaptogenesis during brain development, adult neurons enter a quiescent G0 phase. The action of various toxins such as reactive oxygen species or glutamate can push the neuron into G1. This inappropriate or untimely transition can initiate an apoptotic response. Indeed both in acute and chronic neurological disease models, a role for aberrant cell cycle re-activation leading to an increase in p53 function and subsequent apoptosis of neuronal

cells have been established. These cell death studies include paradigms of  $\beta$ -amyloid, presenilin-1, DNA damage, oxidative stress, depolarization, and 6-hydroxydopamine (6-OHDA) [380-389]. Inhibition of p53 through the use of antisense and dominant negative constructs protects neurons from this wide array of insults [383, 388].

While cell death during ALS is believed to be apoptotic in nature, this is an area of active research and debate. The debate stems from the fact that ALS is a chronic neurodegenerative disease and apoptosis typically is rapid and occurs early during disease pathogenesis. Morphological studies involving apoptotic features in SOD1 transgenic models report a high degree of vacuolation evident in ALS spinal motor neurons. Although vacuoles are not as evident in human post-mortem tissues, other apoptotic features such as chromatolysis, somatodendritic attrition and nuclear condensation have been reported [288]. However, factors such as plausible relatively quick disappearance of apoptotic bodies resulting in low numbers of apoptosis-positive motor neurons have impeded a clear morphological analysis of apoptosis in ALS motor neurons. Increased levels of other apoptotic markers such as the carbohydrate antigen LeY, fractin, p53, Bax, activated caspases, and the apoptosis-related prostate apoptosis response-4 (PAR-4) proteins lend support for an apoptotic mode of cell death in ALS [119, 126, 127, 197, 266, 290, 305, 390-394]. It is plausible that apoptosis is a relevant mechanism albeit not the only one in ALS.

Defective DNA repair and enhanced DNA damage are evident in ALS motor neurons [140, 195, 203, 395]. Increased p53 with concomitant elevation in DNA binding activity has been demonstrated in motor neurons and astroglia of the affected regions of ALS patients but not that of controls [197]. These studies are corroborated with studies in an ALS transgenic mouse over-expressing mutant G86R SOD1 protein [396]. Collectively, these studies suggest a

functional role for p53 and apoptosis during neurodegenerative diseases. However, the role of p53 has been questioned due to results obtained from other SOD1 mice studies. One group generated double transgenics by mating p53<sup>-/-</sup> mice with the mice expressing the high copy number G93A mutation (G93A+) [397]. To summarize their results, they reported that the lack of p53 did not alter disease onset or progression in the double transgenics. Another similar study (with low copy number G93A mutant mice) reported identical results [398]. The pre-symptomatic G93A mice in the second study displayed disease-associated vacuoles irrespective of the genotype of p53. The two reports challenging the role of p53 can however be explained as a mechanism exclusive to FALS or that there are sequential activation of p53-dependent and -independent modes of multiple types of cell death (apoptosis, necrosis or paraptosis). Overall, the role for p53 in ALS remains controversial and unclear.

Amongst the pro-apoptotic genes that p53 regulates are BAX, Apaf-1, SIVA, PUMA and Fas [371, 399-402]. Pro-apoptotic protein levels such as that of active homodimeric Bax, Bad, Bid, and Harakiri levels are increased in vulnerable CNS regions in ALS patients [119, 392, 396, 403, 404]. Conversely, the levels of anti-apoptotic proteins such as Bcl-2 and Bcl-X<sub>L</sub> are decreased. These alterations in the G93A SOD1 transgenic mice are significantly noticeable as the neurodegenerative process progresses. In animal studies, the pro-apoptotic proteins activate caspases that effect the final death blow to the motor neuron. The role for caspases in ALS is supported by the reports of caspase inhibitors significantly reducing motor neuron death in G93A mice and PC12 cells [290]. Increased activity of caspase-1, an inflammatory-associated protease and caspase-3, the effector protease has been reported in human spinal cord as also in G37R, G85R and G93A SOD1 transgenics [126]. Caspase-12, associated with ER stress has also been implicated in ALS [405]. In addition the TNF- $\alpha$  / caspase-8 pathway has been associated with

being a delayed contributor to the degenerative process in a mouse model of ALS [404]. Bax through the apoptosome / mitochondrial pathway and Fas via the death-receptor / caspase-8 pathway activate the effector caspase (caspase-3), which result in DNA fragmentation. Programmed cell death involving the Fas / caspase-8 / caspase-3 apoptotic cascade has been documented in embryonic motor neurons and also in primary motor neurons from the G37R, G85R and G93A mutant SOD1 ALS transgenics [406].

In spite of all these reports, there is no study addressing the role for p53 and an apoptotic death cascade downstream of aberrant activation of G1 to S phase regulators. *Therefore we hypothesized that alterations in the cell cycle regulator, p53, will result in concurrent changes in apoptotic death markers during ALS (Fig 12).* We present evidence for increased accumulation of p53 in the nucleus of ALS spinal cord motor neurons but not neurons of the motor cortex. The lack of p53 in the motor cortex contradicts previous reports [197]. Laser scanning confocal microscopy demonstrates that the G1 to S phase cell cycle regulators co-localize with markers of apoptosis (TUNEL and Caspase-3). Hence, these results suggest a role for p53 and caspases in conjunction with aberrant re-activation of cell cycle regulators during ALS.

### **3.3. Materials and Methods**

Protocols for source of tissue samples (2.3.1), immunohistochemistry for light microscopy (2.3.3), protein extraction (2.3.4), immunoblotting (2.3.5) and statistical analysis (2.3.7) are described in detail under section 2.3.

### **3.3.1. Antibodies**

Monoclonal antibodies were used to detect p53 (Santa Cruz, DO-1), and FAS (Santa Cruz, B10). Polyclonal antibodies were utilized to detect Actin (Chemicon), BAX (Pharmingen), Caspase-3 (Cell Signaling), Caspase-8 (Biomed), p73 (Santa Cruz, H79). For light microscopy, these antibodies were utilized at dilutions of 1:100 (Caspase-8), 1:150 (p53, Caspase-3, BAX), 1:200 (BAX). For confocal laser scanning microscopy, we used primary antibody concentrations of 1:80 (ppRb, p53, Caspase-3, Caspase-8, Fas), 1:60 (E2F1).

### **3.3.2. Electrophoretic Mobility Shift Assay (EMSA)**

Gel mobility shift assays were performed as described in section 2.3.6 with the following modifications. The sequences used to probe for p53 specific DNA binding activity were: WT p53 5'-TACAGAAC **A T G** TCTAAGCATGCTGGGGACT -3'; MT p53 5'-TACAGAAT**TCGCT**TCTAAGCATGCTGGGGACT -3'. For competition reactions, unlabeled p53 competitor (3, 30, and 100ng) or unlabeled unrelated competitor (5'-GATCATT**CAGGTC**ATGACCTGA-3'; 100, and 300ng) oligos were preincubated with the protein for 5 min on ice prior to addition of labeled probe. The positive control for p53 DNA binding activity was camptothecin-treated SHYSY5 neuroblastoma cells.

### **3.3.3. Terminal deoxynucleotidyl transferase-mediated biotinylated UTP nick end labeling staining (TUNEL)**

DNA fragmentation was assayed using the fluorescein based apoptosis detection system as per manufacturer's instructions (Promega, USA). Briefly, paraffin embedded sections were processed as for immunohistochemistry and post-blocking were treated with Proteinase K

(20µg/ml) for 15m. They were then incubated with TdT enzyme / nucleotide mix for 1h at 37°C. For double labeling with confocal laser scanning microscopy, the sections were immunolabeled with p53 or ppRb after TUNEL labeling. Negative (no enzyme) and positive (DNase I treated) samples were utilized. Motor neurons positive for TUNEL and cell cycle proteins (ppRb, p53) were quantified. A total of 30-40 and 20-30 motor neurons in the spinal cord and cortex were counted respectively at X400 magnification. The study was conducted in a blinded fashion using 11 ALS and 6 age-matched control cases.

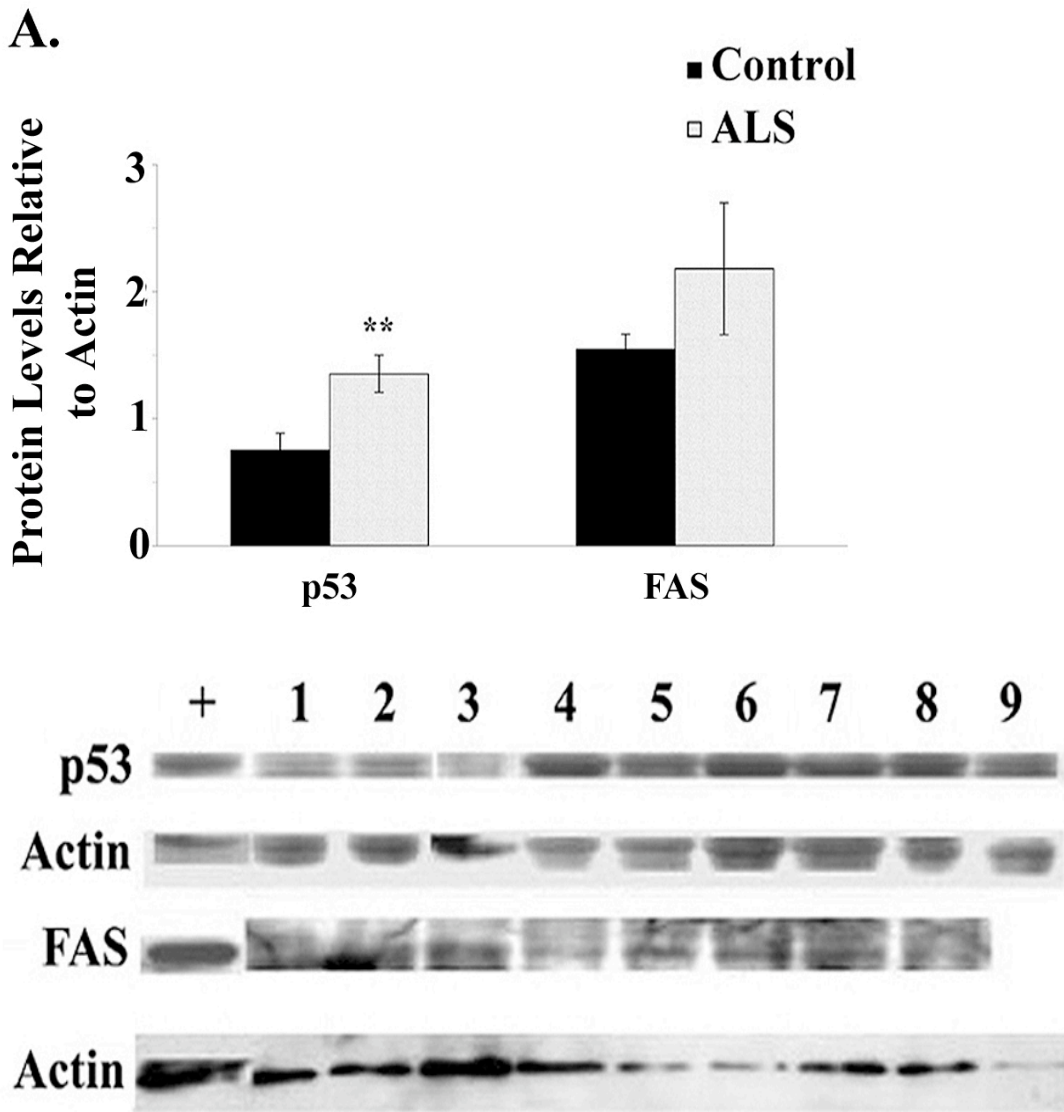
### **3.4. Results**

Aberrant re-activation of G1 to S phase cell cycle proteins can have downstream effects on cell survival by activating molecules such as p53. To further characterize the role of p53 and apoptosis in neuronal cell death during ALS, we investigated the levels of p53, Bax, Fas, Caspases-8 and -3 in human post-mortem tissues from ALS and age-matched control cases. As described in the previous chapter, we utilized tissue samples from both lumbar spinal cord and motor cortex (mid- and superior-motor cortical region). The dorsal horn of the spinal cord and sensory cortex were the internal controls for immunohistochemistry.

#### **3.4.1. Analysis of death marker protein levels by Western immunoblotting**

Western immunoblotting was performed using nuclear, soluble and total tissue lysates from lumbar spinal cord and motor cortex of 18 ALS and 10 control cases. We show representative immunoblots from 3 controls and 6 ALS (Fig 22, A and B (Fas and Caspases)) and 5 controls and 7 ALS (Fig 22B, p53 and p73). All immunoblot signals were normalized to actin and quantitated as previously described. The levels of activated p53 were significantly

increased in the nuclear extracts and the total lysates of ALS spinal cord (Fig 22, A and B). Since p53 can transactivate pro-apoptotic molecules such as Bax, we examined the levels of Bax and other pro-death proteins such as Fas, caspase-8 and caspase-3. Interestingly, the level of the transmembrane receptor, Fas, was increased in the nuclear lysates in addition to the total tissue lysate (Fig 22, A and B).



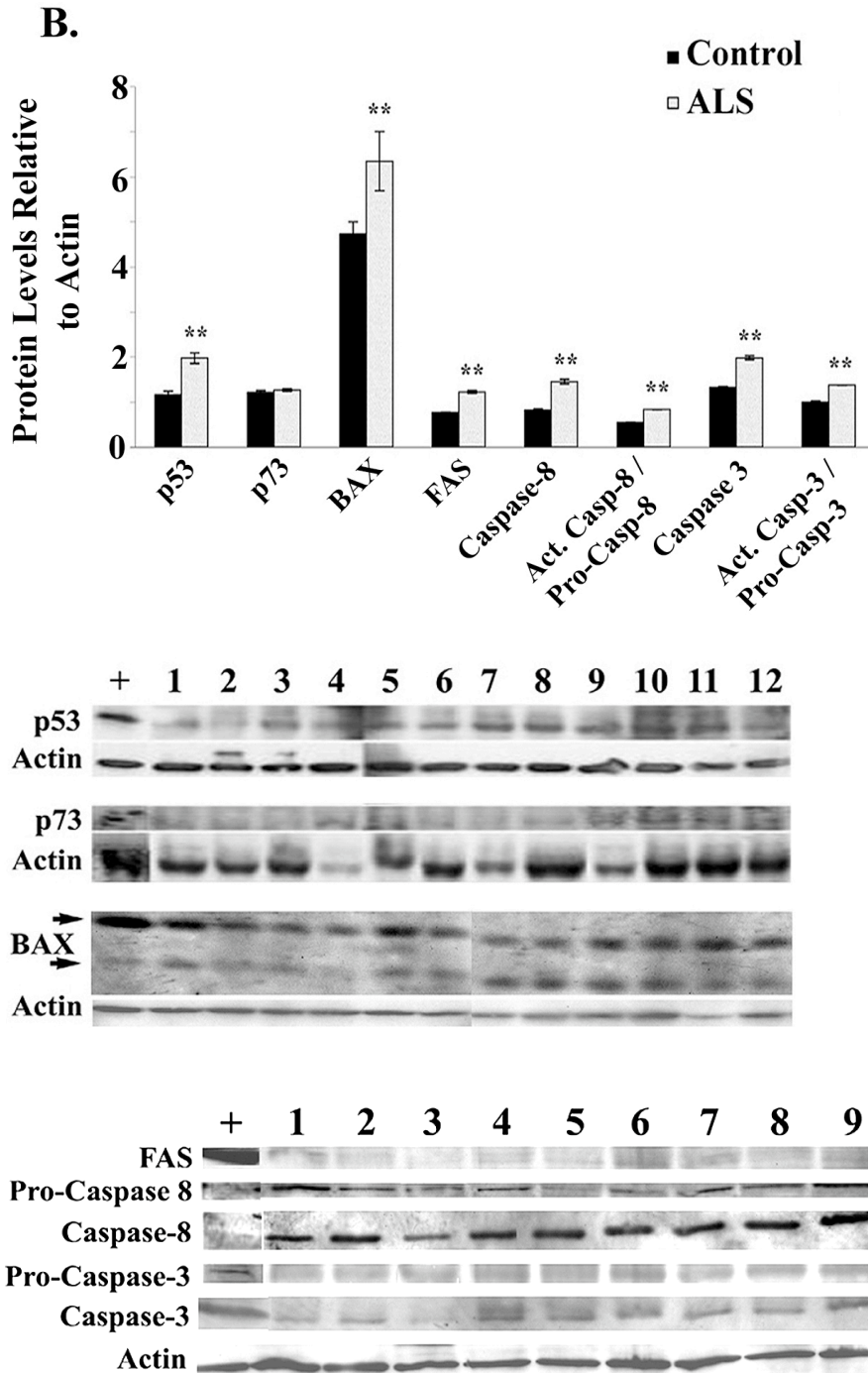


**Figure 22** Increased p53 and death markers in ALS spinal cord tissue lysates

(A) Quantitation of protein expression in nuclear extracts from spinal cord. Black bars are control cases (n=3) and the gray bars are ALS cases (n=6). Statistical analysis was performed

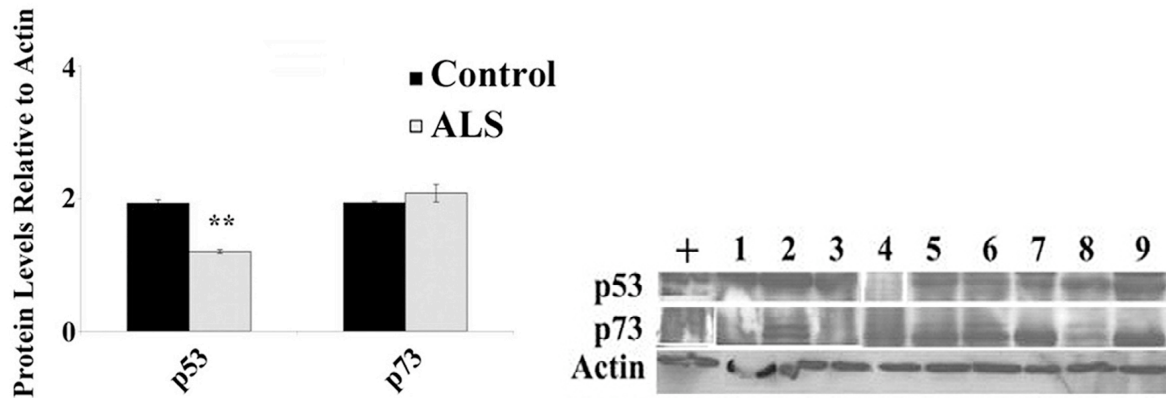
using single-factor ANOVA and asterisks indicate  $p \leq 0.05$ . The  $p$  values for p53 and Fas were 0.0006 and 0.089, respectively. All of these were normalized to Actin.

The respective immunoblots are also presented below the graph. “+” indicates positive control, lanes 1 to 3 are control cases and lanes 4 to 9 are ALS cases.

(B) Quantitation of protein expression in total tissue extracts from spinal cord. Black bars are control cases ( $n=10$ ) and the gray bars are ALS cases ( $n=18$ ). Statistical analysis was performed using single-factor ANOVA and asterisks indicate  $p \leq 0.05$ . The  $p$  values for p53, p73, Bax, Fas, caspase-8 and caspase-3 were 0.009, 0.75, 0.009, 0.03 and 0.018, respectively. All of these were normalized to Actin. The  $p$  values for the ratios of active- to pro caspase-8 and caspase-3 were 0.008 and 0.008, respectively. The lane assignments for the p53, p73 and Bax immunoblots are as follows: “+” indicates positive control, lanes 1 to 5 are control cases and lanes 6 to 12 are ALS cases. Lanes for the Fas and Caspases are as follows: “+” indicates positive control, lanes 1 to 3 are control cases and lanes 4 to 9 are ALS cases. The arrows to the right of the BAX blots indicate that there are two bands (p19 and p21kDa) recognized by the antibody.

We next examined protein expression in the motor cortex by immunoblot (Fig 23). In contrast to our results from lumbar spinal cord tissues, we observed that p53 was significantly decreased in nuclear extracts and undetectable in total lysates (Fig 23, A and B). Since E2F-1 can also activate other members of the p53 family such as p73, we performed immunoblotting to analyze its levels in ALS motor cortical tissues. While there was no difference in its levels in the nuclear extracts, it was significantly decreased in the total lysates (Fig 23B). Fas and Caspase-8 exhibited no significant changes in protein levels and the levels of Bax and caspase-3 were undetectable (Fig 23B).

**A**



**B**

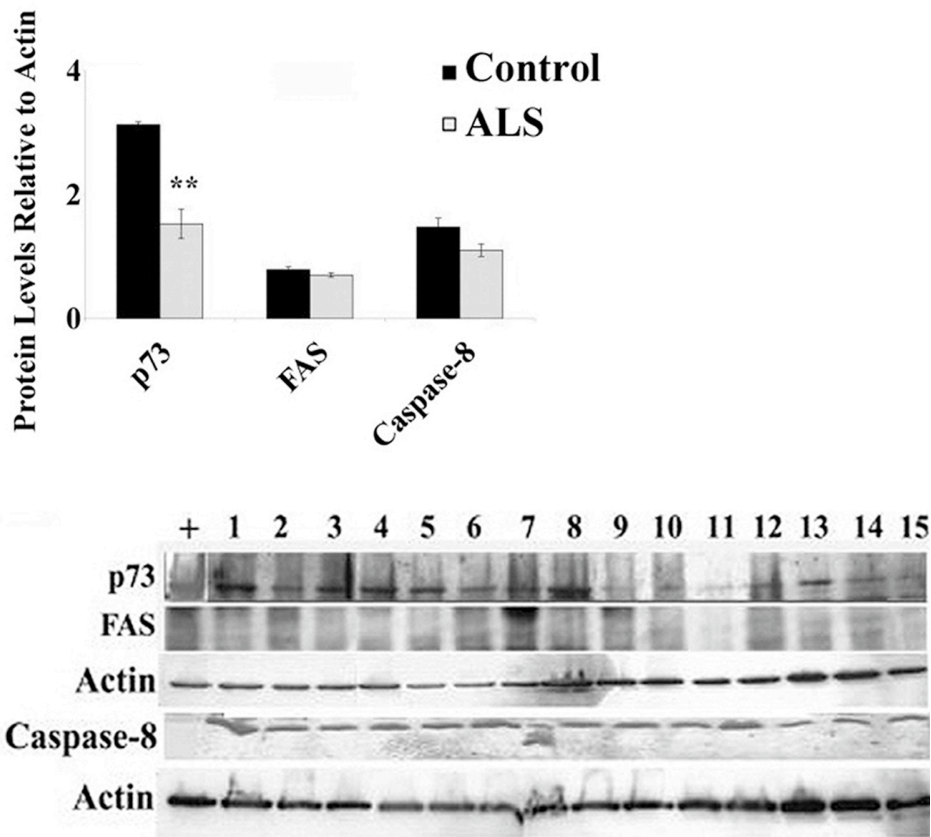


**Figure 23** Decreased p53, p73 and no change in death markers in ALS motor cortex tissue lysates

*(A) Quantitation of protein expression in nuclear extracts from motor cortex. The p values for p53 and p73 were 0.007 and 0.68, respectively. All other details are as described for Fig 22A.*

*Quantitation of protein expression in total tissue extracts from motor cortex. The p values for p73, Fas, and caspase-8 were 0.0007, 0.62, and 0.22, respectively. The lane assignments are as follows: “+” indicates positive control, lanes 1 to 6 are control cases and lanes 7 to 15 are ALS cases. All other details are as described for Fig 22B.*

### **3.4.2. Increased immunoreactivity of p53 in ALS spinal cord but not motor cortex**

Western immunoblotting of tissue extracts presents the caveat of having a mixed population of cells. Therefore we utilized immunohistochemistry to analyze cell specific and subcellular localization of p53 in ALS tissues. Paraffin-embedded sections from lumbar spinal cord and motor cortex of human ALS and age-matched control cases were analyzed by light microscopy.

The percentage of p53 immunoreactive motor neurons was only 38.3% in control subjects (Fig 24A). Much of the p53 in the control cases was cytoplasmic in its localization. Approximately 83.5% (from a total of 200) of the spinal cord motor neurons in ALS cases exhibited abundant nuclear accumulation of p53 (Fig 24B). It was negligible or absent in the dorsal horn sensory neurons (Fig 24C). We then examined if p53 was increased in the surviving Betz cells of the motor cortex. Sections at different regions of the motor cortex were analyzed for p53 levels. p53 immunoreactivity was absent in both the motor and sensory neurons of ALS and the age-matched controls (Fig 24, D to F).

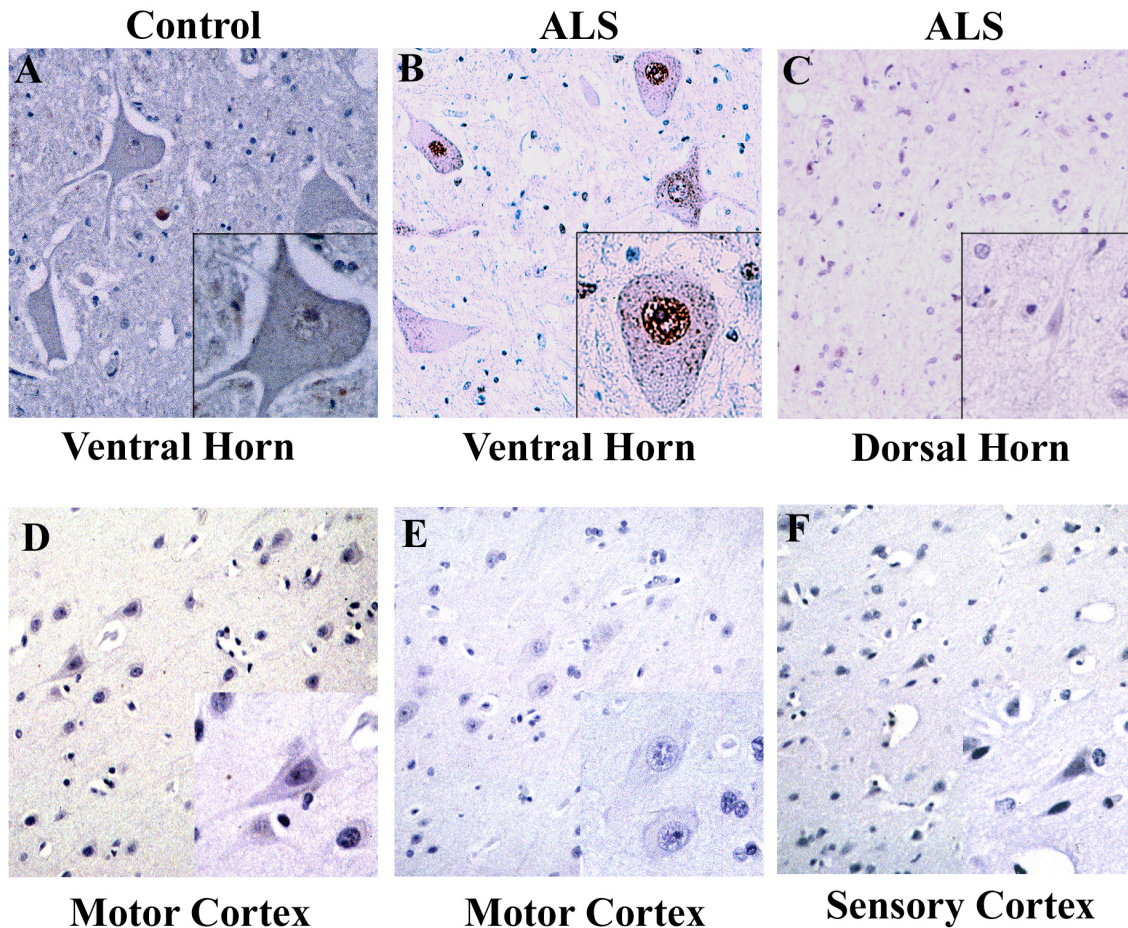


**Figure 24** Increased immunoreactivity of p53 in spinal cord motor neurons but not in the motor cortex

*Lumbar spinal cord (A to C) and motor cortex (D to F) tissues from 18 ALS and 9 non-neurological disease controls were immunostained for p53 using a phospho-specific anti-p53 antibody. Each panel is at X200 magnification with the insets at X400. All insets are of the same cases as the lower magnification. Relative to panels A and D (controls), there is nuclear abundance of p53 in ALS spinal cord (B) but not motor cortex (E). Panels C and F are the internal controls for the respective regions.*

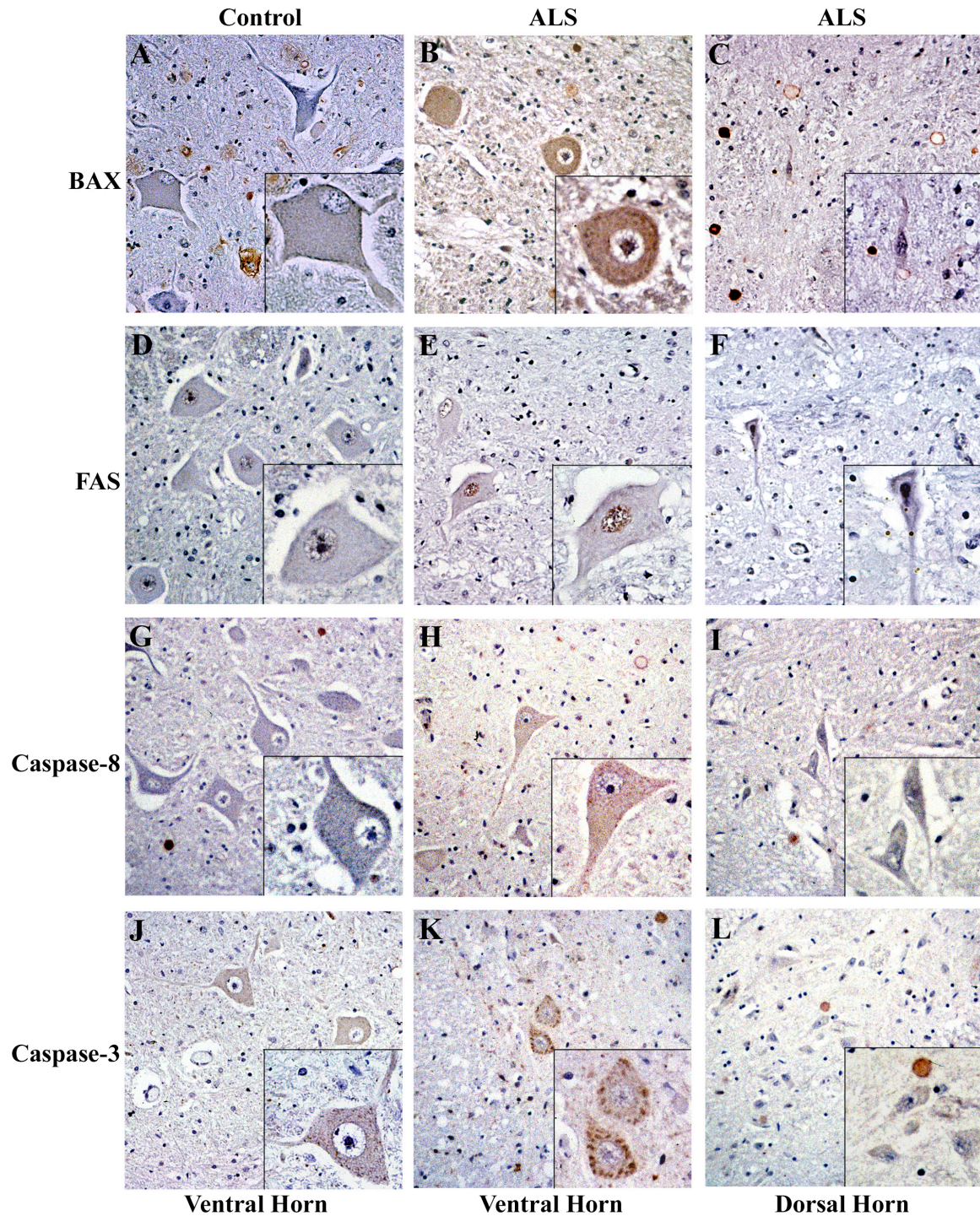


**Figure 25 Increased immunoreactivity of death markers in spinal cord motor neurons**

*Lumbar spinal cord tissues from 18 ALS and 9 non-neurological disease controls were immunostained for BAX (A to C), Fas (D to F), caspase-8 (G to I) and caspase-3 (J to L). Each*

panel is at X200 magnification with the insets at X400. All insets are of the same cases as the lower magnification. Relative to panels A, D, G and J (controls), there is increased BAX (B), nuclear Fas (E), caspase-8 (H) and caspase-3 (K) in ALS spinal cord motor neurons. Panels C, F, I and L represent negative staining in unaffected sensory neurons of the ALS spinal cords.

### **3.4.3. Subcellular distribution of apoptotic death markers in spinal cord and motor cortex**

Similar to p53, we analyzed the distribution of other pro-apoptotic proteins by immunohistochemistry. Bax immunoreactivity was significantly elevated in ALS spinal motor neurons but not in the dorsal horn sensory neurons (Fig 25, A to C). Since death receptor mediated neuronal cell death is evident during development and also *in vitro*, we examined the levels of Fas, which associate with death domains containing adaptor proteins (FADD). In the spinal cord motor neurons of ALS cases, we document increased and specific nuclear localization for Fas (Fig 25, D to F). Caspase-8 is a downstream effector of Fas activation. We observed increased active caspase-8 immunoreactivity in the spinal cord motor neurons (Fig 25, G to I). Finally since both Bax and Fas-mediated death pathways converge on caspase-3, the effector protease, we analyzed its immunoreactivity in the two affected regions of ALS cases. We report increased caspase-3 in the spinal motor neurons (Fig 25, J to L). Furthermore, immunoreactivity to p73 showed no difference in spinal cord or motor cortex of ALS cases (data not shown).

In the motor cortex, there was positive BAX immunoreactivity in neurons but it was not very specific to the remaining large pyramidal neurons (data not shown). Fas immunoreactivity was negligible in the large pyramidal neurons of the motor cortex (Fig 26A). Caspase-8 staining

in the motor cortex was predominantly non-specific with little immunoreactivity (Fig 26B) and was not significantly different from that in the control cases (data not shown). Although the neurons in the motor cortex exhibited caspase-3 signal (Fig 26C), this was non-specific and its immunoreactivity was also detected in the cortical neurons of control cases (data not shown).

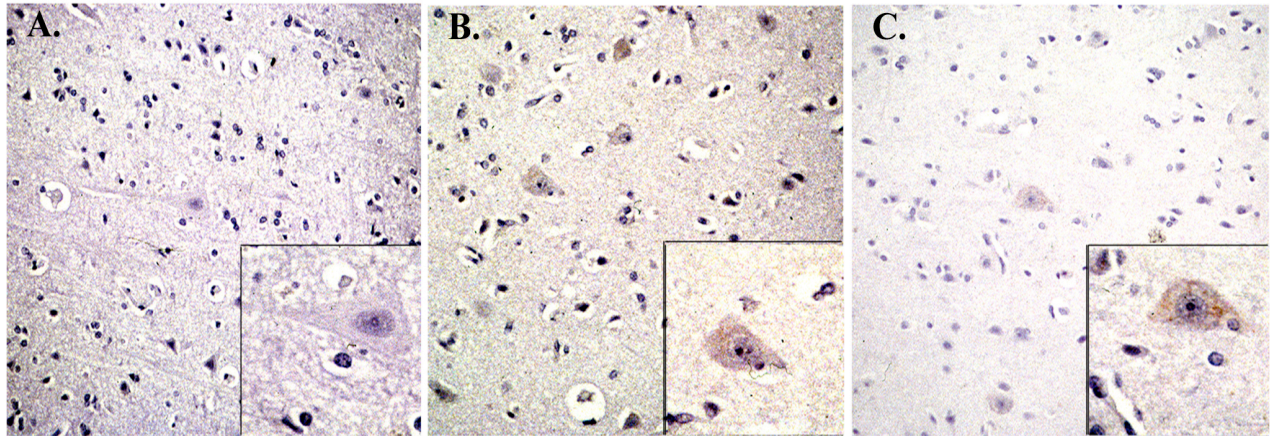


**Figure 26 No change in immunoreactivity of death markers in cortical motor neurons**

*Motor cortex tissues from 18 ALS and 10 non-neurological disease controls were immunostained for Fas (A), caspase-8 (B) and caspase-3 (C). Each panel is at X200 magnification with the insets from the same cases at X400.*

#### **3.4.4. Co-localization of cell cycle proteins and apoptotic death markers in ALS spinal cord and motor cortex**

In the previous chapter, we reported co-localization of p53 with ppRb and E2F-1 in spinal cord motor neurons (Fig 16, A and B).

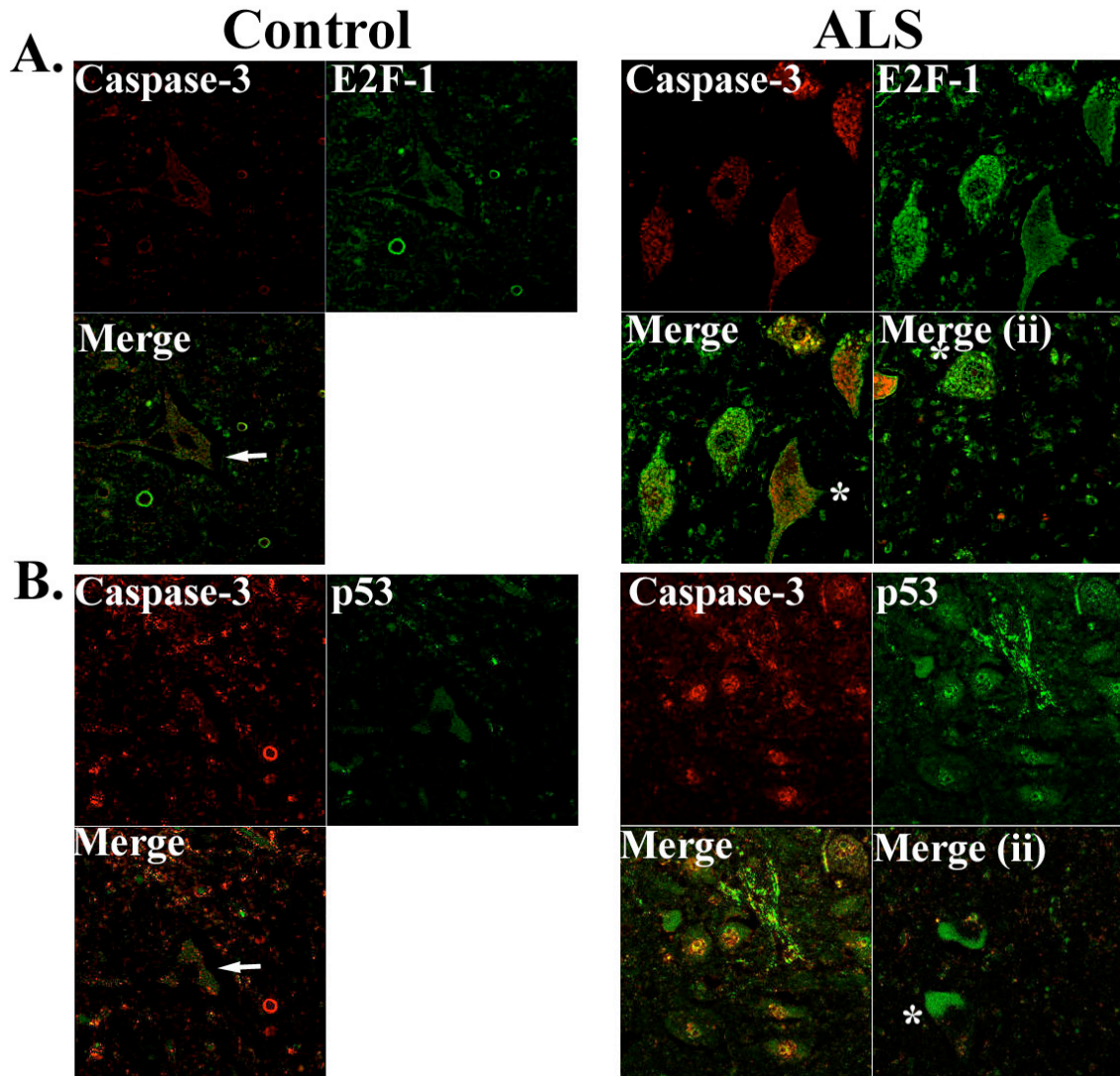


**Figure 27 Cell cycle transcription factors co-localize with death markers in spinal motor neurons (A and B)**

*Lumbar spinal cord (A and B) from 11 ALS and 6 age-matched controls were labeled with the combinations of p53 or E2F-1 (alexa green conjugated secondary antibody) with active caspase-3 (Cy5 conjugated secondary antibody). Arrows in the control panels indicate motor neurons. Asterisk in the Merge (ii) panel indicate ALS motor neurons that are positive for E2F-1 (A) and p53 (B) but not caspase-3.*

We further analyzed the co-localization of the transcriptional regulators E2F-1 and p53 with caspase-3, a marker of apoptosis, by laser scanning confocal microscopy. An increased number of ALS spinal motor neurons exhibited co-localization of p53 / caspase-3 (36.9%) (Fig 28A) and E2F-1 / caspase-3 (21.8%) (Fig 27B). A total of 73 motor neurons from 12 tissue sections were counted. Caspase-3 positive motor neurons in the ALS cases were not widespread, i.e., not all motor neurons were positive for caspase-3 (asterisks in Merge (ii) of Fig 27A and B). The motor neurons in control cases lack E2F-1 immunoreactivity and exhibited low levels of cytoplasmic caspase-3 (<1%). However, in the few neurons of these control cases that were only positive for p53 (12.3%) the staining was cytoplasmic. In neurons of the ALS motor cortex p53 and caspase-3 immunoreactivity was negligible or absent corroborating the results from immunoblotting (Fig 28A). However these motor neurons were positive for ppRb (data not shown) and E2F-1 (arrowhead in Fig 28B).

Furthermore, we observed that the death receptor Fas co-localized with caspase-8 in the cytoplasm of spinal cord motor neurons (34.2%) (Fig 29). Both proteins were present in the nucleus with caspase-8 also localized in the cytoplasm. The nuclear staining of Fas confirmed the results from light microscopy. In the cortical motor neurons, there was negligible staining for either protein (data not shown).

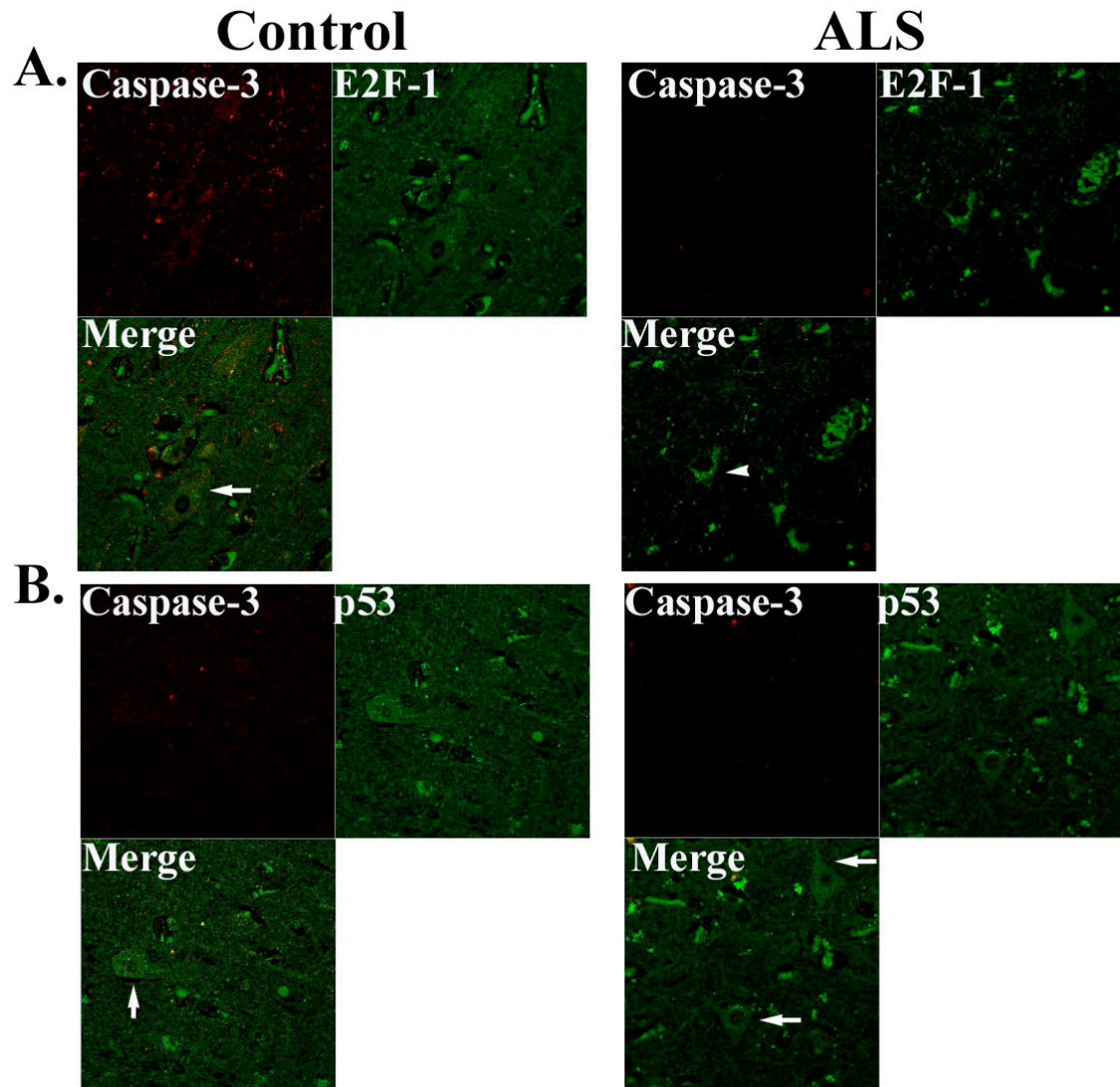


**Figure 28** Cell cycle transcription factors co-localize with death markers in cortical motor neurons (A and B)

*Motor cortex from 11 ALS and 6 age-matched controls were labeled with the combinations of p53 or E2F-1 (alexa green conjugated secondary antibody) with active caspase-3 (Cy5 conjugated secondary antibody). Arrows indicate motor neurons negative for E2F-1, p53 and Caspase-3. Arrowhead in (A) indicates ALS motor neuron that is positive for E2F-1 but not caspase-3.*

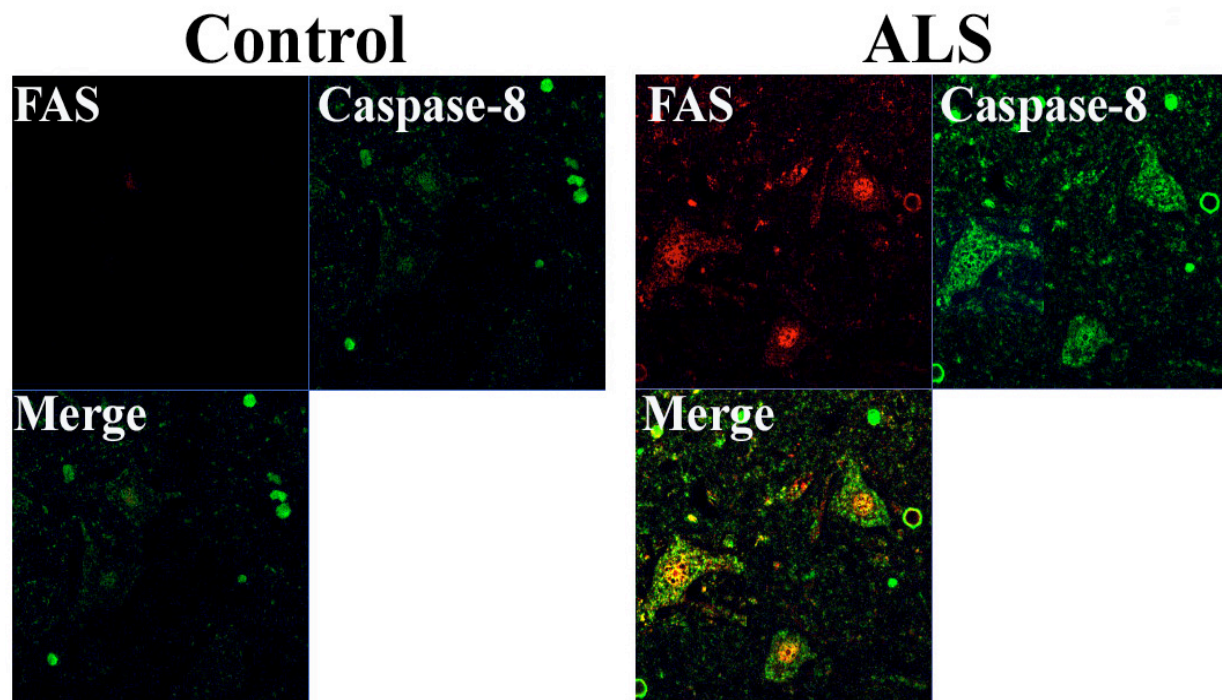
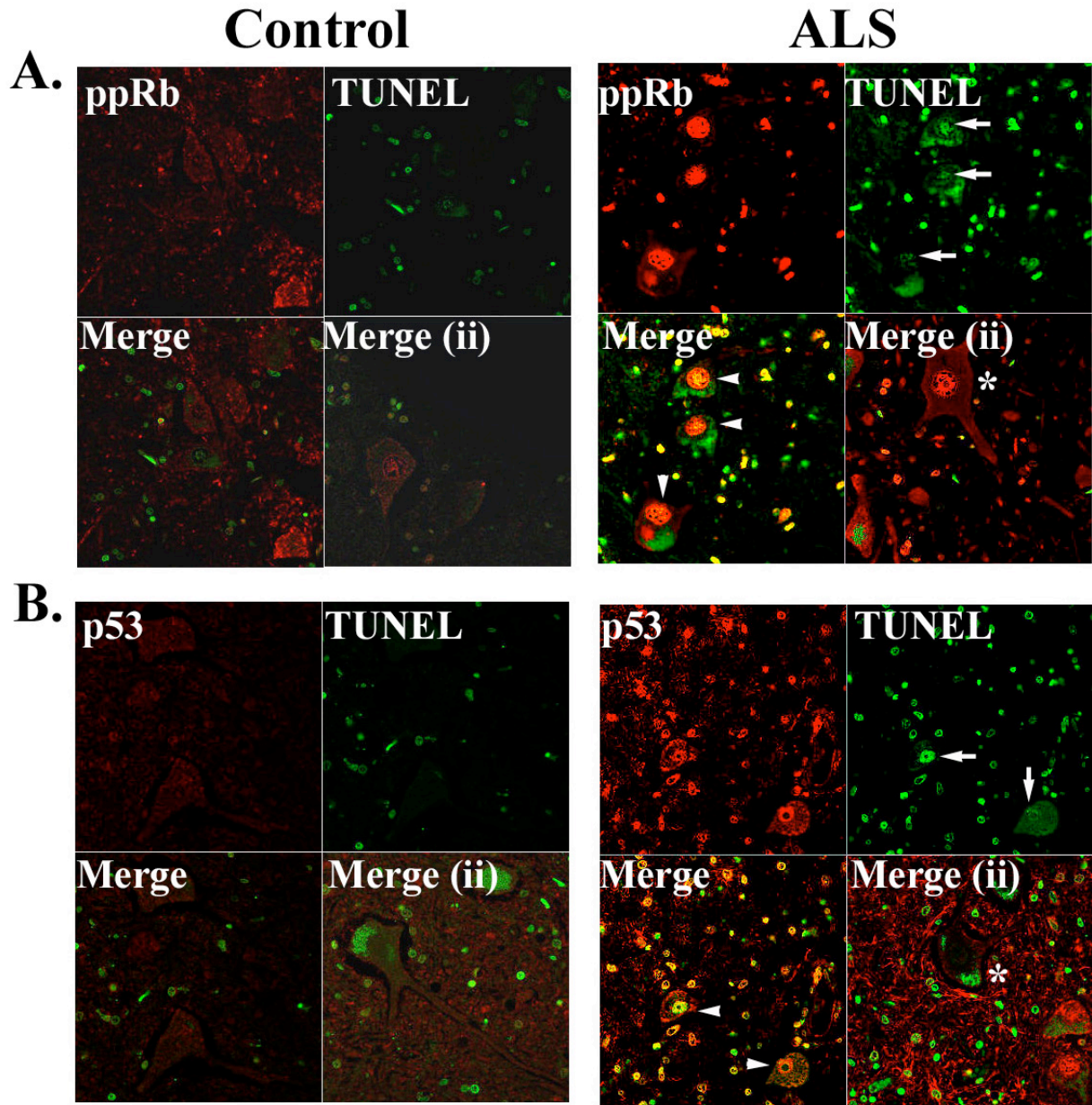


**Figure 29 Fas and Caspase-8 co-localize in spinal motor neurons**

*Lumbar spinal cord sections from 11 ALS and 6 age-matched controls were labeled with the combination of caspase-8 (alexa green conjugated secondary antibody) with Fas (Cy5 conjugated secondary antibody). In the ALS motor neurons, Fas (red signal) is present in the nucleus and co-localized with caspase-8 (yellow color in the bottom left merged image).*

### **3.4.5. DNA fragmentation as a marker for apoptosis**

In addition to caspase-3, terminal deoxynucleotidyl transferase-mediated biotinylated UTP nick end-labeling (TUNEL) staining has been used as a measure of nicked or fragmented DNA, a feature characteristic of apoptosis. There was increased evidence for TUNEL positive motor neurons in ALS spinal cord but not the motor cortex.



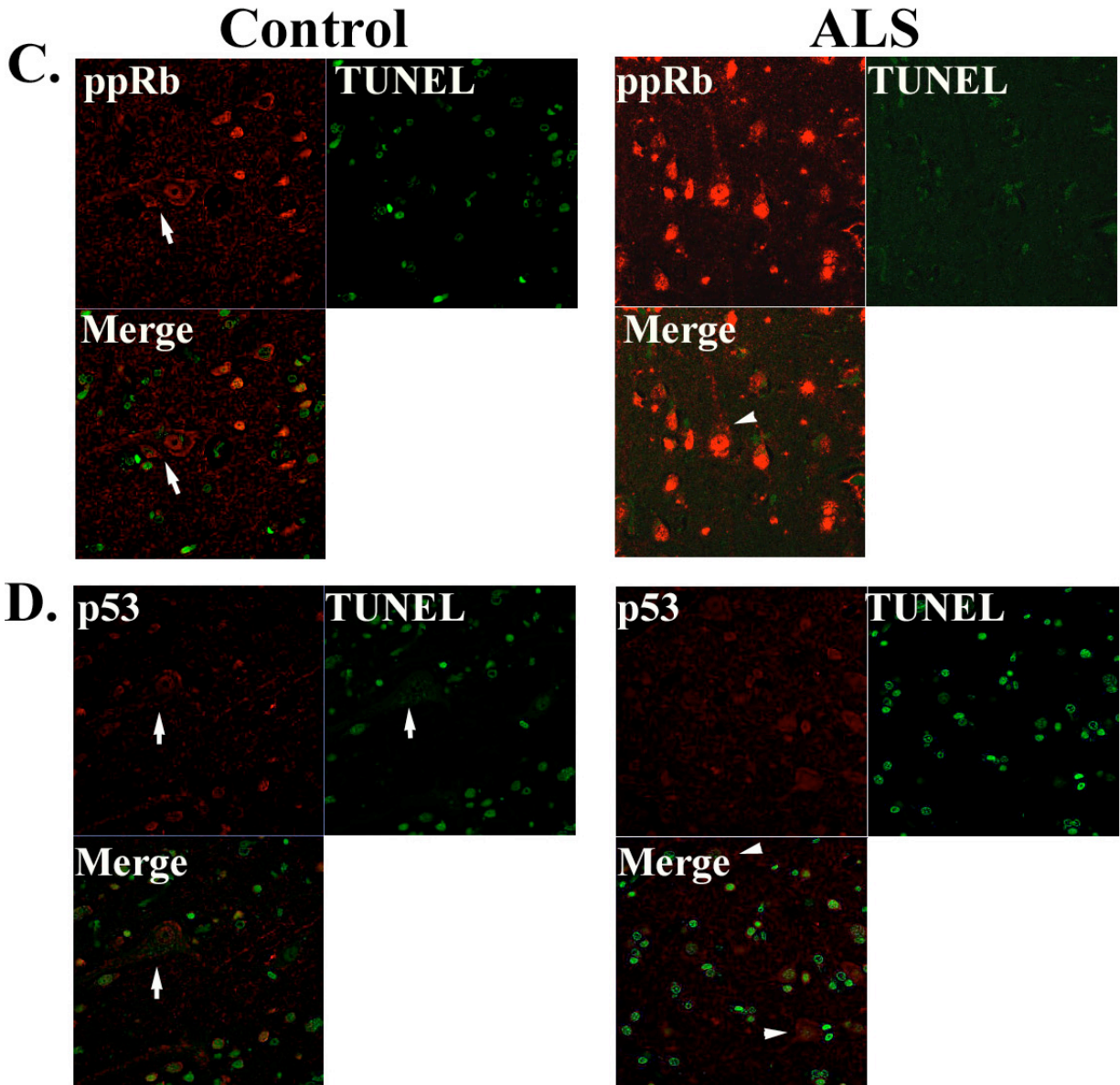


**Figure 30 Increased DNA fragmentation in spinal but not cortical motor neurons**

*Lumbar spinal cord (A and B) and motor cortex (C and D) sections from 11 ALS and 6 age-matched controls were double-labeled for TUNEL (FITC-conjugated) and p53 or ppRb (Cy-5 conjugated). Control cases exhibited negligible percentage of double positive (merge) neurons. Arrows in A and B indicate TUNEL positive motor neurons. ppRb/TUNEL as also p53/TUNEL were present in the same motor neuron (merge; arrowheads) in the spinal cord (A and B). The*

*asterisk in (A) depicts a ppRb(+) but TUNEL(-) ALS motor neuron and the single asterisk in (B) indicates a p53(-) TUNEL(-) healthy looking motor neuron. Arrowheads in A and B indicate double positive ALS motor neurons. The cortical motor neurons in ALS cases appeared positive for ppRb (C) and negative for p53 (D). In both C and D, the motor neurons appear negative for TUNEL. Arrows indicate control motor neurons and arrowheads indicate ALS motor neurons.*

Sections were also analyzed to determine if ALS spinal motor neurons that exhibited increased ppRb or p53 were positive for TUNEL staining. While we observed about 25% (9/36) of the ppRb positive neurons to be TUNEL positive, 30.5% (11/36) of the p53 positive motor neurons were positive for TUNEL staining (arrowheads in Fig 30, A and B, respectively). We also identified ppRb or p53 positive but TUNEL negative ALS motor neurons (asterisk in Fig 30, A and B, merge (ii) panel). Approximately 75% of the motor neurons that exhibited TUNEL also contained activated p53. Furthermore, the motor neurons that were positive both for TUNEL and p53/ppRb appeared shrunken with fewer processes (arrows in Fig 30, A and B). The neurons that were TUNEL negative were observed to be larger with intact somatodendritic morphology (asterisk in Fig 30, A and B, merge (ii) panel). The control cases showed largely a lack of TUNEL staining (absence of green signal) with little (ppRb, Fig 30A, bottom right quadrant) or no (p53, Fig 30B, merge (ii) panel) immunoreactivity. In the motor cortex, approximately 64% (22/34) of the remaining large pyramidal neurons were positive for ppRb (Fig 30C) while only 9% (3/34) of them were p53 positive (Fig 30D). None of the large pyramidal neurons exhibited DNA fragmentation. There was some amount of non-specific TUNEL immunofluorescence in small cells in the gray matter of the cortex but not in any of the surviving motor neurons (green fluorescence in Fig 30, C and D).

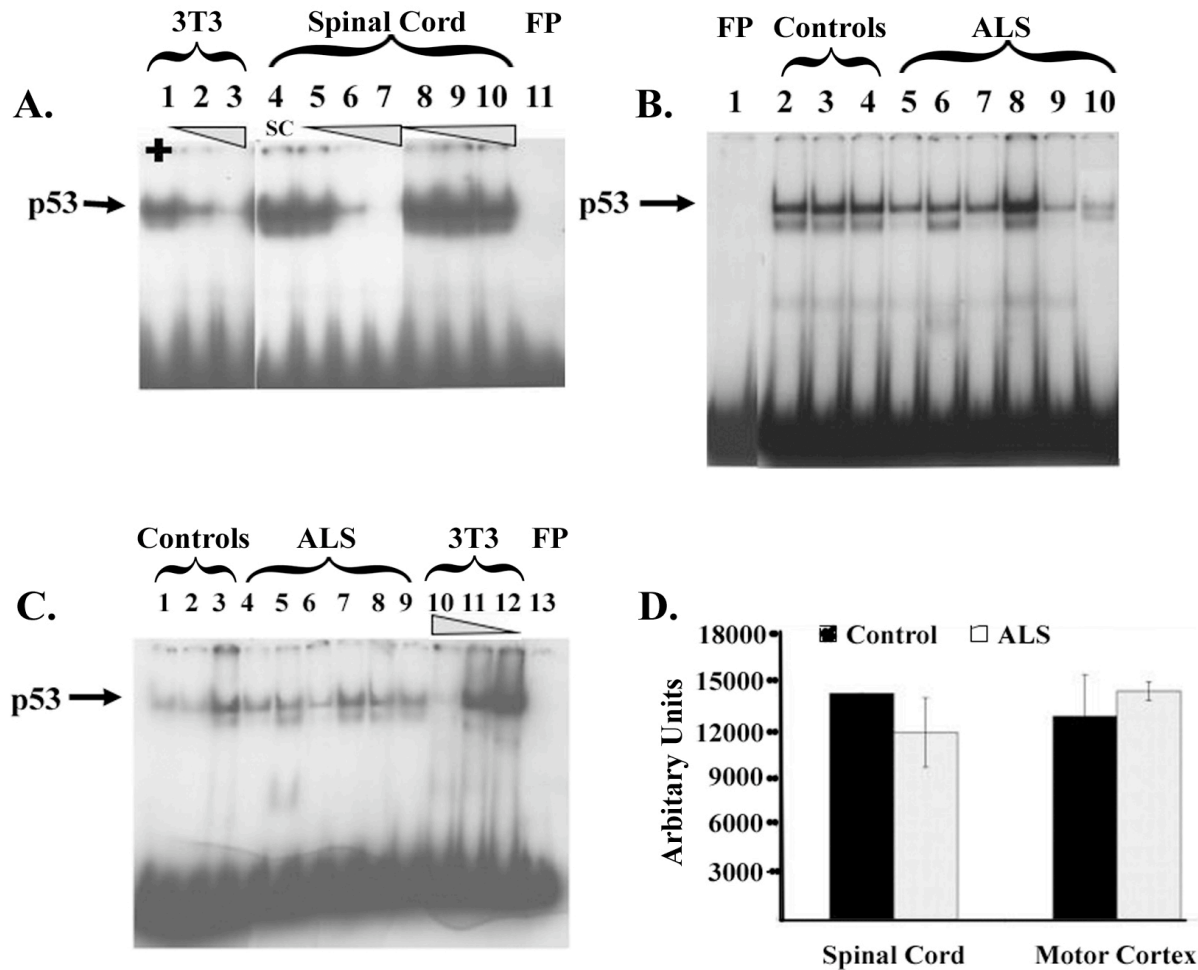


**Figure 31 No change in p53 DNA binding activity in ALS motor neurons**

Nuclear extracts from lumbar spinal cord and motor cortex of six ALS and three age-matched control cases were used for EMSA. (A) Competition EMSA using radiolabeled p53 oligo and either extract from NIH3T3 cells (positive control) (lanes 1 to 3) or spinal cord nuclear extracts (25µg; lanes 4 to 7) indicating a concentration dependent competition (lanes 2 to 3 and 5 to 7) when excess cold oligos were used in the binding reaction. The complex remains unaltered when excess unrelated oligos (lanes 8 to 10) were utilized in the binding reaction. Lane assignments were as follows: Lane 1: 3T3 extract with hot probe (HP); 2 and 3: 3T3 extract with hot probe and excess cold oligos (3ng and 100ng, respectively); 4: Spinal cord extract (SCE) with hot

probe (HP); 5 to 7: SCE with HP and excess cold oligos (3ng, 30ng and 100ng, respectively); 8 to 10: SCE with HP and excess unrelated oligos (30ng, 100ng and 300ng, respectively); 11: Free probe.

Panel B is an EMSA using radiolabeled p53 oligo and spinal cord nuclear extracts. Lane assignments: 1: Free probe; 2 to 4: Control cases; 5 to 10: ALS cases.

Panel C is an EMSA using radiolabeled p53 oligo and motor cortex nuclear extracts. Lane assignments: 1 to 3: Control cases; 4 to 9: ALS cases; 10: 3T3 extract with 100ng excess cold oligo; 11: 3T3 extract with 3ng excess cold oligo; 12: 3T3 cells with probe and no cold oligo; 13: Free probe alone.

Panel D depicts densitometric measurement of the p53:DNA complex using NIH 1.58 software indicating unaltered levels of DNA binding activity. Controls are denoted in black bars (n=3) and ALS cases in stippled bars (n=6). The p-values were  $\geq 0.05$  for both the regions of the CNS using single-factor ANOVA with a 95% confidence interval.

#### **3.4.6. DNA-binding activity of p53**

To determine the functional status of p53 in ALS, DNA binding activity was analyzed using nuclear extracts of spinal cord and motor cortex. [ $^{32}$ P]-labeled double-stranded oligonucleotides containing the consensus p53-binding site were incubated with 25 $\mu$ g of the nuclear extracts. The p53-DNA complex formation was competed by excess unlabeled p53 oligos but not by mutant p53 oligos thus determining the specificity of the binary complex (Fig 31A). The p53 DNA binding activity in the spinal cord or motor cortex tissues showed no significant difference in ALS cases compared to the age-matched controls (Fig 31, B to D).

### 3.5. Discussion

The balance between pro- and anti-apoptotic proteins can modulate survival and the mode of neuronal cell death. There are many studies correlating levels of these proteins to an apoptotic mode of cell death during ALS. However, there is no study that links aberrant activation of G1 to S phase regulators to apoptosis in this chronic neurodegenerative disease. p53 is an important nuclear regulatory protein that plays a role both during cell cycle and apoptosis. In fact, high expression of both cyclin D1 and p53 leads to apoptosis, similar to overexpression of p53 and c-myc [407] or p53 and E2F-1 [408]. We report here the altered levels of p53 and pro-death molecules of the apoptotic cascade in human ALS post-mortem tissues. Interestingly p53 protein levels were increased in the motor neurons and glia of the ALS spinal cord but only in glia of the motor cortex.

We have previously determined that there is an aberrant activation of G1 to S phase regulators in ALS motor neurons marked by altered levels of ppRb and E2F-1 [122]. We have also demonstrated the co-localization of these proteins with p53 (Section 2.4.4). This protein can be divided into three regions: (1) the amino terminus, containing the transcriptional activation region; (2) the central portion of the molecule containing highly conserved sequence blocks throughout which are present oncogenic mutations; (3) the carboxyl terminus, containing both oligomerization and nuclear localization sequences. While p53 is negatively regulated by direct protein-protein interactions with modulators such as mdm-2 it is stabilized by the action of CDK inhibitors such as p14<sup>ARF</sup>, which is a gene product transactivated by E2F-1. Post-translational modifications such as phosphorylation can enhance the transcriptional activity of p53 [409].

Our Western immunoblotting results indicate increased levels of phosphorylated p53 in the nuclear fractions of spinal cord tissue extracts. In normal conditions, p53 is a protein with a

very short half-life and is rapidly degraded. The presence of elevated levels of p53 in ALS patients suggests that this protein is aberrantly stabilized either by the down-regulation of proteins that negatively regulates p53 such as mdm2 or through reduced degradation of p53 via the proteasomal machinery. It is well documented that the proteasomal machinery is compromised in neurodegenerative diseases such as ALS with concomitant increases in aggregate formations. It is also possible that the p53 transcripts are better stabilized in disease states through RNA binding proteins or post-translational modifications can affect the half-life of p53 and its consequent activity. It is likely that the accumulation in p53 is due to these effects.

In a previous study, protein levels of nuclear p53 and its DNA binding activity was increased in affected CNS regions of ALS patients [197]. Contrary to our expectations, we found no significant difference in the DNA binding activity of p53 in spinal cord in spite of its enhanced nuclear localization. This is probably due to the fact that the extracts used for both Westerns and EMSA represent a heterogeneous population of cells (neurons and glia). Our preliminary analysis at the transcriptional activity of p53 using real-time PCR do suggest an increase in its nuclear activity as one of its target genes (p21) was up-regulated in ALS spinal cord tissue extracts but not controls (data not shown). It is likely that in addition to having an effect at the level of transactivation, p53 could modulate protein-protein interactions both in the nuclear and cytoplasmic compartments during the disease.

We further dissected p53 localization through immunohistochemistry whereby the presence of abundant nuclear accumulation of p53 in spinal motor neurons and activated glial cells suggests the involvement of the cell cycle in motor neuronal death. Such subcellular alterations in p53 could be in response to DNA damage in addition to re-entry into cell cycle with subsequent E2F-1 dependent transactivation. DNA damage can activate proteins that induce

cell cycle arrest and / or DNA repair. However, extensive DNA damage induces neuronal apoptosis. The presence of p53 in the nucleus of motor neurons that apparently lack dendritic processes with a rounded cell body suggest that altered localization of active p53 may correspond to cell atrophy and death.

The results obtained in the spinal cord of ALS patients however were in stark contrast to that in the motor cortex of these patients. It was surprising that the remaining large pyramidal cells and other neurons in the motor cortex of these patients showed negligible to no p53 immunoreactivity. The level of this protein was undetectable in any fraction of tissue lysate and there was no difference in the DNA binding activity. This dichotomous pattern of protein expression although intriguing suggests two different pathways for loss of motor neurons, one that is p53 dependent in the lower motor neurons and one p53 independent in the upper motor neurons. Differential role for p53 might also relate to differences in the site of disease onset (bulbar vs lumbosacral), which warrants further investigations. In addition, studies in adult mice and neuronal cell cultures show evidence for localized transcription-independent mechanism of p53 action in the synapses [410]. In these studies, oxidative and excitotoxic insults increased the levels of active (phosphorylated) p53 in isolated cortical synaptosomes, which preceded the loss of synapsin I. This suggests that p53, independent of transactivating its downstream targets, can have an effect on the dysfunction and degeneration of synapses during neuropathologic conditions. In addition, DNA damage can also cause alterations to the glial cells and subsequently affect the motor neurons via a bystander effect. The lack of p53 in the surviving motor cortex neurons but its presence in the astrocytes of the cortex may indicate such a phenomenon. For instance, damage to the astrocytic transporters (EAAT2) or the glial component of the cortical region could initiate a cascade of chemokine / cytokine release, which

will have an effect on the adjacent neurons. In effect, p53 can damage motor neurons directly or indirectly. In support of such a theory are the recent findings of increased PARP immunoreactivity in reactive astrocytes of SALS patients and also in an G93A SOD1 mouse model [200, 411].

Other homologs of p53 such as p73 are regulated by E2F-1 and there are prior reports of altered levels of p73 in AD brain [412, 413]. In the absence of p53, we hypothesized that a homolog such as p73 may exhibit alterations in ALS motor cortex. However, we observed reduced p73 levels in the motor cortex. In this light, alterations in chromatin structure through inappropriate regulation of nuclear factors such as p53 or p73 can make DNA increasingly susceptible to further damage. Mutations or damage to proteins such as Alsin that is implicated in FALS and with sequence homology to the regulator of chromatin condensation may result in exacerbating DNA damage. Other events as also acetylation of nuclear factors such as p53 or p73 can greatly influence a cell to trigger apoptosis. These areas of research warrant further investigations.

Irrespective of the mechanism that induces cell death, apoptosis involves the induction of pro-apoptotic genes with downstream activation of caspases. Our Western immunoblots and confocal microscopy studies suggest the involvement of apoptosis downstream of the aberrant activation of cell cycle regulators. Both a mitochondrial pathway (increased Bax and caspase-3) and a death receptor mediated pathway (increased Fas, caspase-8 and caspase-3) may be involved in the lower motor neuron death in ALS. Caspase-3 staining in the spinal motor neurons appeared cytoplasmic and punctate. This might suggest its probable association with mitochondria. The antibody used in immunohistochemistry recognizes active form of caspase-3 and our confocal images do indicate its nuclear localization.

Fas mediated death pathway in cultured motor neurons from SOD1 mutant transgenics have been reported [406]. There is evidence for p53 to mediate apoptosis through other mechanisms other than Bax, one of which, is the Fas mediated death signaling pathway [284]. It is also known that prostaglandins in ALS spinal cord phosphorylates and activates p53 [414]. Hence it is likely that p53 might act on both the apoptotic pathways with the activation of Fas possibly due to increased prostaglandins. However, it was intriguing to find Fas, a death-domain containing membrane receptor, in the nucleus of spinal cord motor neurons. There is no precedent to this occurrence in scientific literature. Since we have performed peptide blocking and other control experiments to test the specificity of its localization, we believe that our immunohistochemical evidence is real and that it may be a processed form of the receptor. The mode of its nuclear translocation or its nuclear function is unknown. Thus from this study we can conclude that a caspase-dependent apoptotic mode of cell death occurs in the spinal cord motor neurons but not in neurons of the motor cortex. A caspase-independent apoptotic mechanism in the motor cortex however cannot be ruled out by this study. In order to make sure that we are not biasing our investigation by examining just one area of the motor cortex that project to the spinal cord, we analyzed sections from the mid- and superior regions of the motor cortex (regions #2 - #7 in Fig 6B) and report consistent findings. Although these findings contradict earlier reports wherein alterations of apoptotic proteins were evident in both the spinal cord and motor cortex, it fits well with the current idea that multiple pathways are involved in neuronal cell death. Alternatively, it is possible that cell death may not be as extensive in the motor cortex as it is in the spinal cord. In fact, many of the ALS cases utilized in this study do not exhibit motor cortex atrophy by gross neuropathological assessment.

As a measure of DNA damage and apoptosis, we used DNA fragmentation as a marker using TUNEL staining. When nucleases cleave or nick DNA strands, they result in 3'-hydroxyl ends being exposed. These hydroxyl groups then serve as substrates for the terminal deoxynucleotidyl transferase (TdT), which adds deoxyribonucleotides in a template-independent manner. It was noteworthy to find that there was increased evidence for fragmented DNA in spinal cord but not the motor cortex. In the spinal cord, the presence of p53 immunoreactivity in 75% of the TUNEL positive motor neurons suggests that DNA damage results in p53 accumulation but is not the only indicator of DNA damage as only 30.5% of the p53 positive neurons were TUNEL positive. The lack of TUNEL positive motor neurons in the cortex is consistent with the immunohisto-chemical data presented in this Chapter. Furthermore, these results are strengthened by the lack of Bax and caspase-3 protein levels in the Betz cells. It is indeed true that this technique does not differentiate between single-strand (necrosis) and double-strand (apoptosis) DNA breaks. Nevertheless, our results do indicate the presence of nicked DNA that co-localizes to the G1 to S phase regulators. These observations coupled with the presence of activated caspases lend further support for an apoptotic mode of cell death in the spinal cord.

In conclusion, we have reported alterations in the G1 to S phase transition of cell cycle with concomitant increases in p53 levels in the spinal cord of ALS patients may direct susceptible motor neurons to an apoptotic mode of cell death. The same may not be true of the Betz cells in the motor cortex as illustrated by the apparent lack of p53 or any death markers. Therefore, these findings suggest a differential mechanism of neuronal cell death in ALS. It is true that in a chronic neurodegenerative disease such as ALS, it will be difficult to document apoptosis in post-mortem tissues given the rapidity of the cell death process. However, this study

in addition to discerning a potential role for p53 and other G1 to S phase regulators in motor neuronal death provides additional evidence for an apoptotic mode of cell death in ALS.

## **4. Assessment of human CSF Proteome stability by SELDI-TOF-MS**

### **4.1. Abstract**

Mass spectrometry-based clinical proteomics is being used to identify diagnostic biomarkers and surrogate endpoints for a number of human diseases. However, this technique is sensitive and reliable only to the extent to which samples are appropriately handled and stored. Assessment of sample-handling conditions is critical to ensure proper utilization of valuable samples such as cerebrospinal fluid (CSF) in order to obtain reliable and reproducible data. The aim of this study was to examine the effects of storing samples at room temperature and at 4°C on the proteome of human CSF using surface-enhanced laser desorption/ionization – time of flight mass spectrometry (SELDI-TOF-MS). Analysis of variance indicates that differences in protein profiling were evident within 4 hours at room temperature but after 8 hours when stored at 4°C. This chapter highlights the importance of standard operating procedures to maintain integrity of clinical samples.

## 4.2. Introduction

Biomarker discovery for neurodegenerative diseases and neuropsychiatric disorders is at the forefront of biomedical science research [307]. There are a number of ongoing studies to identify biomarkers for diagnostics, drug design and discovery in neurological diseases such as AD, ALS, HIV-encephalitis, and schizophrenia [315, 316, 318, 320, 326, 337, 415-419]. Since neurons and glial cells of the central nervous system (CNS) are bathed in the CSF, it provides an ideal medium for clinical neuroproteomics [315, 420]. However, CSF and serum sample integrity and stability is important for the successful use of very sensitive techniques such as mass spectrometry-based clinical proteomics. Many of the proteomic studies utilizing CSF or serum are collaborative multicenter efforts. Proper handling of these valuable samples is key to obtaining interpretable and reproducible data. When samples are obtained through surgical procedures or routine specimen collection such as venipuncture, it is likely that pre-analytical errors such as prolonged storage at room temperature or in the cold can plague the final data analysis. In a clinical study involving human patients, identification and proper assessment of biological, pathological and pharmacological variation is important. In addition, instrument variations such as mass inaccuracy can add to the difficulty for data interpretation. Therefore it is important to reduce experimental variation by implementing standard operative procedures for collection, handling, and storage of valuable subject samples.

Despite many clinical proteomic studies using CSF and mass spectrometry, there are no reports on the stability of CSF proteome over time when stored at different temperatures. While efforts are made to minimize the time from when the sample is procured till it is processed and placed in long-term storage, quite often this time is variable from sample to sample or between institutions. There is a study using proton nuclear magnetic resonance suggesting alterations in

CSF proteome stability after 72hrs at room temperature but this study has not been performed at various time points [421]. Recent studies have highlighted the importance of standard operating protocols (SOP) for clinical plasma samples using a 2D-GE proteomic approach [422]. Another group published results related to the reproducibility of protein profiles in urine samples analyzed many months apart [339]. However, there are no reports regarding the SOP for clinical CSF samples using mass spectrometry. In this report, we utilize CSF from healthy control subjects and MS-based proteomics to test the stability of the CSF proteome to variations of temperature and time. We detail evidence that protein stability as inferred from the CSF proteomic profiling reduces over time when samples are stored at room temperature. Alterations in the proteomic profile are less pronounced when samples are stored at 4°C prior to its use on protein chip arrays. This analysis is important to further the field of MS-based clinical proteomics and develop standardized protocols to proper handling of valuable clinical samples in a multicenter study.

### **4.3. Materials and Methods**

#### **4.3.1. Study Population and Sample Preparation**

For study of protein stability, two CSF samples were used from the University of Pittsburgh. The samples were from healthy adult subjects. CSF was obtained via lumbar puncture protocol approved by the University of Pittsburgh IRB. Cerebrospinal fluid (CSF) was immediately centrifuged at 1500 rpm for 5 min at 4°C to remove cellular debris and either directly used or frozen at -80 °C and thawed on ice prior to use. IRB-approved informed consent for this procedure was obtained from all subjects. Replicate sample sets either at room temperature or at 4°C was used within each experiment. Each sample set contained seven

replicate tubes and incubated for each of the time points – 0, 2, 4, 6, 8, 12, 16 and 24 hours. The experiments were repeated twice.

CSF samples (20 $\mu$ l) were diluted in 1% trifluoroacetic acid (TFA) to a final TFA concentration of 0.1% (v/v). Samples were fractionated using C4 ZipTip pipette tips (Millipore) according to manufacturer's instructions and eluted onto the spots using a gradient of 75% acetonitrile (ACN) / 0.1% TFA, 50% ACN / 0.1% TFA and 90% ACN / 0.1% TFA.

#### **4.3.2. Chip Preparation**

Strong anion exchange surface (SAX2 or Q10) ProteinChips (CIPHERGEN Biosystems, Inc., Palo Alto, CA) were chosen as initial optimization experiments with this chip yielded reproducible spectral profiles. The 8 spots on SAX2 chips were equilibrated with 100mM Tris-HCl pH 8.5 and then fractionated samples were added to the spots (one sample per spot). CSF samples (20 $\mu$ l) were diluted in 1% trifluoroacetic acid (TFA) to a final TFA concentration of 0.1%. Samples were fractionated using C4 ZipTip pipette tips (Millipore) according to manufacturer's instructions and eluted onto the spots using a gradient of 50% acetonitrile (ACN) / 0.1% TFA, 75% ACN / 0.1% TFA and 90% ACN / 0.1% TFA. A saturated matrix solution of 4-hydroxy- $\alpha$ -cinnamic acid (containing 50% acetonitrile (v/v) in HPLC-grade water and 0.3% (v/v) TFA) was then added to the spots. The spots were dried at room temperature before acquiring spectra using the CIPHERGEN PBSIIc ProteinChip Reader equipped with an autoloader.

#### **4.3.3. SELDI-TOF-MS**

The spectra of proteins/analytes were generated using a laser intensity range of 190-200 and a detector sensitivity range of 8-9 with a mass deflector setting of 1000 Da for the low mass

range (1-20kDa). These settings were kept constant for all chips in each experiment. In addition, we performed two separate experimental runs for each ProteinChip array. Each experiment was repeated twice. For each experiment one CSF sample was used as an internal standard to measure intra-assay variability of the mass spectra. The percent coefficient of variance (CV) for selected mass/charge ( $m/z$ ) signals (20 peaks) was less than 30%. External calibration of the ProteinChip Reader was performed using the Ciphergen Biosystems 5-in-1 peptide mix [(vasopressin (1084.247 Da), somatostatin (1637.903 Da) porcine dynorphin A (2147.5 Da), human ACTH (2933.5 Da), bovine insulin B chain (3495.941 Da), human recombinant insulin (5807.653 Da), hirudin (7033.614 Da)]. Human SOD1 (15591.4 Da) was added to this mix.

#### **4.3.4. Data Analysis**

Total ion current of all profiles was used to normalize each of the spectrograms. An average spectrum for each of the time points was obtained and the raw spectral data consisting of about 18,400 peak values were utilized for further analysis. Variance (VAR) is a measure of the average distance between each of a set of  $m/z$  features and their mean peak intensity. In other words, it is the square of the deviation from the mean ( $(SD)^2$ ). Coefficient of variation (COV) is a relative measure wherein the percent dispersion is a ratio of the magnitude of the standard deviation to its mean (SD/Mean). The value of VAR or COV is directly proportional to the degree of variation. The COV for each time point were then used to calculate a whole-profile grand sum mean deviation (GMSD) from the 0 hour time point of each temperature condition. All measures of variability were plotted against time. Furthermore the average intensity of all the  $m/z$  values within each time point was analyzed in comparison to zero hour time point by single-factor analysis of variance (ANOVA) with corresponding f-value and p-value. The null

hypothesis that two sets of proteome profiles were statistically different was considered significant when the *p-value* less than 0.05.

#### **4.4. Results and Discussion**

Calibration with external calibrants, normalization to total ion density and analysis of all the samples (replicates) from every time point in an experiment was performed at the same time. An average normalized spectrum of all the replicates for each time point from an experiment was generated. These were then compared for any differences in protein profiles over time at ambient temperature and 4 °C. The complete spectral profile in the range between 2 and 20kDa appeared fairly similar across the different time points for each of the two conditions. However, closer examination of certain regions of these spectra revealed differences, which increased over time (Fig 32). In Fig 32, differences in relative abundance and also peak resolution are apparent as depicted in the *m/z* range of 11-15kDa. While they appeared within 2-4hrs when samples were placed at ambient temperature, these differences were noticeable as late as 12hrs when the same samples were stored at 4°C (Fig 32, see arrows and asterisk).

At ambient temperature arrows ‘a’ and ‘b’ indicate loss of peak resolution by 2hrs and 3-fold increase in relative abundance within 6hrs, respectively. In addition at ambient temperature, arrows ‘d’ and ‘e’ represent the loss in peak resolution as early as 2hrs and the appearance of a shoulder by 2hrs, which is sustained at all subsequent time points. However, in this same magnified *m/z* region at 4 °C, we do not observe as much variation. At 4 °C, there is a 3-fold increase within 2hrs in the peak with the same *m/z* as the arrow ‘b’ represents in the ambient temperature spectra. It is interesting to note that while the 0hr spectra at room temperature appears fairly similar to the 4hr spectral profile at 4 °C, the 6hr ambient temperature profile

appears identical to the 12hr 4 °C profile (see ‘asterisk’). The peaks represented by the ‘asterisk’ suggest that the CSF proteome becomes increasingly unstable. In addition, comparison of the profiles at 8-12hrs suggests a delayed instability of the CSF proteome when samples are placed at 4 °C.

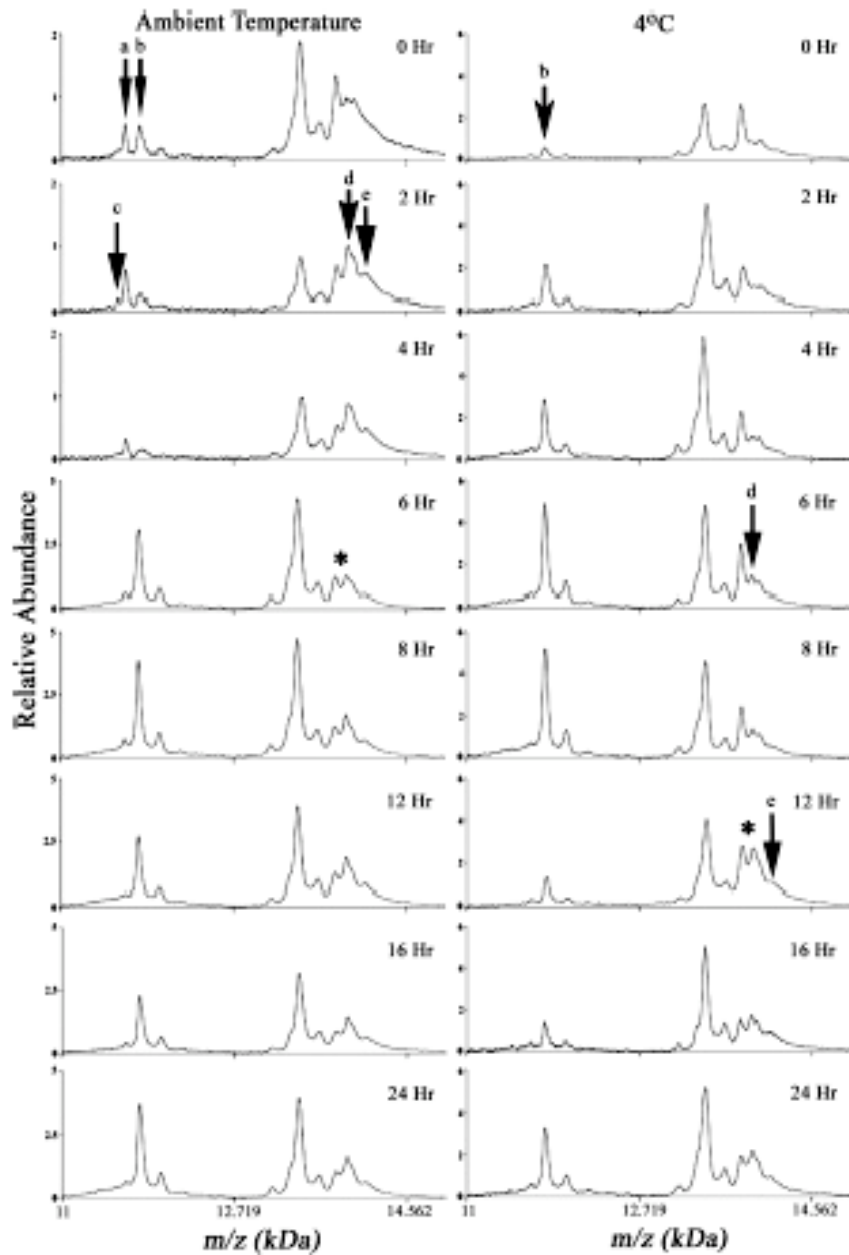


**Figure 32** CSF spectra representing m/z region of 11 to 15kDa depicting temperature dependent changes in proteome stability

*Left and right columns represent SAX2 spectra from individual replicates obtained by thawing and incubating samples at ambient temperature and 4°C for specified timepoints, respectively. Arrows (a-e) represent alterations in relative abundance or loss of peak resolution over time. Asterisk depicts a peak doublet present at 6hrs at ambient temperature that is present as late as 12 hrs at 4°C.*

These spectral profiling results suggest that as hypothesized the CSF protein spectral profiles changed much earlier when stored at room temperature when compared to 4°C. They retained their integrity for an additional 4-6hrs when stored at 4 °C as opposed to ambient temperature. Furthermore, when peak “b” at room temperature is compared to the peak at 4°C in Fig. 32, it initially disappears but re-appears at a later time point. While this peak at room temperature re-appears as early as 6hrs, it re-appears as late as 24hrs at 4°C. These are indications of gross effects of temperature on the CSF proteome stability. It is also possible that these apparent differences in peak “b” might be due to the emergence of a very different protein, possibly a proteolytic fragment of a larger protein. Such changes are important from the context of peak clustering software and further analysis of mass spectrometric data.

Raw spectral data output from each of the time points, which included about 18,400 m/z features, were then utilized for analysis of variance. The average variance, a measure of the deviation from the mean, was determined for the whole profile at each time point with corresponding standard errors (Fig 33A). There was a gradual increase in VAR up to 8hrs at 4°C with a delayed sharp increase at 24hrs. In contrast at ambient temperature an increased variance was noticed as early as 6hrs and this appeared biphasic with a similar sharp increase in variance at 16hrs. In addition, the average COV across the profile was determined for each time point (Fig 33B). The COV at 4°C and ambient temperature showed negligible differences with a sharp

increase at 24hrs when stored at 4°C and by 2-4hrs at room temperature. The minimal magnitude of variations obtained from the VAR and COV results suggest that the CSF proteome is reproducible within each time point. In other words, the rate of alterations in the proteome stability is fairly consistent within each of the time points. The observed small changes could indicate baseline variations present within each time point. Having established the reproducibility within time points we analyzed if there was any variance across them.

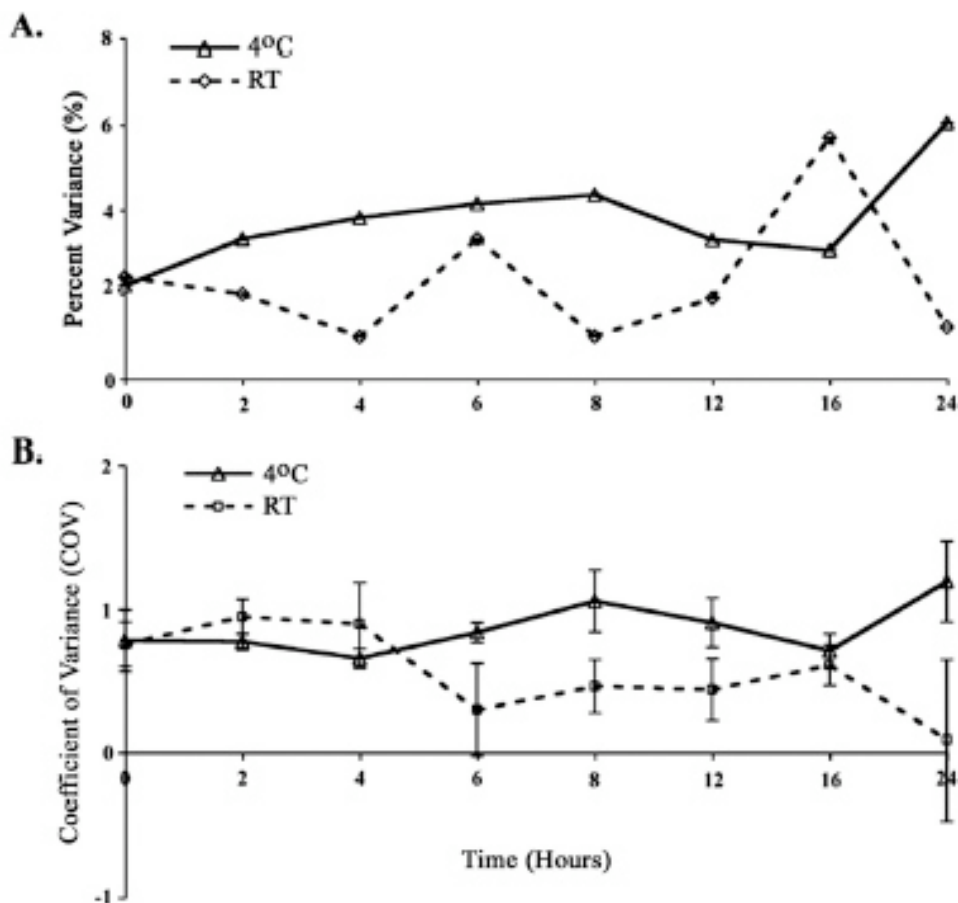


**Figure 33** Percent variance (A) and coefficient of variance (B) as measures of CSF proteome stability

(A) Variance of the  $m/z$  values within all replicate samples at each time point was calculated for each of the 18,400 mass peaks within the raw spectral data. The average overall variance (VAR)

was then computed for each time point and represented as percent variance with corresponding standard errors of mean. (B) The COV for each time point was determined as the ratio of the standard deviation over its mean for each of the 18,400 peak values at each time point. The average COV for each time point was then plotted. In both (A) and (B), solid line represents samples incubated at 4°C and dashed line represents those at room temperature (RT).

While VAR and COV relate to differences within each time point, GMSD is a statistical measure that represents true variances relative to the control time point (zero hour). As demonstrated in Fig 34, the GMSD was fairly constant up to 8hrs signifying that the proteome is stable with an increase in GMSD or instability in the proteome at 24hrs when stored at 4°C. This however was not the case at room temperature wherein there was variance as early as 4hrs with a very sharp significant increase at 24hrs. The measure of GMSD clearly suggests that the rapidity with which the proteome becomes unstable is greater at room temperature than at 4°C.

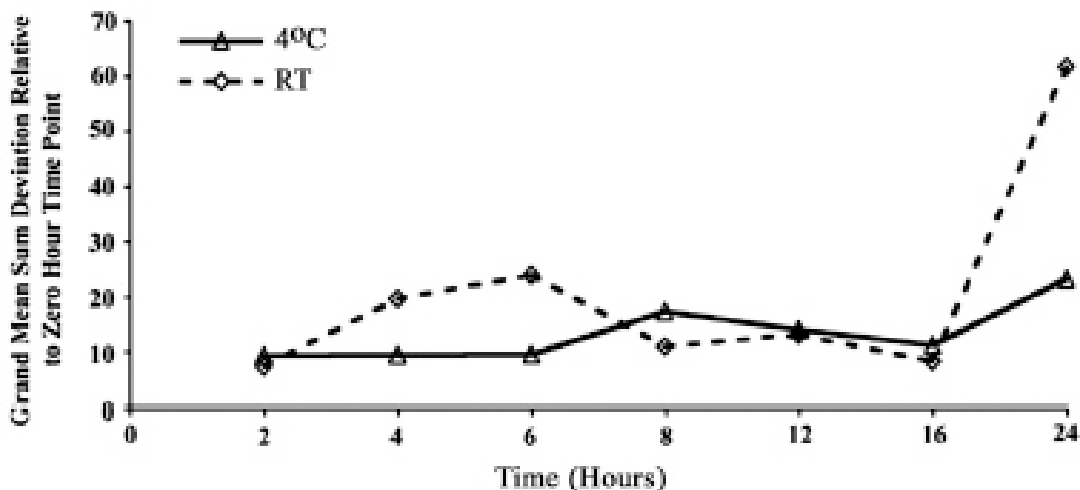


**Figure 34** GMSD as a statistical measure of variance in the CSF proteome

The difference in mean intensities at each time point relative to the 0 hr time point were determined and plotted as the GMSD. These values represent the overall deviation or alteration in the whole profile at each of the seven time points from time zero. While at room temperature,

*variation occurs as early as 2-4hrs with an addition peak between 16 and 24hrs, at 4°C the overall variation of the profiles does not differ by much until 8hrs.*

Additionally, ANOVA of the average intensities yielded statistically significant p values as early as 2hrs at room temperature and as delayed as long as 16hrs at 4°C (data not shown) indicating that the profiles at these time points are significantly different from that at the 0hr time point. These studies were repeated using CSF that was first frozen at -80°C and then thawed on ice prior to use, i.e., after one freeze/thaw cycle. We obtained comparable results suggesting no additional proteome alterations.

Our results demonstrate that the CSF proteome stability depends significantly on the storage conditions as hypothesized. The proteome is unstable as early as 4hrs when stored at ambient temperature and within 8hrs with a sharp increase at 24hrs when stored at 4°C. Instability of the CSF proteome may be a result of proteolytic changes or other post-translational modifications induced by temperature changes. It would be expected that the spectral patterns at 0hr time point both at ambient and 4°C should be similar but there is an apparent difference (Fig 32). Even though the peak intensities are different, the pattern appears fairly similar. Moreover, represented is an individual spectrum (from 7 replicates). When average peak intensities for the whole profile are determined the variance at the 0hr time point between the two temperature conditions is absent (Fig 33). Treating samples with protease inhibitors would further validate some of the spectral differences. It is the first such study using MS-based proteomics that addresses measures for quality control. This study demonstrates the necessity to carefully monitor the time taken to procure and process the CSF samples. Minute alterations in sample handling conditions can significantly affect protein signals obtained from the mass spectrometer thus skewing the mass peaks and the resultant efforts of biomarker discovery and validation.

Furthermore, if such samples are used for 2D-GE based proteomics, temperature induced alterations in pH / pI can greatly affect the migratory pattern of proteins and hence data interpretation. Such proteomic changes in clinical plasma samples in a 2-dimensional gel have been demonstrated [422]. Reducing the time that these CSF samples are placed at ambient or 4°C prior to storage at -80°C will greatly enhance the quality of the samples for proteomic approaches. It will also aid in generating interpretable proteomic profiles using the mass spectrometry based proteomic approach. In conclusion this study underlines the importance of proper handling and storage of valuable clinical samples.

## 5. Post-mortem CSF is not an ideal candidate for biomarker discovery

### 5.1. Abstract

Many neurodegenerative diseases, including amyotrophic lateral sclerosis (ALS), have no clear diagnostic biomarkers or long-term intervention drugs. Extensive research at the gene and protein level using post-mortem tissues, animal models and body fluids has indeed provided molecular targets for clinical trials. Genetic and protein alterations during ALS can be studied using body fluids such as serum and cerebrospinal fluid (CSF). The latter represents an ideal medium for analysis because it bathes glial and neuronal cells. CSF may thus present with protein differences as a result of pathological changes that occur in the CNS during neuronal death. These differences however may vary quite extensively in samples from living and those procured at autopsy. *Using ALS as a model for neurological disorders, we hypothesized that CSF profiling for protein alterations from living patients will yield biomarkers that better defines disease progression than those, which result in CSF obtained at autopsy.* Mass spectrometry-based proteomics using Ciphergen protein chips was utilized for the protein profiling. The CSF proteome from post-mortem (16 controls and 17 ALS) and living (17 controls and 20 ALS) subjects were analyzed using a strong anion exchange chip array. Through univariate and multivariate analysis of resulting spectra, we identified differences in the spectral patterns. This is the first study outlining spectral differences in CSF proteome from post-mortem and living ALS subjects using a mass spectrometric approach. These differences suggest the importance of utilizing CSF from living ALS patients for the identification of early diagnostic biomarkers.

## 5.2. Introduction

The reported incidence of CNS related disorders and neurodegenerative diseases are ever increasing. Although scientific advances have been made in understanding the pathogenic mechanisms of diseases such as AD, PD, Down's syndrome, ALS, multiple sclerosis (MS) and other neuro-psychiatric disorders, none has yet to yield significant biomarkers or long-term interventions. Proteomic approaches via 2D-GE to study protein alterations in these neurodegenerative diseases have been extensively utilized. These studies have revealed oxidative modifications to proteins in diseases such as AD and PD [317, 319-321, 416]. There have been a number of proteins such as GFAP, myelin basic protein (MBP), neurofilament (NF), nitrated proteins, S100B protein and ApoE reported to act as a diagnostic measure of CNS disorders but none have yet to be proven to achieve the level of specificity required for proper early diagnosis of the disease. This is partly because some of these studies have utilized samples (CSF or tissue lysates) obtained at autopsy from diseased patients. Due to differing post-mortem interval times and pre-mortem or agonal state of the patient, protein alterations unrelated to the disease can affect proteomic analysis. Although there have been a few reports of such changes occurring in the brains of animals, there are no such studies utilizing human CSF and a MS-based proteomic approach.

Although CSF is an appropriate sample for biomarker discovery, it is not only important to properly handle these samples but also make sure that the sample used does not yield uninterpretable results due to proteome instability (see Chapter 4). There are many factors such as differences in age, sex, drug regimens that present as confounding factors in addition to other disease un-related issues such as post-mortem interval time and improper handling of samples. These factors can strongly influence a clear discrimination between disease state and normal

controls. Protein alterations that are observed in such situations cannot be ideally referred to as biomarkers for a disease. It is therefore important to evaluate proteomic alterations that may exist between living subjects and post-mortem samples. In this study, *we hypothesized that the CSF proteome profile from a living ALS patient will be very different from that of a post-mortem ALS case.* We have utilized CSF samples from living subjects diagnosed with ALS and those acquired at the time of autopsy. In each category, we have included non-neurological and neurological (AD) control cases. We conclude that there are numerous spectral differences in the proteome between these groups of clinical samples. These results suggest the importance of choosing the right kind of sample for biomarker discovery in CNS related diseases.

### **5.3. Materials and Methods**

#### **5.3.1. Study Population**

CSF samples from 20 subjects of recently diagnosed / living ALS (L-ALS) and 17 subjects of non-ALS age-matched living controls (L-Ctl) were obtained from the Boston cohort through our collaborators at Massachusetts General Hospital, MA. Control group included the following cases: 16 non-neurodegenerative or with no neurologic complaints; one with probable AD. The average time from clinical onset (date when the patient first reported symptoms) to when CSF was procured was 352.8 days for the living ALS patients. CSF acquired at time of autopsy from 17 ALS (PM-ALS), 8 AD and 8 non-neurological control (PM-Ctl) cases from the University of Pittsburgh cohort was also utilized. These samples were age-matched and matched for the post-mortem interval time. While the average ages (years) of the ALS and control patients from the Boston cohort were  $49.04 \pm 2.78$  and  $43.4 \pm 4.23$ , respectively; those from the Pittsburgh cohort were  $54 \pm 2.5$  and  $60 \pm 3.3$ , for ALS and control cases, respectively. The

average post-mortem interval times (hours) for the ALS and control cases from the Pittsburgh cohort were  $6.7 \pm 1$  and  $5.9 \pm 0.45$ , respectively. The ratio of males to females in the Boston cohort was 2:1.08 whereas in the Pittsburgh cohort, it was 1.66:1.08.

### **5.3.2. Sample and Chip Preparation**

Sample and chip preparations were as described in section 4.3.1 and 4.3.2 except that 0.5-4  $\mu$ g of the CSF was utilized. 2D-Quant kit (Amersham, USA) was used to determine protein concentrations (0.06  $\mu$ g/ $\mu$ l to 0.6  $\mu$ g/ $\mu$ l).

### **5.3.3. SELDI-TOF-MS**

Experiments were first performed to optimize the Ciphergen ProteinChip (Ciphergen Biosystems, Inc., Palo Alto, CA) types and binding conditions used in subsequent experiments. A total of four chip types were used to assay CSF samples: H4 (hydrophobic surface), SAX2 (strong anion exchange surface), WCX2 (weak cation exchange surface), and Zinc-IMAC30 (immobilized metal binding surface) at multiple pH binding conditions. Two protein chips, SAX2 (strong anionic exchange) and Zn-IMAC30 (immobilized metal affinity chip) exhibited the best spectral data. The SAX2 chip was utilized for further differential analysis of the post-mortem and living CSF proteomes. The 8 spots on SAX2 chips were equilibrated with 100mM Tris-HCl pH 8.5 and then fractionated samples were added to the spots (one sample per spot) (see section 4.3.2).

The spectra of proteins/analytes were generated using a laser intensity range of 179-185 and a detector sensitivity range of 7-9 with a mass deflector setting of 1000 Da for the low mass range (2-20kDa). These settings were kept constant for all chips in every experiment. For each

individual experiment all CSF samples were analyzed in duplicate (two separate spots on two different ProteinChips) as a measure of inter-experimental variability. We also used one common CSF sample on every chip of an experiment to assess intra-experimental variability. In addition, we performed multiple separate experimental runs for each ProteinChip array. The method to discern percent coefficient of variation (CV) between the chips and calibrants used for calibration were as described in section 4.3.3.

#### **5.3.4. Data Analysis**

Total ion current of all profiles was used to normalize each of the spectrograms. The Ciphergen 3.1 Biomarker Wizard application autodetected mass peaks by clustering and analyzed the output using a non-parametric statistical test, which constituted the univariate analysis of the data. Peak labeling was performed using second-pass peak selection with a signal to noise ratio of 1.5. Statistically significant alterations in analyte levels ( $p < 0.05$ ) were identified.

For multivariate analyses, protein peaks were analyzed with the Ciphergen 3.1 Biomarker Pattern Software (BPS) (Ciphergen Biosystems, CA, USA). BPS is a classification algorithm defining pattern recognition and building classification trees using mass peaks defined by Biomarker Wizard. Tree-building algorithms determine a set of “IF-THEN” logical conditions that permit accurate predictions or classification of cases (splits) [332]. Each tree comprises a parent node and branch or terminal nodes. The key rules to this analytical package are that each node in a tree is split into exactly two branch nodes (binary), the decision to assign a tree to be complete and also assigning each branch node to a class outcome. Splitting rules based on a “IF  $\square$  to a threshold value, THEN – Yes, if not – No” are rank ordered on the basis of the quality of

splits criterion utilizing the GINI and Twoing rules. Once a splitting rule is identified, the algorithm repeats the process for each branch node until such time when further splitting is not possible. There is a relative cost value associated with the classification, with a short tree size defining a low cost value and better classification. BPS is also predictive of sensitivity (correct classification of disease) and specificity (correct classification of control cases). We employed 10-fold cross validation to predict the error rate of selected trees. During this process, class is predicted on 10% of withheld samples based on a set of predictors built on the remaining samples. This process is iterated for each sample and the cumulative error rate is calculated. This provides a reliable estimate of the independent predictive accuracy of each tree.

#### **5.4. Results and Discussion**

The spectra obtained from all experiments were performed in duplicate and analyzed using the Ciphergen-based software for univariate and multivariate analysis. To account for reproducibility a CSF sample was used on every chip and the coefficient of variation was determined to be less than 30% for a total of 25 peaks. Comparison of CSF mass spectra in the range of 2 to 20kDa in ALS and controls from post-mortem cases and living patients revealed a number of differences in peak patterns. Differences in peak intensities are illustrated in Figure 35A using representative spectra from each of the four categories of samples analyzed (L-ALS, L-Ctl, PM-ALS and PM-Ctl). Closer examination of the spectrograms in the m/z range of 4 to 8kDa revealed numerous differences (Figures 35B).

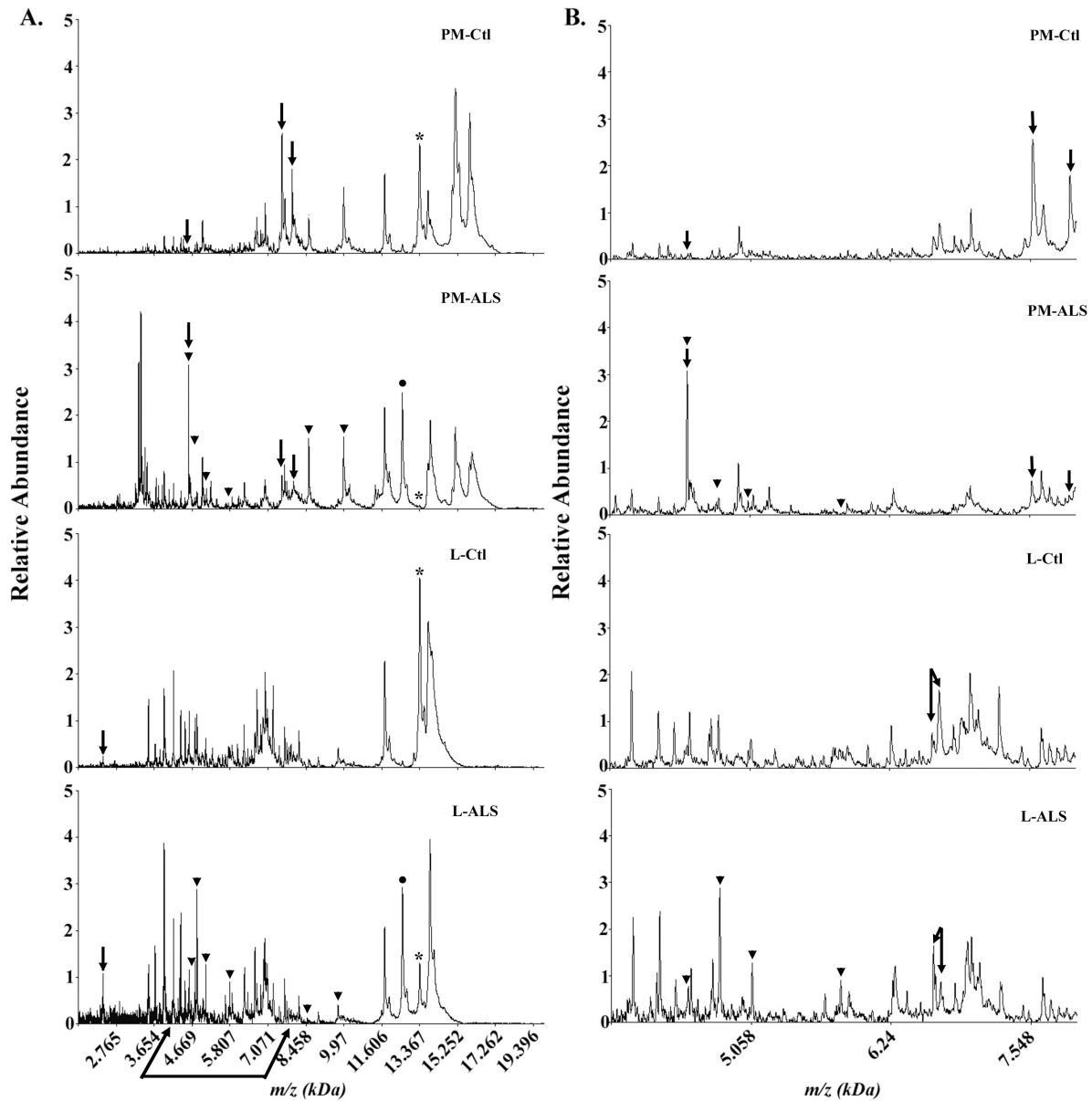


**Figure 35** Representative spectrogram illustrating differences in CSF proteome profile of post-mortem and recently diagnosed ALS patients in the mass range of 2 - 20kDa (A) and 4 -8kDa (B)

*There are distinct differences between PM-ALS and L-ALS indicated by arrowheads in A and B, the peak at approximately 12.7kDa appears in both these cases (black circle). Arrows in A and B represent the differences between control and the respective ALS case. The peak at about*

*13.367kDa (asterisk) represents a peak that is present in high intensity in the control cases but reduced in L-ALS CSF and absent in the PM-ALS CSF.*

The m/z differences in spectral peak patterns observed when comparing the groups PM-Ctl / PM-ALS (4.6kDa, 7.5kDa, 7.9kDa) and L-Ctl / L-ALS (2.5kDa and a doublet at around 6.5kDa) are represented by arrows in Fig 35A and B. Interestingly, the intensities of the 6.5kDa doublet (arrows in Fig 35B) in L-ALS patient was flipped when compared to that of L-Ctl. This could relate to the 6.5kDa peak being a protein variant in the L-ALS CSF. There were also observable differences in peak intensities between PM-ALS and L-ALS (approximate m/z 4.6kDa, 4.75kDa, 5kDa and 5.8kDa; arrowheads in Fig 35, A and B). Similarities between PM-ALS and L-ALS patients were very few or negligible with only one peak at approximately 12.7kDa (black circle in Fig 35A). It is interesting to note that the relative intensity of the peak of m/z 13.367kDa varied amongst the four groups (L-Ctl > PM-Ctl > L-ALS > PM-ALS). The intensity of the peak was significantly reduced in PM-ALS compared to the other three categories (asterisk in Fig 35A).

This underlines the importance of analyzing CSF samples from recently diagnosed ALS patients if the goal is to identify diagnostic biomarkers. The absence of this peak in the PM-ALS cases could also be a result of the intrinsic proteome instability during agonal state and signifies the necessity to assay for biomarkers early on in the disease process.

Additionally when CSF drawn early after onset of disease symptoms (d190) and from other patients at later times (d390 and d1400) were compared to that of CSF drawn at autopsy, the spectrograms revealed differences (Fig 36). The spectral patterns were strikingly different in the post-mortem sample when compared to CSF from recently diagnosed and other living patients. These differences are most likely due to biological alterations since the sample handling

conditions for all of these samples were kept consistent. Such differences can have a profound effect on biomarker discovery. Utilizing post-mortem samples can provide for erroneous differences that can skew biomarker discovery and validation.

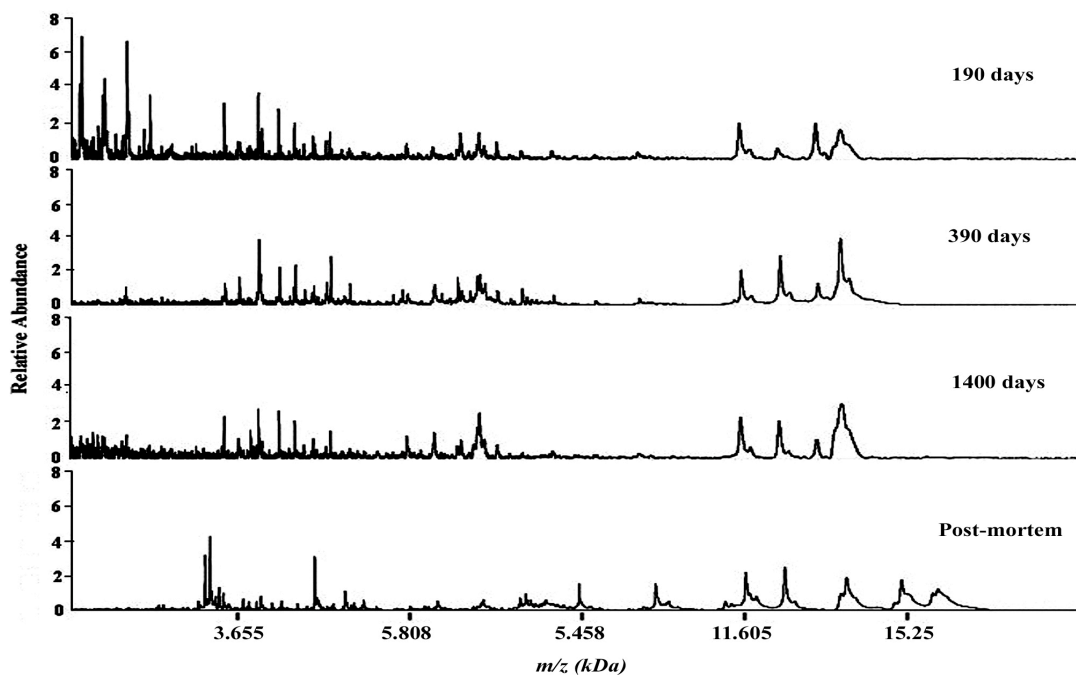


**Figure 36** Differences in spectral patterns when CSF from living ALS patients (190, 390 or 1400 days from time of symptom onset) are compared to post-mortem (PM) CSF sample

*The x-axis represents the m/z in the range of 2-20kDa and on the y-axis is the relative abundance of the peaks. The spectra of the PM CSF appear quite different from the rest with the appearance (about 8-9kDa and about 15kDa) and the disappearance of certain peaks (less than 3kDa).*

Having established differences in the spectrogram, we performed statistical analysis of the differences in the CSF proteome between post-mortem and recently diagnosed ALS patients. Using the CIPHERGEN 3.1 biomarker wizard clustering software, peaks were auto-detected and the output analyzed using a non-parametric univariate analysis. A sample of such a clustering

comparing PM-ALS and L-ALS is illustrated in Figure 37. The larger the separation between the two groups in the cluster for a peak along the y-axis, better is its predictive value.

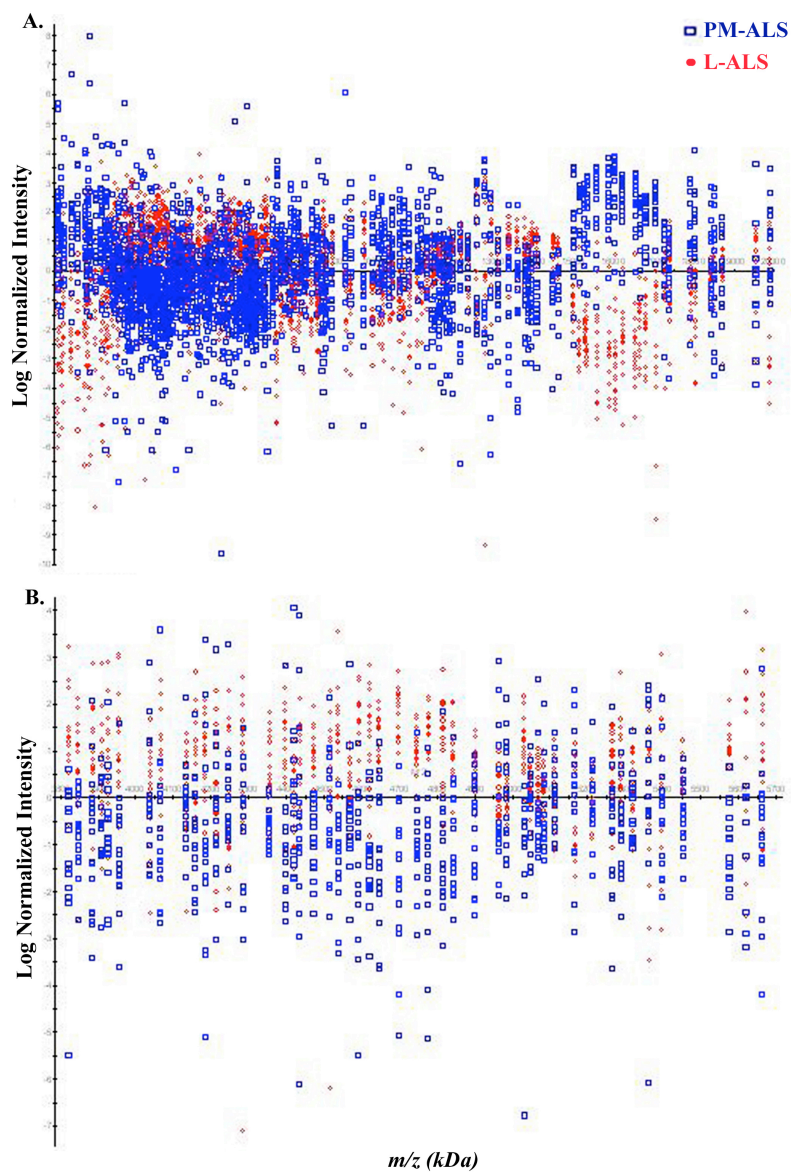
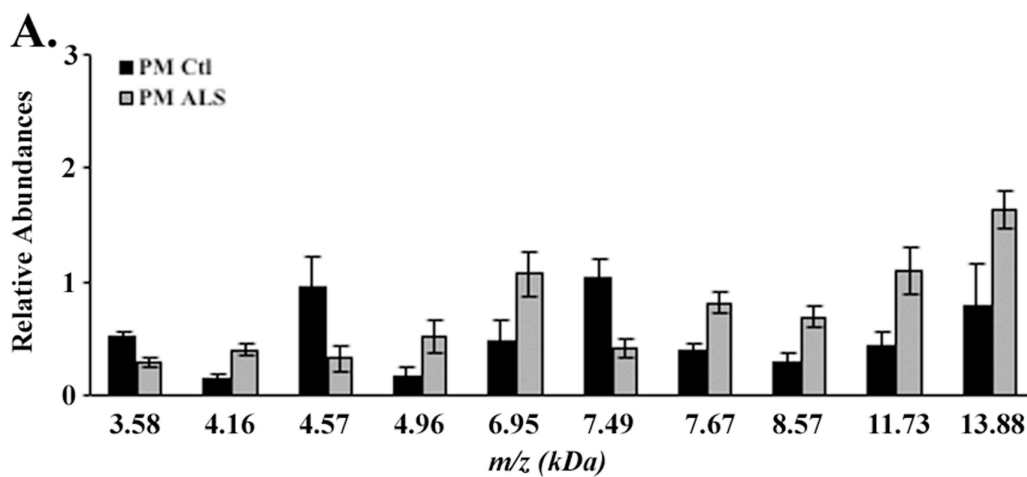


**Figure 37** Clustering of spectra using BPS

(A) Representative cluster of protein peaks between 2-20kDa comparing L-ALS and PM-ALS.

(B) The same cluster in between 4-8kDa. The red circles and blue squares denote L-ALS ( $N = 11$ ) and PM-ALS ( $N = 16$ ) samples, respectively. The y-axis indicates normalized intensity values in the log scale.

Pair-wise univariate comparisons were made between PM-ALS / PM-Ctl, PM-ALS / PM-AD, L-ALS / L-Ctl and PM-ALS / L-ALS samples from three independent experiments performed in duplicates. The peaks common to at least two different experiments and those that were statistically significant with a p value  $\leq 0.02$  are represented by histograms (Fig 38 A to D). The number of peak differences produced by comparing PM-ALS / PM-Ctl, PM-ALS / PM-AD and L-ALS / L-Ctl pairs were 10, 9 and 8, respectively. However, comparing PM-ALS / L-ALS samples yielded as many as 27 peak differences. Two m/z signals (6.88kDa and 13.77kDa) were common to the sample pairs of PM-ALS / PM-AD and L-Ctl / L-ALS. However, the peak signal at 6.88kDa is the double charged protonated form of the peak at 13.77kDa. Furthermore, the 13.77kDa peak appeared statistically different in PM-Ctl / PM-ALS samples in one of the three experimental runs. It is notable to mention that while in the PM-ALS this peak was elevated compared to PM-AD (Fig 38B) or PM-Ctl (data not shown), this intensity of this peak appears to be significantly decreased in L-ALS compared to L-Ctl CSF samples (Fig 38C). In addition to these stark differences between PM and recently diagnosed ALS patient sample, there is only one peak that is similar between the two pairs of samples (Fig 35A, black circles).



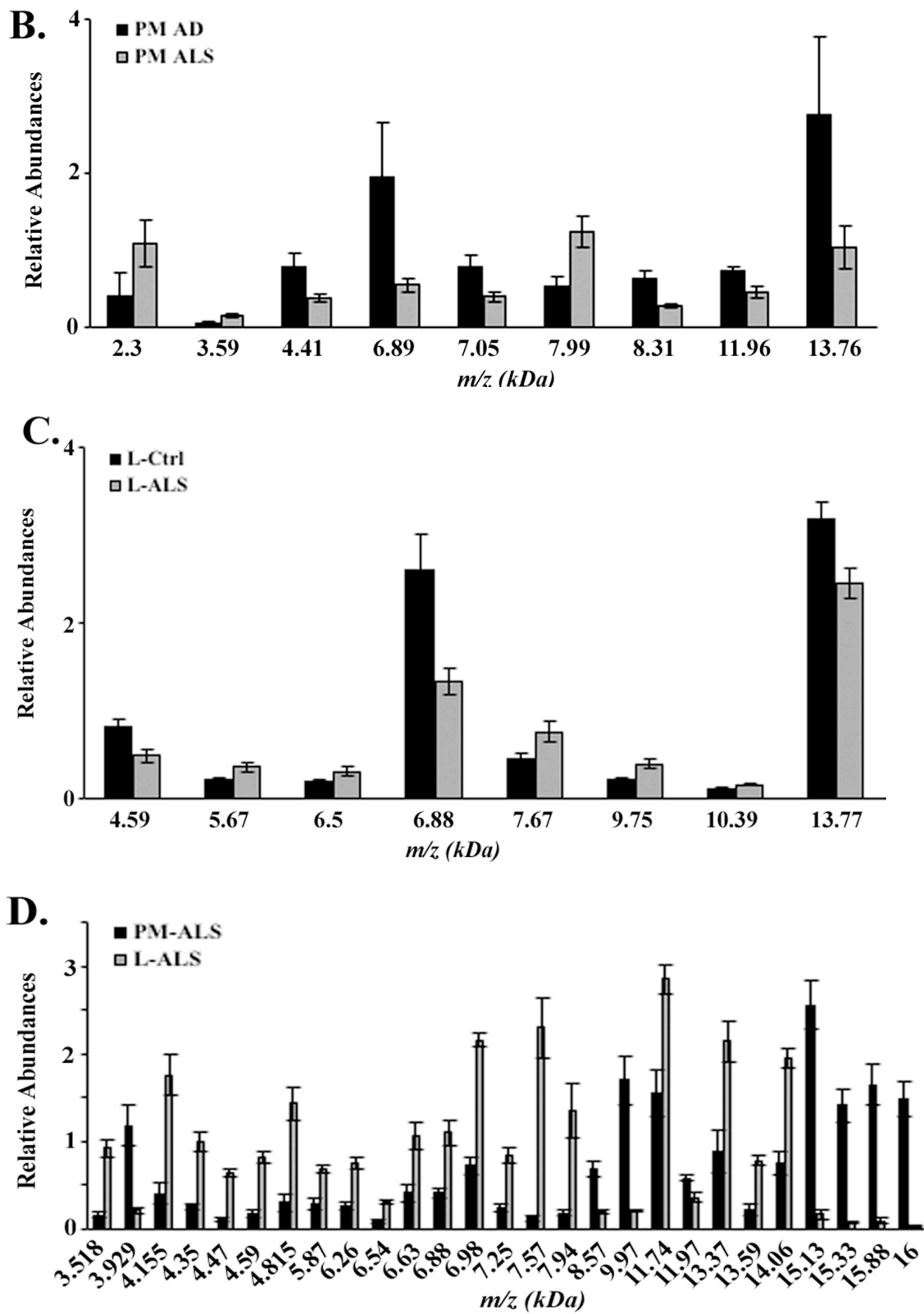


Figure 38 Univariate analysis of CSF from living patients and post-mortem cases

(A) Ten peaks with statistically significant differences ( $p$  value  $\leq 0.01$ ) when comparing CSF from post-mortem ALS (PM-ALS grey bars,  $N = 17$ ) and control (black bars,  $N = 8$ ) cases.

(B) Eight of the nine peaks had a statistically significant difference with a  $p$  value  $\leq 0.01$  when comparing CSF from PM-ALS (grey bars,  $N = 17$ ) and AD (black bars,  $N = 8$ ) cases. The 2.3kDa had a  $p$  value of 0.02.

(C) When CSF from recently diagnosed ALS patients (grey bars,  $N = 20$ ) and age-matched controls (black bars,  $N = 17$ ) were compared, 8 peaks with  $p$  values  $\leq 0.01$  were observed.

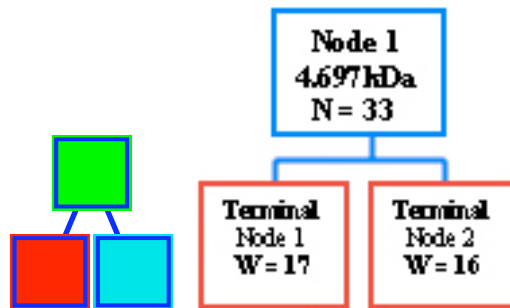
(D) 27 peaks with  $p$  values less than  $1 \times 10^{-4}$  were observed when CSF from recently diagnosed ALS (L-ALS, grey bars,  $N = 20$ ) and PM-ALS cases, (black bars,  $N = 17$ ) were compared by Mann-Whitney non-parametric univariate analysis.

These results suggest that proteomic differences between post-mortem CSF and that from recently diagnosed patients or those from living control individuals are very different. Such differences are further illustrated by the presence of as many as 27 peak differences when the PM-ALS and L-ALS samples are compared.

Further analysis of the datasets was performed using the biomarker pattern software algorithm (CIPHERGEN Biosystems). This multivariate analysis is based on learning a set of rules on two-thirds of the sample using the features (m/z peaks) as selected by the biowizard clustering software. With the learnt set of features and a process of cross-validation the rest of the samples are classified to either of two groups. The percentage of correctly classified control and disease cases signify the specificity and sensitivity of classification, respectively.

When the PM-Ctl and PM-ALS samples were compared, a total of 17 m/z features were used to construct 16 trees with an average specificity of 78% and sensitivity of 80.5%. The BPS classification tree with the best level of sensitivity and specificity for this group comparison is

illustrated in Figure 39. Four additional peaks were used in the classification but these were double charged signals (values in parentheses in row 1, Table 4). The average values of specificity and sensitivity for the pair of L-Ctl and L-ALS were 80% and 91% from 7 trees constructed using 6 peaks. A classification with the 3.44kDa peak as the root node represented the best peak with a sensitivity and specificity of 100% and 91%, respectively (data not shown). While the attribute at 3.44kDa was used as the parent node in as many as 4 different trees, the 2.06kDa peak was present in two different trees as a branch node. This probably implies that these m/z features may represent attributes with strong predictive value. This failed to occur when the post-mortem controls and ALS cases were classified using BPS. This constituted a significant increase (11.5%) in accurately predicting disease state when the samples were from recently diagnosed cases and not from samples obtained at autopsy.



**Prediction Success for Learn Set**

Actual Class	Total Cases	Percent Correct	Ctl N=16	PM-ALS N=17
Ctl	16	100	16	0
PM-ALS	17	100	0	17

**Prediction Success for Test Set**

Actual Class	Total Cases	Percent Correct	Ctl N=17	PM-ALS N=16
Ctl	16	94	15	1
PM-ALS	17	88	2	15

**Figure 39 BPS classification analyzing post-mortem ALS (N = 17) and age-matched post-mortem non-neurological (N = 8) and neurological (N = 8) controls (total N = 16)**

(A) Based on a threshold intensity value,  $m/z$  signal is used as a parent node (4.697kDa) and the total number of samples ( $N = 33$ ) is split into 2 terminal nodes.

(B) The algorithm learns using the  $m/z$  features and predicts on the entire dataset ( $N = 33$ ) considered the “Learn Set”. This resulted in 100% specificity and sensitivity.

(C) The samples are randomized and tested based on the learnt set of features. This produced a specificity and sensitivity of 94% and 88%, respectively. One control and two PM-ALS cases were misclassified.

Groups Compared	Peaks (kDa) used by BPS for Classification Trees
Post-mortem controls and ALS	<u>2.04</u> , <b>2.25</b> , <b>4.53</b> , <u>4.7</u> , 4.82, 5.06 (2.5), 5.33, <u>5.57</u> (2.77), 5.76 (2.88), 6.63 (3.28), <b>6.86</b> , <b>6.98</b> , <b>7.04</b> , 7.14, <b>7.43</b> , <b>7.92</b> , 16.8
Recently diagnosed ALS patients and Living controls	<u>2.06</u> , 3.44, <u>4.74</u> , <b>5.57</b> , 7.49, 8.91
Recently diagnosed ALS patients and Post-mortem ALS cases	2.19, <b>3.5</b> , 3.81, <b>3.91</b> , <b>4.475</b> , <b>4.82</b> , 5.58, <b>7.15</b> , <b>7.55</b> , <b>7.98</b> , 13.748, 14.979, <b>15.13</b> , <b>15.3</b> , 15.4, 15.5, <b>15.78</b> , <b>16</b> , 16.16, 16.5, 16.6

**Table 4** Features utilized by BPS for classification and prediction

Peaks denoted in kilodaltons (kDa) were utilized in classifications and predictions in the different groups indicated on the left column. The bold-faced peaks were also identified by the univariate analysis (see Fig 38 A to D).  $m/z$  features in parentheses indicate that are the double charged signals. Underlined peaks represent those common to post-mortem and living samples.

This multivariate analysis tool was then used to compare datasets of post-mortem ALS cases and recently diagnosed ALS patients obtained from three independent experiments. BPS yielded 31 classification trees using 21 peaks with an average prediction of 89.83% and 91.25% for PM-ALS and L-ALS cases, respectively (Table 4). A classification with the 3.81kDa peak as the root node represented the best peak with a sensitivity and specificity of 100% each (data not

shown). The peaks at 7.55, 15.13, 15.3, 15.5, 16.16 and 16.6kDa were used in multiple trees again suggesting their possible higher predictive value. There were three peaks recognized by BPS that were common to post-mortem cases and living subjects (2.04, 4.7 and 5.57kDa, underlined in Table 4). It is an interesting observation in that it may represent early changes and remain different throughout the course of the disease. It is likely that the levels of these protein peaks could fluctuate and may represent a marker for disease progression. A longitudinal study would help in providing answers to these questions.

The important finding from this study is that CSF obtained at autopsy of an ALS patient reveals a proteomic profile quite different from that procured from a recently diagnosed patient. Such proteomic alterations that occur in post-mortem cases might represent an epiphenomenon and may not necessarily relate to disease-specific changes. Alternatively, the changes observed in CSF obtained at autopsy may represent degradative products. Even if they happen to be disease-specific alterations, they most likely represent the end-stage of ALS. From a clinical diagnostics viewpoint, it is better to obtain early disease biomarkers rather than markers at end-stage. This supported the hypothesis that post-mortem samples are not ideal candidates for biomarker discovery. Carefully handled tissue samples from animal models of neurological diseases wherein the disease progression can be studied in a time-controlled fashion can be valuable assets to biomarker discovery and validation. It is indeed true that a number of studies have been conducted using human post-mortem tissues and other samples in an effort to dissect the molecular mechanisms of a disease. In order to better understand molecular pathways and to obtain molecular targets for therapeutics, multiple approaches including the use of samples procured at autopsy are valuable. Characterization of differentially expressed proteins from post-mortem samples in conjunction with data from other experimental models can lead to a

hypothesis-driven functional approach to dissecting the mechanisms of neurodegeneration. However, they are not ideal in attempts to discover biomarkers for CNS-related diseases. In fact a recent study detailed potential biomarkers for brain injury with relevance to neurodegeneration via a 2D-GE approach utilizing post-mortem CSF [317]. Although they report alterations in interesting proteins some of which are associated with rare forms of familial PD, these cannot be attributed as ‘biomarkers’ but purely as protein alterations using which one can hypothesize disease-specific mechanisms.

## 6. Discovery and identification of ALS-specific biomarkers by mass spectrometry-based proteomics

### 6.1. Abstract

Pathological hallmarks for amyotrophic lateral sclerosis (ALS) include degeneration and loss of motor neurons, protein aggregates in surviving motor neurons and astrogliosis. Although the molecular mechanisms for this debilitating disease are considered multifactorial, how the disease initiation and progression remain largely unclear. Recent advances in understanding ALS pathogenesis have not yielded diagnostic biomarkers or any long-term drug interventions. Proteomic techniques are a sensitive and valuable tool to discover biomarkers and novel therapeutic targets within disease-specific biochemical pathways. *We hypothesized that examination of the proteomic profile of cerebrospinal fluid (CSF) from ALS and control subjects will yield ALS specific protein biomarkers and provide insight into the molecular pathways that govern this disease.* Since CSF bathes the neurons and glia affected during ALS, it may harbor protein biomarkers at sufficient concentration for detection. CSF samples were fractionated and profiled on Ciphergen ProteinChip arrays and surface enhanced laser desorption/ionization-time of flight-mass spectrometry (SELDI-TOF-MS). Univariate analysis performed using the Ciphergen clustering software yielded statistically significant ( $p \leq 0.01$ ) differences in spectral peak intensities of approximately 8% of the spectral peaks using two protein chip subtypes (SAX2 and Zn-IMAC30). Two multivariate analytical algorithms yielded putative biomarker panels with the Rule Learning (RL) algorithm yielding putative biomarker panels with high predictive value for ALS. In addition, we have identified a panel of 11 biomarkers from the two chip arrays through RL analysis that can discriminate the site of disease onset (Bulbar vs Limb

onset). Furthermore, using ion exchange chromatography followed by tandem MS/MS, we have enriched and identified three of the spectral signals to be carboxy terminus of the neuroendocrine secretory protein 7B2 (3.45kDa), cystatin C (13.38kDa) and monomer form of transthyretin (13.78kDa). These proteins have been validated through SELDI-TOF and western immunoblotting. The identification and validation have provided plausible targets for drug design and therapeutics. This is the first such study utilizing CSF samples from ALS patients for proteomic profiling and the identification of diagnostic biomarkers for ALS.

## 6.2. Introduction

The common thread to a diverse range of neurodegenerative diseases such as Alzheimer's disease (AD), Parkinson's disease (PD), Huntington's disease (HD), and ALS are the functional loss of selective populations of neurons. Many of these diseases lack effective diagnostics and treatment. A few of these fatal diseases such as ALS have very minimal drug interventions that have marginal improvement in life span. Given the dearth for diagnostic biomarkers and long-term therapeutic interventions, the impetus in the scientific community is for high-throughput screening for drug targets and also develop a sensitive approach to disease-specific proteomic profiling.

ALS, one of the most common adult motor neuron diseases, affecting one in every 20,000 individuals exists in both sporadic and familial forms (see Chapter 1). Genetic mutations observed in FALS may not fully explain the pathogenesis observed in SALS, which is considered multifactorial [423, 424]. Many approaches, including transgenic animal models, *in vitro* models and human post-mortem studies, have been used to try and understand the pathogenesis of ALS [122, 141, 151, 199, 425-429]. Although these studies have yielded therapeutic targets, there is only one marketed drug, riluzole, and it has only a modest effect on survival [302, 303, 430-433]. There are other molecules that have shown promise in animal studies such as the efficient retrograde delivery of insulin-like growth factor -1 (IGF-1) [206]. However, many of these studies have failed to transform into long-term therapeutic interventions for ALS patients.

Many neurodegenerative diseases including ALS are termed "proteinopathies", characterized by the accumulation of protein abnormalities [434]. Changes in protein composition of the CSF or serum between non-neurological controls and ALS patients may be

indicative of alterations in central nervous system (CNS) protein expression or degradative patterns [435]. New drug targets can be discovered and validated through a systematic combination of proteomic and bioinformatic approaches, analyzing body fluids from patients. Identification of ALS specific biomarkers through functional proteomics would aid in rapid clinical diagnosis, unmasking potential therapeutic targets, and testing drug efficacy in clinical trials. However alterations can be produced due to reduced stability through improper handling and storage conditions as enumerated in Chapter 4. In addition, the CSF proteome can be very different if post-mortem samples are used instead of from recently diagnosed patients and normal controls (see Chapter 5). These factors necessitate the utilization of properly controlled samples from patients who have been recently diagnosed with ALS and also samples from normal controls.

Protein maps from developmental and adult rats, human brains have all been constructed by the use of two-dimensional gel electrophoresis (2D-GE) coupled to MS [436]. Such studies have provided information about the diversity of nervous system-specific proteins that can then be compared in response to injury or disease. AD is associated with a number of defects such as loss in synaptic function, decreased metabolism with mitochondrial deficiencies, oxidative stress, defects in proteasome machinery and protein folding. Proteomic approaches by 2D-GE and MS using AD brain tissues, CSF and animal models have demonstrated alterations in proteins involved in a number of pathways. Such proteomic studies have also been conducted in forms of cognitive impairment such as fronto-temporal dementia (FTD), HIV-1 associated cognitive loss, neuropsychiatric disorders such as schizophrenia, Down's syndrome, and neurodegenerative diseases such as PD and HD [316, 318-321, 418, 437].

Most of the studies in ALS research have utilized a genomic approach or biochemical assays such as enzyme-linked immunosorbent assays (ELISA) for detecting changes in gene expression or protein, respectively [149, 191, 438-440]. Proteomic approaches for ALS is limited with one report each of analysis using *in vitro* culture models and post-mortem samples [419, 441]. None of the studies have produced a sensitive and specific biomarker. Mass spectrometric (MS) analysis on the effects of G93A and G37R mutant SOD1 transfected into a motor neuron-like cell line suggested alterations in proteins associated with antioxidant defenses, proteasome machinery and nitric oxide metabolism [441]. A recent study identified increased levels of ceramides, sphingomyelins and cholesterol esters in spinal cords of ALS patients and transgenic mice using MS/MS, suggesting that MS analysis is a powerful tool [419].

The goal of this study was to identify ALS-specific markers and proteins involved in different molecular pathways, which can then be used for diagnostics and as molecular targets for therapeutics. We performed proteomic profiling of CSF from recently diagnosed ALS patients and control subjects using SELDI-TOF-MS. Diagnostic biomarkers at the clinical onset of ALS were sought in CSF obtained from ALS patients on average of 385 days from onset of clinical symptoms. Utilizing two Ciphergen Biosystems ProteinChip arrays and two computer assisted algorithms (RL and BPS), we have identified disease specific protein peaks. We report statistically significant changes in 30 mass spectrometric signals ( $p \leq 0.01$ ). We have also identified predictive biomarker panels by RL that differentiate ALS from control subjects in blinded test subjects [442]. Peptide mass fingerprinting and sequencing of these markers have yielded three protein identities. In addition, we identified markers with high predictive value to discriminate the site of disease onset in these patients. This is the first study to identify a panel of predictive protein biomarkers in CSF of recently diagnosed ALS patients.

### **6.3. Materials and Methods**

#### **6.3.1. Study Population and CSF**

For the biomarker discovery and identification phase of proteomic study, the training group included 21 control subjects and 15 patients with a recent clinical diagnosis of ALS by board certified neurologists specializing in motor neuron diseases. While 14 of the ALS subjects were sporadic cases, one familial non-SOD1 subject was included (ALS 2, Table 5). The average ages of the ALS and control cohorts were  $49.6 \pm 3.4$  and  $45.2 \pm 3.4$ , respectively. Control group included the following cases: 12 non-neurodegenerative or with no neurologic complaints; one with metabolic myopathy; two each with neuralgia and neuropathy; one case each of meningitis, demyelinating disorder, slowly progressing atypical MND and probable AD. The average time from clinical onset (date when ALS patient first reported symptoms) to when CSF was obtained was  $385 \pm 49.1$  days (113-730 days). We also used a separate test group of 20-blinded subjects as a “diagnostic” set to predict disease status based on predictions generated using the training group. Among 23 ALS samples, the clinical presentations were either with bulbar onset (N = 7) or with limb onset (N = 16). These details are summarized in Tables 5 and 6.

#### **6.3.2. SELDI-TOF-MS**

The samples and chips were prepared as enumerated in sections 5.3.2 and 5.3.3. The IMAC30 arrays were treated with 100mM zinc sulfate followed by washing with 50mM sodium acetate. These were then repeatedly washed with HPLC-grade water (SIGMA) and phosphate-buffered saline. The CSF samples that were desalted and concentrated using ZipTips with C4 columns as explained in section 4.3.1 were then applied to the chip arrays. The settings for SELDI-TOF-MS are as mentioned in 5.3.3.

Group	Diagnosis	Age	Gender	Dz Duration (Days)	Site of Dz Onset
Control 1	Normal	37.7	F	NA	NA
Control 2	Normal	49.5	M	NA	NA
Control 3	Normal	26	M	NA	NA
Control 4	Normal	72.3	F	NA	NA
Control 5	Myopathy	41.2	F	NA	NA
Control 6	Slowly Prog. MND	41.8	F	765	NA
Control 7	Neuralgia	43.8	F	NA	NA
Control 8	Neuropathy	34.4	M	NA	NA
Control 9	Neuropathy	80.5	F	NA	NA
Control 10	Normal	60.9	M	NA	NA
Control 11	Normal	29.5	F	NA	NA
Control 12	Probable AD	50.5	F	NA	NA
Control 13	Normal	68.2	M	NA	NA
Control 14	Normal	26.3	M	NA	NA
Control 15	Neuralgia	39.1	M	NA	NA
Control 16	Demyelinating Dz	30.6	F	NA	NA
Control 17	Normal	28.7	M	NA	NA
Control 18	Normal	40.2	M	NA	NA
Control 19	Normal	34.4	F	NA	NA
Control 20	Meningitis	54.8	M	NA	NA
Control 21	Normal	59.4	F	NA	NA
ALS 1	ALS	34.3	M	192	Limb
ALS 2	Familial ALS	51.3	F	568	Limb
ALS 3	ALS	57	M	406	Limb
ALS 4	ALS	46.1	M	251	Bulbar
ALS 5	ALS	50.3	M	224	Limb
ALS 6	ALS	56.7	M	572	Limb
ALS 7	ALS	75.4	M	467	Bulbar
ALS 8	ALS	31.8	M	113	Bulbar
ALS 9	ALS	39.3	M	175	Bulbar
ALS 10	ALS	26.6	M	615	Limb
ALS 11	ALS	39.3	M	389	Bulbar
ALS 12	ALS	60.5	F	730	Bulbar
ALS 13	ALS	60.3	F	367	Limb
ALS 14	ALS	59.7	M	190	Limb
ALS 15	ALS	56.2	F	529	Bulbar

**Table 5** List of cases in the training set

*Dz – Disease; MND – Motor neuron disease; AD – Alzheimer’s Disease*

Group	Diagnosis	Age	Gender	Dz Duration (Days)	Site of Dz Onset
Control 1	Normal	80.1	F	NA	NA
Control 2	Meningitis	30.5	F	NA	NA
Control 3	Normal	41.1	F	NA	NA
Control 4	Normal	31.6	F	NA	NA
Control 5	Stroke	75.9	M	NA	NA
Control 6	Normal	37.1	M	NA	NA
Control 7	Normal	40.6	F	NA	NA
Control 8	Lymes Dz	43	F	NA	NA
Control 9	Normal	23.9	F	NA	NA
Control 10	Neuropathy	54.2	F	NA	NA
ALS 1	ALS	29.7	M	360	Limb
ALS 2	ALS	73.7	F	1110	Limb
ALS 3	ALS	61.2	F	392	Limb
ALS 4	ALS	47.5	M	3913	Limb
ALS 5	ALS	58.8	M	289	Limb
ALS 6	ALS	48.8	M	380	Limb
ALS 7	ALS	36.1	M	928	Limb
ALS 8	ALS	74.5	M	1339	Bulbar
ALS 9	ALS	47.4	M	324	Limb
ALS 10	ALS	50.6	M	254	Limb

**Table 6** List of cases in the blinded test set

*The groups and site of disease (Dz) onset were revealed post-analysis*

### 6.3.3. Data Analysis

Analysis of the spectrograms using Univariate analysis and BPS were performed as explained in section 5.3.4. In addition, the samples were analyzed using another bioinformatics tool called the Rule Learner (RL) algorithm. The RL algorithm was first used for predicting mass spectra of complex organic molecules [333]. RL creates and searches possible rules by successive specialization, guided by raw spectral data in a training set and by prior knowledge

about the data (e.g., clinical diagnosis or symptoms) to define diagnostic biomarkers [334]. RL learns a set of conditional rules of the form IF-THEN or  $P_1, \dots, P_k \Rightarrow C$ , where the left-hand side (LHS) are premise clauses that describe tests on values of one or more attributes of the training set (e.g., spectral peaks). The concept conclusion (C) is an assertion that any subject with features matching the conditions on the LHS of rule is a member of a class (e.g., ALS). RL learns predictive patterns by starting from rules with a single feature and adding one feature at a time to partial rules that look most promising. Each partial rule is matched against the training cases to see how many of the positive cases are correctly predicted and how many of the negative cases are incorrectly predicted, thus providing statistical guidance to the search. Based on the training data, quantitative attributes such as spectral peaks are converted to ranges of discrete values. These are then divided into groups of values representing mean and levels of standard deviation away from the mean for each attribute. Due to the large amount of data (about 27,000 m/z datapoints), RL was run separately on 10 almost equal subsets of the data to pick representative biomarkers from each subset. In order to allow these biomarkers to compete among one another, we performed a final run of RL with the union of such features selected from each of the previous runs. A 3-fold cross-validation was utilized to tune the RL input parameters during the training, which produced the final set of rules (i.e., predictors). Evidence gathering is performed using “weighted voting” wherein each coded sample is assigned a group (ALS or control) by the casting of a “weighted vote” (the number of training samples that defines a particular rule). For instance, if a coded sample is predicted to be ALS based on three rules of which one of them has defined it to be control, then the other two rules that defines the right hand side (RHS) to be ALS would have “outweighed” the “control” rule. The predictions are then compared to known clinical diagnosis to determine sensitivity and specificity. Different

kinds of statistics are employed during data analysis, including an estimation of certainty factor, together with its positive predictive value and p-value.

#### **6.3.4. Biomarker Identification by Mass Spectrometric Analysis**

Samples (500ul CSF) were fractionated (anion exchange) by gravity flow using Q HyperD F matrix (Ciphergen Biosystems, USA) in Biospin columns (BioRad, USA). The columns were first equilibrated using 50mM Tris-HCl at pH 9. Fractions were collected using buffers at pH of 9 (20mM Tris-Hcl / 0.1% Triton X-100), pH 7 (50mM HEPES / 0.1% Triton X-100), pH 5, and 4 (100mM Sodium Acetate / 0.1% Triton X-100) and pH 3 (50mM Sodium Citrate / 0.1% Triton X-100). The column was then washed with a 33% isopropanol / 17% acetonitrile (ACN)/ 0.1% trifluoroacetic acid (TFA) solution (organic fraction). These different fractions were spotted on SAX2 and NP20 (normal phase) chip to confirm the presence and purity of relevant spectral peaks.

The aliquots of 50-500 $\mu$ l aliquots were concentrated using YM3 or YM10 filtration devices (Millipore). The resulting fractions were electrophoresced on a 1D-SDS PAGE and trypsin digested. Destained and excised bands of interest were incubated with 200 $\mu$ l of 40% methanol / 10% acetic acid solution to remove SDS. After incubation with 200 $\mu$ l of ACN, the gel pieces were dried in a speed-vacuum or at 37°C for 10 mins. In order to elute the protein, the gel pieces were incubated with 20 $\mu$ l of 50% formic acid / 20% ACN / 15% isopropanol (FAPH) solution for 2 hrs with strong agitation. A small amount of the eluted proteins was spotted onto a NP20 chip and the rest were dried in a speed-vacuum. The protein pellet was then re-hydrated in 10 $\mu$ l of 25mM ammonium bicarbonate (pH8) containing 0.02 $\mu$ g/ $\mu$ l of sequencing grade - modified trypsin (Promega) and incubated at 37°C for 16 hrs. The tryptic digests (1-2 $\mu$ l eluates)

were tested again on NP20 chip surface and the fragments were compared to ProFound protein databases. These fragments were also applied for sequencing using QStar-TOF-TOF MS/MS (in collaboration with Ciphergen Biosystems).

### **6.3.5. Biomarker Validation**

#### **6.3.5.1. Immuno-SELDI-TOF-MS**

The identified proteins were validated using a pre-activated antibody chip array and Western immunoblotting. Anti-rabbit polyclonal antibodies against cystatin C (DAKO, Denmark) and transthyretin (DAKO, Denmark) were used for SELDI-TOF and immunoblotting. Immunoprecipitation for transthyretin using pre-activated chip arrays were performed as published [443]. Briefly, 5  $\mu$ l of protein A (Sigma, St. Louis, USA) beads (0.1 mg/ml in PBS) were added to the spots of PS10, pre-activated ProteinChip array, (Ciphergen Biosystems, USA) and incubated in an humidity chamber for 1hr at room temperature. To reduce non-specificity, residual active sites were blocked using 100mM Tris-HCl, pH 8.0 for 25mins at room temperature. The array was washed in 1X PBS three times for 5mins each followed by incubation of each of the spots with the anti-transthyretin antibody at a concentration of 4.1  $\mu$ g/ $\mu$ l for 1.5hrs on a slow shaker. The unbound antibodies were then washed away with three 5min washes in a 15ml tube with 1X PBS. 5  $\mu$ g of the ZipTip fractionated CSF samples from controls (n = 7) and ALS (n = 7) subjects were added to the spots and incubated in a humidity chamber for 1.5hrs at room temperature. Spots were washed three times by placing 5  $\mu$ l of 1X PBS on the spot followed by rinsing once with 5  $\mu$ l of HPLC-water. Once the EAM (SPA, see section 4.3.2) was added to the spots, the chip was loaded onto the ProteinChip reader (PBS IIc, Ciphergen

Biosystems, USA). The settings for laser intensity and sensitivity were 215 and 9, respectively. The chip was processed and instrument calibrated as explained in sections 4.3.3 and 5.3.3.

#### **6.3.5.2. Immunoblotting**

Western immunoblotting for cystatin C and transthyretin was performed as enumerated in section 2.3.5 with the following modifications. 25ng (Cystatin C Westerns) and 50ng (TTR Westerns) of the CSF sample from controls (n = 7) and ALS (n = 7) cases were electrophoresced on a 10-20% Tris-Tricine Ready Gels (BioRad Laboratories, USA) and transferred to a PVDF membrane. The primary antibodies were used at a dilution of 1:500. Purified cystatin C protein (Calbiochem, USA) and transthyretin (Biodesign, USA) were also utilized. While they were utilized at a concentration of 1µg for SELDI-TOF, purified TTR at 50ng and cystatin C at 10ng were utilized for Western immunoblotting.

#### **6.3.5.3. Immunohistochemistry**

Immunohistochemistry for transthyretin by light microscopy using paraffin embedded sections of lumbar spinal cord from archived human post-mortem tissues was performed as described in section 2.3.3. Anti-rabbit polyclonal antibodies (DAKO, Denmark) were used at a concentration of 1:300 to probe sections from 8 control and 16 ALS cases .

## **6.4. Results**

SELDI-TOF-MS was used to characterize CSF analytes of ALS and control subjects. By comparing spectra from the same CSF samples analyzed on SAX2 and IMAC30 chips during an interval of multiple months, we determined that adequate reproducibility between experiments was achieved (data not shown). To account for variability within the experiments, we assayed one CSF sample on a spot of each chip within an experiment and determined that the coefficient of variability was less than 30% (data not shown). Having established the reproducibility of the spectral data, we analyzed CSF samples from the training group.

### **6.4.1. Identification of differentially expressed protein peaks in ALS by univariate analysis**

Direct comparison of spectra from SAX2 or Zn-IMAC30 chips between control and ALS subjects revealed very similar protein profiles (Fig 40A), with discernible differences in some signal intensities (Fig 40B, numbers). The clustering software (CIPHERGEN version 3.1 BioWizard) autodetected a total of 366 peaks (207 on SAX2 and 159 on Zn-IMAC30 chip) in the training group (N=36). We used the same software to perform a univariate analysis of both the SAX2 and Zn-IMAC30 datasets (366 peaks) to identify CSF spectral peaks that exhibited statistically significant relative peak intensities (Fig 41). We identified 15 protein peaks each from the SAX2 (Fig 41A) and the Zn-IMAC30 (Fig 41B) datasets, approximately 8% of total peaks that had a statistically significant difference ( $p < 0.01$ ) in peak intensity (either increased or decreased relative abundance). Furthermore, there were 22 other signals from both datasets with statistically significant difference ( $p \leq 0.05$ ) in peak intensities (data not shown). Thus a

total of 52 signals (14.2%) exhibited significant alterations in peak intensity, thus representing putative biomarkers.

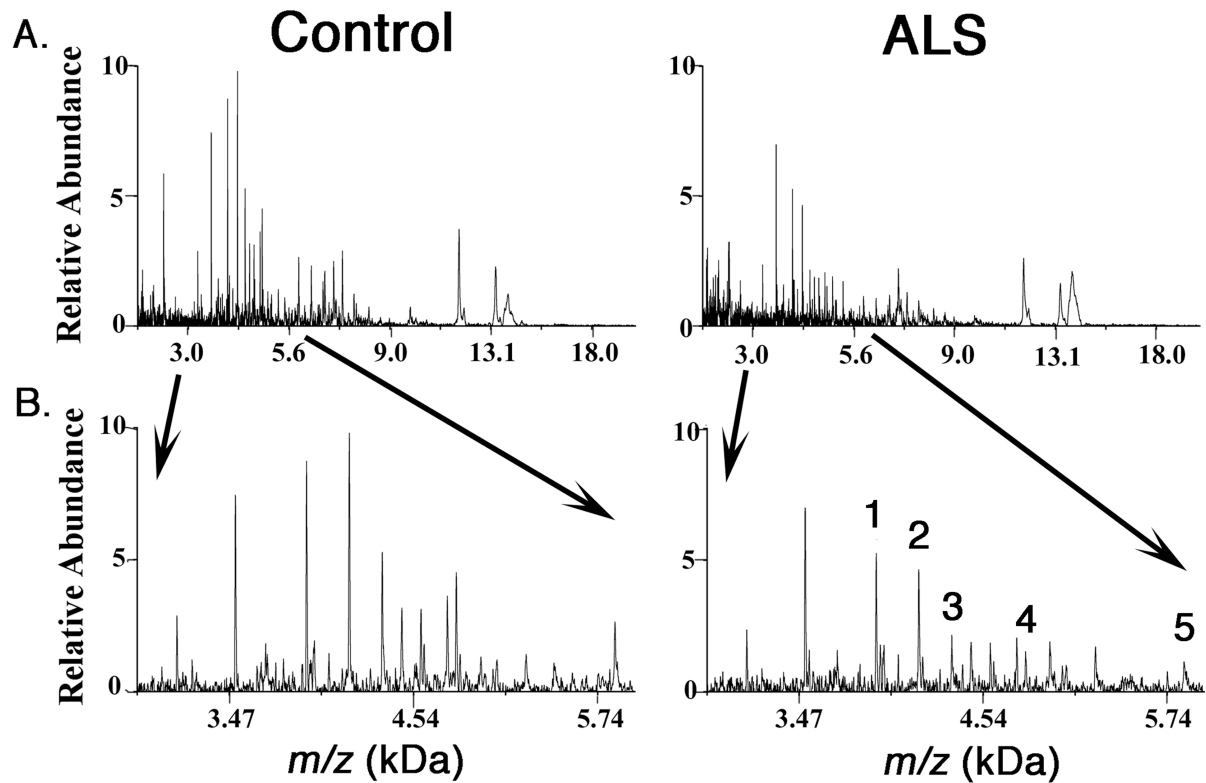


**Figure 40 Comparison of mass spectra between ALS and Controls using SAX2 chip**

*Panel A depicts representative spectral peaks of ALS and control subjects on SAX2 chip and is representative of three independent experiments. Mass-to-charge ratio in kilodaltons (2-20 kDa) is shown on the x-axis, and the relative abundances (peak intensities) on the y-axis. Panel B is the magnification (indicated by the arrows) of the spectra in the range of 3 and 6 kDa. Numbers denote spectral peaks with significant differences ( $p < 0.05$ ) in relative abundance between control and ALS subjects as determined by univariate analysis. Numbers 1 – 5 correspond to spectral peaks 3.923, 4.115, 4.468, 4.807 and 5.866 kDa.*

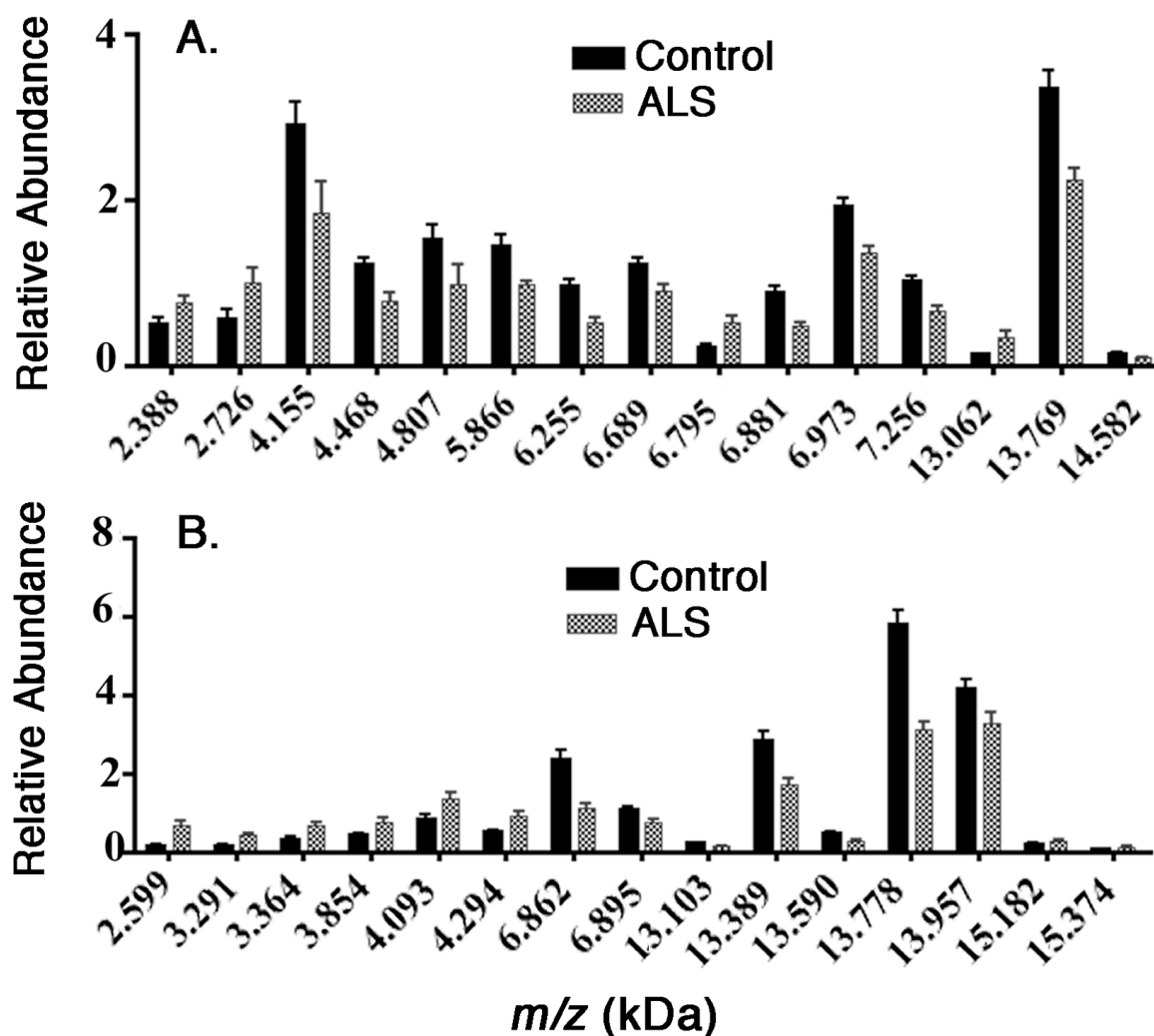


**Figure 41 Univariate analysis of analytes from SAX2 and Zn-IMAC30**

*SAX2 (A) and Zn-IMAC30 (B) datasets exhibited peak intensities with statistical significance ( $p \leq 0.01$ ) between ALS (stippled bars) and control (solid black bars) subjects. Mass in kilodaltons (kDa) is shown on the x-axis, and the mean peak intensity values on the y-axis. Error bars correspond to standard error of mean (SEM). All analyte signals appeared in greater than 30% of subjects. CIPHERGEN biomarker wizard 3.1 - based non-parametric Mann-Whitney test was used for statistical analysis.*

## 6.4.2. CSF Biomarker panels

### 6.4.2.1. BPS Analysis

Two computer-assisted algorithms were used to identify potential diagnostic biomarkers from the CSF spectra in the training group. BPS creates classification trees containing one or more protein peaks that are used to predict disease status. Protein peaks auto-detected from the raw data are used in building trees. An example of a classification tree for the SAX2 dataset is shown in Fig 42A.

The parent or the root node used a peak at 13.77 kDa. 19 subjects with a threshold value greater than 2.824 placed in the right terminal node were controls. The left node contained 17 subjects that were further split at a 2.19 kDa peak. All three subjects in the resultant left node with a threshold value of  $\leq 0.313$  were controls. The 14 subjects in the right terminal node were all ALS subjects. This tree resulted in a misclassification of an ALS subject, yielding 93% sensitivity and 100% specificity during the training phase. BPS then randomizes the dataset through a 10-fold cross-validation and uses the classification tree to make predictions on all 36 samples that are then compared to the known subject diagnosis. The above tree predicted ALS subjects during the validation phase with 80% sensitivity and 95% specificity. Additional trees used peaks observed at 2.014, 2.157, 3.827, 4.964, 6.255, 6.53, 6.79, 6.89, and 6.97 kDa with an overall sensitivity of 73% and specificity of 83%.

BPS was also used to identify potential biomarkers from the Zn-IMAC30 ProteinChip dataset (Fig 42B). In this classification tree, the signal at 3.36 kDa is the parent node. 17 subjects present in the left terminal node with a threshold value of  $\leq 0.342$  were all control subjects. The 19 subjects in the right node were split further using the peak of 2.33 kDa. The resulting right terminal node with a threshold value of  $> 4.122$  contained three controls. The 16

subjects in the left node were further split using the 2.01 kDa signal. All of the 15 subjects in the right terminal node belonged to the ALS group. This classification tree predicted ALS with 100% sensitivity and specificity during the training phase. The classification tree predicted subjects as ALS with 93% sensitivity and 95% specificity through cross-validation of the training set. Additional trees used signals observed at 3.29, 3.44, 6.48, 6.86, 13.1, and 13.78 kDa as nodes with an overall sensitivity of 87% and specificity of 86% for the prediction of ALS.

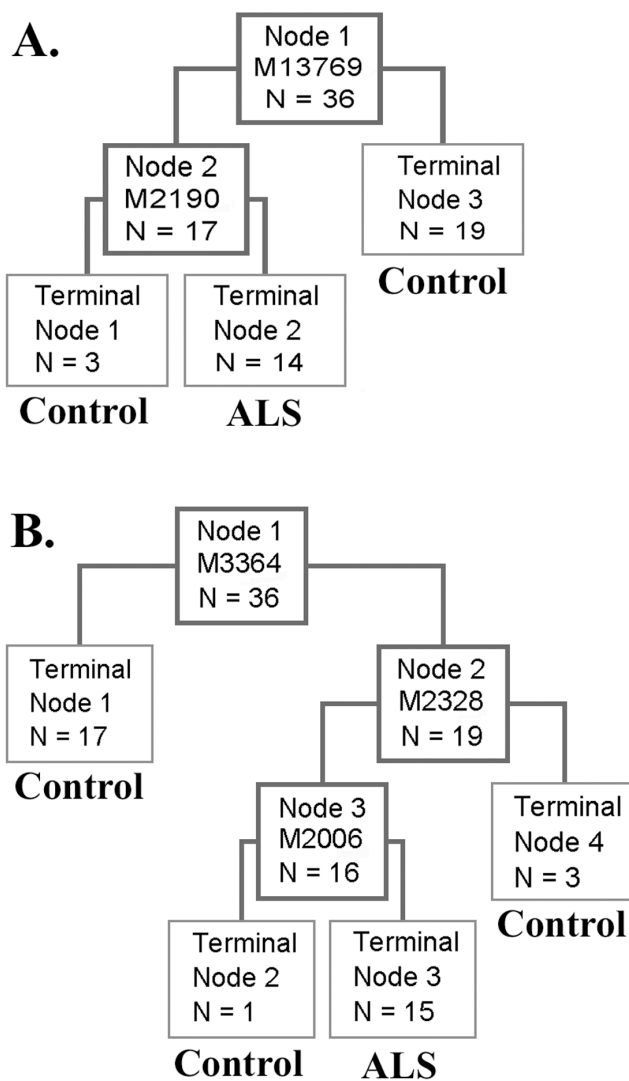


**Figure 42** Multivariate analysis of SAX2 (A) and Zinc-IMAC30 (B) datasets using BPS

(A) Tree representing the SAX2 datasets ( $N = 3$ ). The relative cost value is 0.248. The sensitivity and specificity based on cross-validation based on 12 samples is 80% and 95%, respectively.

(B) Tree representing the Zn-IMAC30 datasets ( $N = 2$ ). The relative cost value is 0.114. The sensitivity and specificity based on cross-validation of 12 samples is 93% and 95%, respectively.

BPS classification trees cannot, however, be applied to spectra to make predictions of a blinded test group. Therefore, we used the Rule Learning (RL) algorithm to create a biomarker panel that can be directly applied to test subjects for diagnostic predictions. RL creates a series of learned rules using raw mass spectral data containing 18,000 m/z data points, which are then used to predict disease status of subjects. RL predicted disease status on one-third ( $N=12$ ) of the training set using rules generated on two-thirds ( $N=24$ ) of the training set.

#### **6.4.2.2. RL Analysis**

For the SAX2 dataset, RL identified 8 rules using 9 mass spectrometric signals (2.649, 3.707, 5.101, 5.828, 10.639, 10.989, 13.681, 14.62 and 15.599 kDa). When these rules were applied to the 12 coded subjects from the training group, RL predicted ALS with 67% sensitivity, 83% specificity and 75% accuracy. RL algorithm was also applied to the Zn-IMAC30 dataset and generated 5 rules using 6 protein peaks (2.201, 5.378, 11.546, 12.874, 15.21, and 16.733 kDa). When these Zn-IMAC30 RL rules were applied to one-third ( $N=12$ ) of the training set, RL predicted ALS with 100% sensitivity, 50% specificity and 70% accuracy. Two of the three control cases that were incorrectly predicted using the Zn-IMAC30 RL rules were predicted correctly by SAX2 RL rules. Furthermore, an ALS case incorrectly predicted by SAX2 rules was predicted correctly by the Zn-IMAC30 rules. These results suggest that using

rules generated from both chip datasets increases the overall predictive value, and the combination of our ALS data resulted in overall predictive values of 89% sensitivity, 72% specificity and 86% accuracy. Therefore, we generated “combined” RL rules from both the SAX2 and Zn-IMAC30 chip datasets validating them first on one-third (N=12) of the training set (Table 7).

“IF”	“THEN”
(SAX2 3.707 in $-0.113 \leq x < 0.078$ )	Control
(Zn 13.395 in $0.079 \leq x < 0.137$ )	Control
(Zn 8.931 in $0.170 \leq x < 0.289$ )	Control
(Zn 16.595 in $0.048 \leq x < 0.072$ )	Control
(Zn 3.052 in $0.24 \leq x < 0.516$ )	Control
(SAX2 7.775 in 4-High)	ALS
(Zn 17.087 in 2-Low)	ALS
(SAX2 11.524 in 2-Low)	ALS
(Zn 8.616 in 2-Low)	ALS
(Zn 9.098 in 2-Low)	ALS

**Table 7      Multivariate analysis of blinded dataset using RL**

*A representative set of “IF-THEN” rules generated by the RL algorithm. A 3-fold cross validation test was used and a final set of 10 “combined” rules generated from a total of 36 subjects (15 ALS and 21 control) for diagnostic prediction from both SAX2 and Zn-IMAC30 datasets. These rules were applied for the “diagnostic” test set of 20-blinded samples. The certainty factor and p value for all the rules generated were 1.0 and less than 0.001, respectively.*

Furthermore, this set rules was applied to make diagnostic predictions from a set of 20-blinded test subjects. The predictive values for the set of 10 “RL biomarkers” were 80% sensitivity, 59% specificity and 73% accuracy (Table 8). It is important to note that the time from symptom onset to CSF draw for the two ALS subjects incorrectly predicted by the biomarker panel was 1339 (ALS 8, Table 6) and 3913 days (ALS 4, Table 6), respectively. A 10-year duration from symptom onset to CSF draw best represents a slowly progressing MND, akin to one subject included within the control group of the training set (Control 6, Table 5). ALS subjects used to create the biomarker panel had a time from symptom onset until CSF draw of 385 days, significantly closer to clinical onset and suggesting that our biomarker panel is most predictive for subjects near the time of clinical symptom onset. Removal of these two slowly progressing MND cases from the analysis increased the predictive values to 100% sensitivity and 76% accuracy for this group of test subjects (N=18). Thus the overall predictive values for ALS in all blinded test subjects [N=30, (12+18)] were 92% sensitivity, 59% specificity, and 79% accuracy (Table 8).

Predicted \ Actual	ALS	Control	NP
ALS	12	3 (1*)	0
Control	5	10	2

<b>Sensitivity</b>	80% (92%*)
<b>Specificity</b>	59%
<b>Accuracy</b>	73% (79%*)
<b>Coverage</b>	94%

**Table 8 RL analysis of validation (n=12) and blinded (n=20) sample sets**

*After the predictions were made based on the RL rules, the codes were broken and the predictions compared to the known clinical diagnosis for each case. The sensitivity and accuracy was 80% and 73%, respectively. The asterisk indicates the two ALS cases with long duration of*

*symptom onset to CSF draw (1339 and 3913 days). When these cases were not considered, the sensitivity and accuracy indicated with the asterisk increased to 92% and 79%, respectively. Coverage refers to the percentage of number of predicted cases (ALS + Controls) excluding the no predictions (NP).*

Additionally, using RL, we analyzed all of the samples ( $n = 52$ ). This set included all the cases listed in Tables 5 and 6 excluding the cases - ALS 4, ALS 8 in Table 6; Controls 5 and 6 in Table 5. Uniform sampling created subsets of attributes (approximately 1000 m/z per subset) and training models were learnt on each of these subsets using 40 of the cases. Then a union of all the m/z attributes that occurred in all the models was chosen (about 1200 m/z values) by a 5-fold cross-validation approach. The rules learnt from all the 40 samples were then tested on the remaining 12 samples. This resulted in 11 m/z peaks or attributes from 12 models, with 7 of the peaks appearing in 10 or more different models (Table 9).

By differing the parameters of the algorithm such as the certainty factor threshold (as this value tends towards 1, higher the predictive value of a rule) data was generated by applying the set of 11 attributes to the test set. The average percent prediction accuracy and percent coverage from these 12 different model sets were  $77 \pm 4.8$  and  $88 \pm 1.2$ . The percent average specificity and sensitivity were  $82 \pm 7.7$  and  $68 \pm 2.8$ , respectively. The chosen attributes in the best model were: 2.4, 2.46, 6.88, 12.28, 13.64kDa (SAX2 chip array) and 3, 3.4, 8.9kDa (Zn-IMAC30 array). This model had an average accuracy, coverage, specificity and sensitivity of 91%, 92%, 100% and 75%, respectively. One of the ALS cases was predicted incorrectly 10 of 12 times that the model was tested. The 2.4kDa peak was chosen as a rule that predicted the RHS of the rule as control. In each case, it was this rule in combination with another rule that outweighed the 3kDa peak, which was predicted as ALS.

<i>Type of ProteinChip Array</i>	<i>m/z Attributes (kDa)</i>
<i>SAX2</i>	<i>2.4, 2.46, 6.88, 12.28, 13.647, and 13.674</i>
<i>Zn-IMAC30</i>	<i>3, 3.4, 7, 8.93, and 12</i>

**Table 9 RL analysis of all subjects (Training set and Blinded set)**

*The table represents the peaks that were utilized by the algorithm when all the samples were used to build models from the raw datasets obtained from the two chip arrays. The bold-faced peaks appeared in at least 10 of a total of 12 different models.*

#### **6.4.2.3. Site of Disease Onset**

We also analyzed the predictive value for site of disease onset by utilizing all the ALS samples except the outliers (ALS 2, 4 and 8 in Table 6). This set constituted a total of 15 subjects with limb onset and 7 with bulbar onset. The datasets acquired from both SAX2 and Zn-IMAC30 chip arrays were analyzed using the RL algorithm. This analysis yielded a panel of 11 m/z attributes (2.01, 2.72, 3.44, 9.68, 13.93, 15.3 and 17kDa peaks from SAX2 and 2.6, 5.34, 6.7 and 9.41kDa peaks from Zn-IMAC30 chip). Amongst these peaks, the algorithm used the 3.44kDa peak iteratively to make correct predictions, suggesting its high positive predictive value (PPV). RL classified correctly 14 of the 15 limb onset subjects without predicting on one of them (ALS 6 in Table 5). Amongst the 7 bulbar onset cases, it correctly and incorrectly predicted on two and one subject, respectively. It did not predict on 4 of the 7 subjects. Thus these analyses provided a prediction accuracy of 95% (Table 10).

Predicted \ Actual	Limb	Bulbar	NP
Limb	14	0	1
Bulbar	1	2	4

**Table 10 RL analysis of site of disease onset in ALS subjects**

*Amongst 15 and 7 cases with limb and bulbar as the site of disease onset, the RL algorithm correctly predicted in 14 and 2 cases, respectively. While one limb onset case was a no prediction (NP), 4 of the bulbar cases were not predicted upon with one bulbar case being incorrectly predicted. The overall prediction accuracy was 95%..*

### **6.4.3. Protein Identification**

Having established a panel of putative biomarkers through univariate and multivariate analyses, we sought to identify some of these mass spectroscopic signals. Commercially available CSF samples as also the CSF from control and ALS subjects were enriched through anion exchange chromatography and the different fractions were collected (see section 6.3.4). The application of these fractions onto a SAX2 and NP20 (normal phase) chip arrays revealed the enrichment of some of the peaks that were identified by the univariate and multivariate analyses (Fig 41, Tables 7 and 9). Specifically, the peaks enriched in these different fractions included 3.45 (pH 7), 3.8 (pH 5), 6.25 (pH 4), 6.88 (pH 4) 13.38 (FT / pH 7) and 13.78kDa (pH 4). As mentioned earlier the 6.88kDa peak is the double charged signal of 13.78kDa peak. While the intensity of 3.44 and 3.8kDa peaks were significantly elevated in ALS cases, the 6.25, 6.88, 13.38 and 13.78kDa peak intensities were decreased in ALS cases (Fig 41). The 6.25 and

13.78kDa peaks that were identified in pH4 fraction as also the 13.38kDa peak that was present in the flow through were further analyzed (Fig 43).

The bands identified on a 1D SDS-PAGE were then subjected to in-gel tryptic digestion followed by tandem mass spectrometry. The in-gel tryptic digests of the 13.38 and 13.78kDa peaks from the respective fractions yielded proteins represented by the expected mass spectrometric signals (Fig 44, A, B, and C).

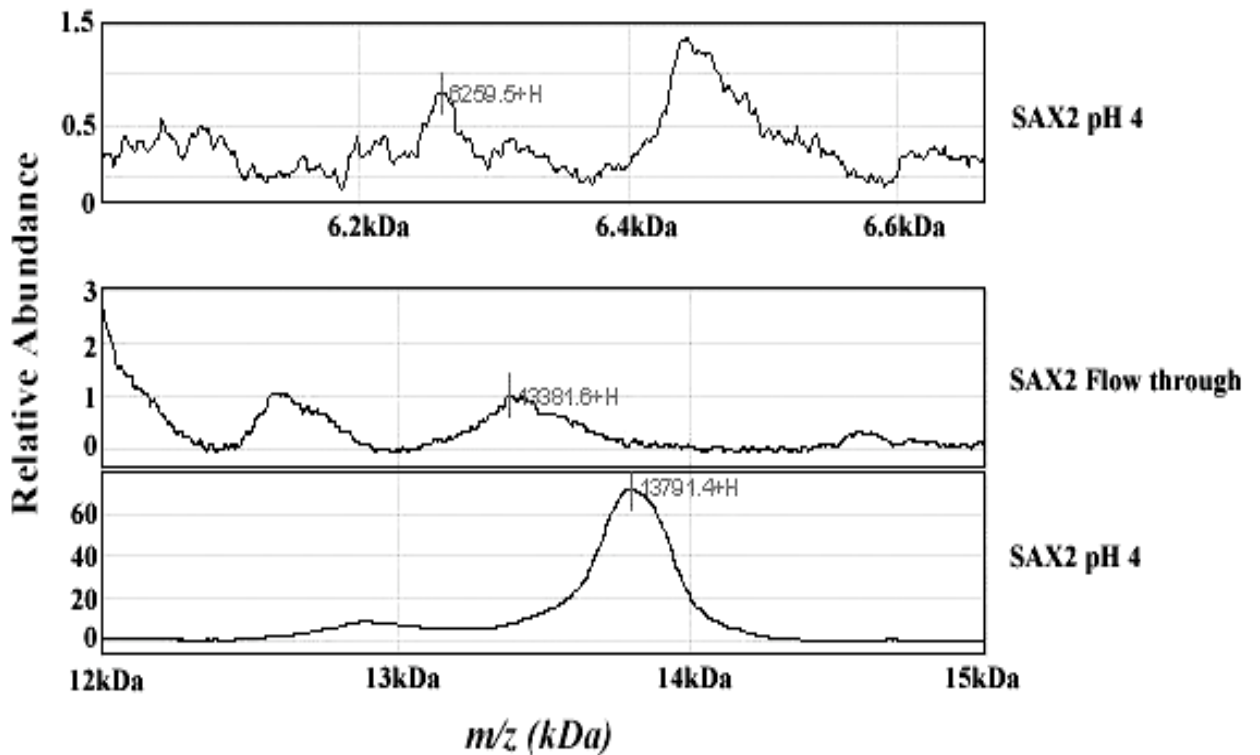


**Figure 43** Enrichment of biomarkers by fractionation

*CSF was fractionated using Q Hyper D matrix at differing pH conditions. The resultant fractions were spotted on SAX2 and NP20 (normal phase) chip arrays to determine the fraction in which the specific peak appeared. The 6.25 and 13.78kDa peaks appeared in the pH 4 fraction (top and bottom panels, respectively) while the 13.38kDa peak appeared in the flow through (middle panel).*

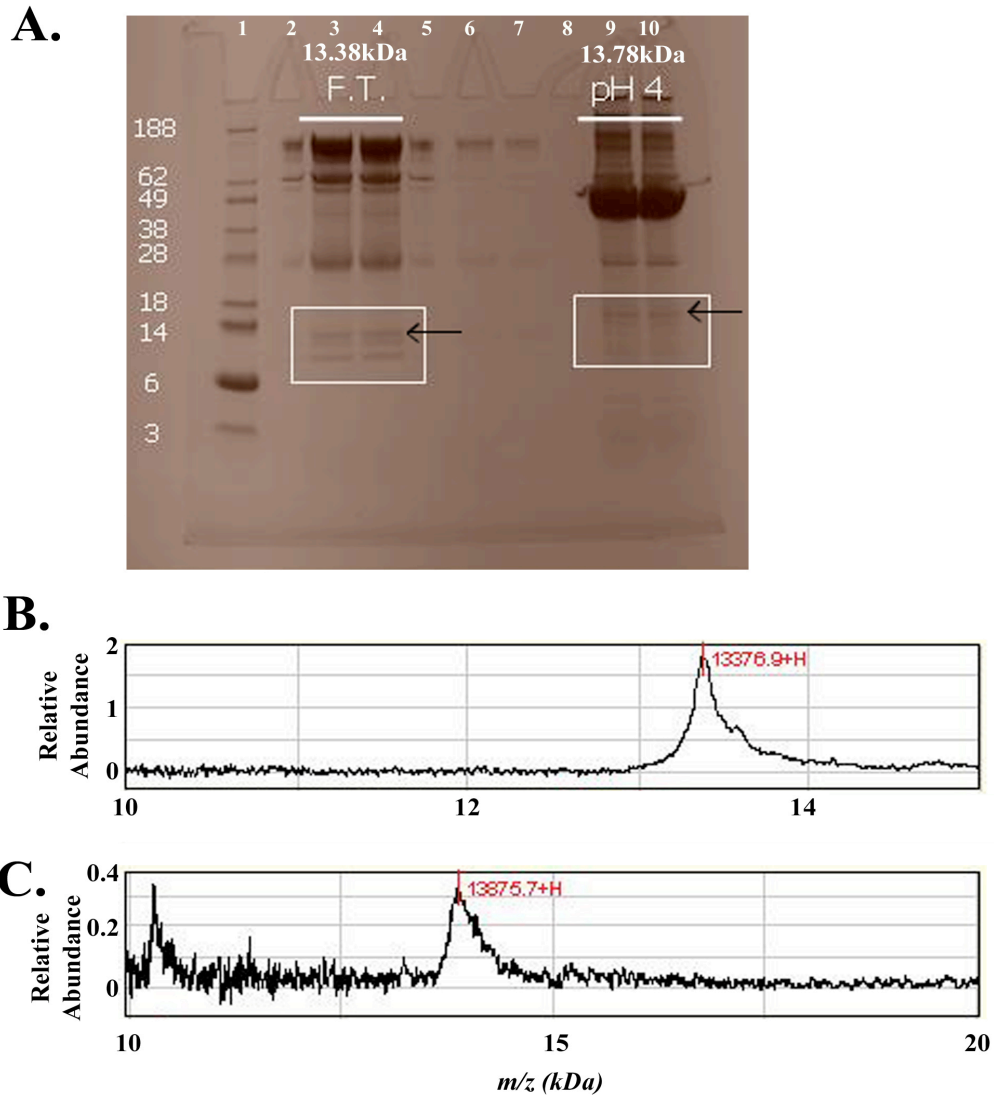


**Figure 44** 1D SDS-PAGE (A), in-gel tryptic digests of the 13.38kDa (B) and 13.78kDa (C) peaks

(A) Representation of a silver stained 1D SDS-PAGE. Lane 1 - Molecular weight (MW in kDa to the left of the lane); Lanes 2 to 7 - flow through fraction; lanes 9 and 10 - pH 4 fraction. The three bands within the box in lanes 3 and 4 (range of 13.38kDa) and the one band within the box in lanes 9 and 10 (range of 13.78kDa) was used for in-gel tryptic digestion.

(B) The resultant eluate from in-gel tryptic digestion of the band represented by arrow (in lanes 2 and 3 of (A)) was spotted on a NP20 chip. It revealed the identity of the 13.38kDa peak.

(C) *Tryptic digestion of the band represented by arrow (in lanes 9 and 10 of (A)) revealed the 13.78kDa peak.*

Peptide mass fingerprints were obtained by analyzing the tryptic digests of the 13.38 and 13.78kDa peaks using tandem MS/MS (Fig 45, A and B). Obtaining the endogenous tryptic digestion fragments and eliminating the common m/z signals determined specificity of the peptide masses. The masses of the peptide fragments for the 13.38kDa peak were 1012.14, 1096.15, 1226.47, 1382.79, 1400.76, 1660.93, 1793.1, 1817.03 and 1921.23 daltons. For the 13.78kDa peak, the masses of the peptide fragments in the fingerprint were 1366.82, 1495.02, 1522.91, 1529.89, 1834.15, 2075.24, 2451.46, 2516.48, 2607.52, 2645.6 and 3140.51 daltons. The identities of these peptides were searched against the ProFound protein database, which matched the peptide fingerprint of the 13.38kDa peak to human cystatin C and that of the 13.78kDa peak to a monomer form of human transthyretin or retinol binding protein. The estimated Z score for the 13.38kDa peak (pI of 9.3) was 2.42 and for the 13.78kDa peak (pI of 5.5) was 2.33. In addition, fractionated CSF samples were tryptic digested directly from Zn-IMAC30 arrays followed by tandem MS/MS identified the 3.45kDa peak to be the carboxy terminus of the neuroendocrine secretory protein 7B2 (data not shown). When the pH4 fraction for the 6.25kDa peak was concentrated using a YM-30 microcon, the purity of this peak was elevated but the in-gel tryptic digestion of the 6.25kDa peak did not yield any protein. Efforts to purify and identify the 3.8kDa peak also have not yielded positive results.

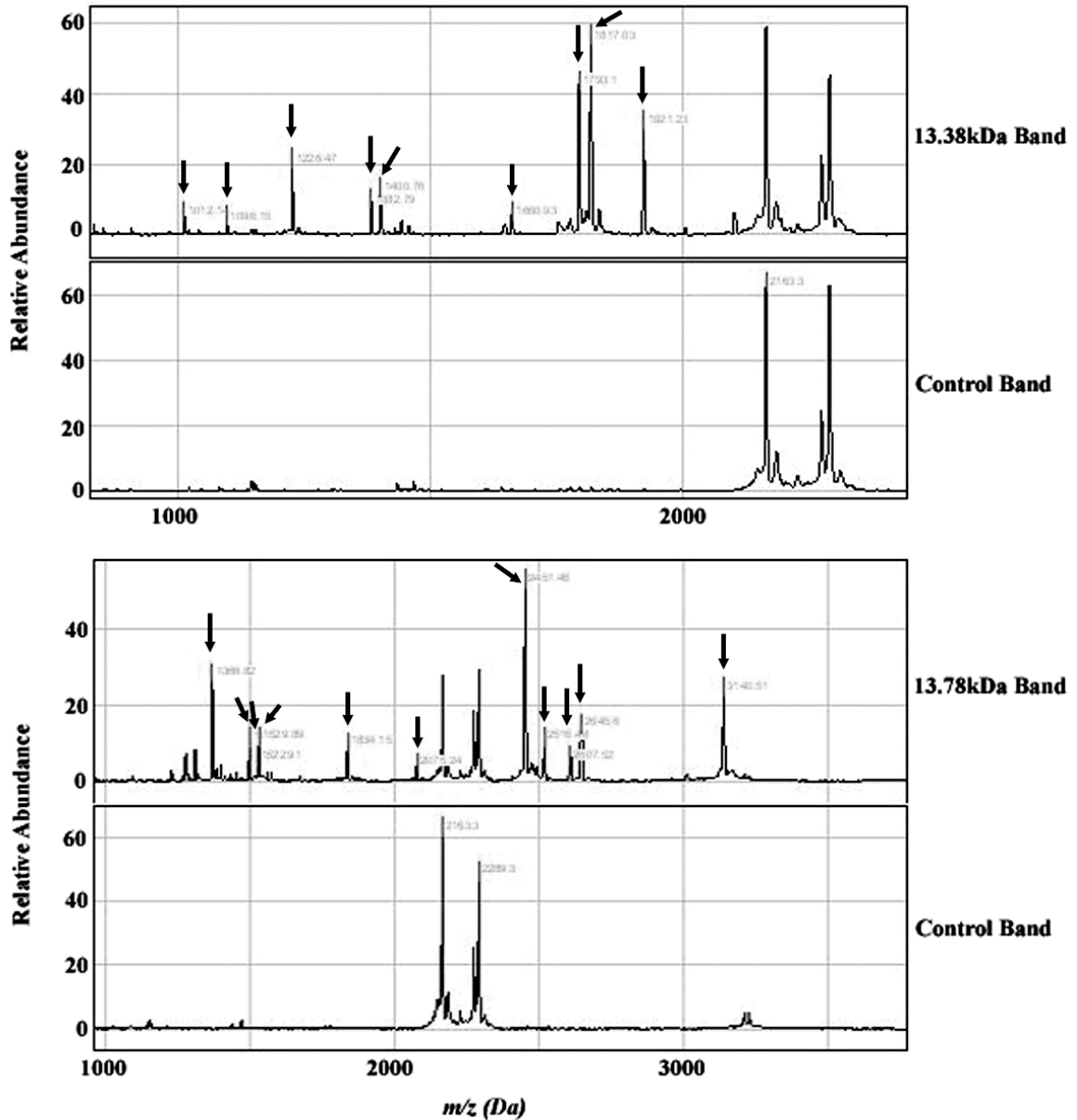


**Figure 45** Peptide mass fingerprinting of the 13.38 (A) and 13.78kDa (B) digests

*The specificity of the peptides was determined using the endogenous tryptic digestion fragments (control band). The peptides identified for both the peaks are represented in A and B in daltons. There were 9 and 11 peptide fragments (arrows) for 13.38 and 13.78kDa peaks, respectively. The  $m/z$  of the fragments are indicated in the text.*

#### 6.4.4. Protein Validation

Immuno-SELDI-TOF-MS was performed (see section 6.3.5) to validate the identified proteins. This resulted in the 13.78kDa and its corresponding double charged peak demonstrating the decrease in ALS CSF sample compared to control (Fig 46).

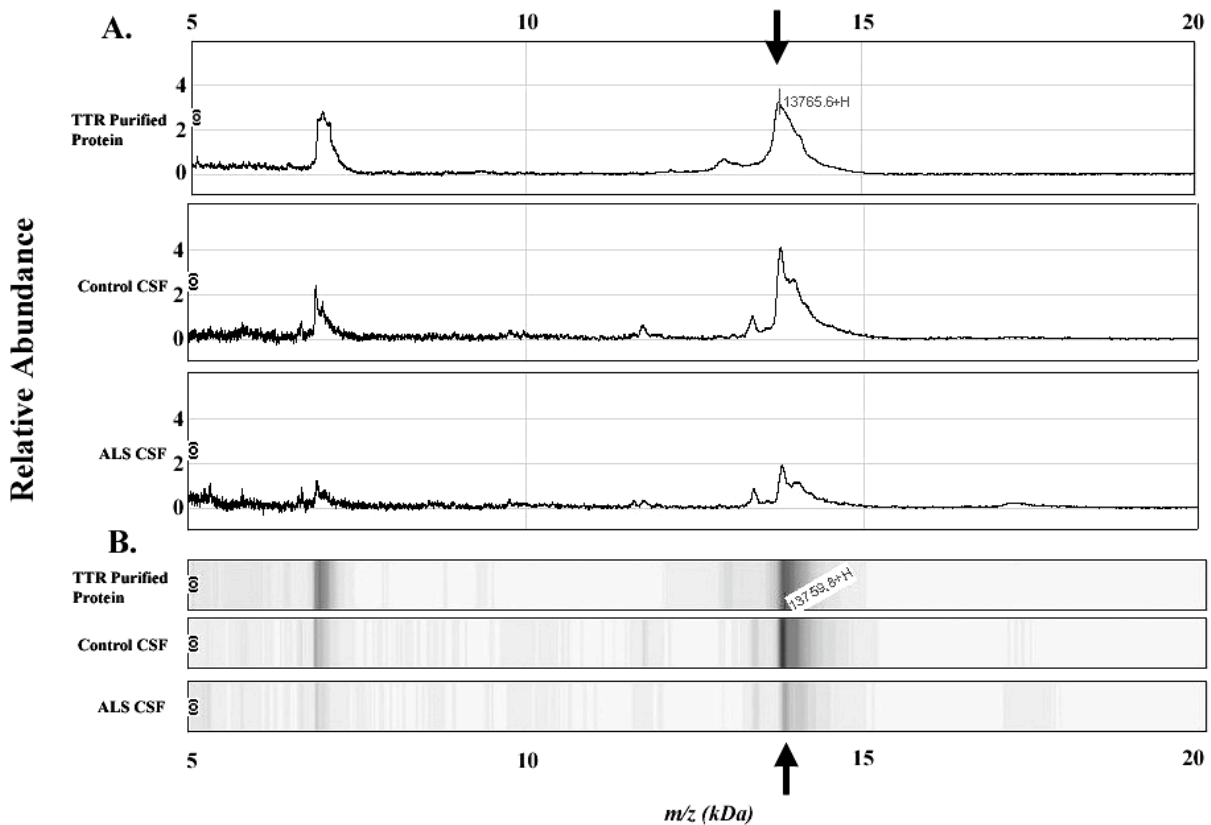


**Figure 46 Validation of transthyretin (monomer) by Immuno-SELDI-TOF-MS**

(A) Single representative spectra of purified human TTR protein (positive control), control ( $N = 7$ ) and ALS ( $N = 7$ ) CSF sample to validate the decreased relative abundance of monomer of transthyretin (arrows) in ALS CSF samples. The difference in the relative peak intensities of the 13.78kDa between controls and ALS determined by this approach was statistically significant ( $p$  value of 0.02).

(B) CIPHERGEN-based software-assisted gel view of the spectra represented in (A)

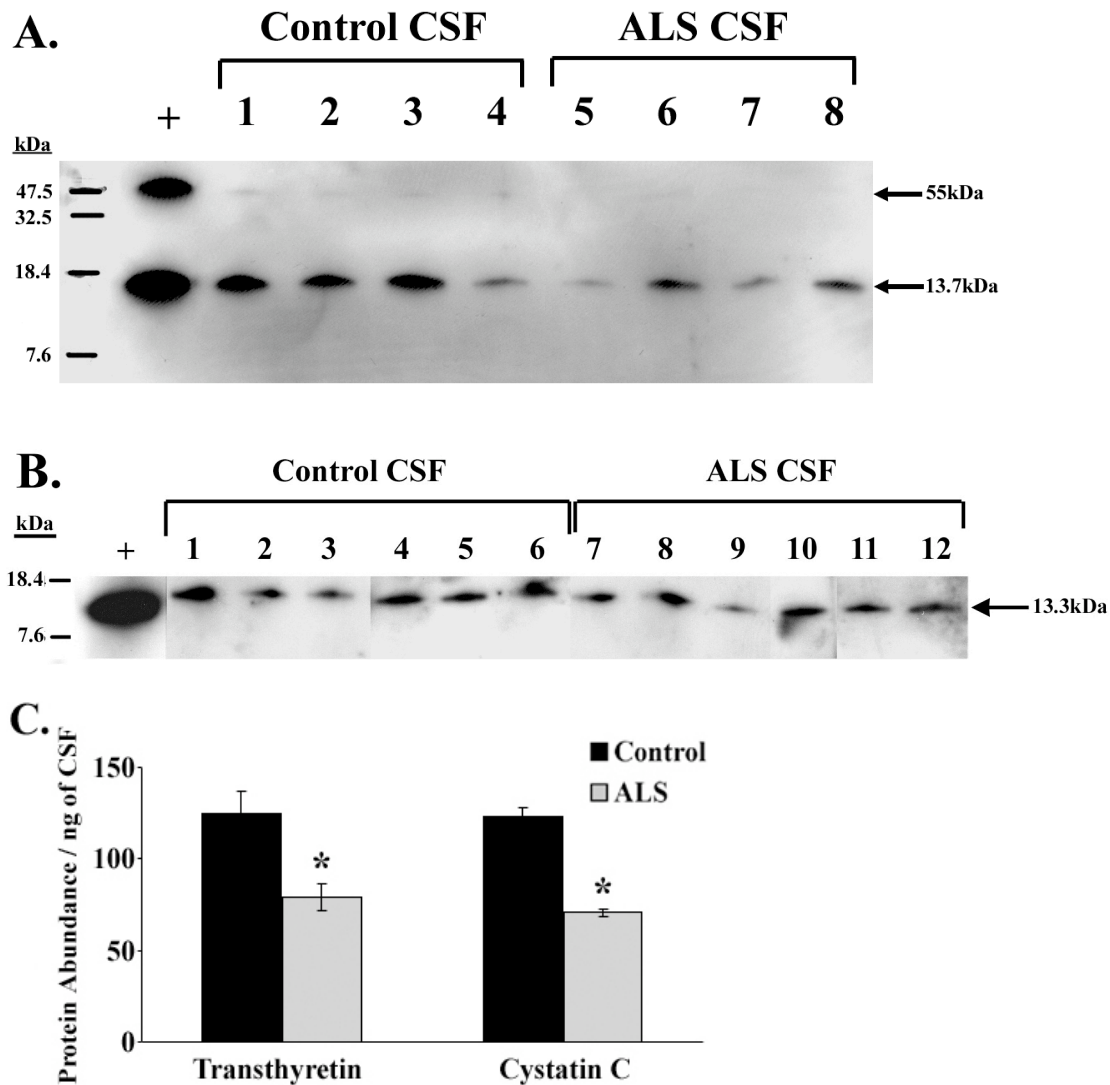


**Figure 47 Validation of the 13.78 and 13.38kDa protein peaks by Western blotting**

(A) 50ng of control ( $n = 4$ ; Lanes 1-4) and ALS ( $n = 4$ ; Lane 5-8) CSF was electrophoresed on 10-20% Tris-Tricine gels and immunoblotted for transthyretin (TTR). The average ages for controls and ALS cases were  $56.75 \pm 5.58$  and  $66.5 \pm 4.97$  yrs, respectively and the average time duration of CSF draw from ALS symptom onset was 572 days. Purified human TTR (50ng) was used as positive control (lane “+”). The arrows on the right indicate the monomer and homotetramer form of TTR protein.

(B) 25ng of protein was used to validate cystatin C by Westerns. The average ages for controls (Lanes 1 – 6) and ALS (Lanes 7 – 12) cases were  $60.66 \pm 1.78$  and  $65.66 \pm 4.44$  yrs, respectively and the average time duration of CSF draw from ALS symptom onset was 548 days. Purified human cystatin C (10ng) was used as positive control (lane “+”). To the left of the positive control lanes in (A) and (B) are the molecular weight markers indicated in kDa.

(C) Densitometric quantitation of the TTR and cystatin C bands using the NIH 1.58 software. The relative abundance was expressed per ng CSF protein that was loaded. Single factor ANOVA was performed with a confidence interval of 95% to compare the protein levels of controls and ALS. The p values for TTR and cystatin C were 0.02 and 0.04, respectively. Asterisks indicate the statistical significance.

#### **6.4.5. Western Immunoblotting for Cystatin C and Transthyretin**

We sought to validate the presence of transthyretin and cystatin C by Western immunoblotting using polyclonal antibodies (DAKO, Denmark). We used purified human TTR and cystatin C proteins as positive controls for the assays. The levels of the 13.78kDa monomer of TTR was significantly reduced in ALS CSF compared to control CSF (Fig 47, A and C; p value = 0.02). The blot also revealed a 55kDa peak, which is the molecular weight of the homotetramer form of TTR (Fig 47A). This band appeared to be increased in control cases compared to CSF from ALS subjects. In addition, we performed immunoblotting to examine the levels of cystatin C and found decreased levels of the protein in ALS CSF (Fig 47, B and C; p value = 0.047).

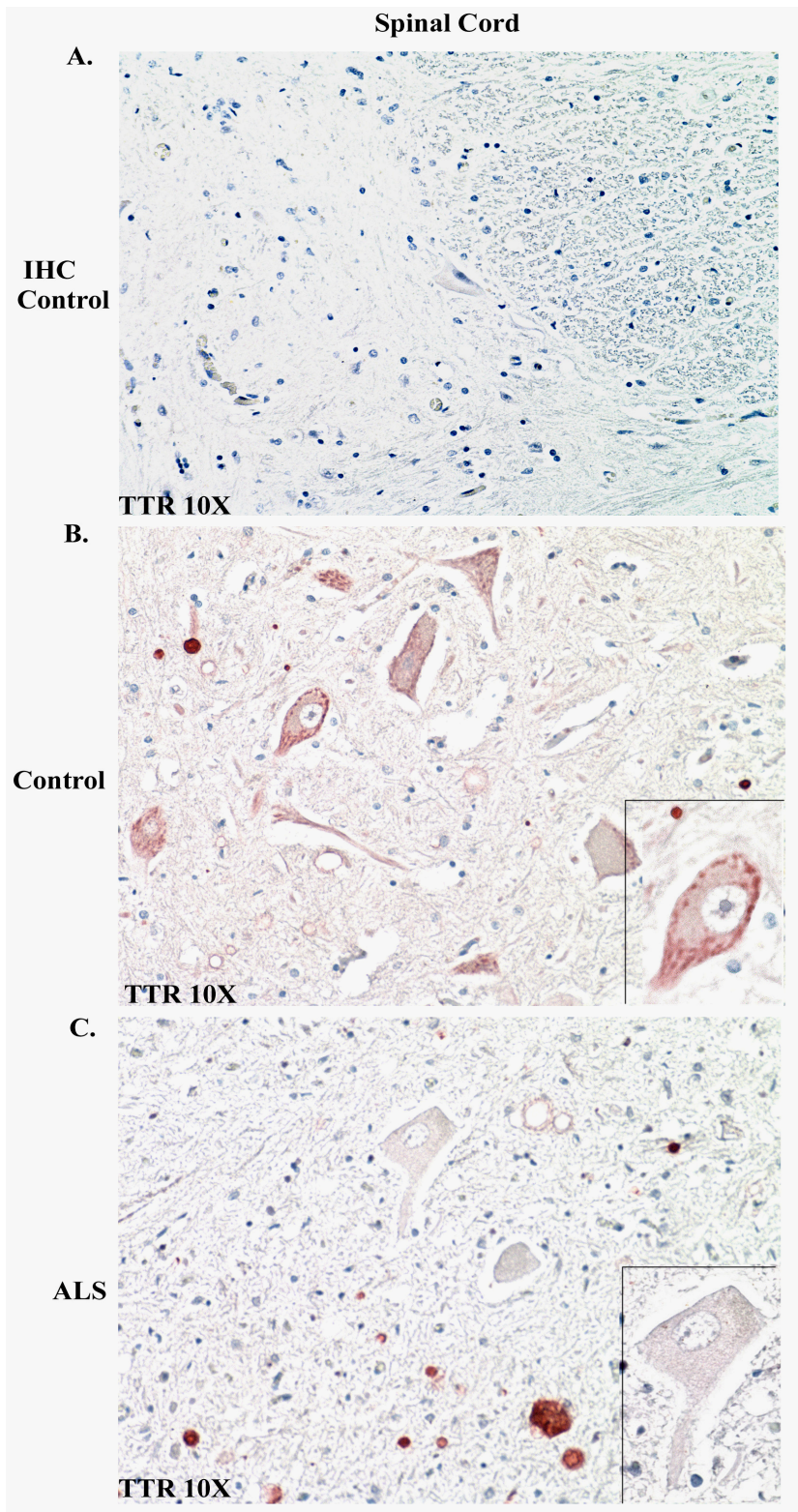


**Figure 48**    **Decreased immunoreactivity of transthyretin in ALS spinal motor neurons**

*Human lumbar spinal cord tissues from 16 ALS and 8 non-neurological age-matched disease control cases were immunostained for transthyretin. The sections were stained with AEC (antigen of interest appears reddish brown) and counterstained with haematoxylin. All panels are at X100 magnification with the insets at X200 magnification.*

*Immunohistochemical (IHC) no primary antibody negative control.*

*(B) Control case shows healthy motor neurons with increased levels of transthyretin.*

*(C) ALS spinal motor neuron present with decreased immunoreactivity for transthyretin.*

#### **6.4.6. Immunohistochemistry for Transthyretin**

In light of a recent finding in transgenic mouse model for Alzheimer's disease for the neuroprotective role for transthyretin, we examined the levels of this protein in human ALS spinal cord tissue sections [444]. Analysis of 8 control and 16 ALS cases revealed increased punctate immunoreactivity in the cytoplasm of spinal motor neurons of control cases when compared to ALS spinal motor neurons (Fig 48).

#### **6.5. Discussion**

In this study we have utilized SELDI-TOF-MS to profile CSF and identify diagnostic biomarkers for ALS using SAX2 and Zn-IMAC30 chips. By univariate analysis, we report 52 spectral peaks with differences in peak intensities between ALS and control subjects. BPS generated a panel of 16 biomarkers (peaks common to SAX2 and Zn-IMAC30 were counted once, i.e., 2.01, 6.48/6.53, 6.86/6.89, 13.77/13.38) from the training group but the algorithm could not be used to predict ALS in blinded test subjects. However, the biomarker panel generated by RL predicted ALS disease status in blinded test subjects (N=30) with 92%

sensitivity, 59% specificity and 79% accuracy. In addition, we have identified three of these peaks to be the carboxy terminus of neuroendocrine secretory protein 7B2, cystatin C and transthyretin. We have also validated the presence of cystatin C and transthyretin in ALS CSF.

The clinical diagnosis of ALS is typically made after exhaustive tests to eliminate other potential causes for the presenting symptoms. A panel of predictive biomarkers would aid in a more rapid clinical diagnosis, which would not only be beneficial to the patient and family but also permit initiation of therapeutics at or near the onset of clinical symptoms. Since our goal is to diagnose ALS at the time of disease onset and ALS affects the motor neurons of the spinal cord and brain, we examined the CSF proteome, which is in intimate contact with motor neurons and other cell types affected during ALS.

Our goal for these biomarker panels is not only for early diagnosis, but also to identify new therapeutic targets and to test drug efficacy in clinical trials. The identification of each protein biomarker may reveal novel targets for drug therapy. While effective drugs are currently unavailable, the development of a biomarker signature pattern for ALS will permit a more rapid discovery of drug therapies. Within clinical trials these biomarkers could be used to determine if a particular drug or drug combination alters the proteomic signature of the disease, thus providing a sensitive method to uncover beneficial drug treatment regimens. It is important to note that the ALS subjects used to identify the biomarker panel had an average time from symptom onset till CSF draw of 385 days. Since we utilized CSF from ALS patients near the time of symptom onset, future experiments will involve a longitudinal study to examine proteomic alterations during disease progression.

In fact in one such longitudinal study, Dr. Pasinetti's group has identified elevated levels of a 4.8kDa peak in CSF drawn every 2 months from 14 ALS patients (unpublished data). In

addition, they have identified decreased levels of two other peaks at 3.8 and 6.3kDa. These were obtained by SELDI-TOF-MS approach and the use of BPS algorithm. It is interesting that our study also reveals peak intensity differences between controls and ALS in these three peaks. However, by univariate analysis the 4.8kDa peak is decreased compared to controls, a trend that seemingly is different from Dr. Pasinetti's findings. The difference in trends can be explained by the fact that while Dr. Pasinetti claims that the marker at 4.8kDa increases as disease progresses, what we believe is that the putative biomarkers from this study constitutes a set of early disease biomarkers. Hence it is likely that CSF drawn at a later date from symptom onset may present a trend as reported by Dr. Pasinetti's group. Furthermore, it is an interesting observation that the 4.8kDa peak is decreased in CSF from post-mortem ALS cases compared to our set of recently diagnosed patients (Fig 38D). This suggests that fluctuations in the levels of this protein might indeed be important for disease progression. With increased sample size, our studies would identify biomarkers with greater sensitivity and specificity, particular protein biomarkers specific to the region of disease onset (bulbar vs lumbar) and also be extended to distinguish a spectrum of motor neuron diseases. In fact our preliminary analysis of predictive value for site of disease onset using 22 ALS CSF samples provided with a marker at 3.44kDa with high positive predictive value and overall prediction accuracy of 94%. Such studies if extended to a larger sample set can yield potential markers that would aid in a clinician determining the type of ALS (bulbar vs limb onset) and devise patient-specific drug regimens thus improving life expectancy for an ALS patient.

Although our initial RL analysis yielded rather low specificity (59%), re-analysis by increasing the training set to 40 samples yielded specificity of 100%. In our study most are

healthy controls. It would be ideal to obtain high levels of specificity given that in most clinical settings the distinction between “likely ALS” from other neurological cases has to be diagnosed.

Data from the Ciphergen-based univariate analysis demonstrate that a number of proteins within the CSF exhibit statistically significant differences in the levels between control and ALS subjects (Fig 41). This implies that numerous protein alterations occur within the CSF of ALS patients near time of symptom onset and that SELDI-TOF-MS is a valuable tool to identify such statistical differences. The proteomic changes may include differential protein expression, altered post-translational modifications or proteolytic processing. Indeed prior studies have demonstrated altered levels of numerous proteins in the CSF of ALS patients [149, 445-449].

Multivariate analysis using two separate bioinformatics algorithms (BPS and RL) identified putative diagnostic biomarkers from the SAX2 and Zn-IMAC30 ProteinChip datasets. BPS classification trees identified 16 putative protein biomarkers (from a total of 366 peaks) and provided predictive values for a correct diagnosis of ALS with an average of 80% sensitivity and 85% specificity. These values were from 10-fold cross-validation of 36 samples but BPS classification trees could not be applied to the 20-blinded test subjects. Since it was not feasible to predict disease status on blinded samples using BPS, we utilized the RL algorithm.

The RL identified 15 protein peaks from the SAX2 and Zn-IMAC30 chip raw datasets (27,000 m/z values) as diagnostic indicators [442]. Combining the rules from both the SAX2 and Zn-IMAC30 chips, RL was able to identify ALS in patients with 89% sensitivity and 72% specificity in the validation phase. To further validate our RL biomarker panels we tested the predictive value of the biomarkers against a set of 20 CSF samples from blinded test subjects. Using RL, there were 6 misclassifications in the blinded set yielding 80% sensitivity and 68% accuracy. Two ALS cases that were misclassified by RL had a time from symptom onset until

the date of CSF draw of 1339 and 3913 days, well beyond that of ALS subjects in the training set. When these two ALS subjects were eliminated for calculations of predictive values, the result was 100% sensitivity and 76% accuracy. This suggests that the biomarker panel identified by RL represent early disease-specific diagnostic predictors. Of the control subjects misclassified, one subject had experienced a change of mental status (confusion) at the end-stage of renal disease, one subject had leg stiffness with an unknown diagnosis (though multiple sclerosis has been ruled out), and another experiences arm numbness with a family history of neurodegenerative disorders.

Having successfully tested the models generated by RL on the blinded set of samples, our attempt at learning on all of the samples (original training plus the blinded set) excluding the four outliers yielded a further 11 peaks as putative biomarkers (Table 10). 2 of the 11 attributes as seen in Table 10 (3 and 8.93kDa peaks from Zn-IMAC30 array) were also part of the “panel of 10 biomarkers” suggesting their possible importance in predicting ALS. This additional analysis performed on a learn set of 40 samples and under different parameter settings yielded a high percentage of accuracy, coverage and specificity but low sensitivity compared to the previous panel obtained from RL (Table 7 and 8). The reduced sensitivity may be the result of using 40 samples for the training set but only 12 for the test group (as opposed to 24 and 20 in the original RL analysis). Increasing the sample size of the test group may increase the sensitivity and specificity in future studies. It was interesting to note that one of the two cases that were predicted appeared incorrect in 10 of the 12 tested models. In each case, the 2.4kDa peak was appeared. These suggested that the reduced sensitivity due to the incorrect recurrence of this ALS case might be due to the drug regimen of the ALS patient affecting the CSF sample. Further analysis is warranted based on the drug regimen of ALS patients.

Although our initial RL analysis yielded rather low specificity (59%), re-analysis by increasing the training set to 40 samples yielded specificity of 100%. In our study, we included some neurologic disease controls within our control group but most were healthy controls. It would be ideal to obtain high levels of specificity given that in most clinical settings the distinction between “likely ALS” from other neurological cases is tenuous. We predict that further analysis with the addition of yet more neurologic non-ALS control subjects in our training set will permit RL to make diagnostic predictions with higher levels of specificity and accuracy. Such studies can then be extended to distinguish ALS from other motor neuron diseases.

Since both algorithms share similarities with respect to parameters used for analysis, comparable outcomes and commonalities in biomarker panels would be expected. We report biomarker panels unique to each algorithm with one common signal (6.8 kDa). This can be attributed to the fact that although BPS utilizes the principle of Classification and Regression Trees (CART), the algorithm uses auto-detected peaks via a clustering software and not the raw data [332]. In addition, the BPS software was unable to predict disease status in blinded test samples. Our study suggests that when the two programs are compared as analysis tools, RL fares better for two reasons: the capability of RL to use the raw data with more than 27,000 m/z spectral values and its ability to provide a means to make diagnostic predictions of blinded test subjects. Taken together, the panel of predictors (a total of 19 m/z attributes, i.e., 10 peaks from table 7 and 9 peaks from table 9) obtained from the statistical analyses performed in this study stress the importance of utilizing multiple bioinformatic algorithms to datamine proteomic datasets.

We have also obtained protein identities on three peaks (3.45kDa, 13.38kDa and 13.78kDa/6.88kDa) from our biomarker panel. These three peaks (6.88kDa is the double charged

signal of the 13.78kDa peak) appeared in the panel obtained from the RL analysis (see tables 7 and 9). While we were unable to validate the presence of the carboxy terminus of the neuroendocrine secretory protein 7B2 (referred to as CT-7B2) due to the lack of commercially available antibodies, attempts at developing antibodies to CT-7B2 are ongoing. 7B2, a highly conserved pituitary protein is selectively expressed in the CNS and endocrine tissues but not glial cells [450, 451]. Human 7B2 protein (27kDa) is localized in the secretory granules of neurons (including motor neurons) and endocrine cells. It interacts with neuroendocrine cell specific prohormone convertases 2 (PC2) within the trans-Golgi network (TGN) and aids in the maturation of pro-PC2. Mature PC2 then catalyzes the conversion of hormone and neuropeptide precursors into their active form. A convertase called Furin cleaves 7B2 within the Golgi into a 21kDa and carboxy terminus fragment (CT-7B2) but is not required for the maturation of pro-PC2. Both the 27kDa full-length protein and the CT-7B2 inhibit the function of PC2. Two lysine residues in the CT of 7B2 are critical for this inhibitory role of the peptide [452]. Furin is important for inactivation of the inhibitory function of CT-7B2 [453]. Thus 7B2 is important as a chaperone in the secretory pathway and the CT-7B2 in regulating the function of PC2.

The 21kDa amino terminal portion of the protein and the CT-7B2 has been found in the CSF [454]. Although it is not an entirely novel occurrence, the presence of CT-7B2 can be linked to ALS at a mechanistic level since one of the early pathological features during ALS is the fragmentation of the golgi complex [168-170]. This event coupled with ER stress may greatly dysregulate the secretory pathway. Motor neurons are highly metabolic and depend on proper protein folding and transport. With the functional loss of these neurons during ALS, secretory chaperone proteins such as 7B2, which are normally localized to the neuronal secretory granules could be released into the local environment and acted upon by various proteases such as Furin.

The peptide fragments can then be released into the CSF that bathes the neurons and glia in the CNS. The loss in integrity of the golgi complex and important chaperone proteins from the secretory granules can affect normal neuronal connectivity by impeding the secretory pathway. In addition, the 7B2 protein has been shown to function as a chaperone in the maturation of growth factors such as IGF-1 [455]. The lack of growth factors and trophic support is a factor implicated during ALS [118]. Hence with the cleavage and release of full-length protein into the CSF, there would be reduced levels of the 7B2 protein in the tissues to carry out their chaperone function.

Cystatin C, a 13.3kDa secreted protein belongs to the class of cysteine protease inhibitors playing an important role in regulating extracellular protein homeostasis in the CNS. During cell death processes that occur in neurological diseases, there are a number of proteases that can cause degradation. However, with high concentrations of the protease inhibitors in the CNS, these proteases can be held in check. In fact, the choroid plexus is a major site for the production of cystatin C and the CSF concentration of this protein is about 5.5-times higher than serum [456]. Mutations in this protein have been associated with a rare disease called hereditary brain amyloid angiopathy wherein amyloid depositions occur along the walls of cerebral vessels this reducing the CSF concentrations of the protein [457]. Initially considered a reliable marker for diseases pertaining to glomerular filtration, it has recently been considered a CSF diagnostic marker for neurodegenerative diseases such as AD, CJD, pain, and brain injury [458-462]. In AD, the protein localizes with  $\beta$ -amyloid. The CSF levels of this protein are increased in AD, CJD and in the dorsal horn during active pain states. Cystatin C localizes to protein aggregates such as Bunina bodies in ALS subjects [463, 464]. It can thus be concentrated in the tissue with subsequent reduction in the CSF. If the protein is sequestered in aggregates and a small part of it

remains in the CSF, it is likely that the altered balance between proteases and their inhibitors (such as cystatin C) can play a role in motor neuron death.

In our study, we observed decreased peak intensities of this protein by mass spectrometry. Our attempts at validating this marker by immuno-SELDI-TOF-MS or Western immunoblotting have barely yielded positive results. The application of anti-cystatin C antibodies and fractionated CSF samples to pre-activated chip arrays resulted in non-specific peaks (data not shown). Future experiments utilizing other antibodies or immunoprecipitation protocols using protein G beads can be performed. The Western blots from controls (n = 6) and ALS (n = 6) yield barely significant differences (p value of 0.047). It is possible that molecular techniques are not able to distinguish the level of differences in CSF cystatin C. Although cystatin C appears to be a marker common to many neurodegenerative diseases and not ALS specific, further analysis of it should not be eliminated. It is likely that validation using antibody chips may be a better approach than Western immunoblotting for cystatin C because the former is more sensitive than immunoblotting. This argument may be strengthened by the fact that the peak intensities of cystatin C based on which it was picked by our statistical analyses to be a marker, was not as significantly different as for instance, transthyretin [444]. In light of this a enzyme-linked immuno sorbent assay (ELISA) using CSF samples for the validation of cystatin C may provide fruitful answers. It would be interesting to correlate the CSF levels of cystatin C to that in the brain and spinal cord tissues.

Transthyretin (TTR) or prealbumin is a 55kDa homotetramer that is synthesized predominantly in the choroid plexus and liver being secreted into the CSF and plasma, respectively [465]. There are variant forms of TTR with both normal and variant forms of TTR present in amyloid fibrils of diseases such as familial amyloidotic polyneuropathy that affects the

peripheral nerves and familial amyloid cardiomyopathy. It is required for the transport of thyroxine and by associating with retinol-binding protein also transports retinol / vitamin A in the brain [466, 467]. One of the important functions of retinoic acid is to serve as an antioxidant. In addition, the ventral spinal cord is a region that specifically expresses retinol-binding protein during neural development [468]. The expression levels of retinol-binding mRNA are elevated in the spinal cord of ALS post-mortem tissues [438, 469]. It is plausible that the levels of TTR protein might also be increased in the ALS spinal cord tissues with a concomitant decrease in the CSF as we observe in the mass spectrometric analysis. Hence, it would be relevant to correlate the levels of TTR by immunohistochemistry and immunoblotting of tissue samples. Indeed the immunoreactivity of transthyretin in ALS spinal motor neurons of human post-mortem tissues was much lesser than those in the spinal motor neurons of age-matched control cases (Fig 48). This finding correlates to the study wherein transthyretin was found to be neuroprotective in transgenic mouse model of Alzheimer's disease [444]. Thus, it is likely that low levels of transthyretin in motor neurons could decrease its neuroprotective function. The mechanism of its neuroprotection is unknown. It is known to form aggregates and since aggregate formation in ALS is well documented, it is possible that transthyretin would sequester proteins critical for normal functioning and survival of motor neurons.

In addition, the choroid plexus is a “sink” for lead and elevated levels of lead in the CNS cause neurotoxicity. Studies have demonstrated that the levels of TTR are decreased in CSF after lead exposure [470]. With the site of production of TTR being in close proximity to the CNS and its association with neurological disorders, it is likely that our results demonstrate the decreased levels of monomeric form of TTR to be a true diagnostic measure for ALS. Although we have not examined levels of the full length TTR protein the fact that the levels of the monomer form

of TTR in ALS patients are greatly reduced compared to normal controls suggests that there is imbalance in the homeostasis of thyroid hormones in the CNS of these patients, most likely as a secondary effect of motor neuron degeneration or may act as a co-factor during disease progression. Alternatively, increased levels of heavy metals may also occur during ALS leading to reduced levels of TTR in the CSF. In fact the levels of TTR are also decreased in CSF of patients with neuropsychiatric disorders such as bipolar syndromes, schizophrenia and depression [471]. Additionally, serum TTR levels are reduced during malnutrition. Thus it has been suggested to act as a nutritional marker and a marker of the metabolic state of the body [472]. Given that MND leads to reduced metabolism and muscle atrophy, one could hypothesize that serum TTR levels in ALS patients should likely be decreased compared to those of the control subjects.

Since the analyzed sample set include patients with CSF drawn at an early stage of the disease (average of 385 days from symptom onset), we believe that proteins such as CT-7B2, cystatin C and TTR could act as diagnostic markers for ALS and also provide information towards molecular pathways. This is the first such study for this fatal neurodegenerative disease and hence we consider these to be “novel biomarkers” for the disease. With two of the three proteins being part of the neuroendocrine system (CT-7B2 and TTR), it is likely that there is a secondary neuroendocrine effect during MND. Further analyses of the spectral patterns with a larger sample size will provide information regarding the ALS specific nature of these proteins. This study points towards a possible role of the neuroendocrine system during ALS. Additional studies are required to obtain amino acid sequence information for more of the putative biomarkers obtained through RL analysis and to characterize the expression pattern and function of each analyte. In conclusion, we have identified CSF markers for ALS that may provide a way

for rapid diagnosis near the time of symptom onset. The identification of at least three of the protein peaks by a SELDI-TOF-MS technique in the CSF of ALS subjects demonstrates the feasibility of the MS approach.

## 7. Future Directions

### 7.1. ***In vitro* motor neuron cultures to dissect the functional role for cell cycle proteins, p53 and pro-death molecules during ALS**

Our study using archived human autopsy tissues from sporadic ALS cases provides evidence for altered expression of cell cycle proteins and transcription factors during ALS. Autopsy tissues reflect end-stage disease thereby necessitating the study of an *in vitro* model system using primary spinal motor neuron cultures from wild type mouse or rat embryos. *In vitro* models permit control over the extracellular environment and monitoring of selective neuronal vulnerability in individual neurons. Using such an *in vitro* model, the hypothesis of aberrant and abortive cell cycle re-entry in response to extracellular insults such as glutamate, hydrogen peroxide or various cytokines could be tested.

Previously published reports and our preliminary results in generating spinal cord cultures from E13 mice embryos provide evidence for the feasibility of the technique [473] (Fig 49). Briefly, a metrizamide density gradient centrifugation procedure was utilized to sort the large cells (motor neurons) from the small cells. The large cells were cultured in complete neurobasal medium supplemented with neurotrophic factors. To provide a more physiological milieu and enhance survival, we used neuronal / astrocytic co-cultures.

Four-well dishes (NUNC) and coverslips in 6-well dishes were used for initial characterization studies to identify the cell types by light and immunofluorescent microscopy. Antibodies for  $\alpha$ -tubulin (Fig 50, Panel A) and microtubule-associated protein (MAP-2) (Fig 50, Panel B) labeled all the neuronal cell bodies and dendritic processes. Neurons with large cell bodies were identified using antibodies against p75, the low affinity neurotrophic receptor (Fig

50, Panel C). Unfortunately efforts to sustain the cultures for further analysis failed and the proposal to identify alterations in aberrant re-activation of cell cycle proteins in this *in vitro* model was aborted. However this model is very useful to test the reactivation of the G1 to S phase regulators and their functional significance in motor neuron death.

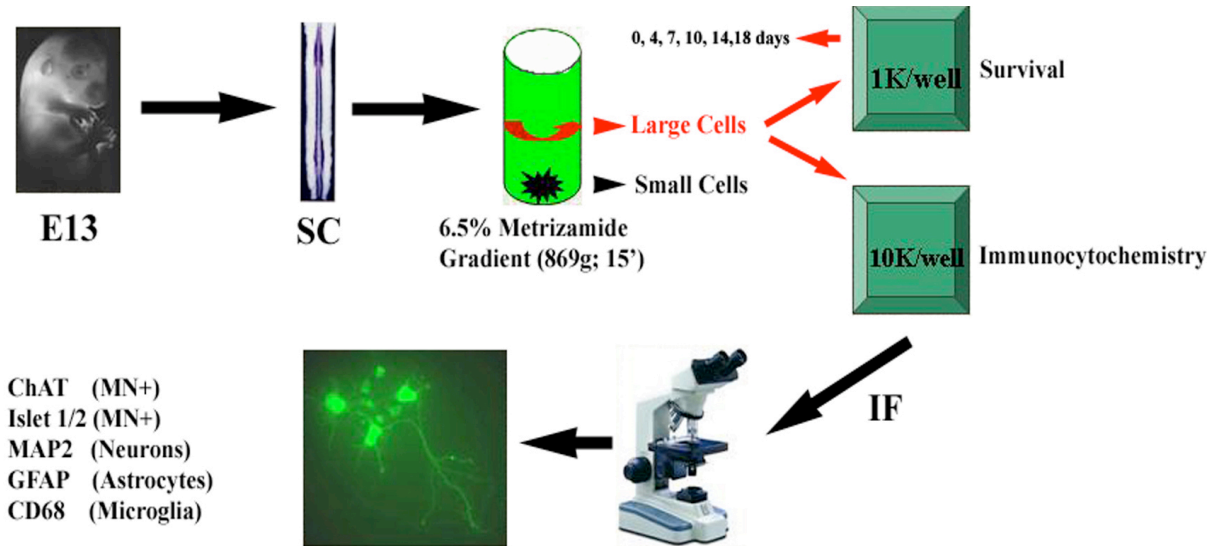


**Figure 49 Schematic representation for murine spinal motor neuron cultures**

*Spinal cords from E13 murine embryos will be dissected, meninges removed and dissociated by triturations followed by pelleting through a 4% BSA/L-15 density cushion. The cells will be centrifuged using a 6.5% metrizamide density centrifugation. A dense band formed at the interface of the medium / metrizamide of large cells will be collected as motor neurons and the small cells with most of them comprised of glial cells will be plated on 4-well dishes for immunocytochemistry with different neuronal and glial markers or toxicity survival assays.*

The *in vitro* culture can be treated with acute/chronic doses of glutamate or peroxide (Fig 51) and assayed for altered cell cycle gene expression, protein localization and transcriptional activity of cell cycle regulators. Glutamate binds to its cognate cell surface receptors resulting in an increase in levels of intracellular calcium and formation of oxidative free radicals. Hydrogen

peroxide results in injury by an increase in hydroxyl radicals ( $\text{OH}^\cdot$ ). Since ALS is a slow progressive disease, a chronic exposure will be a better model for the disease. The role for cell cycle regulators in response to these toxic insults can then be studied using this *in vitro* model.

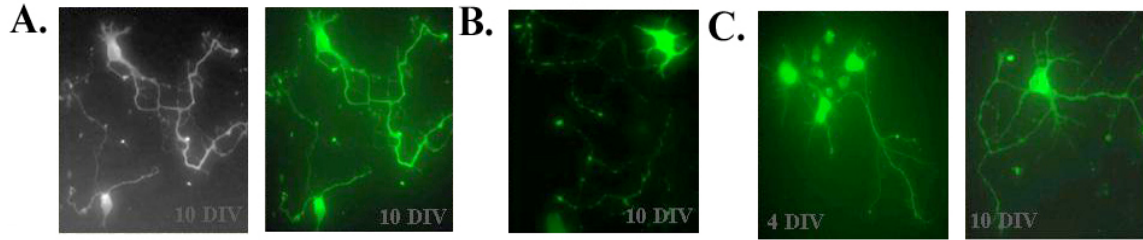


**Figure 50** Immunofluorescent staining for  $\beta$ -tubulin (A), MAP2 (B), p75 (C)

*About 10,000 cells comprised primarily of large motor neurons but also glia were plated on Nunc 4-well plates or coverslips pre-coated with poly-D-ornithine and laminin. Neurons were grown in neurobasal medium supplemented with B27, 1ng/ml BDNF, 10ng/ml GDNF and CNTF for up to 10 days in vitro (DIV) with media replenished 50% every 4 days. These were then fixed in 2% paraformaldehyde / 0.1% glutaraldehyde for 15mins at 37°C. They were then permeabilized in 0.25% triton X-100 / 3%  $\text{H}_2\text{O}_2$ , blocked in 5% milk/PBS and stained with anti- $\beta$ -tubulin (Biogenex), anti-MAP2 (DAKO) and anti-p75<sup>NTR</sup> (Chemicon). The left panel in (A) is a bright field image of 10 DIV motor neuron stained for  $\beta$ -tubulin with the right panel the same image in fluorescence. While  $\beta$ -tubulin and MAP2 are general neuronal markers, p75<sup>NTR</sup> is specific for embryonic motor neurons. Extensive neuronal arborizations are also clearly visualized. All panels are images at X200 magnification.*

Functional role for cell cycle proteins in neuronal death can be tested using pharmacological inhibitors of cdk4, & ppRb, kinase-inactive constructs of cdk4, & dominant negative constructs of DP1, antisense constructs of E2F-1, & p53 proteins and modified oligos of E2F1, & p53 proteins. Based on results from the cultures from wild type mice/rodents, similar

approaches could be used to study the effects of glutamate and hydrogen peroxide in spinal motor neuron cultures from SOD-1 and NF-L transgenics. In addition cultures from E2F-1<sup>-/-</sup> and p53<sup>-/-</sup> could be utilized to define a role for these transcriptional regulators in motor neuron death in response to toxins.

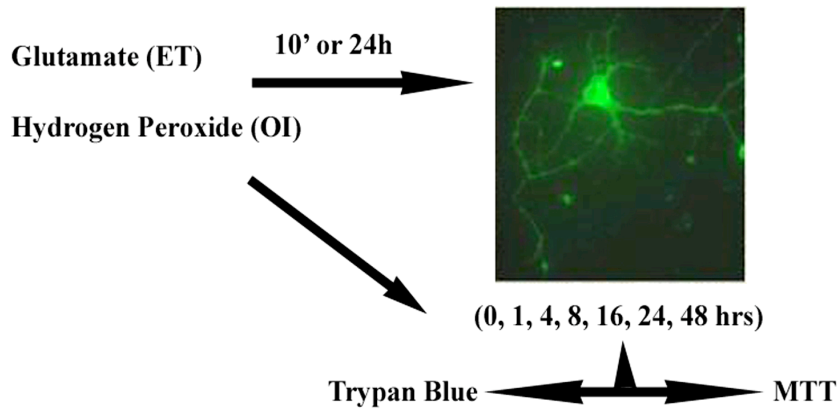


**Figure 51 Motor neuron culture protocol to test aberrant cell cycle hypothesis**

*A schematic flow depicting protocol to test toxicity and survival of in vitro motor neuron cultures when treated with glutamate (excitotoxic injury, ET) and hydrogen peroxide (oxidative injury, OI). Effects on both acute (10min) and chronic (24hr) treatments at a range of time points can be tested. Survival can be tested by trypan blue exclusion and MTT assays.*

Although this *in vitro* model is well established in the field of ALS, there are some drawbacks to the system and its use to test our hypothesis. (i) The yield of motor neurons could pose a problem. To circumvent this problem, anti-p75 or anti-choline acetyltransferase (ChAT) antibodies-based magnetic beads could be used to purify motor neurons and culture them on feeder layers of glial cells. (ii) It is likely that cell cycle re-activation is a downstream effect during ALS pathogenesis and may not relate to insults from any one toxic molecule. This would entail testing the hypothesis by treating the cultures with a combination of these toxic insults.

## **7.2. Dissect the role for re-activation of cell cycle and p53-mediated motor neuron death in animal models of ALS (*in vivo*)**

The SOD1 transgenic animal model developed 10 years ago has been well characterized and used extensively for understanding ALS pathogenesis. The most commonly used model is the high copy number mutant G93A SOD1 transgenic mouse, which exhibits extensive loss of spinal cord motor neurons [103]. Many studies have documented that transgenics with high copy number of G93A remain non-pathological and non-symptomatic until about 60 days (d60). The disease typically progresses from 80 to 110 days with maximal pathological and symptomatic stages at d90 – d105. By d120, the mice develop MND and are sacrificed. In an elegant series of experiments, Kong and Xu characterized the low copy number G93A mouse with slower development of MND symptoms into distinct disease stages [pre-muscle weakness (PMW), rapid decline (RD), slow decline (SD) and paralysis or end-stage (PAR)] based on muscle strength [161]. They document increased vacuolation and mitochondrial degeneration with concomitant loss in muscle strength at the RD stage followed by a slower process of disease progression.

In this set of preliminary experiments, we utilized paraffin embedded spinal cord sections from the different disease stages (PMW, RD, SD and PAR) to examine alterations in the G1 to S phase regulators at the level of light microscopy (see section). Although the levels of ppRb was increased in the 240 days non-transgenic (Fig 52, Top panel A) and the 60 days mutant SOD1 transgenic (Fig 52, Top panel B), all the surviving motor neurons at the RD stage (Fig 52, Top panel D) exhibited elevated ppRb. The increase in levels of ppRb is observed right at the RD stage when motor function is rapidly lost and prior to significant motor neuron cell loss. During the PAR stage when there is an extensive loss of motor neurons, few of them exhibited ppRb

immunoreactivity (Fig 52, Top panel F). There is one report using a G37R mouse model wherein researchers have documented altered levels of CDK4, cyclin D1 and ppRb [244].

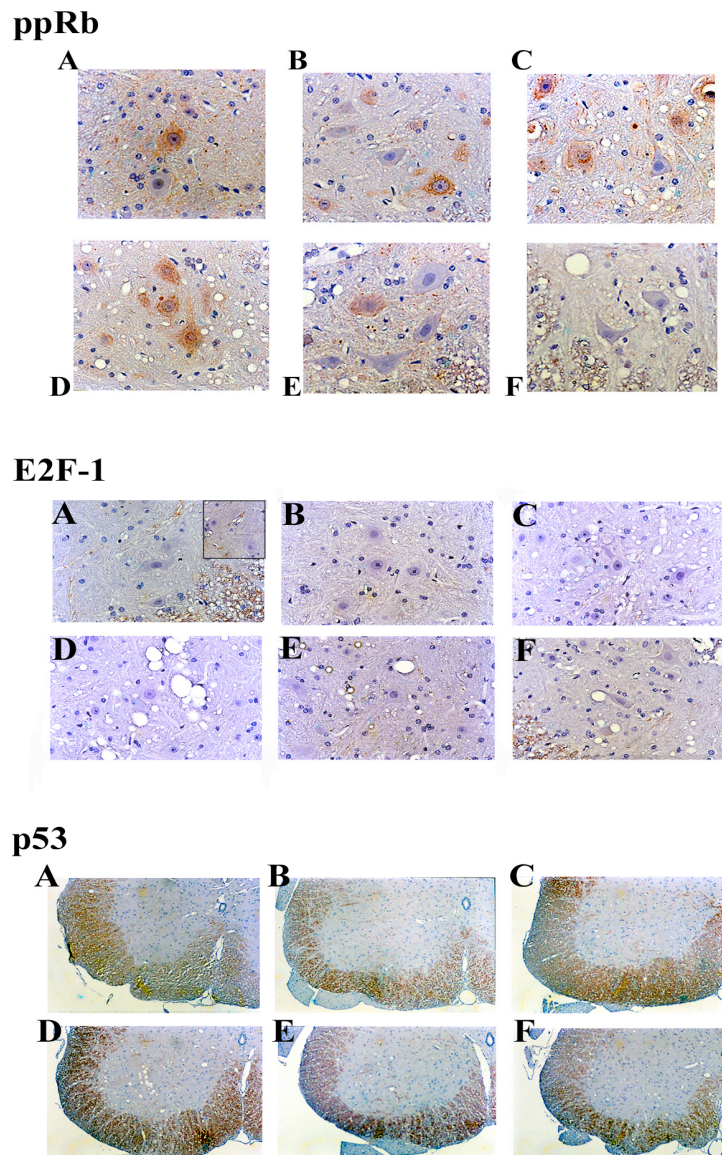


**Figure 52** Spinal cord sections from G93A SOD1 transgenics and non-transgenic littermates immunostained for ppRb (A), E2F-1 (B) and p53 (C)

*For each of the three proteins, the different panels are as follows:*

*(A) 240d Non-transgenic, (B) 60d G93A, (C) pre-muscle weakness (PMW) G93A,*

(D) Rapid decline (RD) G93A, (E) Slow decline (SD) G93A, (F) Paralysis (PAR) G93A. The inset in panel A for E2F-1 is immunostaining in a section of a 240d transgenic for WT SOD1.

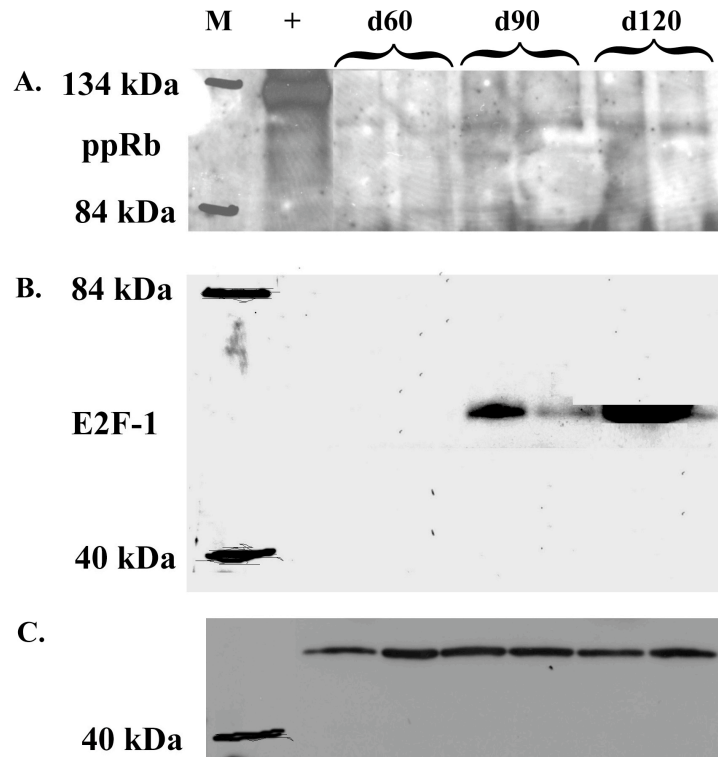


**Figure 53** Western immunoblot for ppRb (A) and E2F-1 (B) in G93A spinal cord

Nuclear lysates from d60 (pre-symptomatic), d90 (disease progression), and d120 (end-stage) G93A spinal cord tissues were prepared as enumerated in Chapter 2. 100µg of protein was loaded on 10% gel, blotted on PVDF membrane and probed with anti-ppRb (A), anti-E2F-1 (B) and anti-actin (C) antibodies. We observe an increase in nuclear ppRb (A) and E2F-1 (B) at d90 and d120 compared to d60. Levels of actin (C) remain unaffected. The number of samples examined per group was only 2. “M” indicates marker lane and “+” indicates the positive control for ppRb.

These results corroborated immunoblots of nuclear extracts from d60 (non-symptomatic), d90 (disease progression) and d120 (end-stage) of the high copy number G93A mice spinal cords

(in collaboration with ALS Therapy Development Foundation, ALS-TDF, MA). There was an increase in ppRb at d90 (n=2) and d120 (n=2) compared to d60 (n=2) (Fig 53). Immunostaining for E2F-1 in the motor neurons fail to exhibit any differences across the different disease stages of the low copy G93A mouse (Fig 52, Middle panels A-F). This could be a phenomenon specific for low copy number because preliminary immunoblot analysis using the high copy G93A mouse revealed an increase in E2F-1 levels at d90 and d120 compared to d60 (Fig 53).

It is possible that ppRb has cellular effects independent of increased E2F-1 through protein-protein interactions. Furthermore, p53 immunostaining was not evident in the motor neurons but there was increased immunoreactivity in the white matter of the low copy number G93A mouse spinal cord sections. This could relate to possible DNA damage induced in the glia that would then have a bystander effect on the neurons. Although these results are preliminary warranting further investigations, it provides avenues to better understand the human disease by in vivo functional analysis at different disease stages. It paves the way to use dominant negative constructs or pharmacological inhibitors and even develop double transgenics such as G93A / E2F-1<sup>-/-</sup> or G93A / p53<sup>-/-</sup> to further dissect cell cycle related pathways to motor neuron death.

### **7.3. Determine the Functional Role for Cytoplasmic E2F-1**

The findings of altered subcellular distribution of the transcription factor, E2F-1, in the affected motor neurons (lower and upper) is consistent with the hypothesis that E2F-1 re-localization may trigger indirect cell death signaling mechanisms. This event deviates from the classical model of E2F-1 mediated activation of gene expression. To discern a role for aberrantly localized E2F-1 in the ALS tissues, we hypothesized that it might associate with anti-apoptotic proteins such as tumor necrosis receptor associated factors (TRAF). Interaction of E2F-1 with

members of the TRAF family of adaptor proteins that mediate intracellular signaling initiates alternative death cascades. The presence of TRAF2 or TRAF6 proteins in the cytoplasm of motor neurons sequesters the death receptors (DR), aiding in survival of the neuron. However, E2F-1 located in the cytoplasm may induce complex formation with TRAF proteins to impede their function, thus releasing death receptors that could now induce cell death via the p75<sup>NTR</sup> pathway or other death pathways [474, 475].

Our preliminary results indicate that E2F-1 co-localize with TRAF2 in 48.5% of the spinal motor neurons. Motor neurons in the controls exhibit cytoplasmic TRAF2 and very negligible E2F-1 (Fig 54). It would be an interesting question to address in response to toxic insults on primary cultures or even examine E2F-1 mediated protein-protein interactions utilizing cultures from the SOD1 transgenics. There is an ever increasing line of evidence for multiple pathways in neuronal cell death and investigations to discern a role for E2F-1 in the cytoplasm will further molecular research and drug design for ALS.

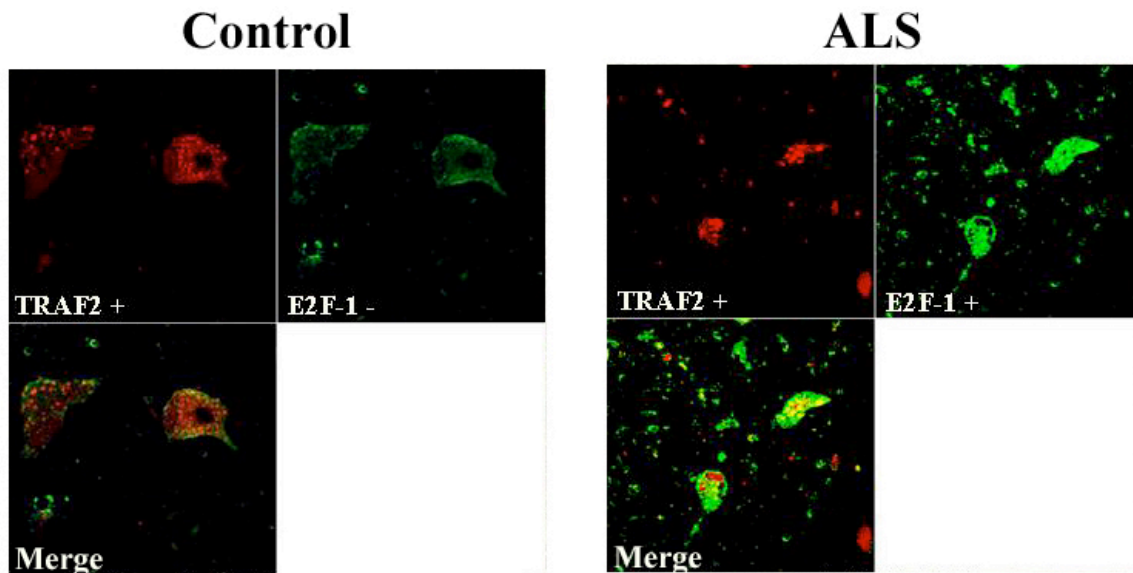


**Figure 54** Human lumbar sections from control (n=6) and ALS (n=11) cases were double-labeled for E2F-1 and TRAF2

*E2F-1 (FITC-conjugated secondary antibody) and TRAF2 (Cy5-conjugated secondary antibody) are present in the same ALS motor neuron (48.7% out of 76 counted MN) as noticed in the merged image with yellow signifying their co-localization (bottom left quadrant). Control cases failed to show this co-localization with negligible E2F-1 but some amount of the anti-apoptotic TRAF2 protein present (red signal).*

Furthermore, it would be interesting to explore the role of transcriptional regulators such as E2F-1, p53 and p73 on chromatin re-modeling during cell death in ALS. In fact one of the gene products associated with FALS is ALSIN (ALS2, see section 1.3.6) that has sequence homology to a regulator of chromatin condensation [107, 476]. Mutations in such proteins and changes to chromatin may make DNA vulnerable to accumulate more damage through the action of ROS. The association of CBP with a DNA repair enzyme (thymine DNA glycosylase) further links transcription, HATs and DNA damage [477]. Although we believe that the re-activation of cell cycle is an abortive attempt and does not proceed beyond the G1 to S phase transition, it would be interesting to examine the role of other cyclin / CDK complexes, G1/M phase markers, and other cell cycle regulators such as the cdc25 family of proteins that may be involved in apoptosis.

#### **7.4. MS-based proteomics approach to study protein alterations during ALS in an animal model using plasma and spinal cord tissue samples**

Having established the feasibility of a mass spectrometric protein profiling approach in identifying disease related changes (see Chapter 6), it could be extended to animal models of the disease. SELDI-TOF-MS could be used to examine the proteome of plasma and spinal cord tissues from G93A mutant SOD1 mice. Comparing the proteome in normal wild type (WT), non-

symptomatic transgenics (G93A, d50-60), during disease progression (d90-105) and end-stage (d120) will help in identifying disease-associated proteomic alterations. Spinal cord tissue samples from these different stages can also be analyzed for region-specific protein changes.

As proof of principle in utilizing spinal cord tissue lysates, we performed experiments using human spinal cord extracts. Analysis using SAX2 chips identified a distinct protein difference at 50kDa (Fig 55A). This peak was elevated in ALS spinal cord tissues compared to control cases. Further analysis of this peak by tryptic digestion of the band from a 1D-SDS PAGE gel (Fig 55B) followed by peptide mass fingerprinting using a MS/MS system (Applied Biosystems 4700) identified the 50kDa peak to be GFAP. This was validated by the use of antibody protein array and SELDI-TOF MS. The surface of the chip was coated with monoclonal anti-GFAP antibody and as a positive control we demonstrated that it could pull down commercially available purified GFAP protein. The antibody also recognized the 50kDa peak in the ALS spinal cord tissue extracts (Fig 55C). Astrogliosis is a pathological hallmark of ALS that has been well documented. GFAP, a marker of activated astrocytes is increased in human and animal ALS tissues through various techniques. This provided a proof-of concept for the use of spinal cord tissues from animal models.

Analysis of plasma and tissue samples from the transgenic mice could provide insight in to ALS pathogenesis. Identification of putative biomarkers through spectral analysis and amino acid sequencing followed by validation through immunoblotting or immunohistochemistry will provide for avenues to test the effectiveness of the markers in diagnostics and therapeutics. These molecular approaches will help identify cell specific and sub-cellular localization of these biomarkers providing clues to their involvement in key biochemical pathways. Proteomic patterns in serum/plasma samples from transgenics and those from human patients from the “U

Pitt” cohort can be compared. These studies will help in validating the animal model for ALS and point plausible mechanistic commonalities between SALS and FALS. If common peaks are not observed, then it is likely that it is a poor model to perform pre-clinical drug screening.

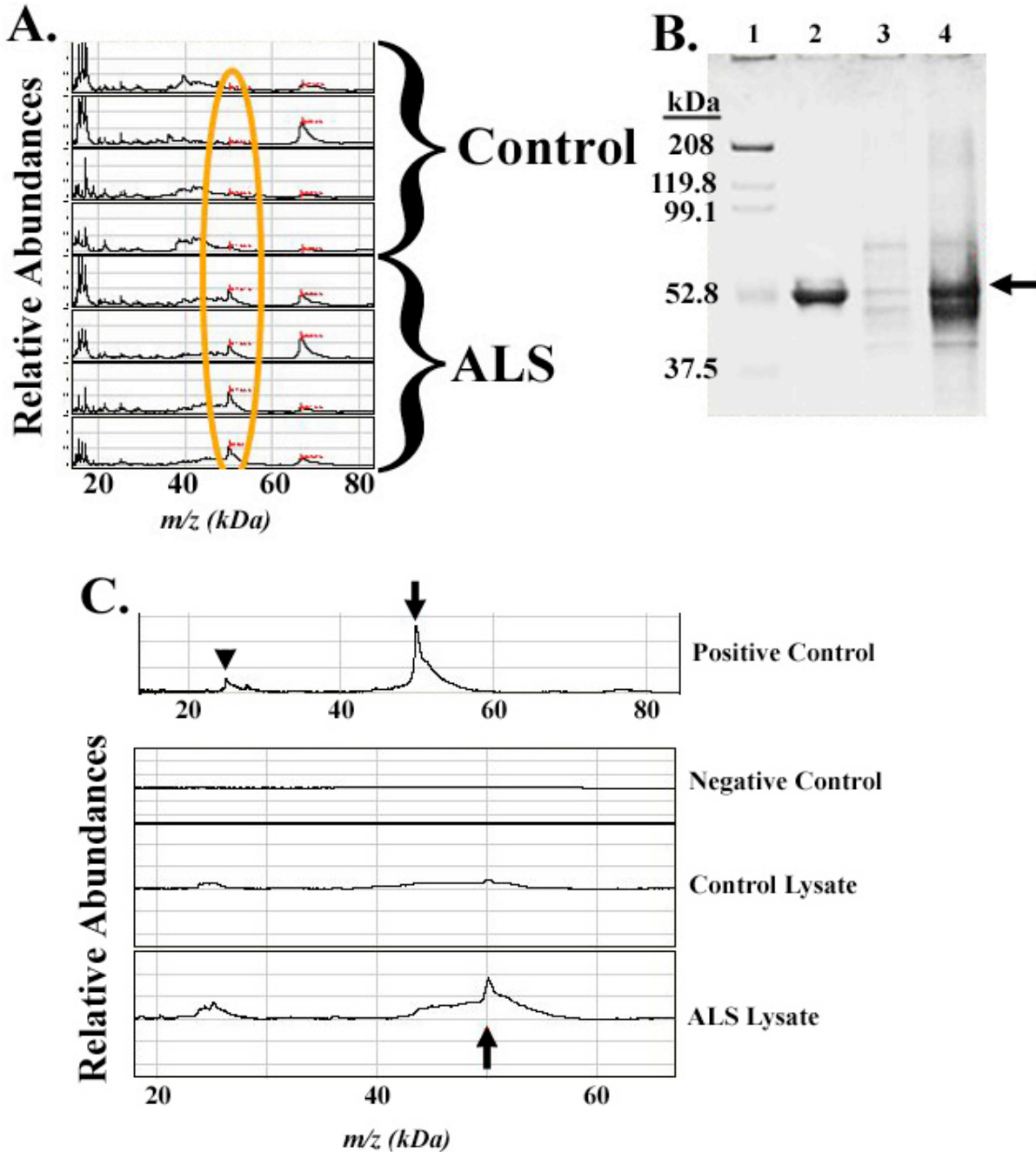


**Figure 55** Identification and validation of glial fibrillary acidic protein (GFAP) in ALS spinal cord lysates

(A) *Representative spectra comparing spinal cord tissue lysates from controls (n = 4) and ALS (n = 4) in the range of 20-80 kDa. The orange oval illustrates the 50kDa peak that differs in peak intensity between controls and ALS.*

*A coomassie-stained 1D SDS-PAGE of spinal cord tissue lysates from a control and ALS case each. Arrow on the right indicates the 50kDa band. The lane assignments are as follows: lane 1 – Molecular weight marker with the mass mentioned on the left in kilodaltons, lane 2 – purified human GFAP protein (10µg), lane 3 –control spinal cord lysate (400µg total protein), lane 4 – ALS spinal cord lysate (400µg total protein).*

(C) *Antibody-chip based SELDI-TOF-MS for validation of the 50kDa protein. 1µg of anti-GFAP antibody coated on each of the spots except in the negative control, which was coated with anti-TNF-α antibody. 5µg of purified GFAP protein was used as the positive control, which reveals a 50kDa peak (arrow) and a double charged peak at about 25kDa (arrowhead). Compared to the control lysate, the ALS tissue lysate reveals a peak at 50kDa similar to the positive control validating that the 50kDa antigen that the antibody is recognizing is GFAP. The negative control that had anti-TNF-α antibody did not recognize the purified GFAP protein.*

## **7.5. A longitudinal biomarker study in ALS patients**

The human CSF biomarker discovery study can be validated with an increased number of samples and then proceed to identify other protein biomarkers. These will be added to the current list of identified biomarkers with continued validation of these in hypothesis-driven disease mechanisms through biochemical and molecular techniques. Similar proteomic approaches towards a longitudinal human study utilizing both CSF and serum samples can be performed. In

fact this has been initiated and a cohort of samples are currently being procured at the University of Pittsburgh under the guidance of Drs. Lacomis and Bowser. Such a study will hopefully identify specific biomarkers as the disease progresses as the CSF / serum donors (ALS patients and non-neurological controls) would have a follow-up visit 6 or 9 months from the initial draw date. This longitudinal study has been undertaken in conjunction with studying the genomics and metabolomics (in collaboration with Day Neuromuscular Center, Harvard Medical School and Metabolon Inc., NC, respectively) providing a three-pronged cutting-edge approach to diagnostics and therapeutics. Such biomarkers may also be valuable as surrogate markers of disease progression that can be used in clinical trials to test drug effectiveness. This would have a dramatic impact on our ability to find effective drug treatments for ALS.

#### **7.6. Proteomics for ALS: The future**

One of the key aspects to identifying disease-specific biomarkers is the recruitment of both the control and patient population. It would be beneficial to obtain a substantial number of non-ALS neurologic control cases and identify protein changes specific to ALS patients by comparing to this group of control cases. Obtaining high degree of specificity in a study comparing these sets of samples is key to classifying protein alterations as obtained through a MS-based proteomic approach as ALS-specific biomarkers. This in itself presents the caveat in that it is difficult to obtain enough number of such non-neurologic cases that present with early clinical symptoms. Another caveat in the field is the presence of a spectrum of motor neuron diseases all of which present with some overlapping clinical symptoms. This necessitates the procurement of clinical samples from patients who have been clearly stratified amongst this spectrum of motor neuron diseases. Diagnostic biomarkers obtained from a carefully selected

patient population can then be tested for their validity. It is possible that a number of these markers could pose a challenge with respect to drug design because some of their functions may be multimodal affecting different physiological arms.

From the context of clinical diagnostics, there are some drawbacks to MS-based proteomic approach using CSF samples. (i) In a clinical diagnostic lab setting, plasma or serum would be the sample of choice as opposed to CSF. Hence, it will be essential to correlate the identified CSF markers to serum / plasma specific markers for ALS. As enumerated earlier in section 7.5, a longitudinal study by procuring both CSF and serum samples from the same patient will greatly substantiate our current findings. (ii) MS-based proteomics cannot infiltrate all diagnostic labs, both from the matters of cost effectiveness and time of assays. MS can still be used for the biomarker discovery and validation phases but one would have to develop molecular techniques such as ELISA in the diagnostic labs.

In conclusion, although our work is incipient for the discovery of ALS-specific biomarkers, it shows promise and has provided a platform for bridging the gap between the basic and clinical science.

## 8. Concluding Remarks

The work performed stretches from dissecting the molecular pathways involved in motor neuron degeneration to biomarker discovery for clinical diagnostics in ALS. We have successfully established a role for cell cycle proteins and our studies demonstrate that the motor neurons in ALS undergo an abortive attempt at re-entry into cell cycle (Chapter 2). This we consider an important factor that contributes to an apoptotic mode of cell death. This however is dichotomous within the surviving motor neurons in the two affected regions in ALS, namely spinal cord and motor cortex (Fig 56). Our studies did not indicate cell death in the motor cortex evident by the absence of p53 and the death markers in the surviving neurons (Chapter 3). Even if altered activation of cell cycle proteins and transcriptional regulators are an epiphenomenon to a primary pathogenic process; it still provides molecular targets for therapeutic interventions. The exact sequence of the events involved in the “abortive re-entry of motor neurons into cell cycle” can be studied using in vitro and animal model systems (Chapter 7). In addition, this study opens avenues to examine the role for DNA damage and chromatin remodeling in the context of the p53 family of transcription factors.

Translating bench work to the bedside is the objective of biomedical research. We have successfully attempted to achieve this goal by the identification and characterization of protein abnormalities in clinical samples as putative biomarkers (Chapter 6). The Ciphergen ProteinChip system is a powerful technique for biomarker discovery and proteomic analysis. We have utilized SELDI-TOF-MS and multiple bioinformatic algorithms to identify putative biomarkers for ALS. Having established this technology, the present study has extensively provided avenues to further the use of MS-based proteomics to identify - (i) molecular markers involved in

different biochemical pathways during onset and progression of ALS; (ii) aid in rapid diagnosis in a clinical setting; (iii) biomarkers to monitor responses to drugs in longitudinal studies.

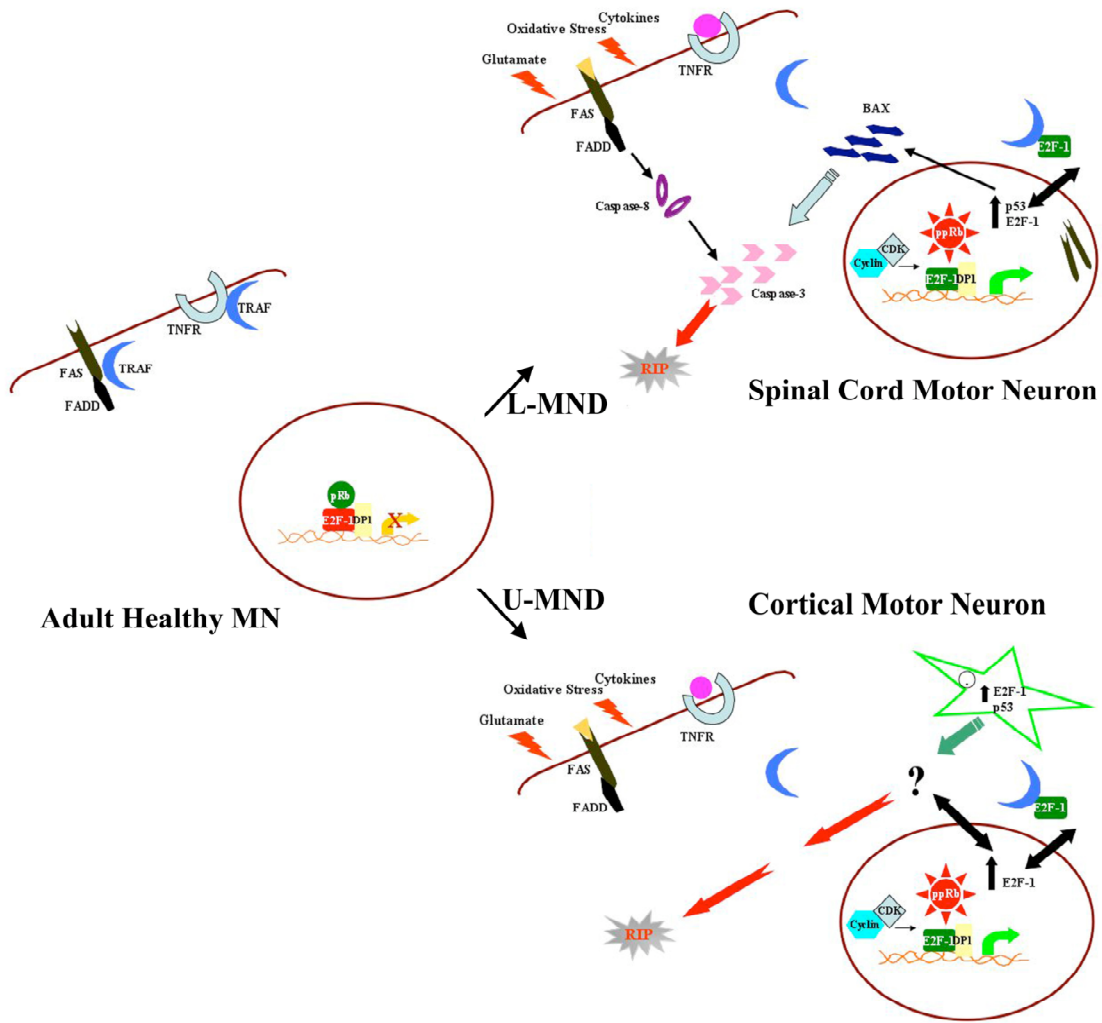


**Figure 56 Motor neuron death in ALS**

*This study provides evidence for dichotomy in the motor neuron death (MND) pathways in spinal cord and motor cortical regions. In a healthy motor neuron the transmembrane receptors such as FAS (dark green bar) and tumor necrosis factor receptor (TNFR; horseshoe) with their death domain adaptor proteins such as (FAS associated via death domain; FADD; black bar) are held*

in check by their association with anti-apoptotic proteins such as TNFR-associated factors (TRAF; blue crescent). In the nucleus (large brown oval), the retinoblastoma (pRb) protein (green circle) in its hypophosphorylated state associates with the E2F-1/DP1 heterodimer (red and yellow boxes) and represses transcription (yellow arrow with a red X). Toxic extracellular insults such as glutamate, oxidative stress and cytokines can re-activate the G1 to S phase regulators in both spinal cord and cortical motor neurons. The re-activation leads to an active cyclin/CDK complex (aqua pentagon/grey box) that hyperphosphorylates pRb (spiked red circle) and de-represses the transcriptional activity of E2F-1 (green block arrow).

Lower Motor Neuron Death (L-MND) - In the spinal cord motor neuron, increase in p53 can lead to increased levels of BAX (blue strips) and caspase-3 (pink “pac mans”). Alternatively, through the interactions of FAS-ligand / FAS, activated caspase-8 (purple ellipse) can result in increased caspase 3. FAS could be mis-localized to the nucleus (dark green bars), the function of which is unknown. TRAFs that are released could associate with the mis-localized E2F-1 and through protein-protein interactions cause L-MND.

Upper Motor Neuron Death (U-MND) - In the cortical motor neurons, there is a lack of p53, BAX, FAS, caspase-8 and caspase-3 in the motor neurons. However, p53 in the astrocytes (green star) can possibly lead to upper MND (U-MND) by yet to be determined pathways. Similar to L-MND, TRAFs could interact with cytoplasmic E2F-1.

**Thus, this body of work has successfully traversed the pathological basis of ALS from molecular mechanisms to biomarker discovery.**

## BIBLIOGRAPHY

1. Shepherd, G.M., *Neurobiology*. 2nd ed. 1988, New York: Oxford University Press. xiv, 685.
2. Parent, A. and M.B. Carpenter, *Carpenter's human neuroanatomy*. 9th ed. 1996, Baltimore: Williams & Wilkins. xii, 1011.
3. Shepherd, G.M., *Foundations of the neuron doctrine*. History of neuroscience ; no. 6. 1991, New York: Oxford University Press. ix, 338.
4. Corvino, V., et al., *S100B protein and 4-hydroxynonenal in the spinal cord of wobbler mice*. Neurochem Res, 2003. **28**(2): p. 341-5.
5. Hirsch, E.C., et al., *The role of glial reaction and inflammation in Parkinson's disease*. Ann N Y Acad Sci, 2003. **991**: p. 214-28.
6. Schofield, E., et al., *Severity of gliosis in Pick's disease and frontotemporal lobar degeneration: tau-positive glia differentiate these disorders*. Brain, 2003. **126**(Pt 4): p. 827-40.
7. Wilson, J.M., et al., *Decrease in glial glutamate transporter variants and excitatory amino acid receptor down-regulation in a murine model of ALS-PDC*. Neuromolecular Med, 2003. **3**(2): p. 105-18.
8. Kandel, E., *Principles of neural science*. 3rd ed ed. 2005.

9. Arendt, T., *Synaptic plasticity and cell cycle activation in neurons are alternative effector pathways: the 'Dr. Jekyll and Mr. Hyde concept' of Alzheimer's disease or the yin and yang of neuroplasticity*. Prog Neurobiol, 2003. **71**(2-3): p. 83-248.
10. Dickey, C.A., et al., *Selectively reduced expression of synaptic plasticity-related genes in amyloid precursor protein + presenilin-1 transgenic mice*. J Neurosci, 2003. **23**(12): p. 5219-26.
11. Arendt, T., *Neurodegeneration and plasticity*. Int J Dev Neurosci, 2004. **22**(7): p. 507-14.
12. Robbins, S.L., R.S. Cotran, and V. Kumar, *Robbins' pathologic basis of disease*. 4th ed. 1989, Philadelphia: Saunders. xiii, 1519.
13. Martin, J.H., *Neuroanatomy : text and atlas*. 2nd ed. 1996, Stamford, Conn.: Appleton & Lange. xxiii, 578.
14. Leigh, P.N. and M. Swash, *Motor neuron disease : biology and management*. 1995, London ; New York: Springer-Verlag. xviii, 468.
15. Kuncel, R.W., *Motor neuron disease*. 2002, London: W. B. Saunders. xiii, 198.
16. Swash, M. and J. Desai, *Motor neuron disease: classification and nomenclature*. Amyotroph Lateral Scler Other Motor Neuron Disord, 2000. **1**(2): p. 105-12.
17. Eisen, A. and C. Krieger, *Amyotrophic lateral sclerosis : a synthesis of research and clinical practice*. 1998, Cambridge ; New York: Cambridge University Press. xx, 303.
18. Kihira, T., et al., *Involvement of Onuf's nucleus in amyotrophic lateral sclerosis*. J Neurol Sci, 1997. **147**(1): p. 81-8.
19. Anneser, J.M., et al., *Glial proliferation and metabotropic glutamate receptor expression in amyotrophic lateral sclerosis*. J Neuropathol Exp Neurol, 2004. **63**(8): p. 831-40.

20. Bergmann, M., M. Volpel, and K. Kuchelmeister, *Onuf's nucleus is frequently involved in motor neuron disease/amyotrophic lateral sclerosis*. J Neurol Sci, 1995. **129**(2): p. 141-6.
21. Charcot, J.M. and C.G. Goetz, *Charcot, the clinician : the Tuesday lessons : excerpts from nine case presentations on general neurology delivered at the Salpãetriãere Hospital in 1887-88 by Jean-Martin Charcot*. 1987, New York: Raven Press. xxx, 193.
22. Goetz, C.G., *Amyotrophic lateral sclerosis: early contributions of Jean-Martin Charcot*. Muscle Nerve, 2000. **23**(3): p. 336-43.
23. Critchley, E.M.R. and A. Eisen, *Diseases of the spinal cord*. Clinical medicine and the nervous system. 1992, London ; New York: Springer-Verlag. xiii, 453.
24. Le Forestier, N., et al., *Does primary lateral sclerosis exist? A study of 20 patients and a review of the literature*. Brain, 2001. **124**(Pt 10): p. 1989-99.
25. Le Forestier, N., et al., *Primary lateral sclerosis: further clarification*. J Neurol Sci, 2001. **185**(2): p. 95-100.
26. Verma, A. and W.G. Bradley, *Atypical motor neuron disease and related motor syndromes*. Semin Neurol, 2001. **21**(2): p. 177-87.
27. Brain, W.R.B., *Diseases of the nervous system*. 6th ed. 1962, London, New York,: Oxford University Press. x, 879.
28. Roling, D.B., A.R. La Spada, and K.H. Fischbeck, *Kennedy's disease*. Neurology, 1993. **43**(11): p. 2424-5.
29. Fischbeck, K.H., *The expanded trinucleotide repeat in Kennedy's disease*. Proc Assoc Am Physicians, 1995. **107**(2): p. 228-30.
30. Fischbeck, K.H., et al., *Androgen receptor mutation in Kennedy's disease*. Philos Trans R Soc Lond B Biol Sci, 1999. **354**(1386): p. 1075-8.

31. Borasio, G.D. and R.G. Miller, *Clinical characteristics and management of ALS*. Semin Neurol, 2001. **21**(2): p. 155-66.
32. Shaw, P.J. and M.J. Strong, *Motor neuron disorders*. Blue books of practical neurology ; 28. 2003, Amsterdam ; Boston: Butterworth-Heinemann. xvi, 569 , [10] of plates.
33. Eisen, A. and M. Weber, *The motor cortex and amyotrophic lateral sclerosis*. Muscle Nerve, 2001. **24**(4): p. 564-73.
34. Majoor-Krakauer, D., P.J. Willems, and A. Hofman, *Genetic epidemiology of amyotrophic lateral sclerosis*. Clin Genet, 2003. **63**(2): p. 83-101.
35. Armon, C., *Western Pacific ALS/PDC and flying foxes: What's next?* Neurology, 2003. **61**(3): p. 291-2.
36. Armon, C., *Environmental risk factors for amyotrophic lateral sclerosis*. Neuroepidemiology, 2001. **20**(1): p. 2-6.
37. Cleveland, D.W. and J.D. Rothstein, *From Charcot to Lou Gehrig: deciphering selective motor neuron death in ALS*. Nat Rev Neurosci, 2001. **2**(11): p. 806-19.
38. Mayeux, R., *Epidemiology of neurodegeneration*. Annu Rev Neurosci, 2003. **26**: p. 81-104.
39. Norris, F., et al., *Onset, natural history and outcome in idiopathic adult motor neuron disease*. J Neurol Sci, 1993. **118**(1): p. 48-55.
40. Rudnicki, S.A., *Estrogen replacement therapy in women with amyotrophic lateral sclerosis*. J Neurol Sci, 1999. **169**(1-2): p. 126-7.
41. Nakamizo, T., et al., *Protection of cultured spinal motor neurons by estradiol*. Neuroreport, 2000. **11**(16): p. 3493-7.

42. Haley, R.W., *Excess incidence of ALS in young Gulf War veterans*. Neurology, 2003. **61**(6): p. 750-6.
43. Horner, R.D., et al., *Occurrence of amyotrophic lateral sclerosis among Gulf War veterans*. Neurology, 2003. **61**(6): p. 742-9.
44. Rose, M.R., *Gulf War service is an uncertain trigger for ALS*. Neurology, 2003. **61**(6): p. 730-1.
45. Brooks, B.R., *El Escorial World Federation of Neurology criteria for the diagnosis of amyotrophic lateral sclerosis. Subcommittee on Motor Neuron Diseases/Amyotrophic Lateral Sclerosis of the World Federation of Neurology Research Group on Neuromuscular Diseases and the El Escorial "Clinical limits of amyotrophic lateral sclerosis" workshop contributors*. J Neurol Sci, 1994. **124 Suppl**: p. 96-107.
46. Brooks, B.R., et al., *El Escorial revisited: revised criteria for the diagnosis of amyotrophic lateral sclerosis*. Amyotroph Lateral Scler Other Motor Neuron Disord, 2000. **1**(5): p. 293-9.
47. Belsh, J.M., *Diagnostic challenges in ALS*. Neurology, 1999. **53**(8 Suppl 5): p. S26-30; discussion S35-6.
48. Ilzecka, J. and Z. Stelmasiak, *Creatine kinase activity in amyotrophic lateral sclerosis patients*. Neurol Sci, 2003. **24**(4): p. 286-7.
49. Iwasaki, Y., et al., *Amyotrophic lateral sclerosis and thyroid function*. J Neurol, 1989. **236**(6): p. 373-4.
50. van Schaik, I.N., et al., *Diagnostic value of GMI antibodies in motor neuron disorders and neuropathies: a meta-analysis*. Neurology, 1995. **45**(8): p. 1570-7.

51. Lamb, N.L. and B.M. Patten, *Clinical correlations of anti-GM1 antibodies in amyotrophic lateral sclerosis and neuropathies*. Muscle Nerve, 1991. **14**(10): p. 1021-7.
52. Niebroj-Dobosz, I., P. Janik, and H. Kwiecinski, *Serum IgM anti-GM1 ganglioside antibodies in lower motor neuron syndromes*. Eur J Neurol, 2004. **11**(1): p. 13-6.
53. Eisen, A., *Clinical electrophysiology of the upper and lower motor neuron in amyotrophic lateral sclerosis*. Semin Neurol, 2001. **21**(2): p. 141-54.
54. Daube, J.R., *Electrodiagnostic studies in amyotrophic lateral sclerosis and other motor neuron disorders*. Muscle Nerve, 2000. **23**(10): p. 1488-502.
55. de Carvalho, M., et al., *Clinical and neurophysiological evaluation of progression in amyotrophic lateral sclerosis*. Muscle Nerve, 2003. **28**(5): p. 630-3.
56. Aggarwal, A. and G. Nicholson, *Detection of preclinical motor neurone loss in SOD1 mutation carriers using motor unit number estimation*. J Neurol Neurosurg Psychiatry, 2002. **73**(2): p. 199-201.
57. Pioro, E.P., et al., *Detection of cortical neuron loss in motor neuron disease by proton magnetic resonance spectroscopic imaging in vivo*. Neurology, 1994. **44**(10): p. 1933-8.
58. Ellis, C.M., et al., *A proton magnetic resonance spectroscopic study in ALS: correlation with clinical findings*. Neurology, 1998. **51**(4): p. 1104-9.
59. Sarchielli, P., et al., *Magnetic resonance imaging and 1H-magnetic resonance spectroscopy in amyotrophic lateral sclerosis*. Neuroradiology, 2001. **43**(3): p. 189-97.
60. Iwasaki, Y., et al., *Muscle morphometry in amyotrophic lateral sclerosis*. Int J Neurosci, 1991. **58**(3-4): p. 165-70.
61. Krivickas, L.S., et al., *Skeletal muscle fiber function and rate of disease progression in amyotrophic lateral sclerosis*. Muscle Nerve, 2002. **26**(5): p. 636-43.

62. Ludolph, A.C. and U. Knirsch, *Problems and pitfalls in the diagnosis of ALS*. J Neurol Sci, 1999. **165 Suppl 1**: p. S14-20.
63. Traynor, B.J., et al., *Amyotrophic lateral sclerosis mimic syndromes: a population-based study*. Arch Neurol, 2000. **57**(1): p. 109-13.
64. Ince, P.G., J. Lowe, and P.J. Shaw, *Amyotrophic lateral sclerosis: current issues in classification, pathogenesis and molecular pathology*. Neuropathol Appl Neurobiol, 1998. **24**(2): p. 104-17.
65. Brooks, B.R., *Diagnostic dilemmas in amyotrophic lateral sclerosis*. J Neurol Sci, 1999. **165 Suppl 1**: p. S1-9.
66. Hayashi, S., et al., *Pathological study of the diffuse myelin pallor in the anterolateral columns of the spinal cord in amyotrophic lateral sclerosis*. J Neurol Sci, 2001. **188**(1-2): p. 3-7.
67. Hirano, A., *Neuropathology of ALS: an overview*. Neurology, 1996. **47**(4 Suppl 2): p. S63-6.
68. Piao, Y.S., et al., *Neuropathology with clinical correlations of sporadic amyotrophic lateral sclerosis: 102 autopsy cases examined between 1962 and 2000*. Brain Pathol, 2003. **13**(1): p. 10-22.
69. Obal, I., et al., *Recruitment of activated microglia cells in the spinal cord of mice by ALS IgG*. Neuroreport, 2001. **12**(11): p. 2449-52.
70. Schiffer, D., et al., *Reactive astrogliosis of the spinal cord in amyotrophic lateral sclerosis*. J Neurol Sci, 1996. **139 Suppl**: p. 27-33.
71. Levine, J.B., et al., *Astrocytes interact intimately with degenerating motor neurons in mouse amyotrophic lateral sclerosis (ALS)*. Glia, 1999. **28**(3): p. 215-24.

72. Oyanagi, K. and M. Wada, *Neuropathology of parkinsonism-dementia complex and amyotrophic lateral sclerosis of Guam: an update*. J Neurol, 1999. **246 Suppl 2**: p. II19-27.
73. Kato, S., et al., *Pathological characterization of astrocytic hyaline inclusions in familial amyotrophic lateral sclerosis*. Am J Pathol, 1997. **151**(2): p. 611-20.
74. Wada, M., et al., *Bunina bodies in amyotrophic lateral sclerosis on Guam: a histochemical, immunohistochemical and ultrastructural investigation*. Acta Neuropathol (Berl), 1999. **98**(2): p. 150-6.
75. Takahashi, T., et al., *Amyotrophic lateral sclerosis with numerous axonal spheroids in the corticospinal tract and massive degeneration of the cortex*. Acta Neuropathol (Berl), 1997. **94**(3): p. 294-9.
76. Toyoshima, I., et al., *Kinesin and cytoplasmic dynein in spinal spheroids with motor neuron disease*. J Neurol Sci, 1998. **159**(1): p. 38-44.
77. Kato, S., et al., *Copper chaperone for superoxide dismutase co-aggregates with superoxide dismutase 1 (SOD1) in neuronal Lewy body-like hyaline inclusions: an immunohistochemical study on familial amyotrophic lateral sclerosis with SOD1 gene mutation*. Acta Neuropathol (Berl), 2001. **102**(3): p. 233-8.
78. Iseki, E., *Dementia with Lewy bodies: reclassification of pathological subtypes and boundary with Parkinson's disease or Alzheimer's disease*. Neuropathology, 2004. **24**(1): p. 72-8.
79. Singleton, A. and K. Gwinn-Hardy, *Parkinson's disease and dementia with Lewy bodies: a difference in dose?* Lancet, 2004. **364**(9440): p. 1105-7.

80. Hamilton, R.L. and R. Bowser, *Alzheimer disease pathology in amyotrophic lateral sclerosis*. Acta Neuropathol (Berl), 2004. **107**(6): p. 515-22.
81. Mackenzie, I.R. and H. Feldman, *Extrapyramidal features in patients with motor neuron disease and dementia; a clinicopathological correlative study*. Acta Neuropathol (Berl), 2004. **107**(4): p. 336-40.
82. Wilson, C.M., et al., *Cognitive impairment in sporadic ALS: a pathologic continuum underlying a multisystem disorder*. Neurology, 2001. **57**(4): p. 651-7.
83. Kasai, K., et al., *Differences in evoked potential characteristics between DRPLA patients and patients with progressive myoclonic epilepsy: preliminary findings indicating usefulness for differential diagnosis*. Epilepsy Res, 1999. **37**(1): p. 3-11.
84. Zoccolella, S., et al., *ALS-plus: 5 cases of concomitant amyotrophic lateral sclerosis and parkinsonism*. Neurol Sci, 2002. **23 Suppl 2**: p. S123-4.
85. Oyanagi, K., et al., *Amyotrophic lateral sclerosis of Guam: the nature of the neuropathological findings*. Acta Neuropathol (Berl), 1994. **88**(5): p. 405-12.
86. Plato, C.C., et al., *Amyotrophic lateral sclerosis and parkinsonism-dementia complex of Guam: changing incidence rates during the past 60 years*. Am J Epidemiol, 2003. **157**(2): p. 149-57.
87. Itoh, N., et al., *Biochemical and ultrastructural study of neurofibrillary tangles in amyotrophic lateral sclerosis/parkinsonism-dementia complex in the Kii peninsula of Japan*. J Neuropathol Exp Neurol, 2003. **62**(7): p. 791-8.
88. Ikemoto, A., A. Hirano, and I. Akiguchi, *Neuropathology of amyotrophic lateral sclerosis with extra-motor system degeneration: characteristics and differences in the*

- molecular pathology between ALS with dementia and Guamanian ALS. Amyotroph Lateral Scler Other Motor Neuron Disord*, 2000. **1**(2): p. 97-104.
89. Bigio, E.H., et al., *Frontotemporal and motor neurone degeneration with neurofilament inclusion bodies: additional evidence for overlap between FTD and ALS. Neuropathol Appl Neurobiol*, 2003. **29**(3): p. 239-53.
  90. Rosen, D.R., et al., *Mutations in Cu/Zn superoxide dismutase gene are associated with familial amyotrophic lateral sclerosis. Nature*, 1993. **362**(6415): p. 59-62.
  91. Hadano, S., et al., *A gene encoding a putative GTPase regulator is mutated in familial amyotrophic lateral sclerosis 2. Nat Genet*, 2001. **29**(2): p. 166-73.
  92. Puls, I., et al., *Mutant dynactin in motor neuron disease. Nat Genet*, 2003. **33**(4): p. 455-6.
  93. Munch, C., et al., *Point mutations of the p150 subunit of dynactin (DCTN1) gene in ALS. Neurology*, 2004. **63**(4): p. 724-6.
  94. Chen, Y.Z., et al., *DNA/RNA helicase gene mutations in a form of juvenile amyotrophic lateral sclerosis (ALS4). Am J Hum Genet*, 2004. **74**(6): p. 1128-35.
  95. Veldink, J.H., L.H. Van Den Berg, and J.H. Wokke, *The future of motor neuron diseaseThe challenge is in the genes. J Neurol*, 2004. **251**(4): p. 491-500.
  96. Deng, H.X., et al., *Amyotrophic lateral sclerosis and structural defects in Cu,Zn superoxide dismutase. Science*, 1993. **261**(5124): p. 1047-51.
  97. Bowling, A.C., et al., *Superoxide dismutase concentration and activity in familial amyotrophic lateral sclerosis. J Neurochem*, 1995. **64**(5): p. 2366-9.
  98. Robberecht, W., et al., *Cu/Zn superoxide dismutase activity in familial and sporadic amyotrophic lateral sclerosis. J Neurochem*, 1994. **62**(1): p. 384-7.

99. Bowling, A.C., et al., *Superoxide dismutase activity, oxidative damage, and mitochondrial energy metabolism in familial and sporadic amyotrophic lateral sclerosis*. J Neurochem, 1993. **61**(6): p. 2322-5.
100. Andersen, P.M., et al., *Amyotrophic lateral sclerosis associated with homozygosity for an Asp90Ala mutation in CuZn-superoxide dismutase*. Nat Genet, 1995. **10**(1): p. 61-6.
101. Marklund, S.L., et al., *Normal binding and reactivity of copper in mutant superoxide dismutase isolated from amyotrophic lateral sclerosis patients*. J Neurochem, 1997. **69**(2): p. 675-81.
102. Reaume, A.G., et al., *Motor neurons in Cu/Zn superoxide dismutase-deficient mice develop normally but exhibit enhanced cell death after axonal injury*. Nat Genet, 1996. **13**(1): p. 43-7.
103. Gurney, M.E., et al., *Motor neuron degeneration in mice that express a human Cu,Zn superoxide dismutase mutation*. Science, 1994. **264**(5166): p. 1772-5.
104. Rosen, D.R., et al., *A frequent ala 4 to val superoxide dismutase-1 mutation is associated with a rapidly progressive familial amyotrophic lateral sclerosis*. Hum Mol Genet, 1994. **3**(6): p. 981-7.
105. Hentati, A., et al., *Linkage of a commoner form of recessive amyotrophic lateral sclerosis to chromosome 15q15-q22 markers*. Neurogenetics, 1998. **2**(1): p. 55-60.
106. Hentati, A., et al., *Linkage of recessive familial amyotrophic lateral sclerosis to chromosome 2q33-q35*. Nat Genet, 1994. **7**(3): p. 425-8.
107. Yang, Y., et al., *The gene encoding alsin, a protein with three guanine-nucleotide exchange factor domains, is mutated in a form of recessive amyotrophic lateral sclerosis*. Nat Genet, 2001. **29**(2): p. 160-5.

108. Otomo, A., et al., *ALS2, a novel guanine nucleotide exchange factor for the small GTPase Rab5, is implicated in endosomal dynamics*. Hum Mol Genet, 2003. **12**(14): p. 1671-87.
109. Chance, P.F., et al., *Linkage of the gene for an autosomal dominant form of juvenile amyotrophic lateral sclerosis to chromosome 9q34*. Am J Hum Genet, 1998. **62**(3): p. 633-40.
110. Blair, I.P., et al., *A gene for autosomal dominant juvenile amyotrophic lateral sclerosis (ALS4) localizes to a 500-kb interval on chromosome 9q34*. Neurogenetics, 2000. **3**(1): p. 1-6.
111. Probst, A., et al., *Axonopathy and amyotrophy in mice transgenic for human four-repeat tau protein*. Acta Neuropathol (Berl), 2000. **99**(5): p. 469-81.
112. Hand, C.K., et al., *A novel locus for familial amyotrophic lateral sclerosis, on chromosome 18q*. Am J Hum Genet, 2002. **70**(1): p. 251-6.
113. Al-Chalabi, A., et al., *Deletions of the heavy neurofilament subunit tail in amyotrophic lateral sclerosis*. Hum Mol Genet, 1999. **8**(2): p. 157-64.
114. Tomkins, J., et al., *Novel insertion in the KSP region of the neurofilament heavy gene in amyotrophic lateral sclerosis (ALS)*. Neuroreport, 1998. **9**(17): p. 3967-70.
115. Lambrechts, D., et al., *VEGF is a modifier of amyotrophic lateral sclerosis in mice and humans and protects motoneurons against ischemic death*. Nat Genet, 2003. **34**(4): p. 383-94.
116. Zheng, C., et al., *Vascular endothelial growth factor prolongs survival in a transgenic mouse model of ALS*. Ann Neurol, 2004. **56**(4): p. 564-7.

117. Guillot, S., et al., *Local GDNF expression mediated by lentiviral vector protects facial nerve motoneurons but not spinal motoneurons in SOD1(G93A) transgenic mice*. Neurobiol Dis, 2004. **16**(1): p. 139-49.
118. Bruijn, L.I., T.M. Miller, and D.W. Cleveland, *Unraveling the mechanisms involved in motor neuron degeneration in ALS*. Annu Rev Neurosci, 2004. **27**: p. 723-49.
119. Mu, X., et al., *Altered expression of bcl-2 and bax mRNA in amyotrophic lateral sclerosis spinal cord motor neurons*. Ann Neurol, 1996. **40**(3): p. 379-86.
120. Nguyen, M.D., W.E. Mushynski, and J.P. Julien, *Cycling at the interface between neurodevelopment and neurodegeneration*. Cell Death Differ, 2002. **9**(12): p. 1294-306.
121. Ranganathan, S., S. Scudiere, and R. Bowser, *Hyperphosphorylation of the retinoblastoma gene product and altered subcellular distribution of E2F-1 during Alzheimer's disease and amyotrophic lateral sclerosis*. J Alzheimers Dis, 2001. **3**(4): p. 377-385.
122. Ranganathan, S. and R. Bowser, *Alterations in G(1) to S phase cell-cycle regulators during amyotrophic lateral sclerosis*. Am J Pathol, 2003. **162**(3): p. 823-35.
123. Bruijn, L.I., et al., *Aggregation and motor neuron toxicity of an ALS-linked SOD1 mutant independent from wild-type SOD1*. Science, 1998. **281**(5384): p. 1851-4.
124. Pasinelli, P., et al., *Caspase-1 and -3 are sequentially activated in motor neuron death in Cu,Zn superoxide dismutase-mediated familial amyotrophic lateral sclerosis*. Proc Natl Acad Sci U S A, 2000. **97**(25): p. 13901-6.
125. Przedborski, S., H. Mitsumoto, and L.P. Rowland, *Recent advances in amyotrophic lateral sclerosis research*. Curr Neurol Neurosci Rep, 2003. **3**(1): p. 70-7.

126. Pasinelli, P., et al., *Caspase-1 is activated in neural cells and tissue with amyotrophic lateral sclerosis-associated mutations in copper-zinc superoxide dismutase*. Proc Natl Acad Sci U S A, 1998. **95**(26): p. 15763-8.
127. Vukosavic, S., et al., *Bax and Bcl-2 interaction in a transgenic mouse model of familial amyotrophic lateral sclerosis*. J Neurochem, 1999. **73**(6): p. 2460-8.
128. Yoshihara, T., et al., *Differential expression of inflammation- and apoptosis-related genes in spinal cords of a mutant SOD1 transgenic mouse model of familial amyotrophic lateral sclerosis*. J Neurochem, 2002. **80**(1): p. 158-67.
129. Deng, H.X., et al., *Two novel SOD1 mutations in patients with familial amyotrophic lateral sclerosis*. Hum Mol Genet, 1995. **4**(6): p. 1113-6.
130. Crow, J.P., et al., *Decreased zinc affinity of amyotrophic lateral sclerosis-associated superoxide dismutase mutants leads to enhanced catalysis of tyrosine nitration by peroxynitrite*. J Neurochem, 1997. **69**(5): p. 1936-44.
131. Boukaftane, Y., et al., *Identification of six novel SOD1 gene mutations in familial amyotrophic lateral sclerosis*. Can J Neurol Sci, 1998. **25**(3): p. 192-6.
132. Gong, Y.H. and J.L. Elliott, *Metallothionein expression is altered in a transgenic murine model of familial amyotrophic lateral sclerosis*. Exp Neurol, 2000. **162**(1): p. 27-36.
133. Nagano, S., et al., *Reduction of metallothioneins promotes the disease expression of familial amyotrophic lateral sclerosis mice in a dose-dependent manner*. Eur J Neurosci, 2001. **13**(7): p. 1363-70.
134. Puttapparthi, K., et al., *Disease progression in a transgenic model of familial amyotrophic lateral sclerosis is dependent on both neuronal and non-neuronal zinc binding proteins*. J Neurosci, 2002. **22**(20): p. 8790-6.

135. Pehar, M., et al., *Peroxynitrite-induced cytotoxicity in cultured astrocytes is associated with morphological changes and increased nitrotyrosine immunoreactivity*. Neurotox Res, 2002. **4**(2): p. 87-93.
136. Cassina, P., et al., *Peroxynitrite triggers a phenotypic transformation in spinal cord astrocytes that induces motor neuron apoptosis*. J Neurosci Res, 2002. **67**(1): p. 21-9.
137. Bruijn, L.I., et al., *Elevated free nitrotyrosine levels, but not protein-bound nitrotyrosine or hydroxyl radicals, throughout amyotrophic lateral sclerosis (ALS)-like disease implicate tyrosine nitration as an aberrant in vivo property of one familial ALS-linked superoxide dismutase 1 mutant*. Proc Natl Acad Sci U S A, 1997. **94**(14): p. 7606-11.
138. Strong, M.J., et al., *Nitration of the low molecular weight neurofilament is equivalent in sporadic amyotrophic lateral sclerosis and control cervical spinal cord*. Biochem Biophys Res Commun, 1998. **248**(1): p. 157-64.
139. Liu, D., et al., *The roles of free radicals in amyotrophic lateral sclerosis: reactive oxygen species and elevated oxidation of protein, DNA, and membrane phospholipids*. Faseb J, 1999. **13**(15): p. 2318-28.
140. Bogdanov, M., et al., *Increased oxidative damage to DNA in ALS patients*. Free Radic Biol Med, 2000. **29**(7): p. 652-8.
141. Subramaniam, J.R., et al., *Mutant SOD1 causes motor neuron disease independent of copper chaperone-mediated copper loading*. Nat Neurosci, 2002. **5**(4): p. 301-7.
142. Azzouz, M., et al., *Prevention of mutant SOD1 motoneuron degeneration by copper chelators in vitro*. J Neurobiol, 2000. **42**(1): p. 49-55.
143. Taylor, J.P., J. Hardy, and K.H. Fischbeck, *Toxic proteins in neurodegenerative disease*. Science, 2002. **296**(5575): p. 1991-5.

144. Wood, J.D., T.P. Beaujeux, and P.J. Shaw, *Protein aggregation in motor neurone disorders*. *Neuropathol Appl Neurobiol*, 2003. **29**(6): p. 529-45.
145. Urushitani, M., et al., *Proteasomal inhibition by misfolded mutant superoxide dismutase 1 induces selective motor neuron death in familial amyotrophic lateral sclerosis*. *J Neurochem*, 2002. **83**(5): p. 1030-42.
146. Hyun, D.H., et al., *Proteasomal inhibition causes the formation of protein aggregates containing a wide range of proteins, including nitrated proteins*. *J Neurochem*, 2003. **86**(2): p. 363-73.
147. Heath, P.R. and P.J. Shaw, *Update on the glutamatergic neurotransmitter system and the role of excitotoxicity in amyotrophic lateral sclerosis*. *Muscle Nerve*, 2002. **26**(4): p. 438-58.
148. Arundine, M. and M. Tymianski, *Molecular mechanisms of calcium-dependent neurodegeneration in excitotoxicity*. *Cell Calcium*, 2003. **34**(4-5): p. 325-37.
149. Perry, T.L., et al., *Amyotrophic lateral sclerosis: amino acid levels in plasma and cerebrospinal fluid*. *Ann Neurol*, 1990. **28**(1): p. 12-7.
150. Rothstein, J.D., et al., *Chronic inhibition of glutamate uptake produces a model of slow neurotoxicity*. *Proc Natl Acad Sci U S A*, 1993. **90**(14): p. 6591-5.
151. Kawahara, Y., et al., *Human spinal motoneurons express low relative abundance of GluR2 mRNA: an implication for excitotoxicity in ALS*. *J Neurochem*, 2003. **85**(3): p. 680-9.
152. Pieri, M., et al., *alpha-Amino-3-hydroxy-5-methyl-isoxazole-4-propionate receptors in spinal cord motor neurons are altered in transgenic mice overexpressing human Cu,Zn superoxide dismutase (Gly93-->Ala) mutation*. *Neuroscience*, 2003. **122**(1): p. 47-58.

153. Van Den Bosch, L., et al., *Protective effect of parvalbumin on excitotoxic motor neuron death*. *Exp Neurol*, 2002. **174**(2): p. 150-61.
154. Ince, P., et al., *Parvalbumin and calbindin D-28k in the human motor system and in motor neuron disease*. *Neuropathol Appl Neurobiol*, 1993. **19**(4): p. 291-9.
155. Lin, C.L., et al., *Aberrant RNA processing in a neurodegenerative disease: the cause for absent EAAT2, a glutamate transporter, in amyotrophic lateral sclerosis*. *Neuron*, 1998. **20**(3): p. 589-602.
156. Rothstein, J.D., L.J. Martin, and R.W. Kuncl, *Decreased glutamate transport by the brain and spinal cord in amyotrophic lateral sclerosis*. *N Engl J Med*, 1992. **326**(22): p. 1464-8.
157. Rothstein, J.D., et al., *Selective loss of glial glutamate transporter GLT-1 in amyotrophic lateral sclerosis*. *Ann Neurol*, 1995. **38**(1): p. 73-84.
158. Meyer, T., et al., *The EAAT2 (GLT-1) gene in motor neuron disease: absence of mutations in amyotrophic lateral sclerosis and a point mutation in patients with hereditary spastic paraplegia*. *J Neurol Neurosurg Psychiatry*, 1998. **65**(4): p. 594-6.
159. Meyer, T., et al., *The RNA of the glutamate transporter EAAT2 is variably spliced in amyotrophic lateral sclerosis and normal individuals*. *J Neurol Sci*, 1999. **170**(1): p. 45-50.
160. Munch, C., et al., *Differential RNA cleavage and polyadenylation of the glutamate transporter EAAT2 in the human brain*. *Brain Res Mol Brain Res*, 2000. **80**(2): p. 244-51.
161. Kong, J. and Z. Xu, *Massive mitochondrial degeneration in motor neurons triggers the onset of amyotrophic lateral sclerosis in mice expressing a mutant SOD1*. *J Neurosci*, 1998. **18**(9): p. 3241-50.

162. Jaarsma, D., et al., *Human Cu/Zn superoxide dismutase (SOD1) overexpression in mice causes mitochondrial vacuolization, axonal degeneration, and premature motoneuron death and accelerates motoneuron disease in mice expressing a familial amyotrophic lateral sclerosis mutant SOD1*. *Neurobiol Dis*, 2000. **7**(6 Pt B): p. 623-43.
163. Higgins, C.M., C. Jung, and Z. Xu, *ALS-associated mutant SOD1G93A causes mitochondrial vacuolation by expansion of the intermembrane space and by involvement of SOD1 aggregation and peroxisomes*. *BMC Neurosci*, 2003. **4**(1): p. 16.
164. Liu, J., et al., *Toxicity of familial ALS-linked SOD1 mutants from selective recruitment to spinal mitochondria*. *Neuron*, 2004. **43**(1): p. 5-17.
165. Flanagan, S.W., et al., *Overexpression of manganese superoxide dismutase attenuates neuronal death in human cells expressing mutant (G37R) Cu/Zn-superoxide dismutase*. *J Neurochem*, 2002. **81**(1): p. 170-7.
166. Albers, D.S. and M.F. Beal, *Mitochondrial dysfunction and oxidative stress in aging and neurodegenerative disease*. *J Neural Transm Suppl*, 2000. **59**: p. 133-54.
167. Strong, M.J., I. Wakayama, and R.M. Garruto, *The neuronal cytoskeleton in disorders of late onset and slow progression*. *Ann N Y Acad Sci*, 1993. **679**: p. 388-93.
168. Gonatas, N.K., et al., *Fragmentation of the Golgi apparatus of motor neurons in amyotrophic lateral sclerosis*. *Am J Pathol*, 1992. **140**(3): p. 731-7.
169. Mourelatos, Z., et al., *Fragmentation of the Golgi apparatus of motor neurons in amyotrophic lateral sclerosis (ALS). Clinical studies in ALS of Guam and experimental studies in deafferented neurons and in beta,beta'-iminodipropionitrile axonopathy*. *Am J Pathol*, 1994. **144**(6): p. 1288-300.

170. Fujita, Y., et al., *The Golgi apparatus is fragmented in spinal cord motor neurons of amyotrophic lateral sclerosis with basophilic inclusions*. Acta Neuropathol (Berl), 2002. **103**(3): p. 243-7.
171. Stieber, A., J.O. Gonatas, and N.K. Gonatas, *Aggregation of ubiquitin and a mutant ALS-linked SOD1 protein correlate with disease progression and fragmentation of the Golgi apparatus*. J Neurol Sci, 2000. **173**(1): p. 53-62.
172. Mourelatos, Z., et al., *The Golgi apparatus of spinal cord motor neurons in transgenic mice expressing mutant Cu,Zn superoxide dismutase becomes fragmented in early, preclinical stages of the disease*. Proc Natl Acad Sci U S A, 1996. **93**(11): p. 5472-7.
173. Rao, M.V. and R.A. Nixon, *Defective neurofilament transport in mouse models of amyotrophic lateral sclerosis: a review*. Neurochem Res, 2003. **28**(7): p. 1041-7.
174. Julien, J.P., S. Couillard-Despres, and J. Meier, *Transgenic mice in the study of ALS: the role of neurofilaments*. Brain Pathol, 1998. **8**(4): p. 759-69.
175. Williamson, T.L., et al., *Absence of neurofilaments reduces the selective vulnerability of motor neurons and slows disease caused by a familial amyotrophic lateral sclerosis-linked superoxide dismutase 1 mutant*. Proc Natl Acad Sci U S A, 1998. **95**(16): p. 9631-6.
176. Beaulieu, J.M. and J.P. Julien, *Peripherin-mediated death of motor neurons rescued by overexpression of neurofilament NF-H proteins*. J Neurochem, 2003. **85**(1): p. 248-56.
177. Kong, J. and Z. Xu, *Overexpression of neurofilament subunit NF-L and NF-H extends survival of a mouse model for amyotrophic lateral sclerosis*. Neurosci Lett, 2000. **281**(1): p. 72-4.

178. Lee, M.K., J.R. Marszalek, and D.W. Cleveland, *A mutant neurofilament subunit causes massive, selective motor neuron death: implications for the pathogenesis of human motor neuron disease*. Neuron, 1994. **13**(4): p. 975-88.
179. Williamson, T.L. and D.W. Cleveland, *Slowing of axonal transport is a very early event in the toxicity of ALS-linked SOD1 mutants to motor neurons*. Nat Neurosci, 1999. **2**(1): p. 50-6.
180. Bajaj, N.P., et al., *Cyclin dependent kinase-5 (CDK-5) phosphorylates neurofilament heavy (NF-H) chain to generate epitopes for antibodies that label neurofilament accumulations in amyotrophic lateral sclerosis (ALS) and is present in affected motor neurones in ALS*. Prog Neuropsychopharmacol Biol Psychiatry, 1999. **23**(5): p. 833-50.
181. Nguyen, M.D., R.C. Lariviere, and J.P. Julien, *Deregulation of Cdk5 in a mouse model of ALS: toxicity alleviated by perikaryal neurofilament inclusions*. Neuron, 2001. **30**(1): p. 135-47.
182. Schiffer, D. and V. Fiano, *Astrogliosis in ALS: possible interpretations according to pathogenetic hypotheses*. Amyotroph Lateral Scler Other Motor Neuron Disord, 2004. **5**(1): p. 22-5.
183. Pramatarova, A., et al., *Neuron-specific expression of mutant superoxide dismutase 1 in transgenic mice does not lead to motor impairment*. J Neurosci, 2001. **21**(10): p. 3369-74.
184. Clement, A.M., et al., *Wild-type nonneuronal cells extend survival of SOD1 mutant motor neurons in ALS mice*. Science, 2003. **302**(5642): p. 113-7.
185. Appel, S.H., et al., *Increased intracellular calcium triggered by immune mechanisms in amyotrophic lateral sclerosis*. Clin Neurosci, 1995. **3**(6): p. 368-74.

186. Offen, D., et al., *Antibodies from ALS patients inhibit dopamine release mediated by L-type calcium channels*. Neurology, 1998. **51**(4): p. 1100-3.
187. Henkel, J.S., et al., *Presence of dendritic cells, MCP-1, and activated microglia/macrophages in amyotrophic lateral sclerosis spinal cord tissue*. Ann Neurol, 2004. **55**(2): p. 221-35.
188. Van Den Bosch, L., et al., *Minocycline delays disease onset and mortality in a transgenic model of ALS*. Neuroreport, 2002. **13**(8): p. 1067-70.
189. Drachman, D.B., et al., *Cyclooxygenase 2 inhibition protects motor neurons and prolongs survival in a transgenic mouse model of ALS*. Ann Neurol, 2002. **52**(6): p. 771-8.
190. Hall, E.D., et al., *Relationship of oxygen radical-induced lipid peroxidative damage to disease onset and progression in a transgenic model of familial ALS*. J Neurosci Res, 1998. **53**(1): p. 66-77.
191. Simpson, E.P., et al., *Increased lipid peroxidation in sera of ALS patients: a potential biomarker of disease burden*. Neurology, 2004. **62**(10): p. 1758-65.
192. Pratico, D. and S. Sung, *Lipid peroxidation and oxidative imbalance: early functional events in Alzheimer's disease*. J Alzheimers Dis, 2004. **6**(2): p. 171-5.
193. Zarkovic, K., *4-hydroxynonenal and neurodegenerative diseases*. Mol Aspects Med, 2003. **24**(4-5): p. 293-303.
194. Rao, A.V. and B. Balachandran, *Role of oxidative stress and antioxidants in neurodegenerative diseases*. Nutr Neurosci, 2002. **5**(5): p. 291-309.
195. Warita, H., et al., *Oxidative damage to mitochondrial DNA in spinal motoneurons of transgenic ALS mice*. Brain Res Mol Brain Res, 2001. **89**(1-2): p. 147-52.

196. Mawrin, C., et al., *Single-cell analysis of mtDNA deletion levels in sporadic amyotrophic lateral sclerosis*. Neuroreport, 2004. **15**(6): p. 939-43.
197. Martin, L.J., *p53 is abnormally elevated and active in the CNS of patients with amyotrophic lateral sclerosis*. Neurobiol Dis, 2000. **7**(6 Pt B): p. 613-22.
198. Cho, K.J., et al., *Reactive astrocytes express p53 in the spinal cord of transgenic mice expressing a human Cu/Zn SOD mutation*. Neuroreport, 1999. **10**(18): p. 3939-43.
199. Kim, S.H., et al., *PARP expression is increased in astrocytes but decreased in motor neurons in the spinal cord of sporadic ALS patients*. J Neuropathol Exp Neurol, 2003. **62**(1): p. 88-103.
200. Koh, S.H., et al., *Epigallocatechin gallate prevents oxidative-stress-induced death of mutant Cu/Zn-superoxide dismutase (G93A) motoneuron cells by alteration of cell survival and death signals*. Toxicology, 2004. **202**(3): p. 213-25.
201. Olkowski, Z.L., *Mutant AP endonuclease in patients with amyotrophic lateral sclerosis*. Neuroreport, 1998. **9**(2): p. 239-42.
202. Kisby, G.E., J. Milne, and C. Sweatt, *Evidence of reduced DNA repair in amyotrophic lateral sclerosis brain tissue*. Neuroreport, 1997. **8**(6): p. 1337-40.
203. Shaikh, A.Y. and L.J. Martin, *DNA base-excision repair enzyme apurinic/apyrimidinic endonuclease/redox factor-1 is increased and competent in the brain and spinal cord of individuals with amyotrophic lateral sclerosis*. Neuromolecular Med, 2002. **2**(1): p. 47-60.
204. Borthwick, G.M., et al., *Mitochondrial enzyme activity in amyotrophic lateral sclerosis: implications for the role of mitochondria in neuronal cell death*. Ann Neurol, 1999. **46**(5): p. 787-90.

205. Lu, Y.Y., et al., *Intramuscular injection of AAV-GDNF results in sustained expression of transgenic GDNF, and its delivery to spinal motoneurons by retrograde transport.* Neurosci Res, 2003. **45**(1): p. 33-40.
206. Kaspar, B.K., et al., *Retrograde viral delivery of IGF-I prolongs survival in a mouse ALS model.* Science, 2003. **301**(5634): p. 839-42.
207. Bilak, M.M., A.M. Corse, and R.W. Kuncl, *Additivity and potentiation of IGF-I and GDNF in the complete rescue of postnatal motor neurons.* Amyotroph Lateral Scler Other Motor Neuron Disord, 2001. **2**(2): p. 83-91.
208. Sun, W., H. Funakoshi, and T. Nakamura, *Overexpression of HGF retards disease progression and prolongs life span in a transgenic mouse model of ALS.* J Neurosci, 2002. **22**(15): p. 6537-48.
209. Kato, S., et al., *Expression of hepatocyte growth factor and c-Met in the anterior horn cells of the spinal cord in the patients with amyotrophic lateral sclerosis (ALS): immunohistochemical studies on sporadic ALS and familial ALS with superoxide dismutase 1 gene mutation.* Acta Neuropathol (Berl), 2003. **106**(2): p. 112-20.
210. Berger, M.M., et al., *Detection and cellular localization of enterovirus RNA sequences in spinal cord of patients with ALS.* Neurology, 2000. **54**(1): p. 20-5.
211. Karpati, G. and M.C. Dalakas, *Viral hide-and-peek in sporadic ALS: a new challenge.* Neurology, 2000. **54**(1): p. 6-7.
212. Nix, W.A., et al., *Failure to detect enterovirus in the spinal cord of ALS patients using a sensitive RT-PCR method.* Neurology, 2004. **62**(8): p. 1372-7.
213. Walker, M.P., et al., *Absence of echovirus sequences in brain and spinal cord of amyotrophic lateral sclerosis patients.* Ann Neurol, 2001. **49**(2): p. 249-53.

214. Jubelt, B. and H.L. Lipton, *ALS: persistent scientists do not find persisting enteroviruses*. Neurology, 2004. **62**(8): p. 1250-1.
215. Ross, M.E., *Cell division and the nervous system: regulating the cycle from neural differentiation to death*. Trends Neurosci, 1996. **19**(2): p. 62-8.
216. Ohnuma, S., A. Philpott, and W.A. Harris, *Cell cycle and cell fate in the nervous system*. Curr Opin Neurobiol, 2001. **11**(1): p. 66-73.
217. Nurse, P., Y. Masui, and L. Hartwell, *Understanding the cell cycle*. Nat Med, 1998. **4**(10): p. 1103-6.
218. Hartwell, L.H. and M.B. Kastan, *Cell cycle control and cancer*. Science, 1994. **266**(5192): p. 1821-8.
219. Hatakeyama, M., et al., *Collaboration of G1 cyclins in the functional inactivation of the retinoblastoma protein*. Genes Dev, 1994. **8**(15): p. 1759-71.
220. Weinberg, R.A., *The retinoblastoma protein and cell cycle control*. Cell, 1995. **81**(3): p. 323-30.
221. Hatakeyama, M. and R.A. Weinberg, *The role of RB in cell cycle control*. Prog Cell Cycle Res, 1995. **1**: p. 9-19.
222. Bagchi, S., R. Weinmann, and P. Raychaudhuri, *The retinoblastoma protein copurifies with E2F-1, an E1A-regulated inhibitor of the transcription factor E2F*. Cell, 1991. **65**(6): p. 1063-72.
223. Chellappan, S.P., et al., *The E2F transcription factor is a cellular target for the RB protein*. Cell, 1991. **65**(6): p. 1053-61.
224. Hiebert, S.W., et al., *The interaction of RB with E2F coincides with an inhibition of the transcriptional activity of E2F*. Genes Dev, 1992. **6**(2): p. 177-85.

225. Black, A.R. and J. Azizkhan-Clifford, *Regulation of E2F: a family of transcription factors involved in proliferation control*. *Gene*, 1999. **237**(2): p. 281-302.
226. Eliyahu, D., et al., *Wild-type p53 can inhibit oncogene-mediated focus formation*. *Proc Natl Acad Sci U S A*, 1989. **86**(22): p. 8763-7.
227. Finlay, C.A., P.W. Hinds, and A.J. Levine, *The p53 proto-oncogene can act as a suppressor of transformation*. *Cell*, 1989. **57**(7): p. 1083-93.
228. Yonish-Rouach, E., et al., *Wild-type p53 induces apoptosis of myeloid leukaemic cells that is inhibited by interleukin-6*. *Nature*, 1991. **352**(6333): p. 345-7.
229. Shaw, P., et al., *Induction of apoptosis by wild-type p53 in a human colon tumor-derived cell line*. *Proc Natl Acad Sci U S A*, 1992. **89**(10): p. 4495-9.
230. Donehower, L.A., et al., *Mice deficient for p53 are developmentally normal but susceptible to spontaneous tumours*. *Nature*, 1992. **356**(6366): p. 215-21.
231. Macleod, K.F., Y. Hu, and T. Jacks, *Loss of Rb activates both p53-dependent and independent cell death pathways in the developing mouse nervous system*. *Embo J*, 1996. **15**(22): p. 6178-88.
232. Phillips, A.C., et al., *Induction of DNA synthesis and apoptosis are separable functions of E2F-1*. *Genes Dev*, 1997. **11**(14): p. 1853-63.
233. Phillips, A.C. and K.H. Vousden, *E2F-1 induced apoptosis*. *Apoptosis*, 2001. **6**(3): p. 173-82.
234. Copani, A., et al., *Activation of cell-cycle-associated proteins in neuronal death: a mandatory or dispensable path?* *Trends Neurosci*, 2001. **24**(1): p. 25-31.
235. Herrup, K., et al., *Divide and die: cell cycle events as triggers of nerve cell death*. *J Neurosci*, 2004. **24**(42): p. 9232-9.

236. Bowser, R. and M.A. Smith, *Cell cycle proteins in Alzheimer's disease: plenty of wheels but no cycle*. J Alzheimers Dis, 2002. **4**(3): p. 249-54.
237. Becker, E.B. and A. Bonni, *Cell cycle regulation of neuronal apoptosis in development and disease*. Prog Neurobiol, 2004. **72**(1): p. 1-25.
238. Morris, E.J. and H.M. Geller, *Induction of neuronal apoptosis by camptothecin, an inhibitor of DNA topoisomerase-I: evidence for cell cycle-independent toxicity*. J Cell Biol, 1996. **134**(3): p. 757-70.
239. Copani, A., et al., *Mitotic signaling by beta-amyloid causes neuronal death*. Faseb J, 1999. **13**(15): p. 2225-34.
240. Park, D.S., et al., *Cyclin-dependent kinases participate in death of neurons evoked by DNA-damaging agents*. J Cell Biol, 1998. **143**(2): p. 457-67.
241. Park, D.S., et al., *Multiple pathways of neuronal death induced by DNA-damaging agents, NGF deprivation, and oxidative stress*. J Neurosci, 1998. **18**(3): p. 830-40.
242. Jordan-Sciutto, K., J. Rhodes, and R. Bowser, *Altered subcellular distribution of transcriptional regulators in response to Abeta peptide and during Alzheimer's disease*. Mech Ageing Dev, 2001. **123**(1): p. 11-20.
243. Kruman, II, et al., *Cell cycle activation linked to neuronal cell death initiated by DNA damage*. Neuron, 2004. **41**(4): p. 549-61.
244. Nguyen, M.D., et al., *Cell cycle regulators in the neuronal death pathway of amyotrophic lateral sclerosis caused by mutant superoxide dismutase 1*. J Neurosci, 2003. **23**(6): p. 2131-40.
245. Jordan-Sciutto, K.L., et al., *Response of cell cycle proteins to neurotrophic factor and chemokine stimulation in human neuroglia*. Exp Neurol, 2001. **167**(2): p. 205-14.

246. Vincent, I., et al., *Aberrant expression of mitotic cdc2/cyclin B1 kinase in degenerating neurons of Alzheimer's disease brain*. J Neurosci, 1997. **17**(10): p. 3588-98.
247. Arendt, T., et al., *Aberrancies in signal transduction and cell cycle related events in Alzheimer's disease*. J Neural Transm Suppl, 1998. **54**: p. 147-58.
248. Jordan-Sciutto, K.L., et al., *Expression patterns of retinoblastoma protein in Parkinson disease*. J Neuropathol Exp Neurol, 2003. **62**(1): p. 68-74.
249. Ogawa, O., et al., *Increased p27, an essential component of cell cycle control, in Alzheimer's disease*. Aging Cell, 2003. **2**(2): p. 105-10.
250. McShea, A., A.F. Wahl, and M.A. Smith, *Re-entry into the cell cycle: a mechanism for neurodegeneration in Alzheimer disease*. Med Hypotheses, 1999. **52**(6): p. 525-7.
251. Yang, Y., D.S. Geldmacher, and K. Herrup, *DNA replication precedes neuronal cell death in Alzheimer's disease*. J Neurosci, 2001. **21**(8): p. 2661-8.
252. Volbracht, C., et al., *Apoptosis in caspase-inhibited neurons*. Mol Med, 2001. **7**(1): p. 36-48.
253. Zhan, R.Z., et al., *Both caspase-dependent and caspase-independent pathways may be involved in hippocampal CA1 neuronal death because of loss of cytochrome c From mitochondria in a rat forebrain ischemia model*. J Cereb Blood Flow Metab, 2001. **21**(5): p. 529-40.
254. Roy, M. and R. Sapolsky, *Neuronal apoptosis in acute necrotic insults: why is this subject such a mess?* Trends Neurosci, 1999. **22**(10): p. 419-22.
255. Sperandio, S., I. de Belle, and D.E. Bredesen, *An alternative, nonapoptotic form of programmed cell death*. Proc Natl Acad Sci U S A, 2000. **97**(26): p. 14376-81.

256. Cuervo, A.M., *Autophagy and aging--when "all you can eat" is yourself*. Sci Aging Knowledge Environ, 2003. **2003**(36): p. pe25.
257. Selimi, F., et al., *Lurcher GRID2-induced death and depolarization can be dissociated in cerebellar Purkinje cells*. Neuron, 2003. **37**(5): p. 813-9.
258. Larsen, K.E., et al., *Methamphetamine-induced degeneration of dopaminergic neurons involves autophagy and upregulation of dopamine synthesis*. J Neurosci, 2002. **22**(20): p. 8951-60.
259. Zhu, X., G. Perry, and M.A. Smith, *Amyotrophic lateral sclerosis: a novel hypothesis involving a gained 'loss of function' in the JNK/SAPK pathway*. Redox Rep, 2003. **8**(3): p. 129-33.
260. Florez-McClure, M.L., et al., *The p75 neurotrophin receptor can induce autophagy and death of cerebellar Purkinje neurons*. J Neurosci, 2004. **24**(19): p. 4498-509.
261. Thornberry, N.A. and Y. Lazebnik, *Caspases: enemies within*. Science, 1998. **281**(5381): p. 1312-6.
262. Li, W.P., et al., *Terminal dUTP nick end labeling (TUNEL) positive cells in the different regions of the brain in normal aging and Alzheimer patients*. J Mol Neurosci, 1997. **8**(2): p. 75-82.
263. Beilharz, E.J., et al., *Mechanisms of delayed cell death following hypoxic-ischemic injury in the immature rat: evidence for apoptosis during selective neuronal loss*. Brain Res Mol Brain Res, 1995. **29**(1): p. 1-14.
264. Hara, H., et al., *Inhibition of interleukin 1beta converting enzyme family proteases reduces ischemic and excitotoxic neuronal damage*. Proc Natl Acad Sci U S A, 1997. **94**(5): p. 2007-12.

265. Schulz, J.B., M. Weller, and M.A. Moskowitz, *Caspases as treatment targets in stroke and neurodegenerative diseases*. *Ann Neurol*, 1999. **45**(4): p. 421-9.
266. Ekegren, T., et al., *Upregulation of Bax protein and increased DNA degradation in ALS spinal cord motor neurons*. *Acta Neurol Scand*, 1999. **100**(5): p. 317-21.
267. Estevez, A.G., et al., *Induction of nitric oxide-dependent apoptosis in motor neurons by zinc-deficient superoxide dismutase*. *Science*, 1999. **286**(5449): p. 2498-500.
268. Dragunow, M., et al., *In situ evidence for DNA fragmentation in Huntington's disease striatum and Alzheimer's disease temporal lobes*. *Neuroreport*, 1995. **6**(7): p. 1053-7.
269. Hirsch, E.C., et al., *Dopaminergic neurons degenerate by apoptosis in Parkinson's disease*. *Mov Disord*, 1999. **14**(2): p. 383-5.
270. Tatton, N.A., *Increased caspase 3 and Bax immunoreactivity accompany nuclear GAPDH translocation and neuronal apoptosis in Parkinson's disease*. *Exp Neurol*, 2000. **166**(1): p. 29-43.
271. Tatton, W.G., et al., *Apoptosis in Parkinson's disease: signals for neuronal degradation*. *Ann Neurol*, 2003. **53 Suppl 3**: p. S61-70; discussion S70-2.
272. Thomas, L.B., et al., *DNA end labeling (TUNEL) in Huntington's disease and other neuropathological conditions*. *Exp Neurol*, 1995. **133**(2): p. 265-72.
273. Martin, L.J., et al., *Injury-induced apoptosis of neurons in adult brain is mediated by p53-dependent and p53-independent pathways and requires Bax*. *J Comp Neurol*, 2001. **433**(3): p. 299-311.
274. Martin, L.J., et al., *Early events of target deprivation/axotomy-induced neuronal apoptosis in vivo: oxidative stress, DNA damage, p53 phosphorylation and subcellular redistribution of death proteins*. *J Neurochem*, 2003. **85**(1): p. 234-47.

275. Friedlander, R.M., *Apoptosis and caspases in neurodegenerative diseases*. N Engl J Med, 2003. **348**(14): p. 1365-75.
276. Ashkenazi, A. and V.M. Dixit, *Death receptors: signaling and modulation*. Science, 1998. **281**(5381): p. 1305-8.
277. Hakem, R., et al., *Differential requirement for caspase 9 in apoptotic pathways in vivo*. Cell, 1998. **94**(3): p. 339-52.
278. Li, P., et al., *Cytochrome c and dATP-dependent formation of Apaf-1/caspase-9 complex initiates an apoptotic protease cascade*. Cell, 1997. **91**(4): p. 479-89.
279. Liu, X., et al., *DFP, a heterodimeric protein that functions downstream of caspase-3 to trigger DNA fragmentation during apoptosis*. Cell, 1997. **89**(2): p. 175-84.
280. Liu, X., et al., *The 40-kDa subunit of DNA fragmentation factor induces DNA fragmentation and chromatin condensation during apoptosis*. Proc Natl Acad Sci U S A, 1998. **95**(15): p. 8461-6.
281. Enari, M., et al., *A caspase-activated DNase that degrades DNA during apoptosis, and its inhibitor ICAD*. Nature, 1998. **391**(6662): p. 43-50.
282. Matsushita, K., et al., *Fas receptor and neuronal cell death after spinal cord ischemia*. J Neurosci, 2000. **20**(18): p. 6879-87.
283. Sakurai, M., et al., *Delayed selective motor neuron death and fas antigen induction after spinal cord ischemia in rabbits*. Brain Res, 1998. **797**(1): p. 23-8.
284. Sharma, K., et al., *Death the Fas way: regulation and pathophysiology of CD95 and its ligand*. Pharmacol Ther, 2000. **88**(3): p. 333-47.
285. Yu, S.W., et al., *Mediation of poly(ADP-ribose) polymerase-1-dependent cell death by apoptosis-inducing factor*. Science, 2002. **297**(5579): p. 259-63.

286. Stringer, J.R., et al., *Increased mutation in mice genetically predisposed to oxidative damage in the brain*. *Mutat Res*, 2004. **556**(1-2): p. 127-34.
287. Klein, J.A., et al., *The harlequin mouse mutation downregulates apoptosis-inducing factor*. *Nature*, 2002. **419**(6905): p. 367-74.
288. Martin, L.J., *Neuronal death in amyotrophic lateral sclerosis is apoptosis: possible contribution of a programmed cell death mechanism*. *J Neuropathol Exp Neurol*, 1999. **58**(5): p. 459-71.
289. Pasinelli, P., et al., *Amyotrophic lateral sclerosis-associated SOD1 mutant proteins bind and aggregate with Bcl-2 in spinal cord mitochondria*. *Neuron*, 2004. **43**(1): p. 19-30.
290. Li, M., et al., *Functional role of caspase-1 and caspase-3 in an ALS transgenic mouse model*. *Science*, 2000. **288**(5464): p. 335-9.
291. Kostic, V., et al., *Bcl-2: prolonging life in a transgenic mouse model of familial amyotrophic lateral sclerosis*. *Science*, 1997. **277**(5325): p. 559-62.
292. Bendotti, C., et al., *Early vacuolization and mitochondrial damage in motor neurons of FALS mice are not associated with apoptosis or with changes in cytochrome oxidase histochemical reactivity*. *J Neurol Sci*, 2001. **191**(1-2): p. 25-33.
293. Kalra, S., D.L. Arnold, and N.R. Cashman, *Biological markers in the diagnosis and treatment of ALS*. *J Neurol Sci*, 1999. **165 Suppl 1**: p. S27-32.
294. Turner, M.R., M.J. Parton, and P.N. Leigh, *Clinical trials in ALS: an overview*. *Semin Neurol*, 2001. **21**(2): p. 167-75.
295. Festoff, B.W., Z. Suo, and B.A. Citron, *Prospects for the pharmacotherapy of amyotrophic lateral sclerosis : old strategies and new paradigms for the third millennium*. *CNS Drugs*, 2003. **17**(10): p. 699-717.

296. Du, Y., et al., *Minocycline prevents nigrostriatal dopaminergic neurodegeneration in the MPTP model of Parkinson's disease*. Proc Natl Acad Sci U S A, 2001. **98**(25): p. 14669-74.
297. Lin, S., et al., *Minocycline blocks 6-hydroxydopamine-induced neurotoxicity and free radical production in rat cerebellar granule neurons*. Life Sci, 2003. **72**(14): p. 1635-41.
298. Tikka, T.M. and J.E. Koistinaho, *Minocycline provides neuroprotection against N-methyl-D-aspartate neurotoxicity by inhibiting microglia*. J Immunol, 2001. **166**(12): p. 7527-33.
299. Kelly, K.J., et al., *Minocycline inhibits apoptosis and inflammation in a rat model of ischemic renal injury*. Am J Physiol Renal Physiol, 2004. **287**(4): p. F760-6.
300. Scarabelli, T.M., et al., *Minocycline inhibits caspase activation and reactivation, increases the ratio of XIAP to smac/DIABLO, and reduces the mitochondrial leakage of cytochrome C and smac/DIABLO*. J Am Coll Cardiol, 2004. **43**(5): p. 865-74.
301. Zhu, S., et al., *Minocycline inhibits cytochrome c release and delays progression of amyotrophic lateral sclerosis in mice*. Nature, 2002. **417**(6884): p. 74-8.
302. Zhang, W., M. Narayanan, and R.M. Friedlander, *Additive neuroprotective effects of minocycline with creatine in a mouse model of ALS*. Ann Neurol, 2003. **53**(2): p. 267-70.
303. Kriz, J., G. Gowing, and J.P. Julien, *Efficient three-drug cocktail for disease induced by mutant superoxide dismutase*. Ann Neurol, 2003. **53**(4): p. 429-36.
304. Friedlander, R.M., et al., *Inhibition of ICE slows ALS in mice*. Nature, 1997. **388**(6637): p. 31.

305. Vukosavic, S., et al., *Delaying caspase activation by Bcl-2: A clue to disease retardation in a transgenic mouse model of amyotrophic lateral sclerosis*. J Neurosci, 2000. **20**(24): p. 9119-25.
306. Cascante, M., et al., *Metabolic control analysis in drug discovery and disease*. Nat Biotechnol, 2002. **20**(3): p. 243-9.
307. Frank, R. and R. Hargreaves, *Clinical biomarkers in drug discovery and development*. Nat Rev Drug Discov, 2003. **2**(7): p. 566-80.
308. Hanash, S., *Disease proteomics*. Nature, 2003. **422**(6928): p. 226-32.
309. Petricoin, E., et al., *Clinical proteomics: revolutionizing disease detection and patient tailoring therapy*. J Proteome Res, 2004. **3**(2): p. 209-17.
310. Fung, E.T., G.L. Wright, Jr., and E.A. Dalmasso, *Proteomic strategies for biomarker identification: progress and challenges*. Curr Opin Mol Ther, 2000. **2**(6): p. 643-50.
311. Chambers, G., et al., *Proteomics: a new approach to the study of disease*. J Pathol, 2000. **192**(3): p. 280-8.
312. Freeman, W.M. and S.E. Hemby, *Proteomics for protein expression profiling in neuroscience*. Neurochem Res, 2004. **29**(6): p. 1065-81.
313. Butterfield, D.A., D. Boyd-Kimball, and A. Castegna, *Proteomics in Alzheimer's disease: insights into potential mechanisms of neurodegeneration*. J Neurochem, 2003. **86**(6): p. 1313-27.
314. Davidsson, P., et al., *Clinical mass spectrometry in neuroscience. Proteomics and peptidomics*. Cell Mol Biol (Noisy-le-grand), 2003. **49**(5): p. 681-8.
315. Morrison, R.S., et al., *Proteomic analysis in the neurosciences*. Mol Cell Proteomics, 2002. **1**(8): p. 553-60.

316. Luo, X., et al., *Macrophage proteomic fingerprinting predicts HIV-1-associated cognitive impairment*. Neurology, 2003. **60**(12): p. 1931-7.
317. Lescuyer, P., et al., *Identification of post-mortem cerebrospinal fluid proteins as potential biomarkers of ischemia and neurodegeneration*. Proteomics, 2004. **4**(8): p. 2234-41.
318. Jiang, L., et al., *Proteomic analysis of the cerebrospinal fluid of patients with schizophrenia*. Amino Acids, 2003. **25**(1): p. 49-57.
319. Castegna, A., et al., *Proteomic identification of oxidatively modified proteins in Alzheimer's disease brain. Part I: creatine kinase BB, glutamine synthase, and ubiquitin carboxy-terminal hydrolase L-1*. Free Radic Biol Med, 2002. **33**(4): p. 562-71.
320. Castegna, A., et al., *Proteomic identification of nitrated proteins in Alzheimer's disease brain*. J Neurochem, 2003. **85**(6): p. 1394-401.
321. Choe, L.H., et al., *Studies of potential cerebrospinal fluid molecular markers for Alzheimer's disease*. Electrophoresis, 2002. **23**(14): p. 2247-51.
322. Lubec, G., et al., *Expression of the dihydropyrimidinase related protein 2 (DRP-2) in Down syndrome and Alzheimer's disease brain is downregulated at the mRNA and dysregulated at the protein level*. J Neural Transm Suppl, 1999. **57**: p. 161-77.
323. Zabel, C., et al., *Alterations in the mouse and human proteome caused by Huntington's disease*. Mol Cell Proteomics, 2002. **1**(5): p. 366-75.
324. Zabel, C. and J. Klose, *Influence of Huntington's Disease on the Human and Mouse Proteome*. Int Rev Neurobiol, 2004. **61**: p. 241-83.
325. Bajo, M., et al., *Proteomic evaluation of intermediary metabolism enzyme proteins in fetal Down's syndrome cerebral cortex*. Proteomics, 2002. **2**(11): p. 1539-46.

326. Kim, S.H., et al., *Human brain nucleoside diphosphate kinase activity is decreased in Alzheimer's disease and Down syndrome*. *Biochem Biophys Res Commun*, 2002. **296**(4): p. 970-5.
327. Karas, M. and F. Hillenkamp, *Laser desorption ionization of proteins with molecular masses exceeding 10,000 daltons*. *Anal Chem*, 1988. **60**(20): p. 2299-301.
328. Hillenkamp, F. and M. Karas, *Mass spectrometry of peptides and proteins by matrix-assisted ultraviolet laser desorption/ionization*. *Methods Enzymol*, 1990. **193**: p. 280-95.
329. Hillenkamp, F., et al., *Matrix-assisted laser desorption/ionization mass spectrometry of biopolymers*. *Anal Chem*, 1991. **63**(24): p. 1193A-1203A.
330. Issaq, H.J., et al., *The SELDI-TOF MS approach to proteomics: protein profiling and biomarker identification*. *Biochem Biophys Res Commun*, 2002. **292**(3): p. 587-92.
331. Boguski, M.S. and M.W. McIntosh, *Biomedical informatics for proteomics*. *Nature*, 2003. **422**(6928): p. 233-7.
332. Breiman, L., *Classification and regression trees*. The Wadsworth statistics/probability series. 1993, Belmont, Calif.: Wadsworth International Group. 358.
333. Feigenbaum, E.A.a.B., B.G., *Dendral and meta-dendral roots: Knowledge systems and expert system applications*. *Artificial Intelligence*, 1993. **59**: p. 233-240.
334. Provost, F.a.F., T., *Robust classification for imprecise environments*. *Machine Learning*, 2001. **42**: p. 203-231.
335. Petricoin, E.F., et al., *Use of proteomic patterns in serum to identify ovarian cancer*. *Lancet*, 2002. **359**(9306): p. 572-7.
336. Sorace, J.M. and M. Zhan, *A data review and re-assessment of ovarian cancer serum proteomic profiling*. *BMC Bioinformatics*, 2003. **4**(1): p. 24.

337. Butterfield, D.A., *Proteomics: a new approach to investigate oxidative stress in Alzheimer's disease brain*. Brain Res, 2004. **1000**(1-2): p. 1-7.
338. Zheng, P.P., et al., *Identification of tumor-related proteins by proteomic analysis of cerebrospinal fluid from patients with primary brain tumors*. J Neuropathol Exp Neurol, 2003. **62**(8): p. 855-62.
339. Rogers, M.A., et al., *Proteomic profiling of urinary proteins in renal cancer by surface enhanced laser desorption ionization and neural-network analysis: identification of key issues affecting potential clinical utility*. Cancer Res, 2003. **63**(20): p. 6971-83.
340. McGregor, E. and M.J. Dunn, *Proteomics of heart disease*. Hum Mol Genet, 2003. **12 Spec No 2**: p. R135-44.
341. Campa, M.J., et al., *Protein expression profiling identifies macrophage migration inhibitory factor and cyclophilin a as potential molecular targets in non-small cell lung cancer*. Cancer Res, 2003. **63**(7): p. 1652-6.
342. Toda, M. and S.J. Ono, *Genomics and proteomics of allergic disease*. Immunology, 2002. **106**(1): p. 1-10.
343. Li, J., et al., *Proteomics and bioinformatics approaches for identification of serum biomarkers to detect breast cancer*. Clin Chem, 2002. **48**(8): p. 1296-304.
344. Ornstein, D.K., et al., *Serum proteomic profiling can discriminate prostate cancer from benign prostates in men with total prostate specific antigen levels between 2.5 and 15.0 ng/ml*. J Urol, 2004. **172**(4 Pt 1): p. 1302-5.
345. Dwek, M.V. and A.A. Alaiya, *Proteome analysis enables separate clustering of normal breast, benign breast and breast cancer tissues*. Br J Cancer, 2003. **89**(2): p. 305-7.

346. Zhang, L., et al., *Contribution of human alpha-defensin 1, 2, and 3 to the anti-HIV-1 activity of CD8 antiviral factor*. Science, 2002. **298**(5595): p. 995-1000.
347. Dyson, N., *The regulation of E2F by pRB-family proteins*. Genes Dev, 1998. **12**(15): p. 2245-62.
348. Heintz, N., *Cell death and the cell cycle: a relationship between transformation and neurodegeneration?* Trends Biochem Sci, 1993. **18**(5): p. 157-9.
349. Dyson, N., *pRB, p107 and the regulation of the E2F transcription factor*. J Cell Sci Suppl, 1994. **18**: p. 81-7.
350. Giovanni, A., et al., *E2F1 mediates death of B-amyloid-treated cortical neurons in a manner independent of p53 and dependent on Bax and caspase 3*. J Biol Chem, 2000. **275**(16): p. 11553-60.
351. Nagy, Z., M.M. Esiri, and A.D. Smith, *The cell division cycle and the pathophysiology of Alzheimer's disease*. Neuroscience, 1998. **87**(4): p. 731-9.
352. Park, D.S., et al., *Involvement of retinoblastoma family members and E2F/DP complexes in the death of neurons evoked by DNA damage*. J Neurosci, 2000. **20**(9): p. 3104-14.
353. Jacks, T., et al., *Effects of an Rb mutation in the mouse*. Nature, 1992. **359**(6393): p. 295-300.
354. Tsai, K.Y., et al., *Mutation of E2f-1 suppresses apoptosis and inappropriate S phase entry and extends survival of Rb-deficient mouse embryos*. Mol Cell, 1998. **2**(3): p. 293-304.
355. Jordan-Sciutto, K.L., L.M. Malaiyandi, and R. Bowser, *Altered distribution of cell cycle transcriptional regulators during Alzheimer disease*. J Neuropathol Exp Neurol, 2002. **61**(4): p. 358-67.

356. Padmanabhan, J., et al., *Role of cell cycle regulatory proteins in cerebellar granule neuron apoptosis*. J Neurosci, 1999. **19**(20): p. 8747-56.
357. Park, D.S., et al., *Cell cycle regulators in neuronal death evoked by excitotoxic stress: implications for neurodegeneration and its treatment*. Neurobiol Aging, 2000. **21**(6): p. 771-81.
358. Lee, S.S., et al., *Cell cycle aberrations by alpha-synuclein over-expression and cyclin B immunoreactivity in Lewy bodies*. Neurobiol Aging, 2003. **24**(5): p. 687-96.
359. Park, D.S., S.E. Farinelli, and L.A. Greene, *Inhibitors of cyclin-dependent kinases promote survival of post-mitotic neuronally differentiated PC12 cells and sympathetic neurons*. J Biol Chem, 1996. **271**(14): p. 8161-9.
360. Park, D.S., et al., *Cyclin dependent kinase inhibitors and dominant negative cyclin dependent kinase 4 and 6 promote survival of NGF-deprived sympathetic neurons*. J Neurosci, 1997. **17**(23): p. 8975-83.
361. Park, D.S., et al., *G1/S cell cycle blockers and inhibitors of cyclin-dependent kinases suppress camptothecin-induced neuronal apoptosis*. J Neurosci, 1997. **17**(4): p. 1256-70.
362. Jordan-Sciutto, K.L., et al., *Induction of cell-cycle regulators in simian immunodeficiency virus encephalitis*. Am J Pathol, 2000. **157**(2): p. 497-507.
363. Miller, F.D., C.D. Pozniak, and G.S. Walsh, *Neuronal life and death: an essential role for the p53 family*. Cell Death Differ, 2000. **7**(10): p. 880-8.
364. Boutillier, A.L., E. Trinh, and J.P. Loeffler, *Selective E2F-dependent gene transcription is controlled by histone deacetylase activity during neuronal apoptosis*. J Neurochem, 2003. **84**(4): p. 814-28.

365. Verona, R., et al., *E2F activity is regulated by cell cycle-dependent changes in subcellular localization*. Mol Cell Biol, 1997. **17**(12): p. 7268-82.
366. Trinh, E., A.L. Boutillier, and J.P. Loeffler, *Regulation of the retinoblastoma-dependent Mdm2 and E2F-1 signaling pathways during neuronal apoptosis*. Mol Cell Neurosci, 2001. **17**(2): p. 342-53.
367. Irwin, M., et al., *Role for the p53 homologue p73 in E2F-1-induced apoptosis*. Nature, 2000. **407**(6804): p. 645-8.
368. Bates, S., et al., *p14ARF links the tumour suppressors RB and p53*. Nature, 1998. **395**(6698): p. 124-5.
369. Furukawa, Y., et al., *Apaf-1 is a mediator of E2F-1-induced apoptosis*. J Biol Chem, 2002. **277**(42): p. 39760-8.
370. Luciakova, K., et al., *Activity of the human cytochrome c1 promoter is modulated by E2F*. Biochem J, 2000. **351**(Pt 1): p. 251-6.
371. Miyashita, T. and J.C. Reed, *Tumor suppressor p53 is a direct transcriptional activator of the human bax gene*. Cell, 1995. **80**(2): p. 293-9.
372. Nahle, Z., et al., *Direct coupling of the cell cycle and cell death machinery by E2F*. Nat Cell Biol, 2002. **4**(11): p. 859-64.
373. Klein, J.A. and S.L. Ackerman, *Oxidative stress, cell cycle, and neurodegeneration*. J Clin Invest, 2003. **111**(6): p. 785-93.
374. Smith, M.A., et al., *Metabolic, metallic, and mitotic sources of oxidative stress in Alzheimer disease*. Antioxid Redox Signal, 2000. **2**(3): p. 413-20.
375. O'Connor, D.J., et al., *Physical and functional interactions between p53 and cell cycle co-operating transcription factors, E2F1 and DP1*. Embo J, 1995. **14**(24): p. 6184-92.

376. Seelan, R.S., et al., *The human p73 promoter: characterization and identification of functional E2F binding sites*. Neoplasia, 2002. **4**(3): p. 195-203.
377. Ramalho, R.M., et al., *Inhibition of the E2F-1/p53/Bax pathway by tauroursodeoxycholic acid in amyloid beta-peptide-induced apoptosis of PC12 cells*. J Neurochem, 2004. **90**(3): p. 567-75.
378. Harvey, M., et al., *Genetic background alters the spectrum of tumors that develop in p53-deficient mice*. Faseb J, 1993. **7**(10): p. 938-43.
379. Clarke, A.R., et al., *Thymocyte apoptosis induced by p53-dependent and independent pathways*. Nature, 1993. **362**(6423): p. 849-52.
380. Blum, D., et al., *p53 and Bax activation in 6-hydroxydopamine-induced apoptosis in PC12 cells*. Brain Res, 1997. **751**(1): p. 139-42.
381. Chan, S.L., et al., *Presenilin-1 mutations sensitize neurons to DNA damage-induced death by a mechanism involving perturbed calcium homeostasis and activation of calpains and caspase-12*. Neurobiol Dis, 2002. **11**(1): p. 2-19.
382. Daily, D., et al., *The involvement of p53 in dopamine-induced apoptosis of cerebellar granule neurons and leukemic cells overexpressing p53*. Cell Mol Neurobiol, 1999. **19**(2): p. 261-76.
383. Tieu, K., et al., *Inhibition of 6-hydroxydopamine-induced p53 expression and survival of neuroblastoma cells following interaction with astrocytes*. Neuroscience, 2001. **103**(1): p. 125-32.
384. Honma, H., L. Gross, and A.J. Windebank, *Hypoxia-induced apoptosis of dorsal root ganglion neurons is associated with DNA damage recognition and cell cycle disruption in rats*. Neurosci Lett, 2004. **354**(2): p. 95-8.

385. Enokido, Y., et al., *Involvement of p53 in DNA strand break-induced apoptosis in postmitotic CNS neurons*. Eur J Neurosci, 1996. **8**(9): p. 1812-21.
386. O'Hare, M.J., et al., *Induction and modulation of cerebellar granule neuron death by E2F-1*. J Biol Chem, 2000. **275**(33): p. 25358-64.
387. Puttonen, K.A., et al., *Increased p53 levels without caspase-3 activity and change of cell viability in 6-hydroxydopamine-treated CV1-P cells*. Cell Biol Toxicol, 2003. **19**(3): p. 177-87.
388. Jordan, J., et al., *Role and regulation of p53 in depolarization-induced neuronal death*. Neuroscience, 2003. **122**(3): p. 707-15.
389. Kitamura, Y., et al., *Hydrogen peroxide-induced apoptosis mediated by p53 protein in glial cells*. Glia, 1999. **25**(2): p. 154-64.
390. Pedersen, W.A., et al., *The prostate apoptosis response-4 protein participates in motor neuron degeneration in amyotrophic lateral sclerosis*. Faseb J, 2000. **14**(7): p. 913-24.
391. Spooren, W.P. and B. Hengerer, *DNA laddering and caspase 3-like activity in the spinal cord of a mouse model of familial amyotrophic lateral sclerosis*. Cell Mol Biol (Noisy-le-grand), 2000. **46**(1): p. 63-9.
392. Shinoue, T., et al., *Upregulation of the pro-apoptotic BH3-only peptide harakiri in spinal neurons of amyotrophic lateral sclerosis patients*. Neurosci Lett, 2001. **313**(3): p. 153-7.
393. Yoshiyama, Y., et al., *Apoptosis related antigen, Le(Y) and nick-end labeling are positive in spinal motor neurons in amyotrophic lateral sclerosis*. Acta Neuropathol (Berl), 1994. **88**(3): p. 207-11.
394. de la Monte, S.M., et al., *P53- and CD95-associated apoptosis in neurodegenerative diseases*. Lab Invest, 1998. **78**(4): p. 401-11.

395. Kikuchi, H., et al., *Impairment of mitochondrial DNA repair enzymes against accumulation of 8-oxo-guanine in the spinal motor neurons of amyotrophic lateral sclerosis*. Acta Neuropathol (Berl), 2002. **103**(4): p. 408-14.
396. Gonzalez de Aguilar, J.L., et al., *Alteration of the Bcl-x/Bax ratio in a transgenic mouse model of amyotrophic lateral sclerosis: evidence for the implication of the p53 signaling pathway*. Neurobiol Dis, 2000. **7**(4): p. 406-15.
397. Kuntz, C.t., et al., *Absence of p53: no effect in a transgenic mouse model of familial amyotrophic lateral sclerosis*. Exp Neurol, 2000. **165**(1): p. 184-90.
398. Prudlo, J., et al., *Motor neuron cell death in a mouse model of FALS is not mediated by the p53 cell survival regulator*. Brain Res, 2000. **879**(1-2): p. 183-7.
399. Fortin, A., et al., *The proapoptotic gene SIVA is a direct transcriptional target for the tumor suppressors p53 and E2F1*. J Biol Chem, 2004. **279**(27): p. 28706-14.
400. Nakano, K. and K.H. Vousden, *PUMA, a novel proapoptotic gene, is induced by p53*. Mol Cell, 2001. **7**(3): p. 683-94.
401. Fortin, A., et al., *APAF1 is a key transcriptional target for p53 in the regulation of neuronal cell death*. J Cell Biol, 2001. **155**(2): p. 207-16.
402. Munsch, D., et al., *Human and mouse Fas (APO-1/CD95) death receptor genes each contain a p53-responsive element that is activated by p53 mutants unable to induce apoptosis*. J Biol Chem, 2000. **275**(6): p. 3867-72.
403. Guegan, C., et al., *Recruitment of the mitochondrial-dependent apoptotic pathway in amyotrophic lateral sclerosis*. J Neurosci, 2001. **21**(17): p. 6569-76.
404. Guegan, C., et al., *Instrumental activation of bid by caspase-1 in a transgenic mouse model of ALS*. Mol Cell Neurosci, 2002. **20**(4): p. 553-62.

405. Wootz, H., et al., *Caspase-12 cleavage and increased oxidative stress during motoneuron degeneration in transgenic mouse model of ALS*. *Biochem Biophys Res Commun*, 2004. **322**(1): p. 281-6.
406. Raoul, C., et al., *Motoneuron death triggered by a specific pathway downstream of Fas. potentiation by ALS-linked SOD1 mutations*. *Neuron*, 2002. **35**(6): p. 1067-83.
407. Evan, G.I., et al., *Induction of apoptosis in fibroblasts by c-myc protein*. *Cell*, 1992. **69**(1): p. 119-28.
408. Wu, X. and A.J. Levine, *p53 and E2F-1 cooperate to mediate apoptosis*. *Proc Natl Acad Sci U S A*, 1994. **91**(9): p. 3602-6.
409. Ryan, K.M., A.C. Phillips, and K.H. Vousden, *Regulation and function of the p53 tumor suppressor protein*. *Curr Opin Cell Biol*, 2001. **13**(3): p. 332-7.
410. Gilman, C.P., et al., *p53 is present in synapses where it mediates mitochondrial dysfunction and synaptic degeneration in response to DNA damage, and oxidative and excitotoxic insults*. *Neuromolecular Med*, 2003. **3**(3): p. 159-72.
411. Chung, Y.H., et al., *Reactive astrocytes express PARP in the central nervous system of SOD(G93A) transgenic mice*. *Brain Res*, 2004. **1003**(1-2): p. 199-204.
412. Stiewe, T. and B.M. Putzer, *Role of the p53-homologue p73 in E2F1-induced apoptosis*. *Nat Genet*, 2000. **26**(4): p. 464-9.
413. Wilson, C., et al., *The p53 homologue p73 accumulates in the nucleus and localizes to neurites and neurofibrillary tangles in Alzheimer disease brain*. *Neuropathol Appl Neurobiol*, 2004. **30**(1): p. 19-29.

414. Kondo, M., et al., *15-Deoxy-Delta(12,14)-prostaglandin J(2): the endogenous electrophile that induces neuronal apoptosis*. Proc Natl Acad Sci U S A, 2002. **99**(11): p. 7367-72.
415. Tilleman, K., et al., *Proteomics analysis of the neurodegeneration in the brain of tau transgenic mice*. Proteomics, 2002. **2**(6): p. 656-65.
416. Korolainen, M.A., et al., *Proteomic analysis of protein oxidation in Alzheimer's disease brain*. Electrophoresis, 2002. **23**(19): p. 3428-33.
417. Butterfield, D.A. and D. Boyd-Kimball, *Proteomics analysis in Alzheimer's disease: new insights into mechanisms of neurodegeneration*. Int Rev Neurobiol, 2004. **61**: p. 159-88.
418. Tsuji, T., et al., *Proteomic profiling and neurodegeneration in Alzheimer's disease*. Neurochem Res, 2002. **27**(10): p. 1245-53.
419. Cutler, R.G., et al., *Evidence that accumulation of ceramides and cholesterol esters mediates oxidative stress-induced death of motor neurons in amyotrophic lateral sclerosis*. Ann Neurol, 2002. **52**(4): p. 448-57.
420. Kim, S.I., et al., *Neuroproteomics: expression profiling of the brain's proteomes in health and disease*. Neurochem Res, 2004. **29**(6): p. 1317-31.
421. Levine, J., et al., *Stability of CSF metabolites measured by proton NMR*. J Neural Transm, 2000. **107**(7): p. 843-8.
422. Hulmes, J.D., et al., *An investigation of plasma collection, stabilization, and storage procedures for proteomic analysis of clinical samples*. Clinical Proteomics, 2004. **1**(1): p. 17-32.
423. Bruijn, L.I., *Amyotrophic lateral sclerosis: from disease mechanisms to therapies*. Biotechniques, 2002. **32**(5): p. 1112, 1114, 1116 passim.

424. Strong, M. and J. Rosenfeld, *Amyotrophic lateral sclerosis: a review of current concepts*. Amyotroph Lateral Scler Other Motor Neuron Disord, 2003. **4**(3): p. 136-43.
425. Rosen, D.R., et al., *Mutations in Cu/Zn superoxide dismutase gene are associated with familial amyotrophic lateral sclerosis*. Nature, 1993. **362**(6415): p. 59-62.
426. Valentine, J.S. and P.J. Hart, *Misfolded CuZnSOD and amyotrophic lateral sclerosis*. Proc Natl Acad Sci U S A, 2003. **100**(7): p. 3617-22.
427. Nagai, M., et al., *Rats expressing human cytosolic copper-zinc superoxide dismutase transgenes with amyotrophic lateral sclerosis: associated mutations develop motor neuron disease*. J Neurosci, 2001. **21**(23): p. 9246-54.
428. Van Westerlaak, M.G., et al., *Chronic mitochondrial inhibition induces glutamate-mediated corticomotoneuron death in an organotypic culture model*. Exp Neurol, 2001. **167**(2): p. 393-400.
429. Menzies, F.M., et al., *Mitochondrial dysfunction in a cell culture model of familial amyotrophic lateral sclerosis*. Brain, 2002. **125**(Pt 7): p. 1522-33.
430. Riviere, M., et al., *An analysis of extended survival in patients with amyotrophic lateral sclerosis treated with riluzole*. Arch Neurol, 1998. **55**(4): p. 526-8.
431. Klivenyi, P., et al., *Neuroprotective effects of creatine in a transgenic animal model of amyotrophic lateral sclerosis*. Nat Med, 1999. **5**(3): p. 347-50.
432. Gurney, M.E., et al., *Benefit of vitamin E, riluzole, and gabapentin in a transgenic model of familial amyotrophic lateral sclerosis*. Ann Neurol, 1996. **39**(2): p. 147-57.
433. Rothstein, J.D., *Of mice and men: reconciling preclinical ALS mouse studies and human clinical trials*. Ann Neurol, 2003. **53**(4): p. 423-6.

434. Paulson, H.L., *Protein fate in neurodegenerative proteinopathies: polyglutamine diseases join the (mis)fold*. Am J Hum Genet, 1999. **64**(2): p. 339-45.
435. Rohlff, C., *Proteomics in molecular medicine: applications in central nervous systems disorders*. Electrophoresis, 2000. **21**(6): p. 1227-34.
436. Fountoulakis, M., *Application of proteomics technologies in the investigation of the brain*. Mass Spectrom Rev, 2004. **23**(4): p. 231-58.
437. Marcotte, E.R., L.K. Srivastava, and R. Quirion, *cDNA microarray and proteomic approaches in the study of brain diseases: focus on schizophrenia and Alzheimer's disease*. Pharmacol Ther, 2003. **100**(1): p. 63-74.
438. Malaspina, A., N. Kaushik, and J. de Belleruche, *Differential expression of 14 genes in amyotrophic lateral sclerosis spinal cord detected using gridded cDNA arrays*. J Neurochem, 2001. **77**(1): p. 132-45.
439. Shibata, N., et al., *Accumulation of protein-bound 4-hydroxy-2-hexenal in spinal cords from patients with sporadic amyotrophic lateral sclerosis*. Brain Res, 2004. **1019**(1-2): p. 170-7.
440. Beuche, W., et al., *Matrix metalloproteinase-9 is elevated in serum of patients with amyotrophic lateral sclerosis*. Neuroreport, 2000. **11**(16): p. 3419-22.
441. Allen, S., et al., *Analysis of the cytosolic proteome in a cell culture model of familial amyotrophic lateral sclerosis reveals alterations to the proteasome, antioxidant defenses, and nitric oxide synthetic pathways*. J Biol Chem, 2003. **278**(8): p. 6371-83.
442. Gopalakrishnan, V., et al., *Proteomic data mining challenges in identification of disease biomarkers from variable resolution mass spectra*. Proceedings of SIAM Bioinformatics Workshop, 2004: p. 1-10.

443. Schweigert, F.J., K. Wirth, and J. Raila, *Characterization of the microheterogeneity of transthyretin in plasma and urine using SELDI-TOF-MS immunoassay*. *Proteome Sci*, 2004. **2**(1): p. 5.
444. Stein, T.D., et al., *Neutralization of transthyretin reverses the neuroprotective effects of secreted amyloid precursor protein (APP) in APPSW mice resulting in tau phosphorylation and loss of hippocampal neurons: support for the amyloid hypothesis*. *J Neurosci*, 2004. **24**(35): p. 7707-17.
445. La Bella, V., J.C. Goodman, and S.H. Appel, *Increased CSF glutamate following injection of ALS immunoglobulins*. *Neurology*, 1997. **48**(5): p. 1270-2.
446. Smith, R.G., et al., *Presence of 4-hydroxynonenal in cerebrospinal fluid of patients with sporadic amyotrophic lateral sclerosis*. *Ann Neurol*, 1998. **44**(4): p. 696-9.
447. Shaw, P.J. and R. Williams, *Serum and cerebrospinal fluid biochemical markers of ALS*. *Amyotroph Lateral Scler Other Motor Neuron Disord*, 2000. **1 Suppl 2**: p. S61-7.
448. Jacobsson, J., et al., *Superoxide dismutase in CSF from amyotrophic lateral sclerosis patients with and without CuZn-superoxide dismutase mutations*. *Brain*, 2001. **124**(Pt 7): p. 1461-6.
449. Spreux-Varoquaux, O., et al., *Glutamate levels in cerebrospinal fluid in amyotrophic lateral sclerosis: a reappraisal using a new HPLC method with coulometric detection in a large cohort of patients*. *J Neurol Sci*, 2002. **193**(2): p. 73-8.
450. Marcinkiewicz, M., et al., *Expression of neuroendocrine secretory protein 7B2 mRNA in the mouse and rat pituitary gland*. *Neuroendocrinology*, 1993. **58**(1): p. 86-93.
451. Marcinkiewicz, M., P. Touraine, and M. Chretien, *Pan-neuronal mRNA expression of the secretory polypeptide 7B2*. *Neurosci Lett*, 1994. **177**(1-2): p. 91-4.

452. Zhu, X., et al., *Internal cleavage of the inhibitory 7B2 carboxyl-terminal peptide by PC2: a potential mechanism for its inactivation*. Proc Natl Acad Sci U S A, 1996. **93**(10): p. 4919-24.
453. Hwang, J.R. and I. Lindberg, *Inactivation of the 7B2 inhibitory CT peptide depends on a functional furin cleavage site*. J Neurochem, 2001. **79**(2): p. 437-44.
454. Stark, M., et al., *Peptide repertoire of human cerebrospinal fluid: novel proteolytic fragments of neuroendocrine proteins*. J Chromatogr B Biomed Sci Appl, 2001. **754**(2): p. 357-67.
455. Chaudhuri, B., et al., *The neuroendocrine protein 7B2 acts as a molecular chaperone in the in vitro folding of human insulin-like growth factor-1 secreted from yeast*. Biochem Biophys Res Commun, 1995. **211**(2): p. 417-25.
456. Davidsson, P., R. Ekman, and K. Blennow, *A new procedure for detecting brain-specific proteins in cerebrospinal fluid*. J Neural Transm, 1997. **104**(6-7): p. 711-20.
457. Coria, F. and I. Rubio, *Cerebral amyloid angiopathies*. Neuropathol Appl Neurobiol, 1996. **22**(3): p. 216-27.
458. Palm, D.E., et al., *Cystatin C, a protease inhibitor, in degenerating rat hippocampal neurons following transient forebrain ischemia*. Brain Res, 1995. **691**(1-2): p. 1-8.
459. Nishio, C., et al., *Involvement of cystatin C in oxidative stress-induced apoptosis of cultured rat CNS neurons*. Brain Res, 2000. **873**(2): p. 252-62.
460. Sastre, M., et al., *Binding of cystatin C to Alzheimer's amyloid beta inhibits in vitro amyloid fibril formation*. Neurobiol Aging, 2004. **25**(8): p. 1033-43.
461. Levy, E., et al., *Codeposition of cystatin C with amyloid-beta protein in the brain of Alzheimer disease patients*. J Neuropathol Exp Neurol, 2001. **60**(1): p. 94-104.

462. Kalso, E., *Biomarkers for pain*. Pain, 2004. **107**(3): p. 199-201.
463. Okamoto, K., et al., *Bunina bodies in amyotrophic lateral sclerosis immunostained with rabbit anti-cystatin C serum*. Neurosci Lett, 1993. **162**(1-2): p. 125-8.
464. Seilhean, D., et al., *Amyotrophic lateral sclerosis with neuronal intranuclear protein inclusions*. Acta Neuropathol (Berl), 2004. **108**(1): p. 81-7.
465. Schreiber, G., *The evolution of transthyretin synthesis in the choroid plexus*. Clin Chem Lab Med, 2002. **40**(12): p. 1200-10.
466. Monaco, H.L., *The transthyretin-retinol-binding protein complex*. Biochim Biophys Acta, 2000. **1482**(1-2): p. 65-72.
467. Power, D.M., et al., *Evolution of the thyroid hormone-binding protein, transthyretin*. Gen Comp Endocrinol, 2000. **119**(3): p. 241-55.
468. Sockanathan, S. and T.M. Jessell, *Motor neuron-derived retinoid signaling specifies the subtype identity of spinal motor neurons*. Cell, 1998. **94**(4): p. 503-14.
469. Malaspina, A. and J. de Bellerocche, *Spinal cord molecular profiling provides a better understanding of amyotrophic lateral sclerosis pathogenesis*. Brain Res Brain Res Rev, 2004. **45**(3): p. 213-29.
470. Zheng, W., et al., *Transthyretin, thyroxine, and retinol-binding protein in human cerebrospinal fluid: effect of lead exposure*. Toxicol Sci, 2001. **61**(1): p. 107-14.
471. Sousa, J.C., et al., *Transthyretin is involved in depression-like behaviour and exploratory activity*. J Neurochem, 2004. **88**(5): p. 1052-8.
472. Mears, E., *Outcomes of continuous process improvement of a nutritional care program incorporating TTR measurement*. Clin Chem Lab Med, 2002. **40**(12): p. 1355-9.

473. Cohen, J. and G.P. Wilkin, *Neural cell culture : a practical approach*. Practical approach series ; 165. 1996, Oxford ; New York: IRL PRes at Oxford University. xx, 248.
474. Khursigara, G., J.R. Orlinick, and M.V. Chao, *Association of the p75 neurotrophin receptor with TRAF6*. J Biol Chem, 1999. **274**(5): p. 2597-600.
475. Ye, X., et al., *TRAF family proteins interact with the common neurotrophin receptor and modulate apoptosis induction*. J Biol Chem, 1999. **274**(42): p. 30202-8.
476. Kanekura, K., et al., *Alsin, the product of ALS2 gene, suppresses SOD1 mutant neurotoxicity through RhoGEF domain by interacting with SOD1 mutants*. J Biol Chem, 2004. **279**(18): p. 19247-56.
477. Tini, M., et al., *Association of CBP/p300 acetylase and thymine DNA glycosylase links DNA repair and transcription*. Mol Cell, 2002. **9**(2): p. 265-77.